TESIS DE LA UNIVERSIDAD DE ZARAGOZA
2022
112

Joana Ines Santos De Almeida

Generation and large-scale expansion of highly functional hPSC-derived hepatocytes for Cellular therapies and bioengineered livers: the unknown role of human microbiome

Director/es
Almeida De Matos Baptista, Pedro Miguel

ISSN 2254-7606

Prensas de la Universidad
Universidad Zaragoza

ISSN 2254-7606

Universidad Zaragoza
1542

Tesis Doctoral

GENERATION AND LARGE-SCALE EXPANSION OF HIGHLY FUNCTIONAL HPSC-DERIVED HEPATOCYTES FOR CELLULAR THERAPIES AND BIOENGINEERED LIVERS: THE UNKNOWN ROLE OF HUMAN MICROBIOME

Autor

Joana Ines Santos De Almeida

Director/es

Almeida De Matos Baptista, Pedro Miguel

UNIVERSIDAD DE ZARAGOZA
Escuela de Doctorado

Programa de Doctorado en Ingeniería Biomédica

2022

Universidad Zaragoza
1542

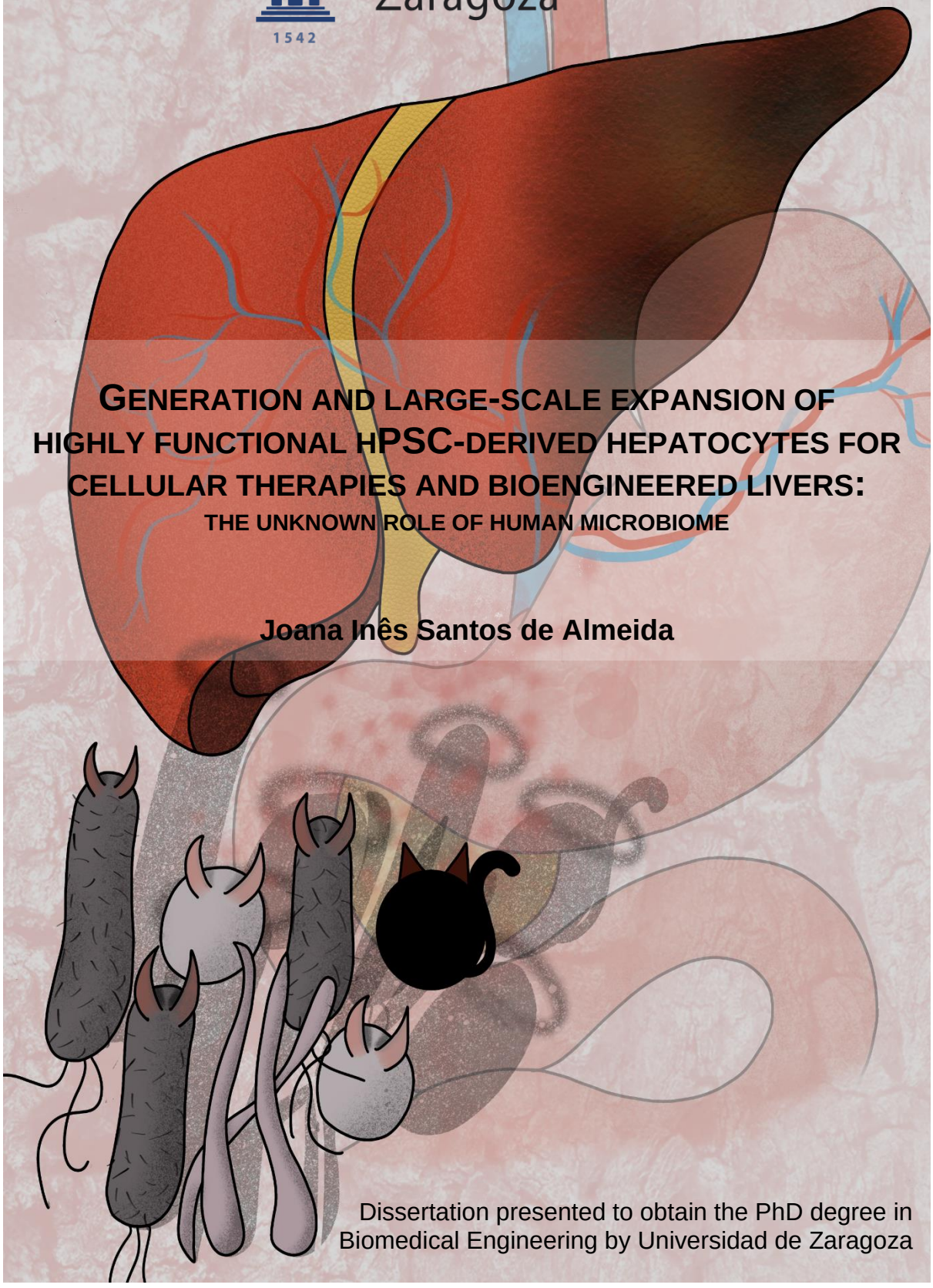

GENERATION AND LARGE-SCALE EXPANSION OF HIGHLY FUNCTIONAL HPSC-DERIVED HEPATOCYTES FOR CELLULAR THERAPIES AND BIOENGINEERED LIVERS:

THE UNKNOWN ROLE OF HUMAN MICROBIOME

Joana Inês Santos de Almeida

Dissertation presented to obtain the PhD degree in Biomedical Engineering by Universidad de Zaragoza

Generation and large-scale expansion of highly functional hPSC-derived hepatocytes for cellular therapies and bioengineered livers:
the unknown role of human microbiome

Joana Inês Santos de Almeida

Thesis to obtain the PhD Degree in
Biomedical Engineering

Supervisor: Pedro Miguel Baptista, PhD

With the financial support from FCT,
under contract SFRH/BD/116780/2016

March 2022

Generation and large-scale expansion of highly functional hPSC-derived hepatocytes for cellular therapies and bioengineered livers:
the unknown role of human microbiome

By Joana Inês Santos de Almeida

Cover: "Blessed bacterial secretome": Illustrative cartoon of human intestinal microbes, represented as "villains" due to their association with the pathophysiology of liver diseases; and now recognized as protectors ("angels"), secreting postbiotics that help the damaged liver to regenerate.

Universidad de Zaragoza
Pedro Cerbuna 12
50009 Zaragoza - España
ciu@unizar.es

Instituo de Investigación Sanitaria de Aragón
Edificio CIBA - Campus San Francisco
Avda. San Juan Bosco, 13
50009 Zaragoza
http://www.iisaragon.es/

Instituto de Biologia Experimental e Tecnológica
Instituto de Tecnologia Química e Biológica António Xavier
Av. da República EAN,
2780-157 Oeiras, Portugal
http://www.ibet.pt

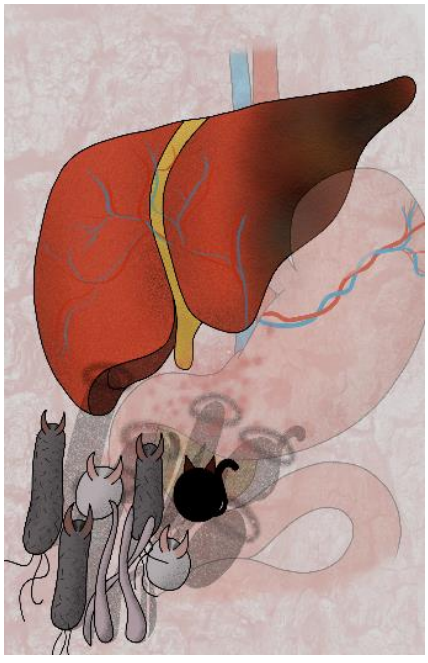

La ejecución del plan de trabajos de esta Tesis Doctoral se ha desarollado en el Instituto de Investigación Sanitaria de Aragón (IIS-Aragón) y en el Centro de Investigación Biomédica de Aragón (CIBA), Zaragoza (España); y en el Instituto de Biologia Experimental e Tecnológica (iBET) en Lisboa (Portugal); y se ha enmarcado dentro de los proyectos: “PI18/00529”, financiado por el Instituto de Salud Carlos III; “LMP226_18” de la Diputación General de Aragón (España); “ERAdicatPH” (E-Rare3/0002/2015) del ERA-NET E-Rare 3 research program y “MetaCardio” (PTDC/BTM-SAL/32566/2017) financiado por la Fundação para a Ciência e Tecnologia (Portugal).

La candidata Joana Inês Santos de Almeida ha disfrutado de una beca predoctoral mista (SFRH/BD/116780/2016) financiada por la Fundação para a Ciência e Tecnologia (Portugal).

Acknowledgements

I would not have been able to complete this work without acknowledging some amazing people for whose help I am immeasurably grateful:

First and foremost, I would like to thank my esteemed supervisor Dr. Pedro Miguel Baptista for accepting me as your student and introducing me to this fascinating field of Regenerative Medicine. Your immense knowledge and unparalleled creativity have always inspired me. I hope we can continue to challenge the limits of science together.

I would like to express my sincere gratitude to my co-supervisor, mentor and friend, Dr. Margarida Serra, for her guidance, encouragement, and immeasurable support throughout this journey.

I would also like to extend my deepest gratitude to Dr. José Manuel García Aznar for always being helpful.

I would like to acknowledge Dr. Paula M. Alves and Prof. Manuel Carrondo for being visionary leaders and providing me with unprecedented professional opportunities.

I gratefully acknowledge Fundação para a Ciência e Tecnologia for the financial support (SFRH/BD/116780/2016).

I want to thank all the present and former members of the Organ Bioengineering and Regenerative Medicine Lab at IIS-Aragón and colleagues and friends from Stem Cell Bioprocessing Lab and ACTU at iBET.

I am deeply indebted to Pedro Vicente and Inês Crespo, “the engines of this project”. Your contributions to this project have been invaluable.

Many thanks to all my dearest scientists and friends: Filipa, Iris, Sofía, Daniela, Nikolaus, Marco, Cláudia, Maria Bia, Laurens, Henrique, Tomás, Marcos and André Barros. I feel very lucky to share this journey with you.

To my best friends: Leticia, Sara, Manel and Julia, for have always been there when homesick hit me harder. This would not have been the same without you.

To my close friends Sara Lopes, Filomena, André Q., Raquel, Daniela G. and Vanessa for understanding my absences but always valuing and treasuring our friendship.

I am grateful for the wisdom of older people who have enriched my world, my grandparents, Avó Isabel and Avô Vasco, Avó Rosa and Avô Santos, I am blessed for still having you here.

To my two godmothers Dina, for being an example of commitment, dedication, and altruism. Paula, for being a special human being, who were always supporting me and encouraging me with their best wishes.

To Lomu and Pablo for showing me the purest forms of love.

To Nik for his unconditional love, patience and endless care. Thank you for enlightening my life and fill it with happiness and dreams. The best part is yet to come. I love you with all my heart and soul.

To my brother. You are my biggest inspiration and an example of strength, focus and resilience. I have been so blessed to have a brother like you. And to my sister Nádia for filling our family with sincere love.

Finally, I wish to express my love and gratitude to my parents for their eternal love, constant support and encouragement. Without you, none of this would be possible.
I hope you understand that all these I accomplished were ultimately for you.

À minha família e Nik

Abstract

Hepatocytes differentiated from human induced pluripotent stem cells (hiPSC), also called hepatocyte-like cells (HLC), provide unprecedented opportunities for cell-based therapies and, therefore, the treatment of a wide range of liver diseases. Regrettably, more than 15 years of research in the field were insufficient to convert HLC into an advanced therapy medicinal product. The immature phenotypes exhibited by these cells, the lack of reliable and reproducible protocols for their scalable production and the uncertainties regarding their ability to engraft into scaffolds (in vitro and in vivo) are some of the reasons that hamper their clinical application. Thus, this thesis aimed to develop efficient strategies to generate clinically relevant numbers of functional and mature HLC for cell therapy and regenerative medicine applications. To achieve this goal, an integrated approach was developed by combining advanced manufacturing platforms with nature-inspired strategies, by unveiling the role of human microbiome on HLC maturation and function preservation.

Recapitulating *in vitro* the physiological liver maturation process is challenging as it takes approximately two years after birth and involves the induction of a wide range of metabolic and detoxification pathways. Recent insights on liver development revealed that the acquisition of adult maturation and function could be strongly associated with the establishment and diversification of the intestinal microbiome.

In **Chapter 1**, the microbial molecules and the molecular mechanisms underlying this crosstalk were revised.

In **Chapter 2**, the effects of the secretome of intestinal microbiota on hPSC-HLC functionality (or maturation) were investigated. Thus HLC, generated from hESC or hiPSC using 2D or 3D culture approaches, were treated with a microbial secretome formulated in vitro in the form of a conditioned medium (CM). Our results showed that HLC exposed to CM showed higher expression of putative hepatocyte markers (e.g., HNF4A, CYP1B1, -3A4, -2C9, -2D6, -2E1, CPS1, PPARA, TLR1, -2, -5, -6, etc.); preserved the basal CYP3A4 activity and/or showed inducible -3A4 metabolism; showed improved expression of ALB and enhanced secretion of some specific liver-plasma proteins, ALB and A1AT, when compared to untreated HLC.

As cell therapies require relevant cells numbers, scalable bioprocesses for the production of HLC as 3D cell aggregates under controlled culture conditions were developed in **Chapters 3** and **4.**

In **Chapter 3**, an integrated bioprocess that combines 3D hiPSC expansion and hepatic differentiation steps was implemented, using stirred-tank bioreactors (STB) operating in perfusion. Using this protocol, hiPSC were able to proliferate as 3D aggregates and further differentiate into HLC that expressed typical hepatic markers and exhibited functional characteristics of hepatocytes including glycogen storage and drug metabolization capacity. Moreover, the incorporation of capacitance sensor in the bioreactor system allowed to demonstrate, for the first time, the potential of dielectric spectroscopy to monitor *in situ* hiPSC expansion and differentiation in STB; the results obtained showed a good correlation between the cell permittivity measured online and the aggregate biovolume measured by standard offline methods.

Aiming to improve further cell expansion and HLC differentiation yields, in **Chapter 4**, the bioprocess was optimized by controlling the dissolved oxygen concentration at low levels (4% O2) during hepatic specification phase. The optimized bioprocess was validated for two hiPSC lines enabling higher HLC production yields (up to 3.2×10^6 cell/mL) and differentiation efficiencies (> 80% $Albumin^+$ cells) when compared to uncontrolled conditions (0.6×10^6 cell/mL). A detailed transcriptomic analysis of HLC at different maturation stages was done, showing that immature and mature hiPSC-HLC differed about 35% in their whole transcriptome, and these differences included pathways related to cell engraftment. Noteworthily, these differences had implications in the cellular ability to engraft into decellularized liver scaffolds, as only mature HLC showed the capacity to adhere, proliferate and remain functional after 14 days in culture.

Finally, in **Chapter 5** a general discussion of the main achievements and conclusions of the work are presented, and future perspectives outlined.

In conclusion, this thesis represents an important first step towards the generation of protocols for production of relevant numbers of HLC with more mature and functional features that will hopefully potentiate the development of hepatic stem cell therapies for patients with end-stage liver disease. This work also opens a new paradigm into

Stem Cell Bioengineering and links it with an unexpected topic, the Human Microbiome.

Resumen

Los hepatocitos diferenciados a partir de células madre pluripotentes inducidas humanas (hiPSC), también conocidos como *hepatocyte-like cells* (HLC), proporcionan una cantidad sin precedentes de posibilidades para el desarrollo de terapias celulares y, con ello, el tratamiento de una gran variedad de enfermedades hepáticas. Sin embargo, más de quince años de investigación en este campo han sido insuficientes para obtener una terapia médica avanzada a base de HLC. Los fenotipos inmaduros que presentan estas células, la falta de protocolos fiables y reproducibles para su producción a gran escala, así como la incertidumbre con respecto a su capacidad para injertarse en andamios (o *scaffolds*), tanto *in vitro* como *in vivo,* son algunas de las razones que dificultan su aplicación clínica. Por lo tanto, el objetivo de esta tesis ha sido el desarrollo de estrategias eficientes para generar HLC maduras y funcionales en cantidades clínicamente relevantes para su uso en terapia celular y medicina regenerativa. Para ello, se ha desarrollado un método integrado que combina plataformas de fabricación avanzada con estrategias inspiradas en procesos naturales, estudiando el efecto del microbioma intestinal humano en la maduración y la preservación de las funciones de las HLC.

Recapitular *in vitro* el proceso de maduración fisiológica del hígado supone un gran reto, ya que dura aproximadamente dos años desde el nacimiento e implica la inducción de una amplia gama de vías metabólicas y de desintoxicación. Investigaciones recientes sobre el desarrollo del hígado han revelado que la maduración y el desarrollo de la función hepática podrían estar altamente asociados con el establecimiento y la diversificación del microbioma intestinal.

En el **Capítulo 1**, discutimos las moléculas microbianas y los mecanismos moleculares que constituyen esta interacción.

En el **Capítulo 2**, investigamos los efectos del secretoma de la microbiota intestinal sobre la funcionalidad (o maduración) de las hPSC-HLC mediante el tratamiento de estas células, generadas utilizando diferentes estrategias en 2D o 3D, con un secretoma microbiano formulado *in vitro* en forma de medio condicionado. Nuestros resultados muestran que las HLC expuestas al medio condicionado presentan una mayor expresión de marcadores hepáticos (p.ej. *HNF4A*, *CYP1B1*, *-3A4*, *-2C9*, *-2D6*,

-2E1, *CPS1*, *PPARA*, *TLR1*, *-2*, *-5*, *-6*, etc.); conservan la actividad basal de CYP3A4 y/o mostraban metabolismo inducible CYP3A4; mejoran la expresión de ALB; y aumentan la secreción de las proteínas hepáticas plasmáticas ALB y A1AT, en comparación con HLC no tratadas con el medio condicionado.

Dado que las terapias celulares requieren una alta producción celular, en los **Capítulos 3** y **4** desarrollamos bioprocesos escalables para la producción de HLC en forma de agregados celulares tridimensionales.

En el **Capítulo 3**, implementamos una estrategia integrada para la producción a gran escala de hiPSC-HLC, que combina la expansión y diferenciación en 3D de las hiPSC usando biorreactores de tanque agitado en modo de perfusión. Mediante este protocolo, las hiPSC son capaces de crecer en agregados 3D y las HLC resultantes expresan marcadores hepáticos típicos y exhiben características funcionales de los hepatocitos, incluyendo el almacenamiento de glucógeno y la capacidad de metabolización de fármacos. Además, la incorporación de un sensor de capacitancia en el sistema del biorreactor nos ha permitido demostrar por primera vez el potencial de la espectroscopia dieléctrica para monitorizar la expansión y diferenciación de hiPSC en los biorreactores de tanque agitado. Los resultados que obtuvimos mostraron una buena correlación entre la permitividad celular medida *on-line* y el biovolumen de los agregados medido por métodos estándar *off-line.*

Con el objetivo de mejorar la expansión celular y el rendimiento de la diferenciación, en el **Capítulo 4** optimizamos el bioproceso al mantener la concentración de oxígeno disuelto en niveles bajos (4% O_2) durante la fase de especificación hepática. Hemos validado esta optimización para dos líneas celulares de hiPSC mejorando el rendimiento de producción de HLC (hasta $3.2x10^6$ células/mL) y la eficiencia de diferenciación (> 80% células Albumina+) en comparación con condiciones no controladas ($0.6×10^6$ células/mL). Un análisis transcriptómico detallado de las HLC en diferentes etapas de maduración muestra que las hiPSC-HLC maduras difieren aproximadamente un 35% en su transcriptoma completo con respecto a hiPSC-HCL inmaduras. Estas diferencias incluyen vías relacionadas con el injerto celular, teniendo implicaciones en la capacidad celular para injertarse en andamios, ya que solo las HLC maduras pueden adherirse, proliferar y mantener su funcionalidad después de 14 días de cultivo.

Por último, en el **Capítulo 5**, presentamos una discusión general de los logros y conclusiones principales del trabajo realizado y delineamos futuras perspectivas a investigar.

En conclusión, este estudio representa un importante primer paso hacia la generación de HLC derivadas de hiPSC más maduras y funcionales que, esperamos, harán que las terapias con células madre hepáticas sean una realidad tangible para los pacientes con enfermedad hepática en etapa terminal. También abre un nuevo cambio de paradigma en la bioingeniería de células madre y lo vincula con un campo inesperado, el microbioma humano.

Thesis Publications

Published

1. **Almeida J.I.**, Tenreiro M.F., Martinez-Santamaria, L., Guerrero-Aspizua, S., Gisbert, J.P., Alves P.M, Serra, M., Baptista, P.M. Hallmarks of the human intestinal microbiome on liver maturation and function. Journal of Hepatology 2022. 76(3):694-725. doi: 10.1016/j.jhep.2021.10.015.

2. Isidro, I.A., Vicente, P., Pais, D. A. M., **Almeida, J.I.**, Domingues, M., Abecasis, B., Zapata-Linares, N., Rodriguez-Madoz, J.R., Prosper, F., Aspegren, A., Alves, P.M., Serra, M. Online monitoring of hiPSC expansion and hepatic differentiation in 3D culture by dielectric spectroscopy. Biotechnology and Bioengineering 2021. 118(9):3610-3617. doi: 10.1002/bit.27751.

In preparation

1. **Almeida J.I.**, Vicente P., Crespo I.E., Serra M., Baptista P.M. Human intestinal microbiota sustains the functionality of hPSC-derived hepatocytes *in vitro*.

2. **Almeida J.I.**, Crespo I.E., Vicente P., Virgolini N., Calmeiro T., Vazão Almeida H., Calleja M.; Rodriguez-Madoz, J.R., Prosper, F., Fortunato E., Alves P.M., Baptista P.M., Serra M. Recellularization of acellular liver scaffolds with highly functional hiPSC-hepatocytes generated using a scalable and optimized bioprocess.

3. Vicente P., **Almeida J.I.**, Crespo I.E., Isidro, I.A., Calleja M.; Rodriguez-Madoz, J.R., Prosper, F., Aspegren, A., Alves, P.M., Serra, M. Massive production of hiPSC-derived hepatocytes and application in primary hyperoxaluria type 1 disease modeling.

Other publications

1. Brovold M., **Almeida J.I.**, Pla-Palacín I., Sainz-Arnal P., Sánchez-Romero N., Rivas J.J., Almeida H., Dachary P.R., Serrano-Aulló T., Soker S., Baptista P.M. Naturally derived Biomaterials for Tissue Engineering Applications. Adv Exp Med Biol 2018. 1077:421-449. doi: 10.1007/978-981-13-0947-2_23.

2. Morini S., Sanchéz-Romero N., Pla-Palacín I., Sainz-Arnal P., Almeida M., Verscheijden L., **Almeida J.I.**, *et al*. Liver Tissue Engineering in Bioreactors for Stem Cell Expansion and Differentiation by Joaquim M S Cabral and Cláudia Lobato da Silva. 2018. Publisher: Boca Raton - Taylor & Francis, 2019

Contents

Acronymous

2D	Two dimensional
3D	Three dimensional
ABC	ATP-binding cassette
ABCB1	ATP binding cassette subfamily B member 1
Abx	Antibiotics
AFM	Atomic force microscopy
AFP	Alpha-fetoprotein
ALB	Albumin
ALD	Alcoholic liver disease
A1AT	Alpha-1 antitrypsin
BMP	Bone morphogenetic protein
ChiPSC18	Cellartis human iPS Cell Line 18
CMs	Conditioned media
CM A	Conditioned media from a healthy donor
CM A+abx	Conditioned media from a donor under antibiotic treatment
CPS1	Carbamoyl-Phosphate Synthase 1
CYP1B1	Cytochrome P450 Family 1 Subfamily B Member 1
CYP2C9	Cytochrome P450 Family 2 Subfamily C Member 9
CYP2D6	Cytochrome P450 Family 2 Subfamily D Member 6
CYP2E1	Cytochrome P450 Family 2 Subfamily E Member 1
CYP3A4	Cytochrome P450 Family 3 Subfamily A Member 4
CYP3A7	Cytochrome P450 Family 3 Subfamily A Member 7
CYP450	Cytochrome P450
DAPI	4′,6-diamidino-2-phenylindole
DE	Definitive endoderm
dECM	Decellularized ECM
DMSO	Dimethyl sulfoxide
DO	Dissolved oxygen
DPBS	Dulbecco phosphate-buffered saline
DR	Dilution rate
ECM	Extracellular matrix
Epcam	Epithelial cell adhesion molecule
FBS	Fetal bovine serum
FDA	Fluorescein diacetate
FGF	Fibroblast growth factor
FMT	Fecal microbiota transplantation
GC-MS	Gas chromatography-mass spectrometry
GF	Germ-free
hESC	Human embryonic stem cells
hiPSC	Human induced pluripotent stem cells
hPSC	Human pluripotent stem cells
HLC	Hepatocyte-like cells
HMM	Hepatocyte maintenance media
HNF4A	Hepatocyte nuclear factor 4 alpha
hPSC	Human induced pluripotent stem cells
HSC	Hematopoietic stem cells
H&E	Hematoxylin and eosin

ICG	Indocyanine green
imHLC	Immature HLC
KC	Kupffer cells
LA	Lithocholic acid
LPS	Lipopolysaccharide
LT	Liver transplantation
mHLC	Mature HLC
MT	Masson's Trichrome
NAFLD	Non-alcoholic fatty liver disease
NFR	Nuclear fast red
OCT	Optimal Cutting Temperature
OSM	Oncostatin M
ON	Over night
PAS	Periodic acid–schiff
PCA	Principal component analysis
PCR	Polymerase chain reaction
PHH	Primary human hepatocytes
pO2	Oxygen partial pressure
PPARA	Peroxisome proliferator activated receptor alpha
rECM+imHLC-7d	Acellular liver scaffolds recellularized with imHLC and cultured for 7 days
rECM+mHLC-7d	Acellular liver scaffolds recellularized with mHLC and cultured for 7 days
rECM+mHLC-14d	Acellular liver scaffolds recellularized with mHLC and cultured for 14 days
RT	Room temperature
RT-PCR	Reverse transcription-PCR
RT-qPCR	RT-quantitative real-time PCR
SAR	Surface aeration rate
SCFA	Short-chain fatty acids
Sc-RNA-seq	Single-cell RNA sequencing
SD	Standard deviation
SEM	Scanning electron microscopy
s-GAGs	Sulphated glycosaminoglycans
SGF	Simulated gastric fluid
SIF	Simulated intestinal fluid
SPF	Specific pathogen-free
STBR	stirred-tank bioreactor
STM	Septum transversum mesenchyme
TLR1	Toll Like Receptor 1
TLR2	Toll Like Receptor 2
TLR4	Toll Like Receptor 4
TLR6	Toll Like Receptor 6
TOPRO-3	TO-PRO™-3 Iodide
UGT(s)	UDP-glucuronosyltransferase(s)
UPLC/MRM-MS	Ultraperformance liquid chromatography-multiple reaction monitoring-multi-stage/mass spectrometry
Vit.K_2	Vitamin K_2

Chapter 1

INTRODUCTION

This chapter is adapted from the Seminar:

Almeida J.I., Tenreiro M.F., Martinez-Santamaria, L., Guerrero-Aspizua, S., Gisbert, J.P., Alves P.M, Serra, M., Baptista, P.M. Hallmarks of the human intestinal microbiome on liver maturation and function. Journal of Hepatology 2022. 76(3):694-725. doi: 10.1016/j.jhep.2021.10.015.

Authors’ contributions

Joana Inês Almeida conceptualized, wrote, and designed the figures of the manuscript.

Contents

1. The Human Liver

1.1. Hepatic function and complexity

In adult life, the liver is the largest solid internal organ and the biggest gland, comprising roughly 2-3% of the total body weight [1]. It is located below the diaphragm on the right side of the abdominal cavity and it is morphologically divided into two portions, a right and a left lobe as viewed from the front (diaphragmatic) surface, even though when seen from the visceral surface two additional lobes may be considered, the caudate and the quadrate lobes [2]. An alternative classification, based on liver's functional anatomy, shows it to be divided into eight independent segments, each composed by approximately 1000 lobules and endowed with their own blood supply and biliary drainage [3,4]. Hepatic lobules, the anatomic units of the liver, are organized into irregular polygons demarcated by connective tissue and composed by plates of hepatocytes radiating outward from the central vein to the portal triads (i.e., hepatic arteriole, portal venule and a bile ductule) at the corners (**Figure 1**). Interestingly, it is estimated that the human liver contains approximately 1 million lobules [5] measuring around 1mm in diameter [6].

The liver is a unique organ in the sense that it receives a dual blood supply [1]. Approximately 75% of the liver's blood corresponds to venous blood that is drained from the spleen, gastrointestinal tract and its associated organs, and carried to hepatic tissues by the portal vein; the remaining 25% corresponds to oxygenated blood that reaches the acinus through the hepatic artery. Within the lobule, mixed arterial and venous blood enter the liver by the portal triads, flowing radially inwards towards a draining central vein through sinusoids. Bile secreted into canaliculi is directed in the opposite direction towards portal regions by specialized hepatocellular microvilli.

Beyond its remarkable anatomical structure, the liver is a critical hub for numerous physiological processes and the most metabolically complex systems in the human body. Approximately 1-2 liters of blood bypass the liver per minute, which corresponds to one-fourth of the total cardiac output at rest in adults [1]. Its complexity is also reflected by recent transcriptomic and proteomic data showing the expression of more than 17396 genes, of which 238 genes were identified as liver enrichment genes, [7] and encoding more than 72% of all human proteins [8]. Therefore, it is not surprising

that a fully mature liver is able to perform up to 500 different functions [9] such as anabolic and catabolic metabolism of macronutrients, detoxification of xenobiotics, bile and protein secretion, immune surveillance, among others [10].

Hepatocytes are the “metabolic factories” of the liver. They are the most predominant parenchymal cell type, accounting for approximately 80% of the adult liver mass [11]. They are polygonal, polarized and polyploid cells (20–30% tetraploid and octaploid [12,13]), perceived as a crucial adaption for high metabolic demand. However, liver functions are not exclusively performed by these cells, and rather result from finely tuned interactions between hepatocytes and the multiple non-parenchyma cells (NPC) that compose the hepatic tissue (i.e., liver sinusoidal endothelial cells, hepatic stellate cells, biliary epithelial cells (or cholangiocytes), kupffer cells (KC) and additional immune cell populations).

Importantly, the liver is not a uniform mass of cells that performs all the above functions equally. In fact, most hepatic tasks are non-homogeneously carried out by different subsets of hepatocytes, a division of labor that is possible due to its remarkable property known as *liver zonation*. Liver zonation, a fascinating example of evolutionary optimization of function, corresponds to the spatial separation of the immense spectrum of different metabolic pathways along the acinus resulting into three distinct ‘zones’ (zone 1, 2, and 3). Each zone possesses very specialized hepatocytes exhibiting morphological and metabolic heterogeneity. For instance, hepatocytes located in zone 1 (or periportal region) are the first and best perfused as well as the ones more devoted to oxidative metabolism (i.e., gluconeogenesis, lipid ß-oxidation, ureagenesis, bile and cholesterol synthesis), while pericentral hepatocytes (zone 3) are mostly implicated in glycolysis, glutamine synthesis, liponeogenesis, ketogenesis and detoxification. Finally, hepatocytes located at zone 2 (i.e., intermediate zone) show a mixed phenotype, preferably assuming the functional attributes of zone 1 hepatocytes in the face of damage or loss of function. Understanding metabolic zonation and its regulation has been comprehensively reviewed from time to time [14,15], and culminated a little more than a decade ago with the discovery of Wnt/β-catenin signaling as a master regulator of zonation in the adult liver [16,17]. More recently, the cell surface complex RSPO–LGR4/5–ZNF3/RNF43 was shown to direct Wnt/β-catenin signaling in this process [18,19]. Beyond the previous master

regulators, zonation is also dynamically regulated by various physical parameters like the gradient of oxygen [20] or by (patho)physiologic factors, the latter including nutrient/hormonal conditions [21], circadian rhythm [22], hepatitis C virus infection and systemic metabolic disturbances such as advanced non-alcoholic steatohepatitis (NASH) [23]. Interestingly, it has also been shown that several liver diseases have zonal preferences [24,25], and that the disturbance of liver zonation and its regulatory mechanisms may result in liver pathology and development of metabolic disorders [23]. These phenomena are deeply reviewed elsewhere [26].

The liver has long been recognized as a key metabolic organ that governs body energy status [10,27]. Briefly, during the postprandial phase, the liver converts glucose into glycogen and lipids, which provide metabolic fuels during fasting. In the fasted state, the liver produces and secretes glucose through both glycogenolysis and gluconeogenesis. The liver also converts fatty acids into ketone bodies, which provide additional metabolic fuels for extrahepatic tissues during fasting. The metabolic switch between the fasted and fed states in the liver is tightly controlled by neuronal and hormonal inputs.

Perhaps the most sophisticated hepatic function is the capacity of metabolizing a wide range of xenobiotics, preventing the body from toxicity. Hepatic drug metabolism can be briefly defined by a three-phase set of enzymatic reactions that convert lipophilic products into more hydrophilic compounds, facilitating their elimination in the urine [28,29]. It occurs preferentially in the microsomes, lysosomes and cytosol of zone 3 hepatocytes. Phase-I biotransformation reactions (also termed as nonsynthetic reactions) include oxidations, reductions and hydrolysis and are catalyzed mostly by enzymes belonging to the complex cytochrome P450 (CYP450) superfamily. Human CYP450 genes comprise more than 115 genes and pseudogenes members and are among the most extensively annotated mammalian genes, starting from CYP1A1 and ending with CYP51P3 [30]. Even though CYP450 enzymes are distributed throughout various tissues and organs in humans, including peripheral blood cells, platelets, aorta, adrenal glands, adipose tissues, nasal tissue, vaginal tissues, seminal vesicles, brain, lung and kidneys, it is in the liver and small intestine that they have their maximum expression. A very detailed meta-analysis reported that among all CYP450 enzymes present in adult liver, CYP3A4 is the most abundant, followed by CYP2E1

and CYP2C9, representing approximately 22.1%, 15.3%, and 14.6% of the total CYP450 (based on protein content), respectively [31,32]. Apart from CYP450 enzymes, other phase I enzymes include flavin-containing monooxygenases, monoamine oxidases, molybdenum hydroxylases, alcohol dehydrogenases, aldehyde dehydrogenases, aldo-keto reductase, NADPH:quinone reductases, and hydrolytic enzymes [28]. In phase-II, drugs or metabolites from phase I pathways are enzymatically conjugated with a hydrophilic group by different reactions including glucuronidation, sulfation, acetylation, methylation, conjugation with glutathione and conjugation with amino acids (e.g., taurine, glutamine, glycine). The UDP-glucuronosyltransferases (UGTs), sulfotransferases, N-acetyltransferases, glutathione S-transferases, thiopurine S-methyltransferases and catechol O-methyltransferases constitute the enzymes involved in this phase [28]. Finally, during phase III the conjugated xenobiotics may be further processed before being recognized by efflux transporters and pumped out of cells. ATP-binding cassette (ABC) and solute carrier transporters are among the major players in this process [28].

The liver intertwines with nearly every system in the body, and so it is prone to many multisystemic diseases. Liver failure after partial hepatectomy or the end-stage liver disease (ESLD) caused by acute or chronic insults results in decompensation in other organs including hepatic encephalopathy, variceal bleeding, kidney impairment, ascites, lungs issues, coma and eventually death. Fortunately, the liver is an extremely resilient organ and the only visceral tissue that possesses the capacity for regeneration. It is known that as much as 51% of the original liver mass can regenerate back to its full size [33]. The overall process of liver regeneration includes three phases: an initial priming stage where hepatocytes become sensitive to growth factors with the aid of some cytokines (e.g., TNF-α and IL-6); a second proliferative phase where the previous factors induce hepatocytes to re-enter in G1 phase; and a termination phase where hepatocytes will discontinue to proliferate to maintain normal liver mass and function. Beyond hepatocytes that contribute for their own maintenance, recent studies suggest the presence of both intrahepatic and extrahepatic stem/progenitor cell populations also serves to maintain the normal organ and to regenerate damaged parenchyma in response to a variety of insults [34]. For a better understanding of liver regeneration the reading of [35–37] is strongly recommended.

Another recent function attributed to liver is its role in immune system support. Immunity has long been attributed exclusively to KC, but hepatocytes are now also being acknowledged as key contributors. Zhou Z. and co-authors reviewed the proteins secreted by hepatocytes that might activate innate immunity. These proteins include bactericidal proteins able to directly kill bacteria, opsonins (e.g. CRP, SAP, etc.) that assist in the phagocytosis of foreign bacteria, iron-sequestering proteins (i.e., transferrin) capable of blocking iron uptake by bacteria, several soluble factors as regulators of lipopolysaccharide (LPS) signaling, interleukins (i.e., IL-6, IL-22, IL-1β and TNF-α), complement proteins (C1r/s, C2, C4, C4bp, C3, B, etc.) and the coagulation factor fibrinogen [38].

As discussed above, the liver is capable of the most extraordinary functions. Others like lipid storage, cholesterol and bile acid homeostasis, vitamin metabolism, urea and plasma protein synthesis, and even destruction of old or faulty red blood cells, were not neglected, just were not revisited here.

The liver and its processes are well conserved among vertebrates, and when fully developed and matured they are imperative for life. But has it always been this way? Does a baby born with all these hepatic functions? Will the fetal liver be the same as the neonatal liver? And are these very different from an adult liver? While many authors have deeply reviewed the development of the liver, giving important insights into organ and tissue morphogenesis [39], less is known regarding the acquisition of hepatic functions and the mechanisms behind fetal to neonatal to adult liver remodeling. Mammalian tissues initially form and begin functioning in the embryo but are extensively remodeled after birth to rapidly adapt and perform adult functions. This process is especially relevant for the liver.

1.2. The emerging liver

During the last half of the 20th century, facilitated by an explosion in molecular biology techniques, novel imaging strategies and genome-wide bioinformatics, the embryonic development of the human liver has been decoded. Understanding its fundamental mechanisms was essential for developmental and cell biology, as it laid out the basis for stem cell research which ultimately may lead to more valuable therapeutic options in regenerative medicine.

The embryonic liver development is characterized by a set of orchestrated events that enable: i) the proliferation and differentiation of progenitor cells that will constitute the main liver cell types; ii) its spatial rearrangement along the acinus and the development of hepatic lobules; iii) the generation of a complex network of intra and extrahepatic bile ducts; iv) the formation of the gallbladder; v) the onset of a complex vasculature and innervation system that, in combination with physiological maturation processes occurring throughout gestation, will build a functional tissue [40]. Due to ethical concerns, studies with human embryos are few and not always time accurate, but recent studies with animal models have shown to be elucidative regarding lineage relationships, signaling pathways and transcriptional programs that orchestrate hepatogenesis [39,41–43].

Briefly, after the commitment of the foregut endoderm, the human liver emerges by the 3rd to 4th weeks of gestation as a result of the hepatic diverticulum (or liver bud) organogenesis, a process remarkably conserved across vertebrate species (**Figure 1**). The hepatic diverticulum is an out-pocket of thickened ventral foregut epithelium adjacent to the developing heart and represents the first structure bearing morphological signs of the embryonic liver. It will be composed by two distinct parts: i) the anterior portion (or *pars hepatica*) that gives rise to the liver and intrahepatic biliary tree; ii) the posterior portion (or *pars cystica*) which forms the gallbladder and extrahepatic bile ducts with no contribution to liver development in humans. By 23-26 days of gestation (3-4 mm embryo), hepatic endoderm cells that from the hepatic diverticulum rapidly grow and invade the adjacent septum transversum mesenchyme (STM), allowing hepatic specification of the hepatic diverticulum (**Figure 1**). Signals from STM, such as FGFs and BMPs, are required for this process. Immediately after, by 31-56 days of gestation, hepatoblasts (i.e., the bipotential hepatic progenitors) proliferate and sinusoids expand, being these events characteristic of the hepatic diverticulum outgrowth. Finally, from 56-58 to ~210 days of gestation, hepatoblasts differentiate into hepatocytes or cholangiocytes (from the intra or extrahepatic bile ducts). Differentiation into hepatocyte lineage requires a core transcription factor network that includes HNF1α, FOXA2, HNF4α1, HNF6, and LRH-1 [44]. The subsequent and final step of hepatocyte maturation requires other factors like oncostatin M (OSM), glucocorticoids, HGF and Wnt. A more detailed review of these mechanisms can be found at [39,42].

Interestingly, since the termination of hepatic lineage differentiation (by day 210 of gestation) till the end of the gestational period (~266-288 days) only ~56-80 days have passed, which corresponds to the period of hepatocyte maturation *in utero* [42]. Is it enough time to mature the "metabolic factories" of the liver? Are hepatocytes functional during and after gestation? Is the newborn liver capable of supporting life? How are hepatic functions acquired?

During fetal life, the liver takes up a very large portion of fetus's abdominal cavity. Szpinda M. *et al*., elegantly described the rapid volumetric growth of liver in human fetuses, reporting an increase in liver weight from 3.09 ± 0.27 g in fetuses aged 12-13 weeks to 161.94 ± 37.78 g in fetuses aged 41-42 weeks [45]. During the gestational period, fetal liver grows dramatically and becomes a pivotal organ involved in fetoplacental metabolism. However, these rapid modifications seem not to follow its maturation process. Most hepatic functions that we know from the adult liver, which are extremely essential for life, are absent in the fetus. Fetal liver immaturity might be related with fetus's dependency of a maternal body supporting basic fetal functions like nutrition and filtration, or simply because the acquisition of liver functions requires more time and needs other stimuli different from those present during uterine life. However, the fetal liver shows other important functions that are not seen in adults. Hematopoiesis, for example, is the main function of the liver during a considerable period of mammalian prenatal development. By 5-7th weeks of gestation (10 mm embryo), soon after hepatoblasts invade the SPM, the fetal liver is colonized by hematopoietic stem cells (HSC) and transiently becomes the major hematopoietic organ. By the 2nd trimester of gestation, the hematopoietic activity increases drastically and approximately 60-70% of the hepatic parenchyma is populated by HSC, mainly due to the optimal hematopoietic environment/niche created by fetal liver hepatic progenitors [46] (**Figure 1**). Interestingly, these HSC appear to be essential for hepatocyte maturation as well because they secrete OSM, responsible for several hepatic cellular responses. In fetal liver, hematopoiesis has a distinct zonal distribution; while the production of erythroid cells is found within the sinusoid (or "bessis islands"), myelopoiesis is located mainly around the vascular structures within the portal triads [47].

By the 24th week of gestation, hematopoietic activity starts to decrease gradually until birth, beginning translocation to the bone marrow. More on hepatic hematopoiesis can be found at [48,49].

Besides hematopoiesis, the fetal liver ensures blood circulation in the fetus, being often described as a “cardiovascular tissue” [50]. Briefly, the fetal liver receives oxygen-rich blood from the umbilical vein, shunting it via ductus venosus to the inferior vena cava and then to the fetus’s heart, where it is pumped to all tissues. By this time, the fetal liver is bi-lobed that seem to function independently with respect on the microcirculation [40]. The right side of the liver is perfused with less well-oxygenated blood, mainly originated from portal blood, and has a greater role in hematopoiesis, while the liver’s left side receives blood mainly from the umbilical vein (**Figure 1**), exhibits a higher content of oxygen-dependent enzymes, and therefore is more active in drug metabolism [51].

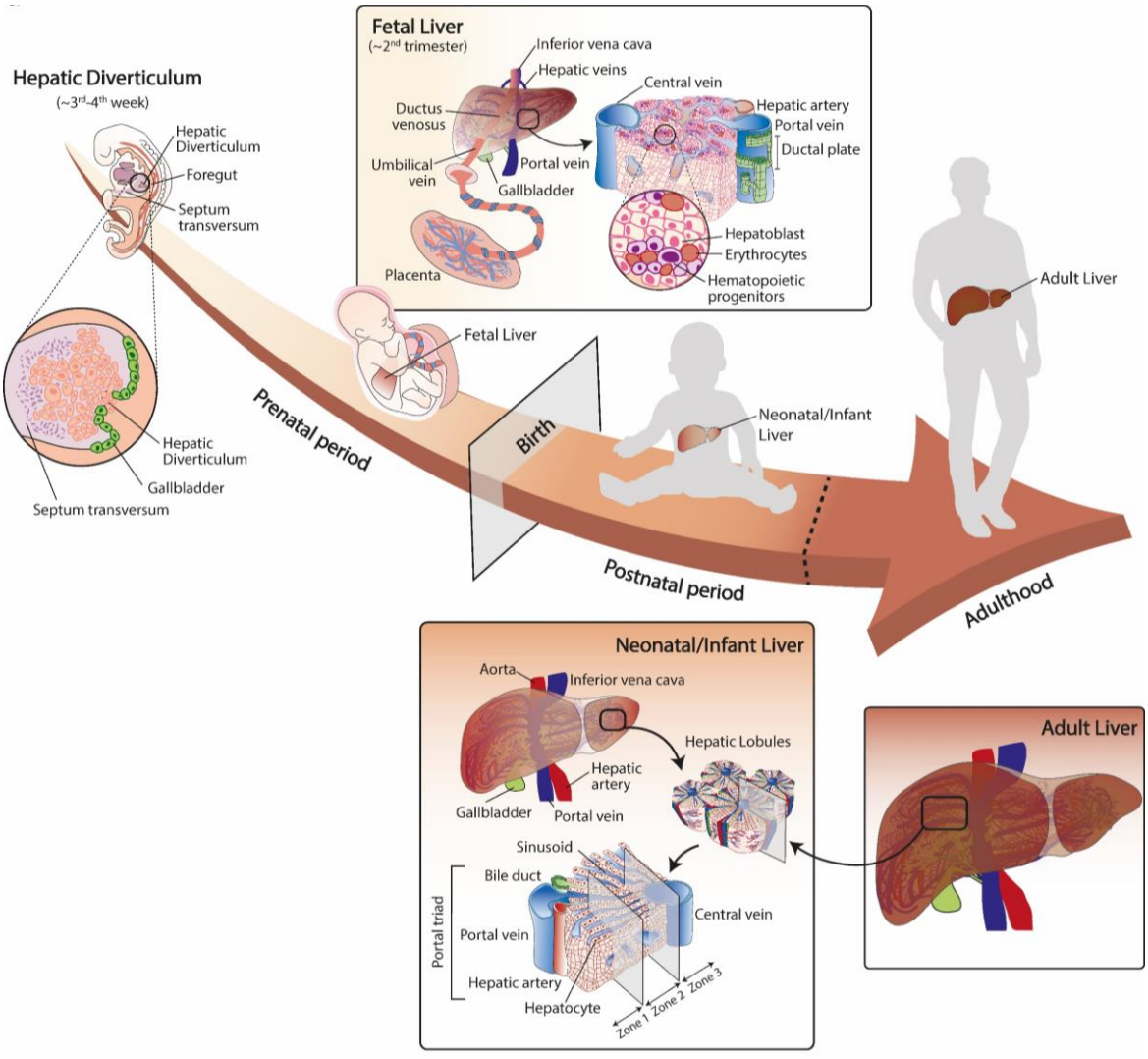

Figure 1. Human liver development. During embryogenesis, the first sign of human liver development corresponds to the formation of the hepatic diverticulum after the commitment of foregut endoderm. Throughout gestation these hepatic progenitor cells, known as hepatoblasts, differentiate into hepatocytes or cholangiocytes, which culminates with the development of hepatic lobules. The fetal liver also supports hematopoiesis, peaking at the 2nd trimester and declining until birth. The maturation of liver cells happens during the last moments before birth, which is not sufficient to establish all hepatic functions that are imperative for adult competence.

What about the other liver functions? Is a fetal liver capable of xenobiotics detoxification, nutrient metabolism, or even protein production?

The dogma that considers the placenta as an impenetrable barrier against most drugs is now broadly questioned. For some years now it has been shown that nearly all drugs administered during pregnancy will enter, to some degree, the fetal circulation via passive diffusion. In fact, approximately 75% of umbilical venous blood passes through the fetal liver [51]. This contains maternal-derived xenobiotics and drugs that are metabolized by the fetal liver, preventing the fetus from cardiac and neuronal toxicity. Therefore, it is not surprising the fetal liver might present some drug detoxification capacity. Recent studies on human fetal liver biopsies have confirmed these beliefs. Enzymatic expression levels of CYP450 were detectable in the fetus's liver, and its expression was relatively stable throughout gestation but represented only ~30% of the levels detected in adulthood. These findings are not surprising given their role in modulating levels of endogenous substrates involved in fetal homeostasis, growth, and differentiation. By 1 year of age, CYP450 reach expression levels comparable to those of adults [52,53]. Within the CYP450 superfamily, individual CYP450 enzymes demonstrate significant differences in expression and activity in the fetus and neonate compared to adults, resulting in vastly different metabolic profiles between neonates and adults [28,54]. As an example, CYP3A7 (involved in steroid metabolism) accounts for up to 50% of total hepatic fetal CYP450 content, whose expression is replaced by CYP3A4 during the first year of life [55]. Others like CYP1A1 and CYP2D6 have also been detected in the human fetal liver [55]. Regarding phase-II enzymes, neonates show a reduced enzymatic glucuronidation capacity, as demonstrated by their limited ability to conjugate bilirubin during early postnatal life, resulting often in hyperbilirubinemia. Coughtrie M. W, et al., reported the fetal liver has low expression levels of hepatic UGT enzymes, and these developed postnatally reaching about 25% of adult levels by 3 months of age [56]. For a detailed revision on fetal hepatic drug elimination the following study is suggested [55].

Fetal energy needs are primarily supported by the transplacental transfer of maternal glucose to the fetus [57]. Therefore no significant levels of gluconeogenesis by the fetus is documented under physiological conditions, even though all the machinery necessary for gluconeogenesis is well developed by the eighth week of gestation [58]. For example, the hepatic glucose-6-phosphatase activity, the final enzymatic step in glycogenolysis and gluconeogenesis, is significantly reduced in the fetus, increasing to 10% of adult levels by term and reaching adult levels by 3 days of age [59].

Fetal plasma protein synthesis is also dissimilar from those found in adults. The main serum protein produced by the fetal liver is alpha-fetoprotein (AFP), whose plasma concentration peaks at the end of the first trimester, but its synthesis dramatically ceases after birth and is replaced by albumin (ALB) as the most produced plasma protein [60]. The role of AFP during prenatal development remains unknown, even though it is postulated it could be a carrier protein similar to ALB. Other research suggests AFP may also take part in bilirubin metabolism [61] and regulate T cell immunity [60]. In mice, AFP has been found to have high affinity to estradiol and so it can sequester estrogens found in maternal blood, preventing the female brain from high exposure to estrogens and ensuring the male brain is mostly exposed to estradiol obtained from testosterone aromatization. AFP is particularly important to imprint prenatal brain sexual dimorphism in mice [62], however human AFP has low affinity to estrogens [63], raising questions regarding its true purpose in humans. Additionally, the synthesis of other plasma proteins, such as coagulation proteins, is only intensified following birth.

The liver is crucial for life but it seems quite immature throughout gestation. Surprisingly, during the first weeks of life the liver experiences a wide range of dramatic changes that promote its maturation through the performance of various function aimed at ensuring newborn survival. But what triggers liver maturation during the early postnatal period?

1.3. Liver remodeling after birth

The transition from a fetus to a newborn is the most complex adaptation that occurs in human experience [64]. Beyond the rapid adaptations for breathing, the newborn must also quickly control its energy metabolism and thermoregulation. The newborn liver

must rapidly adapt and mature to face this challenging new life. Here we briefly revisit some of the environmental and molecular factors that promote hepatocyte differentiation and maturation, as previously identified by Chen et al. [65] (**Figure 2**).

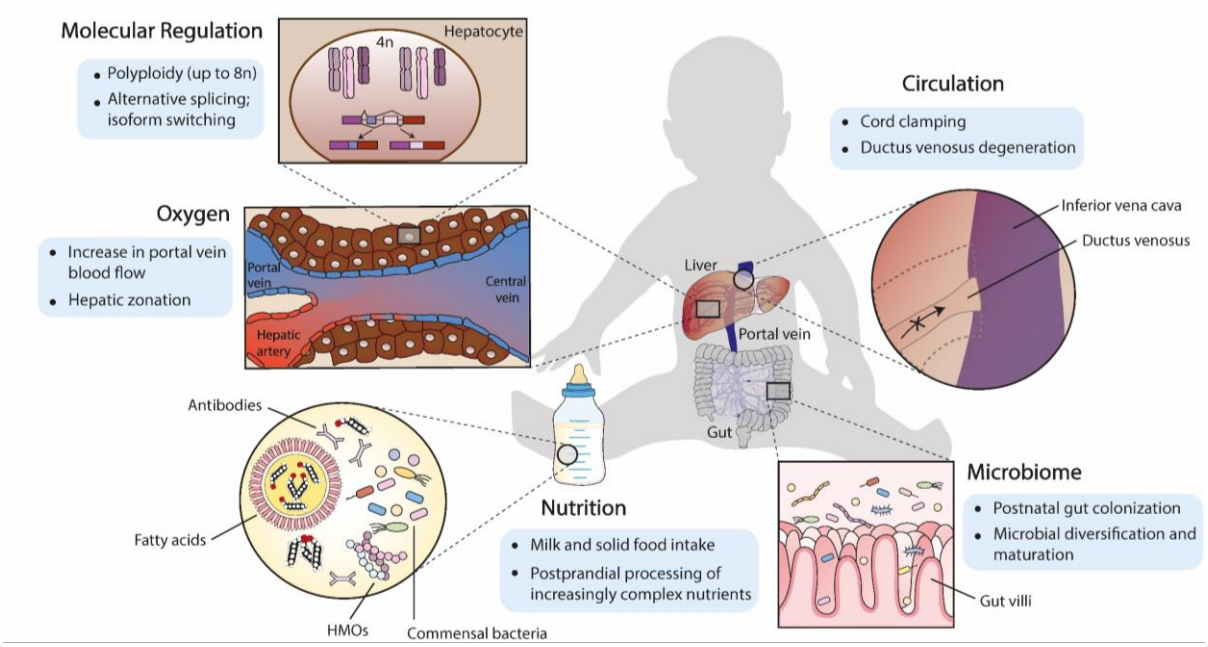

Figure 2. Postpartum changes involved in hepatic maturation. Environmental, cellular and molecular factors that play a part in postpartum liver maturation. Abbreviations: HMO, human milk oligosaccharide.

1.3.1. Circulation and Oxygenation

At birth, the placental circulation is abolished, and as the newborn becomes hypoxic the lungs expand for the first time, commencing pulmonary function and eliminating the need for gas exchange through the placenta. And so, elements that partake in hepatic fetal circulation are no longer needed, such as the extra abdominal portion of the umbilical vein and the ductus venosus. *In utero*, liver perfusion is predominantly carried out by the umbilical vein branches, with a smaller contribution coming from the hepatic artery and portal vein [66]. After birth there is a marked decrease in umbilical venous pressure, and within the first days the ductus venosus closes as a consequence of intracardiac pressure changes and decreased circulating prostaglandins [67]. Interestingly, as a consequence of the fetal blood vessels' degeneration, the remnants of the umbilical vein and ductus venous will give rise to the ligamentum teres and ligamentum venosum in the liver, respectively. The neonatal liver circulation will now be ensured solely by the hepatic artery and the portal system,

the latter representing the greatest contribution of all liver blood flow [68]. In fact, with the beginning of the intestinal function portal trunk doubles its caliber within the first 3 weeks [69]. Since the portal trunk is directed towards the right, the portal circulation will preferentially supply blood to the right lobe, as opposed to the umbilical circulation, and so this will result in a noticeable postnatal change in liver morphology that favors an enhanced growth of the right liver half [69].

These dramatic postpartum changes in liver circulation certainly have consequences for hepatic function, physiology and maturation, which till date have not yet been fully unveiled in the neonate. However, several *in vitro* studies showed that oxygenation increased ALB and urea synthesis in rat hepatocytes [70]. Additionally, oxygen is known to regulate metabolic zonation in the normal liver and under pathological conditions [20,71], and the shear stress was described to increase function of liver parenchymal cells, for example, through polarization [72].

1.3.2. Nutrition

After birth the baby no longer receives intravenous fully processed nutrients from the mother, and so initiation of the digestive and intestinal functions is essential to acquire the necessary nutrients. Birth also imposes dramatic changes upon the newborn diet. During pregnancy, the fetus primarily receives glucose and amino acids from maternal blood as well as lactate synthesized in the placenta. Even though the human placenta is permeable to free fatty acids, the supply of glucose and amino acids is sufficient for oxidative metabolism and fetal growth [73]. After birth, the high-carbohydrate low-fat diet that characterizes fetal nutrition is replaced by a low-carbohydrate high-fat diet as a consequence of suckling.

As the newborn awaits absorption of the new source of nutrients from the milk, glycogen and lipid stores are rapidly exhausted, which briefly leads to hypoglycemia [74]. This transient starvation period results in alterations of pancreatic hormone levels, namely a decrease in insulin concentration and a rise in glucagon secretion. Essentially, this endocrine response to the stress associated with birth will onset various metabolic adaptations that prepare the liver for extrauterine life. In particular, recovering and maintaining normal glycemia levels requires intensification of glucose

production through gluconeogenesis. Lactose is the only carbohydrate present in milk and its hydrolysis yields insufficient glucose to cover the newborn's needs, even when galactose is used as a gluconeogenic substrate [73]. Contrary to the fetal liver, the neonatal liver readily harnesses the ability to synthesize glucose from lactate, pyruvate and amino acids following birth, especially owed to an increase in activity of the gluconeogenesis rate-limiting enzyme phosphoenolpyruvate carboxykinase (PEPCK), that occurs in response to a shift in insulin/glucagon molar ratio [75].

Owing to the high-fat content of milk, newborns must develop ways to cope with a much larger amount of free fatty acids, that were practically absent during uterine life. This requires coordinated regulation of genes involved in fatty acid catabolism and ketogenesis. In fact, postnatal development of fatty acid oxidation and ketone body production is closely related with the appearance of the mitochondrial carnitine palmitoyltransferase (CPT) system and 3-hydroxy-3-methylglutaryl-CoA (HMG-CoA) synthase [76]. Neonatal energy metabolism is particularly dependent upon peroxisome proliferator-activated receptor-alpha (PPARα) transcriptional regulation. In mice, the genes required for lipid catabolism were found to be transcribed before birth under PPARα control, as to prompt efficient energy production from lipidic milk substrates [77]. Fatty acid catabolism not only yields higher energy amounts, it also provides essential co-factors (acetyl-CoA and NADH) to support gluconeogenesis in the liver [73]. Interestingly, the balance between glucose production and oxidation is insufficient to meet neuronal needs [78], and since fatty acids are unable to cross the blood brain barrier, the neonatal liver forcefully has to adapt and provide an additional source of metabolic fuels. Such source comes from ketone body production, which is vigorously intensified in the neonate with a turnover rate comparable to those found in adults after several days of total fasting [79].

1.3.3. Molecular Regulation

Hepatocyte identity is controlled by diverse genetic and molecular mechanisms, ensuring proper lineage specification, differentiation and maturation. Hepatic transcriptional programming is not only regulated by a vast repertoire of transcription factors (e.g., C/EBPα, HNF1α, HNF4α, FOXA family, HNF6) [80], but also by post-translational modifications like alternative splicing (e.g., SRSF3 and ESRP2) able to

control hepatocyte hypertrophic growth, polyploidization and postnatal fetal-to-adult isoform switch [81,82]. In particular, polyploidization only becomes evident after birth [83], and unlike most human cells hepatocytes can become tetraploid (4n) and even octoploid (8n). Hepatic polyploidy is typically associated with senescence, terminal differentiation and maturation, even though it has been suggested as a way of enhancing tissue-specific functions [84], a clear advantage in the liver due to its vast catalogue of functions. Besides genome-wide adaptations, gradual decreases in membrane fluidity [85] and alterations is extracellular matrix composition [86] also seem to contribute for postnatal hepatocyte maturity.

1.3.4. Microbiome

Efforts in characterizing the composition and functionality of microbial communities in the first years of life have undoubtedly elucidated the assembly and maturation of gut microbes during this critical time frame is necessary for proper physiological development. Although some support prenatal microbial colonization via extraembryonic tissues/fluids [87,88], others only detected meaningful traces of microbial communities after birth [89]. Notwithstanding, postnatal events such as delivery, early feeding practices and environmental exposures are the greatest contributors for postnatal gut colonization and progressive functional maturation [90]. Among all organs, the liver is likely to receive the greatest amount of macro and micronutrients that are actively produced by gut microbes, which is made possible due to its proximity to the gut via the portal system.

The implications of human intestinal microbiome on the acquisition of adult hepatic function and maturation are addressed extensively in the following chapters.

2. Unraveling the crosstalk between gut and liver

The term “gut-liver axis”, first described in the 1980s [91,92], refers to the bidirectional communication between the gut (with its microbiota) and the liver, in which there is an active participation of signals from dietary, genetic and environmental origin (**Figure 3 a**). In the past decade, strong evidence from both animal models and clinical studies have suggested perturbations to the gut-liver axis influence liver disease progression, namely in non-alcoholic fatty liver disease (NAFLD), non-alcoholic steatohepatitis (NASH), alcoholic liver disease (ALD), cirrhosis and hepatocellular carcinoma (HCC) [93]. The burden of these gastrointestinal-associated liver diseases has, consequently, placed the gut-liver axis on the scientific agenda. While much is known about its role in disease [94], its physiological contribution to liver development and homeostasis is less appreciated.

The liver and the gut are connected by the biliary tract and the portal venous system. The common bile duct joins the pancreatic duct at the anatomical transition from foregut to midgut, known as the hepatopancreatic ampulla, where both bile and pancreatic enzymes are allowed to enter the major duodenal papilla during the postprandial period (**Figure 3 b**). In particular, the bile contains bile acids that aid lipid and fat-soluble vitamin emulsification, solubilization and absorption along the ileum. Due to its finger-like evaginations (i.e., villi), the gut is one of the body’s largest interfaces, where host, environmental factors, antigens and microorganisms interact (**Figure 3 c**). Among the players involved, bile acids, for instance, can instruct enterocytes to produce antimicrobial agents during periods of increased microbial exposure, and so mediate gut eubiosis [95]. Most of these bile acids (~ 95%) will return to the liver through the portal venous system to be recycled and secreted back to the biliary tract, completing the so-called enterohepatic circulation. The portal venous system is established early on, between the 4^{th} and 12^{th} weeks of gestation [96,97], and is responsible for toxin and nutrient drainage from the gastrointestinal tract to the liver. In fact, portal blood flow represents 75% of the total hepatic blood flow, with approximately one liter of blood reaching the liver per minute in healthy individuals [98]. Apart from reabsorbed bile acids, nutrients and minerals, a vastly rich repertoire of microbial metabolites also travels along the portal circulation (**Figure 3 d**). Once they reach the liver, these molecules are sensed by specific hepatocyte receptors and

initiate distinct signal transduction pathways that result in multiple cellular responses (**Figure 3 e, f**). Below, we briefly introduce the microbial communities that inhabit the gut and enumerate compounds they produce that might reach and influence the liver parenchyma.

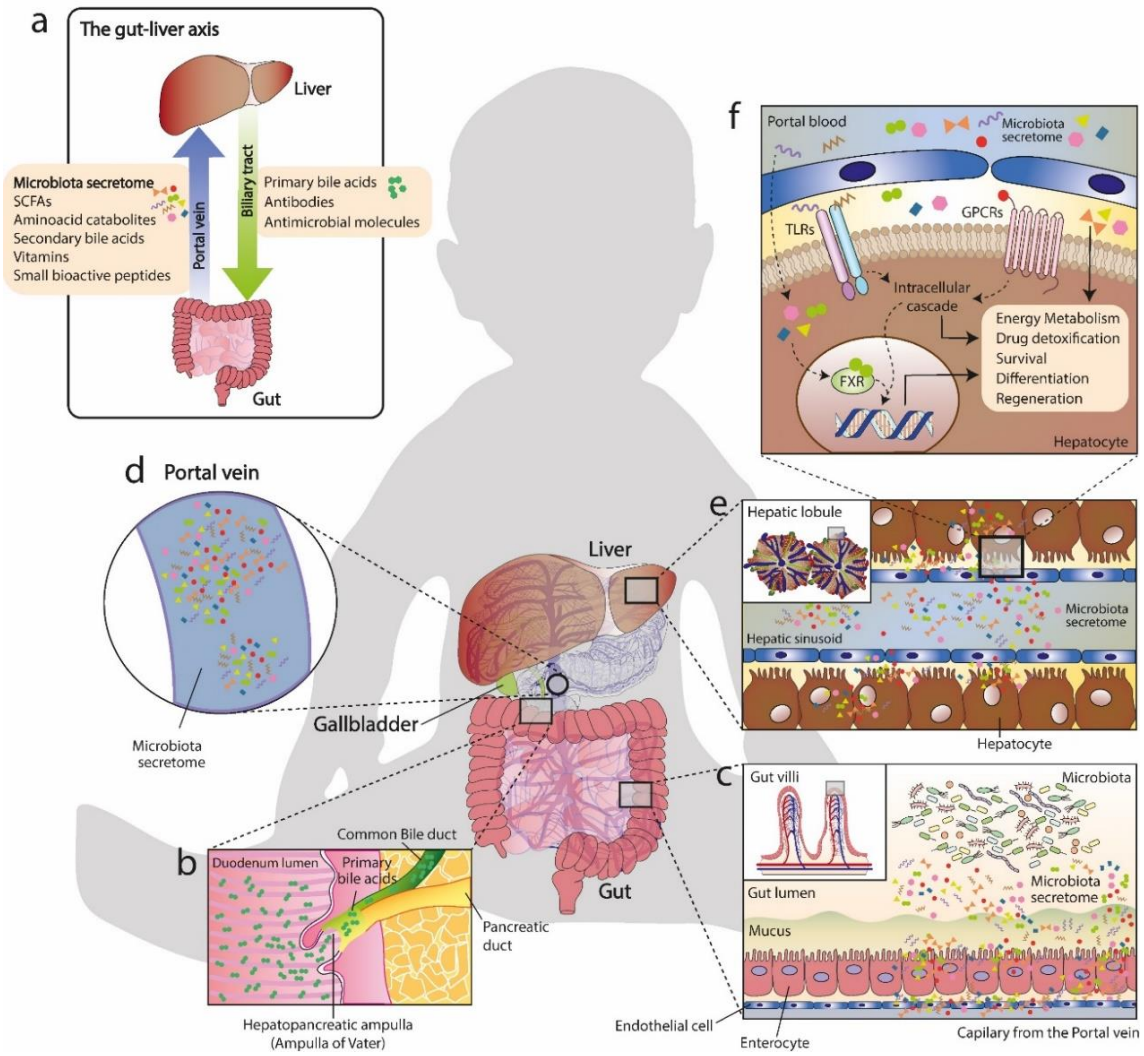

Figure 3. The gut-liver axis. The bidirectional communication between gut and liver (a) is intensified soon after birth and persists throughout life. The liver is anatomically connected with the gut via the hepatopancreatic ampulla (or ampulla of Vater) and provides it with bile acids to ease lipidic nutrient digestion and absorption and antimicrobial molecules to prevent bacterial overgrowth (b). In turn, microbes inhabiting the gut produce a wide variety of compounds (e.g., short-chain fatty acids, aminoacid catabolites, secondary bile acids, vitamins, and small bioactive peptides) that are absorbed across the intestinal lumen (c) and reach hepatic sinusoids in the liver via portal vein circulation (d, e). These microbial-derived metabolites are sensed by receptors localized at the plasma membrane of hepatocytes, influencing the parenchyma in multiple ways (f). Abbreviations: FXR, farnesoid X receptor; GPCRs, G protein-coupled receptors; SCFAs, short-chain fatty acids; TLRs, Toll-like receptor.

2.1. The gut microbiota

It is estimated that, during a lifetime, around 60 tons of food pass across the gut, along with high amounts of environmental toxins and microorganisms. These external inputs take part in the development of gastrointestinal's immunity and establish its unique

microbial community, the gut microbiome, which refers to the collection of bacteria (bacterial microbiome), archaea (archaeal microbiome), fungi (mycobiome), protists (meiofauna) and viruses (virome). The Human Microbiome Project, launched by the NIH in 2007, has been providing a comprehensive identification and characterization of the human microbiome [99]. There are circa 100 trillion of microorganisms inhabiting the human gut, which encompasses more than ~ 10 times the number of human cells in the body [100]. Such an ecosystem is unique simply because it allows cooperative growth and maturation of many species that exist nowhere else together in nature. Some authors even acknowledge the gut microbiome as a ‘forgotten organ’ or ‘hidden organ’ [101], since it collectively encodes 500 times more genes than the human genome [99,102], and can regulate a complex framework of metabolic activities equal to a virtual organ.

Gut microbes have a remarkable organization along the intestine, which is determined by physiological variations along its length such as pH and oxygen gradients, antimicrobial concentration, nutrient competition with the host, and the establishment of an indirect contact with the intestinal epithelium [103]. The later, are sealed tightly together and are protected against microorganisms by a thick layer of mucus, thus avoiding local inflammation and systemic translocation. Nonetheless, this barrier is selectively permeable to a wide variety of microbial metabolic products, so-called postbiotics, that can influence the host in numerous ways not only in the gut but also throughout the body, including the liver.

2.2. Microbial molecules from the gut and their effect on the liver

The current knowledge about the composition and organization of microbial communities inhabiting us vastly surpasses the knowledge about microbial molecules produced by these communities and their importance on human physiology. The gut microbial metabolome is complex as nutrient biotransformation requires community-level interactions in which different microbes and even the host have specific roles within each metabolic pathway.

We currently have only a loose grasp of the full spectrum of the gut microbiome metabolome, even though significant efforts have been made to crack the "black-box".

Biological function mapping of metagenomic sequences, targeted or/and untargeted metabolomics, integrating pathway prediction into the metabolomics workflow and even using systems biology approaches have proven robust tools to identify physiologically relevant classes of microbial metabolites. Readers are referred to the recent article by Donia et al, which reviewed some of the major gut microbiome-derived metabolites identified to date and the methodologies used to identify those molecules [104]. Here, we highlight the key microbial molecules that participate in gut-liver crosstalk and have proven to play a role in hepatic function. Table 1 comprehensively presents these metabolites and their hepatic molecular targets identified.

2.2.1. Short-chain fatty acids

Various soluble dietary fibers and resistant starch that escape digestion can be fermented by gut saccharolytic microbes, which harbor a broader range of carbohydrate-degrading enzymes. Bacterial fermentation of undigestible fibers mainly produces short-chain fatty acids (SCFAs) [105], a subset of fatty acids with 6 or less carbon atoms in their backbone. Around 500-600 mmol of SCFAs are produced in the gut every day [106], depending on dietary fiber consumption, and among these, acetate (C2), propionate (C3) and butyrate (C4) account for >95% of intestinal SCFA content [105].

In the gut, SCFAs maintain intestinal barrier integrity [107], mediate mucus secretion [108] and gut immunity [109]. SCFAs also fuel colonocyte metabolism, especially butyrate, which provides up to 70% of its energy through β-oxidation [110]. In fact, the colonic epithelial layer of germ-free mice is under an energy-deprived state that promotes colonocyte autophagy [111].

Animal studies using ^{13}C radiolabeling have demonstrated absorbed SCFAs can be transported into the portal circulation [112], from where they can reach various organs. In humans, portal blood contains on average 258 μM of acetate, 88 μM of propionate and 29 μM of butyrate, but these concentrations drop in hepatic venous circulation to 115 μM, 21 μM and 12 μM, respectively [105]. Peripheral blood concentration is even lower and so, compared to other tissues, the liver receives the greatest proportion of

microbial SCFAs. Hepatic gene expression can be regulated by SCFAs, as they control various metabolic pathways involved in lipogenesis [112,113], lipolysis or fatty acid oxidation [114–119], gluconeogenesis [120,121] and insulin sensitivity [116–118]. SCFAs might influence hepatic metabolism via interaction with the G-protein coupled receptors GPR43/FFAR2 and GPR41/FFAR3 [122], but also by regulating histone deacetylases [113,116] and hormone levels [117,123]. Fluxomics analysis have also revealed SCFAs can simply serve as intermediate substrates in *de novo* lipid [112,113], cholesterol [124] and glucose [124,125] synthesis in the liver.

Besides this, SCFAs have also been reported to influence stem cell fate. It has been shown the invaginated architecture of the intestinal epithelium, together with a natural limiting gradient imposed by diffusion, allows the majority of butyrate to be absorbed by the surface layer of differentiated colonocytes, thus shielding stem/progenitor cells from this metabolite that would otherwise suppress their proliferative capacity [126]. In turn, acetate is involved in goblet cell differentiation, besides increasing their mucin production and its glycosylation [127]. As the liver is a privileged site enriched in SCFA content, it is tempting to speculate their role in hepatic commitment and specification, similar to what happens in the gut. *In vivo* data is lacking to support such an hypothesis, but *in vitro* butyrate has shown capable of promoting hepatic endoderm specification of human pluripotent stem cells (hPSC) [128,129] and hepatic transdifferentiation of human fibroblasts [130].

2.2.2. Amino acid catabolites

Unlike some carbohydrates, protein fermentation in the gut can be carried out by the host or the microbiome [131], which brings into question the role of the microbiota in protein metabolism and renders distinction of the metabolite source more difficult. Typically, proteins that escape digestion by host proteases can be taken up by colonic bacteria to synthesize microbial proteins or catabolized through different pathways. Bacterial metabolites from protein catabolism positively correlate with longer transit times, and so only after depletion of carbohydrates occurring in the proximal to the distal colon transition causes bacteria to switch from carbohydrate to protein metabolism [132]. Protein fermentation can yield a wider range of metabolites,

including SCFAs, branched-chain fatty acids (BCFAs), ammonia, amines, hydrogen sulfide, phenols and indoles [131].

The most striking way microbial protein metabolism impacts the host is via aromatic amino acid (AAA) catabolism, which by far yields the more diverse set of metabolites, such as indolic and phenolic compounds. The essential amino acid tryptophan is catabolized by commensal bacteria resulting in several molecules, such as tryptamine, indole, indole-3-acetic acid (IAA), indole-3-propionic acid (IPA) and skatole. Microbiota undoubtedly plays a role in systemic tryptophan balance, as corroborated by the fact germ-free mice have increased levels of circulating tryptophan [133]. Indole appears to be the most abundant microbial tryptophan catabolite in the gut averaging 2.59 mM [134], even though other derivates are still present in a µM range [135]. In the gut, tryptophan catabolites induce secretion of glucagon-like peptide 1 by enteroendocrine cells [136], serve as ligands of the aryl hydrocarbon receptor (AhR) to stimulate mucosal defense [137] and decrease intestinal permeability via pregnane X receptor (PXR) activation [138]. Nonetheless, tryptophan-derived compounds have been detected in human serum (indole: 0.72 µM [139]; IAA: 1.30 µM [140]; IPA: 1.01 µM [140]), suggesting a potential systemic effect. Particularly in the liver, these metabolites can act via AhR to reduce inflammation [141,142] by modulating the NF-κB pathway [143,144] and attenuate cytokine-mediated lipogenesis [141,144]. Moreover, indole [145–148], IAA [149] and skatole [145,146,150,151] can interact with various detoxification enzymes. Besides tryptophan, bacteria can also metabolize phenylalanine and tyrosine. The systemic effects of phenylalanine catabolites on host physiology are not yet clear, even though phenylacetic acid was found elevated in non-diabetic obese women with hepatic steatosis [152]. Tyrosine catabolism mainly yields phenolic compounds, in particular *p*-cresol (or 4-methylphenol), a known uremic toxin elevated in chronic kidney disease [153]. *p*-cresol is metabolized in the liver, thereby interacting with various detoxification enzymes and drug transporters [149,154,155], and can be traced in urine averaging a concentration of 10.54 µM [156].

2.2.3. Secondary bile acids

The bile acid fraction that escapes absorption (~5%) enters the large intestine and is metabolized by gut microbes, which transforms primary to secondary bile acids via

reactions including deconjugation, 7α-dehydroxylation, oxidation, epimerization, esterification and desulfation [157]. These transformations ultimately yield over 50 different secondary bile acids [158], which notably increases the chemical diversity of the bile acid pool. As expected, in germ-free mice the bile acid pool is mainly composed of primary bile acids [159]. Among secondary bile acids, deoxycholic acid (DCA), lithocholic acid (LA) and ursodeoxycholic acid (UDCA), as well as its derivates, account for the majority of bile acids present in the cecum, reaching a concentration of up to 1 mM [160]. They are then either absorbed by passive diffusion or excreted in feces.

Over the past decades, not only primary but also secondary bile acids have been recognized as signaling molecules. Bacterially modified bile acids were shown to modulate gene expression as well as alter cell survival and proliferation. Perhaps the most well-known example is bile acid synthesis regulation, which is under negative feedback control through farnesoid X receptor (FXR) activation. Both DCA and LA serve as agonists to the hepatic FXR, resulting in CYP7A1 inhibition, the rate-limiting enzyme in bile acid synthesis, thus repressing overall *de novo* synthesis [161]. Albeit to a lesser extent, DCA has proven capable of also inhibiting other enzymes involved in bile acid synthesis, such as CYP8B1 [162] and CYP27A1 [163],through FXR-independent mechanisms [164]. Interestingly, LA has been reported to function mainly as a FXR antagonist, inhibiting bile salt export pump (BSEP, encoded by *ABCB11*) that consequently represses bile acid transport to bile canaliculi [165]. Unlike its more hydrophobic counterparts, the secondary bile acid UDCA poorly interacts with FXR [166]. However, the hydrophobicity of bile acids can be toxic to hepatocytes, and so their proper clearance (either excretion or reconjugation) is of utmost importance. In particular, LA can activate PXR [167–169] and vitamin D receptor (VDR) [170], which induces expression of genes involved in detoxification of xenobiotics.

Aside from nuclear receptors, bile acids have also been reported to interact with the G-protein receptor TGR5 [171] in peripheral tissues, particularly in brown adipose tissue, where TGR5 activation increases intracellular cAMP levels to promote energy expenditure [172]. Even though TGR5 is solely expressed in hepatic nonparenchymal cells [173], secondary bile acids can serve as ligands in mitogen-activated protein kinase pathways [174,175] and still be able to regulate hepatic energy metabolism.

Dysregulations in gut-liver crosstalk mediated by secondary bile acids may be detrimental to hepatocytes, ultimately compromising cell viability and liver function. DCA elevations induce apoptosis [176–178] and oxidative stress [177,179,180] in hepatocytes, while UDCA is hepatoprotective during liver injury by promoting cell survival [181–184] and acting as an antioxidant agent [179,185,186]. Nonetheless, the coordinated action of bile acids is critical during tissue- and even organ-level response to hepatic injuries, as shown by a reduced liver regrowth following partial hepatectomy in $FXR^{-/-}$ mice [187]. This effect is particularly evident for secondary bile acids [188,189].

2.2.4. Vitamins

Vitamins participate in vital biochemical reactions in almost every cell of the human body. Human cells are unable to synthesize them in sufficient quantities to meet their needs, so vitamin acquisition is heavily reliant upon diet. Surprisingly, gut bacteria regulate both biosynthesis and metabolism of several essential vitamins. As of the establishment of the first germ-free animals, the role of gut microbes as a source of vitamins has become evident, since these animals require dietary vitamin supplementation [190], especially B and K vitamins, which is not needed by their eubiotic conventional counterparts.

Despite B vitamins being mainly absorbed across the small intestine, there is an additional source of B vitamins absorbed along the colon, and these are mainly from bacterial origin. A comprehensive study analyzed genome annotations of 256 common gut bacteria and revealed an intricate cooperation between bacteria across distinct B vitamin biosynthetic pathways [191]. It also became clear that gut-resident bacteria cannot provide the host with the daily recommended intake of B vitamins, and even those that are produced in higher amounts (e.g., pyridoxine, folate and niacin) are possibly taken up by host-competing microbes in order to ensure cooperative ecosystem survival. Nonetheless, microbial B vitamins likely impact host health, as illustrated by the fact infantile malnutrition has been associated with a gut microbiome underrepresented of bacteria involved in niacin/NADP biosynthesis [192]. In fact, B vitamins shape the gut environment in numerous ways. For instance, thiamine is needed for B cell immunometabolism [193], pyridoxine/folate participate in host-

microbiome drug co-metabolism [194] and cobalamin influences microbe fitness [195]. Notwithstanding, microbial B vitamins can enter systemic circulation and reach peripheral tissues. At a cellular level, B vitamins can function as coenzymes in a myriad of biological processes, namely those related with carbohydrate [196,197], fatty acid [197–199], glucose [198], amino acid [197,200,201] and nucleic acid metabolism [201]. When taken up by liver parenchymal cells they can even have additional roles, such as to prevent inflammation and oxidative stress [202–207], promote cell survival [208–210], reduce lipid accumulation [211–214], control glucose levels [214,215], or simply stored [216]. It remains to be elucidated, however, if B vitamins from microbial origin have different roles from those of dietary origin in the liver.

Similar to B vitamins, K vitamins are essential nutrients for host health. The various forms of vitamin K are related with the length and degree of saturation of their quione ring side-chain. While vitamin K_1 (or phylloquione) is obtained exclusively through diet, vitamin K_2 (or menaquione) can be obtained either from selected foods or from gut bacteria. Nonetheless, the proportion of microbial vitamin K_2 that enters portal circulation is likely low [217], as the majority of vitamin-K_2 producing bacteria reside in the colon and, due to the fat-soluble nature of K vitamins, their absorption requires bile acids that are mainly localized in the small intestine. All forms of vitamin K serve as cofactors for enzymes involved in the biosynthesis of anti-coagulant factors, a process that primarily takes place in the liver [218,219]. Interestingly, vitamin K_2 has shown to have a positive impact in *in vitro* differentiation [220] and maturation [167,220] of hPSC-derived hepatocytes, which is associated with PXR activation and increased gap junction intracellular communication. This could allude to a potential role of vitamin K_2 during prenatal and postnatal liver development, with a partial contribution coming from the gut microbiome.

2.2.5. Microbial-derived peptides

Host-microbiome mutualism does not exclusively involve metabolic and nutritional aspects, but also includes the interaction between the microbiota and immunity. In recent years, numerous studies have revealed the molecular mechanisms orchestrating this crosstalk with the immune system and redefined how the microbiome can promote health and mediate critical illness [221,222]. In particular,

studies on germ-free animals have proved that the gut microbiota is required to maintain intestinal crypt integrity and the architecture of intestinal-associated lymphoid tissues [223], in order to prevent the surface adhesion of pathogens as well as promote the development and maturation of mucosal immunity.

While most attention has focused on the innate recognition of immune-stimulatory bacterial molecules, such as cell wall components, nucleic acids and diet-dependent microbial metabolites, the creation of “Mechanism of Action of the Human Microbiome” (MAHMI) database changed this paradigm and turned the attention to microbial extracellular surface-associated proteins and other small peptides [224]. The MAHMI database (http://www.mahmi.org) [225] is an online bioinformatic platform fueled by the public Metahit project metagenomes, a vast compilation of the amino acid sequence and the predicted bioactivity of peptides encrypted in the human gut metaproteome. The immunomodulatory activity of some of these peptides has been assessed using the MAHMI pipeline. More specially, 15 out of the 300 million peptides contained in this database were synthesized and screened *in silico* for the ability to activate human peripheral blood mononuclear cells (PBMCs). Results showed that the bacterial peptides FR-16 and LR-17 had the highest immunomodulation capability over PBMCs, increasing Th17 and decreasing Th1 cell responses, together with an induction of IL-22 production [226]. Another study identified the bacterial peptides B7 and B12 as capable of controlling the intestinal cytokine milieu by modulating circulating antigen presenting cells, and this immunomodulation was disrupted in intestinal bowel disease (IBD) [227]. Several other peptides elicit an immune response by the host, namely serine-threonine peptide, serpin (AAN23973) and CHWPR peptide, which is comprehensively reviewed elsewhere [228].
Gut bacteria can also secrete other peptides like ribosomally synthesized and post-translationally modified peptides (RiPPs) (i.e. lantibiotics, bacteriocins, microcins and TOMMs), however these are essentially associated with competitive and social prokaryotic interactions in the gut [104]. Intriguingly, the microbial effects on the immune system are not confined to local responses, but are rather associated with extra-intestinal organs and integrated with systemic immunity [229]. Studies on germ-free animals showed a significant reduction in IgA-secreting plasma cells [230] and fewer regulatory T cells [231]. Additionally, microbiome composition has been shown to be predicative of cancer immunotherapy efficacy in humans, both locally in the gut

[232], or systemically [233]. The effect of bacterial derived peptides has been increasingly recognized under different healthy and inflammatory scenarios. Although their physiological role in other organs remains unveiled. Their absorption and transport to the liver through portal blood, and ultimately, their effect in the liver and other organs, represent a “black-box” with high discovery potential but still with too many unknowns.

Table 1. Microbial molecules from the gut and their known/predicted effects on the liver**.**

Class	Compound	Known/predicted function in liver/hepatocytes	Molecular targets
Short Chain Fatty Acids	**Acetate**	**Lipogenesis**	• Serves as an intermediate metabolic precursor and is converted into acetyl-CoA for *de novo* lipid synthesis in an ACSS1/2-dependet manner. [112,113] • Up-regulates *FASN* and *ACACA* in HepG2 hepatocytes [113] and fructose-fed mice. [112]
		Anti-lipogenic **Fatty acid oxidation**	• Reduces triglyceride accumulation in bovine hepatocytes. • Increases AMPK phosphorylation, and downstream increases the transcriptional activity of PPARα (up-regulates *ACO, CPT1, CPT2, L-FABP*) and decreases the transcriptional activity of SREPB-1c and ChREBP (down-regulates *ACCA, FASN, SCD1*) in bovine hepatocytes. [114]
		Cholesterol synthesis	• Serves as an intermediate metabolic precursor and is converted into acetyl-CoA for *de novo* cholesterol synthesis in mice. [124]
		Epigenetic regulator	• Induces histone 3 acetylations (H3K9, H3K27, H3K56) at *FASN* and *ACACA* promotor regions in an ACSS1/2-dependent manner in HepG2 hepatocytes. [113]
	Propionate	**Gluconeogenesis**	• Serves as an intermediate metabolic precursor and is converted in succinate for *de novo* glucose synthesis in mice. [124] • Increases hepatic pyruvate cycling and pyruvate carboxylase activity in mice. [125] • Induces hepatic hyperglycemia via increased secretion of glucagon and FABP4 in mice and humans. [123]
		Anti-gluconeogenesis	• Binds to hepatic GPR43 and mediates AMPK phosphorylation via Ca^{2+}/CaMKKβ. Down-regulates G6Pase and PEPCK in HepG2 hepatocytes. [120]
		Anti-lipogenic	• Reduces triglyceride accumulation and ω6:ω3 ratio in HFD mice and HepG2 hepatocytes. [115] • Down-regulates ACLY, ACAC and SCD1 in HFD mice. [115]
	Butyrate	**Anti-lipogenic** **Fatty acid oxidation**	• Induces GLP-1R expression in HepG2 hepatocytes and prevented its downregulation in NAFLD mice, consequently increasing GLP-1 sensitivity. [116] • Decreases leptin and adiponectin serum levels in HFD mice. [117] • Prevents triglyceride accumulation by activating the hepatic AMPK/ACC pathway in HepG2 hepatocytes and NAFLD/HFD mice (reduces steatosis). [116–118] • Up-regulates PPAR-ɣ, FGF21, PGC1-α and FFAR2 and down-regulates endotoxin-associated TLR4, CD14, TLR2 and TLR9 in MCD/NAFLD mice. [118,119]
		Gluconeogenesis	• Up-regulates PEPCK, G6Pase, FOXO1, PGC-1α and HNF4α in primary mouse hepatocytes via cAMP/CREB pathway activation. [121]
		Cholesterol synthesis	• Serves as an intermediate metabolic precursor and is converted into acetyl-CoA for *de novo* cholesterol synthesis. [124]
		Insulin sensitivity	• Up-regulates insulin receptor/IRS-1 pathway in HepG2 hepatocytes and NAFLD/HFD mice. [116,117] • Increases Akt phosphorylation and *GLUT2* up-regulation in HepG2 hepatocytes and HFD/NAFLD mice. [117,118]
		Anti-inflammatory	• Decreases pro-inflammatory cytokine (TNF-α, IL-1β and MCP-1) levels in HFD/NAFLD/MCD [117–119] mice via NF-κB pathway modulation [118]. • Down-regulates F4/80 expression in NAFLD/MCD mice. [118,119]
		Mitochondrial function **Antioxidant**	• Promotes mitochondrion fusion and an increase in volume density in HFD mice. [117] • Increases proton leak in HFD mice. [117] • Increases antioxidant enzyme activity (NQO1, GST and higher GSH:GSSG ratio) in HFD mice. [117]
		Epigenetic regulator	• Inhibits HDAC2 in HepG2 hepatocytes and in NAFLD mice. [116]
		Hepatic Differentiation	• Promotes hepatic specification (but not by-itself) of definitive endoderm cells derived from hESC [128,129], hiPSC [129] and human fibroblasts [130].
	Tryptophan **tryptamine**	**Anti-inflammatory**	• Decreases pro-inflammatory cytokine secretion (TNF-α and IL-1β) by RAW 264.7 murine macrophages. Reduces RAW 264.7 murine macrophage migration towards MCP-1. [141]

Aminoacid catabolites		**indole**	**Anti-inflammatory**		• Modulates the NF-κB pathway and downstream down-regulates murine pro-inflammatory genes (*Nlrp3*, *Il-1β* and *Il-18*) in *ex vivo* liver slices. [143]
			Cholesterol metabolism regulation		• Increases 4β-hydroxycholesterol hepatic levels in HFD mice. [143]
			Xenobiotic metabolism		• Induces CYP2A6 protein expression in pig hepatocytes. [145,146] • Metabolized and converted to indoxyl by CYP2E1 [147] and then to indoxyl sulfate by SULT1A1 [148] for renal clearance.
		indole-3-acetate indole-3-acetic acid	**Anti-inflammatory**		• Decreases TNF-α secretion by RAW 264.7 murine macrophages and its recruitment mediated by MCP-1. [141]
			Antioxidant		• Decreases ROS production and increases superoxide dismutase activity in HFD mice. [142]
			Anti-lipogenic		• Attenuates cytokine-mediated lipogenesis in AML12 murine hepatocytes in an AhR-dependent manner (down-regulates *Fasn* and SREBP-1c). [141]
			Xenobiotic metabolism		• Interacts and inhibits in a dose-dependent manner drug transporters (OATP1B1 and OATP1B3). [149]
		indole-3-propionic acid	**Anti-inflammatory**		• Modulates the NF-κB pathway and downstream down-regulates pro-inflammatory cytokine levels (TNF-α, IL-1β and IL-16) in NAFLD mice. [144]
			Anti-lipogenic Anticholesterolemic		• Decreases triglyceride and cholesterol accumulation and partially reverses steatosis in NAFLD mice. [144]
		skatole (indole-3-methyl)	**Xenobiotic metabolism**		• Induces CYP2A6 [145,146] and CYP2E1 [150] protein expression in pig hepatocytes. • Induces up-regulation of *CYP1A1*, *CYP1A2* and *CYP1B1* via AhR activation in HepG2 and primary human hepatocytes. [151]
	Phenylalanine	**phenylacetic acid**	**Lipogenesis**		• Promotes triglyceride accumulation in primary human hepatocytes (up-regulation of lipid metabolism genes *LPL* and *FASN*) and in mice (steatosis). [152]
			Insulin resistance		• Reduces insulin uptake in primary human hepatocytes (down-regulation of *INSR* and *GLUT2*) by inhibiting Akt phosphorylation. [152]
	Tyrosine	***p*-cresol** (4-methylphenol)	**Xenobiotic metabolism**		• Metabolized and converted to *p*-cresol sulphate for renal clearance. • Interacts and inhibits in a dose-dependent manner hepatic phase I/II metabolic enzymes (CYP2E1, CYP3A4, UGT1A1, UGT1A9, UGT2B7 [154] and SULT1A1 [155]) and drug transporters (OATP1B1 and OATP1B3) [149].
Secondary Bile Acids	**Deoxycholic Acid** (DCA) **Lithocholic Acid** (LA) **Ursodeoxycholic Acid** (UDCA)		**Bile acid synthesis repression**	**DCA LA**	• Bind to FXR, down-regulate CYP7A1 and reduce LXRα transactivation activity in HepG2 hepatocytes. [161]
				DCA	• Binds to FXR, reduces HNF4α transactivation activity and downstream down-regulates *CYP8B1* in HepG2 hepatocytes. [162] • Binds to FXR and down-regulates *CYP27A1* in HepG2 hepatocytes. HNF4α may also be a target for bile acid mediated *CYP27A1* repression. [163] • Activates JNK and down-regulates *Cyp7a1* via an ASM/FAS-dependent mechanism in primary mouse hepatocytes. [164]
				LA	• Binds to PXR and down-regulates *Cyp7a1* in mice. [168]
			Bile acid transport Repression	**LA**	• Down-regulates BSEP by inactivating FXR in HepG2 hepatocytes. [165]
			Xenobiotic metabolism	**LA**	• Binds to PXR and induces CYP3A4 expression in mice. LA serves as a substrate for CYP3A4 hydroxylation. [169] • Binds to PXR and up-regulates *Cyp3a11* and *Oatp2* expression in mice. [168] • Induces PXR activation and up-regulation in hESC-derived and isolated fetal hepatocytes. Up-regulates *CYP3A4* and *CYP2C9.* [167] • Binds to VDR and induces Cyp3a11 expression in mice (independent of PXR activation). [170]
			Energy metabolism	**DCA**	• Activates the ERK1/2 and Akt pathways via a ROS-dependent manner in primary mouse hepatocytes; consequently, this inactivates phosphotyrosine phosphatases resulting in EGFR activation. [174]

				DCA **UDCA**	• Taurine-conjugated DCA, glycine-conjugated DCA and taurine-conjugated UDCA activate the ERK1/2 and Akt pathways through $S1P_2$ in primary mouse hepatocytes. [175]
			Apoptosis	**DCA**	• Activates in a dose-dependent manner the p53/miR-34a/SIRT1 proapoptotic pathway through downstream JNK1 phosphorylation in mice. [176] • Activated in a dose-depended manner the miR-21/PDC4 proapoptotic pathway by downstream inhibiting NF-κB transcriptional activity in mice. [177] • Inhibits in a dose-dependent manner the EGFR/Ras/MAPK pathway and potentiates FAS-mediated apoptosis in primary mouse and human hepatocytes. [178]
			Oxidative stress **Lipid Peroxidation**	**DCA**	• Induces oxidative stress and caspase-2 activation in a PIDD-dependent manner by inhibiting NF-κB transcriptional activity in mice. [177] • Disrupts mitochondrial transmembrane potential through increased ROS production, leading to translocation of the apoptosis regulator BAX and release of cytochrome c in primary mouse hepatocytes. [179] • Inhibits mitochondrial NADH dehydrogenase and NADH:ferricytochrome c oxiredutase activities, increasing ROS production in primary mouse hepatocytes. [180] • Taurine-conjugated DCA increases TBARS production in primary mouse hepatocytes. [180]
			Cell Survival	**UDCA**	• Suppresses in a dose-dependent manner the p53/miR-34a/SIRT1 proapoptotic pathway in mice. [181] • Protects FAS-ligand-induced apoptosis, without reducing FAS trimerization, in mice. [182] • Taurine-conjugated UDCA activated the p38/ERK/MAPK and PI3K pathways, delaying apoptosis in primary mouse and HepG2 hepatocytes. [183] • Prevents CYP2B1, CYP2E1, CYP3A2, CYP2C6, CYP2C11 and CYP4A1 down-regulation in mice with DCA-induced injury. [184]
			Antioxidant	**UDCA**	• Reduced the mitochondrial membrane permeability transition in mice with DCA-induced injury. [185] • Prevented mitochondrial release of cytochrome c and BAX accumulation in mitochondria of primary mouse hepatocytes with DCA-induced injury. [179] • Increases GSH and metallothionein levels in primary mouse hepatocytes. [186]
			Liver Regeneration	**DCA**	• Delays early regeneration in mice after two-thirds PH, due to altered expression of cell-cyle markers cyclins A, B, D1 and D3. By day 8 regeneration is much accelerated, as shown by a 20% increase in hepatic mass relative to controls. [188] • Promotes cholestatic hepatitis and a damage-induced hepatocyte proliferation in mice after 40% PH (SGPT and bilirubin elevations). [189]
				UDCA	• Promotes hepatocellular proliferation without hepatotoxic effects in mice after 40% PH. [189]
Vitamins	**B vitamins**	**Thiamine** (B_1)	**Coenzyme**	• Increases (by itself or when transformed into thiamine phosphate) the specific activity of branched chain α-ketoacid dehydrogenase in the human liver [196], which is necessary for carbohydrate metabolism.	
		Riboflavin (B_2)	**Coenzyme**	• Serves as a substrate for the biosynthesize of FAD in rat liver mitochondria [198], which is necessary for acetyl-CoA dehydrogenation in β-oxidation.	
			Antioxidant **Anti-inflammatory**	• Protects hepatocytes against ischaemia/reperfusion injury in mice. [202] • Protects against oxidative-mediated hepatotoxicity induced by thioacetamide in rats (in combination with nicotinamide and vitamin C). [203] • Provides protective effects against the risk of cirrhosis in human subjects (in combination with vitamin B_{12}). [204]	
		Niacin (B_3)	**Antioxidant** **Anti-inflammatory**	• Inhibits lipid accumulation and oxidative stress (through DGAT2 and NADPH respectively), and reduces the production of IL-8 in HepG2 and human primary hepatocytes. [205]	
			Anti-lipogenic	• Decreases hepatic triglyceride synthesis and subsequent VLDL/LDL secretion by directly and noncompetitively inhibiting DGAT2 in HepG2 cells. [211] • Inhibits *de novo* lipogenesis via a GPR109A-mediated PKC–ERK1/2–AMPK signalling pathway in HFD mice. [212]	
		Pantothenic acid (B_5)	**Coenzyme**	• Serves as a substrate for the biosynthesis of coenzyme A and acyl carrier protein [199], which are necessary for fatty acid catabolism and sterol metabolism.	
			Antioxidant **Anti-inflammatory**	• Shows hepatoprotective and anti-oxidant effects in experimental models of CCl4-induced toxicity. [206]	
			Anti-lipogenic	• Decreases hepatic, perinephric, and plasma lipid accumulation in rats fed with pantothenic acid free diet and/or under ethanol regimen. [213]	

		Pyridoxine (B_6)	**Coenzyme**	• Serves as a substrate for the biosynthesis of pyridoxal 5'-phosphate in the liver [200], which can be transported to other tissues/organs and participate in amino acid metabolism.
			Antioxidant	• Pyridoxine deficiency increases TBARS production, glutathione peroxidase activity and glutathione reductase activity in the rat liver. [207]
		Biotin (B_7)	**Coenzyme**	• Serves as a covalently bound coenzyme for various carboxylases (acetyl-CoA 1 and 2, pyruvate carboxylase, propionyl-CoA carboxylase, 3-methylcrotonyl-CoA carboxylase) [197], which are necessary for fatty acid, carbohydrate and amino acid metabolism.
			Glucose metabolism	• Improves glucose metabolism and protein expression levels of IRS-1, PPAR-γ, and NF-κB in rats (in combination with chromium histidinate). [215]
		Folate (B_9)	**Coenzyme**	• Serves as a coenzyme and either accepts or donates one-carbon moieties in reactions involving amino acid metabolism and purine and pyrimidine biosynthesis. [201]
			Anti-glycemic	• Chronic folate deficiency reduced the *p-Akt/Akt* ratio in response to insulin in mice. [214]
			Anti-lipogenic	• Chronic folate deficiency increases serum triglyceride levels, upregulates *Acc1* and *Fasn*, and downregulates Cd36 and ApoB mRNA levels in mice. [214]
			Anti-apoptotic	• Protects hyperhomocysteinemia mice from apoptosis via CFTR-activated endoplasmic reticulum stress. [208] • Attenuates apoptosis caused by arsenic-induced toxicity in Chang human hepatocytes [209]. • Folate deficiency enhances perturbations in hepatic methionine metabolism and DNA damage, besides promoting alcoholic liver injury. [210]
		Cobalamin (B_{12})	**Storage**	• Stored in liver parenchymal cells, and from there can be transported to the bone marrow and other sites where it is involved in nuclear maturation processes [216] (serves as a co-factor for methionine synthase in the biosynthesis of purines and pyrimidines).
	Vitamin K_2 (menaquinone)		**Anticoagulant factor synthesis**	• Serves as an intermediate precursor for the synthesis of the anticoagulant factors II, VII, IX and X by parenchymal cells in the human liver. [218,219]
			Hepatic Differentiation	• Increases the expression of plasma proteins (*ALB* and *AAT*), genes associated with cell-cell communication (*Cnx32* and *CLDN1*), urea cycle (*CPS1* and *OTC1*), hepatic phase I (*CYP3A4*), II (*UGT1A1, UGT1AB, UGT1A4* and *UGT2B7*) and III (*OATP1B1* and *MDR1*) metabolic enzymes, and hepatic nuclear receptors (*SHIP, FXR, LXRA* and *PPARα*) in hESC-derived hepatocytes. [220]
			Hepatic Maturation	• Increases albumin secretion, urea production, LDL uptake, triglyceride accumulation and glycogen storage in hESC-derived hepatocytes. [167,220] • Promotes higher expression of genes involved in PPAR signaling, xenobiotic metabolism by CYP450, pentose and glucuronate interconversions, glycine, serine and threonine metabolism, and complement and coagulating cascades in hESC-derived hepatocytes. [220] • Induces PXR activation and up-regulation in hESC-derived and isolated fetal hepatocytes. Together with LCA, promotes inducible CYP450 activity. [167] • Promotes formation and assembly of gap junctions enriched in Cnx32 by inhibiting the MAPK/p38 pathway in hESC-derived hepatocytes, thereby increasing gap junction intracellular communication. [220]
Probiotic extracellular proteins and bioactive peptides	**FR-16 LR-17; Peptide B7; Peptide B12 SerineThreonine peptide (STp)**		**Unknown**	Unknown

Abbreviations: ACAC, acetyl-CoA carboxylase; ACACA/Acc1, acetyl-CoA carboxylase 1; ACCA, acetyl-coenzyme A carboxylase carboxyl transferase subunit α; ACLY, ATP citrate lyase; ACO, 1-aminocyclopropane-1-carboxylate oxidase; ACSS1/2, acyl-CoA synthetase short chain family member 1/2; AhR, aryl Hydrocarbon Receptor; Akt (or PKB), protein kinase B; AMPK/ACC, AMP-activated protein kinase/acetyl-CoA carboxylase (pathway); APOB, apolipoprotein B; ASM, acid sphingomyelinase; BAX, Bcl-2-associated X protein; BSEP, bile salt export pump; Ca2+/CaMKKβ; calcium/calmodulin-dependent protein kinase kinase β; cAMP/CREB, cAMP- response element binding protein (pathway); CCl4, carbon tetrachloride; CD14/36, cluster of differentiation 14/36; CFTR, cystic fibrosis transmembrane conductance regulator; ChREBP, carbohydrate-responsive element-binding protein; Cnx32/43, connexin-32/43; CPT1/2, carnitine palmitoyltransferase I/II; CYP, cytochromes P450; DGAT2, diacylglycerol acyltransferase 2; EGFR, epidermal growth factor receptor; ERK(1/2), extracellular signal-regulated protein kinase (1/2); FABP4, fatty acid-binding protein 4; FAD, flavin adenine dinucleotide; FASN, fatty acid synthase; FFAR2, free fatty acid receptor 2; FGF21, fibroblast growth factor 21; FOXO1, forkhead box protein O1; FXR, farnesoid X receptor; G6Pase, glucose 6-phosphatase; GLP-1, glucagon-like peptide-1; GLP-1R, glucagon-like peptide-1 receptor; GLUT2, glucose transporter; GPR43, G-protein-coupled receptor 43; GPR109A, hydroxycarboxylic acid receptor 2 (HCA2); GSH, reduced glutathione; GSSG, oxidized

glutathione; GST, Glutathione S-transferase; HDAC2, histone deacetylase 2; HNF4α, hepatocyte nuclear factor 4α; hESC, human embryonic stem cells; HFD, high fat diet; hiPSC, human induced pluripotent stem cells; IL-1β/8/16/18, interleukin-1β/8/16/18; INSR, insulin receptor; IRS-1, insulin receptor substrate-1; JNK(1), c-Jun N-terminal kinase (1); LDL, low density lipoprotein; L-FABP, liver-type fatty acid binding protein; LPL, lipoprotein lipase; LPS, lipopolysaccharide; LXRα, liver X receptor α; MAPK, mitogen-activated protein kinase; MCD, methionine-choline deficient (diet); MCP-1, monocyte chemoattractant protein-1; miR, micro RNA; MRP, multidrug resistance-associated protein; NADH, nicotinamide adenine dinucleotide (NAD) + hydrogen (H); NADPH, nicotinamide adenine dinucleotide phosphate; NAFLD, non-alcoholic fatty liver disease; NF-κB, nuclear factor kappa light chain enhancer of activated B cells (pathway); Nlrp3, NOD-, LRR- and pyrin domain-containing protein 3; NQO1, NAD(P)H dehydrogenase [quinone] 1; NTCP, Na+-taurocholate cotransporting polypeptide; OATP, organo anion transporter; p-Akt, phospho-protein kinase B; PDC4, programmed cell death 4; PEPCK, phosphoenolpyruvate carboxykinase; PGC1-α, peroxisome proliferator-activated receptor gamma coactivator 1-alpha; PH, partial hepatectomy; PI3K, phosphatidyl ionositol 3-kinase; PIDD, p53-induced protein with a death domain; PKC, protein kinase C; PPARα/ɣ, peroxisome proliferator-activated receptor α/ɣ; PXR, pregnane X receptor; ROS, reactive oxygen species; $S1P_2$, sphingosine-1-phosphate receptor 2; SCD1, stearoyl-CoA desaturase-1; SGPT, serum glutamic pyruvic transaminase; SIRT1, sirtuin 1; SREPB-1c, sterol regulatory element-binding protein-1c; SULT, sulfotransferase; TBARS, thiobarbituric acid reactive substances; TNF-α, tumor necrosis factor α; TLR2/4/9, toll-like receptor-2/4/9; UGT, UDP-glucuronosyltransferase; VDR, vitamin D receptor; VLDL, very low density lipoprotein.

3. The evolving microbiome: cues for liver maturation, function and homeostasis

As mentioned earlier, the gut microbiome could be easily compared to a virtual organ, containing millions of genes that participate in a myriad of biological processes that ultimately expand the host's metabolic capacity and provides it with a vast catalogue of important metabolites. Efforts in characterizing the structure and function of the human microbiome have made clear that the presence/absence of microorganisms are indispensable, as its absence, has detrimental implications in development and health. Sommer et. al previously reviewed the role of the microbiome in health, acknowledging its critical role not only for immune system development but also during the morphogenesis and postnatal maturation of the gut [234]. In fact, germ-free animals have reduced intestinal surface area, reduced regeneration, decreased intestinal peristaltic activity, prolonged gastrointestinal transit time, altered intestinal barrier integrity with reduced epithelial permeability, among other abnormalities [234]. As the liver receives a considerable amount of macro and micronutrients absorbed across the intestines, including those produced by microbes, it can be expected that the gut microbiome similarly impacts the liver throughout life. In this section, we describe how the gut microbiome evolves throughout the various stages of life (**Figure 4**), highlighting compelling research that identify it as a key player in liver maturation, function and homeostasis.

3.1. Prenatal period

For nearly a century, it has been thought that placenta acts as a barrier able to prevent fetal contamination by maternal toxins and microbes, thus preserving fetal sterility and ensuring proper development. Bacterial colonization of the womb was most commonly described in the context of clinical infection of the fetal membranes and amniotic fluid, preterm birth and/or maternal conditions such as obesity, gestational diabetes mellitus (GDM) and preeclampsia. The detection of bacteria and microbial DNA/RNA/and other derived products in healthy placental tissue, umbilical cord, and amniotic fluid [235,236] challenged the long-held belief of a sterile environment nurturing the developing fetus.

An elegant study from Aagaard et al., in which 320 healthy placentas were analyzed, revealed a unique microbiome mainly composed of non-pathogenic commensal bacteria from the *Firmicutes*, *Tenericutes*, *Proteobacteria*, *Bacteroidetes*, and *Fusobacteria* phyla [87]. At the species level, *Lactobacillus* spp., *Propionibacterium* spp. and members of *Enterobacteriaceae* family appear to dominate placental microbial communities [235]. While some studies claim that the placental microbiome may originate from vertical ascension from the vagina, digestive or urinary tracts, Aagaard et al. reported more similarities with the oral microbiome [87], possibly acquired by hematogenous route. Besides placental tissue, bacteria were also found in the amniotic fluid, even without amniotic sac ruptures, and the work from Jiménez et al. revealed the presence of commensal bacteria (e.g., *Enterococcus*, *Streptococcus*, *Staphylococcus*, and *Propionibacterium*) in the umbilical cord blood of healthy full-term neonates [88]. Nevertheless, in a recent well-designed controlled study, de Goffau et al. analyzed placental samples collected from 537 women and confirmed that the placenta does not contain a reservoir of microbes [89]. Positive signals of detected microorganisms were either related to acquisition of bacteria during labor and delivery, or due to contaminations of laboratory reagents and equipment with bacterial DNA. Only *Streptococcus agalactiae* was identified in 5% of placental tissue, a maternal pathogenic microbe that can undergo intrauterine transmission and is associated with neonatal sepsis.

Even though de Goffau and colleagues presented compelling evidence to dispute the existence of a placenta microbiome, it also becomes clear that the womb may not be entirely microbe-free during pregnancy, opening several questions whether it would be possible for bacteria to bypass the extraembryonic fetal tissues' barriers and onset gut colonization *in utero*. Studies on neonatal meconium (the first stool after birth) showed levels of bacterial DNA and its derived molecules like acetate and propionate, further supporting a possible *in utero* route of colonization. At the phylum level, meconium was dominated by *Proteobacteria* and *Firmicutes*. *Acinetobacter* - known to be protective against the development of hypersensitivity reactions (allergies) - was the most abundant genus, followed by *Pelomonas*. Interestingly, Ardissone et al. reported that more than 50% of bacteria present in meconium also colonized amniotic fluid, possibly in part as a consequence of amniotic fluid swallowing during the last trimester of pregnancy [237].

Despite uncertainties surrounding transfer of microbes from mother to the evolving fetus *in utero*, normal fetal development occurs in symbiosis with the maternal microbiome, which could still be an indirect influence on fetal well-being. But what is the impact or the role of these maternal microbial communities in the evolving fetus?

Due to technical and ethical issues, most of existing research is focused on longitudinal studies rather than using invasive prenatal diagnostic tools (e.g., cordocentesis, amniocentesis, chorionic villus sampling and fetoscopy). This suggests that alterations in microbiota composition predisposes to placental pathologies, adverse pregnancy outcomes and development of several diseases later in life and adulthood, even though the underlying mechanisms are elusive.

Of note, maternal nutrition has revealed an impact on offspring microbiome composition. Ma et al. showed in a primate model that a gestational high fat diet (HFD) altered offspring gut microbiome with significant depletion of *Proteobacteria* and selectively favored microbes involved in amino acid, carbohydrate and lipid metabolism [238]. Perinatal nutrition is believed to act via epigenetic modifications that may persist after birth however its effect on developing organs, such as the liver, is still not fully understood. Mice offspring of HFD dams have shown differences in methylation or acetylation near promotor regions of key hepatic genes associated with metabolism [239], cell cycle [240] and circadian rhythm [241]. These alterations may predispose the neonate to develop hepatic steatosis [242], and Wankhade et al. observed worse fatty liver phenotype and bile acid metabolism dysregulation in male offspring of HFD mice [243]. Maternal obesity and gestational weight gain are also relevant factors of dysbiosis in pregnant women, promoting higher abundances of *Bacteroides* and *Staphylococcusin* spp. [244]. More recently, Soderborg et al. used stool microbes from 2-week old human neonates born from obese mothers to colonize the gut of germ-free mice, and detected altered bile acid metabolism, increased hepatic peri-portal inflammation and impaired macrophage function, all in agreement with features of advanced pediatric NAFLD [245]. Additionally, other factors including gestational age, GDM status, vaginal infection, periodontitis, pre-/probiotic supplementation and antibiotic exposure can also have adverse effects on maternal microbial composition [246,247], thus affecting fetal health.

Much less is known regarding the physiological role of prenatal microbiome in fetal development. Prenatal microbial gut colonization is believed to play a role in immune [248,249] and metabolic [238] programming, and potentially, future well-being. However, there are still a lot of open questions: What are the mechanisms underlying this? Could the fetal gut microbiome modulate organ growth and maturation? Does it persist after birth and shape the early neonatal development? In a landmark study, Kimura et al. demonstrated in mice that colonic SCFAs reached the embryo via maternal liver and bloodstream, and were sufficient to activate the G-protein coupled receptors GPR41 and GPR43, thereby promoting sympathetic neuronal, enteroendocrine and pancreatic β cell differentiation [250]. Maternal SCFAs, especially propionate, shaped the development of energy metabolism, as evidenced by the fact offspring of germ-free mothers were more predisposed to metabolic syndrome. Even if maternal microbiota is unable to onset fetal gut colonization, with the work of Kimura et al. it becomes clear its intermediates are instrumental for proper development, rendering metabolomics a powerful tool to correlate microbiota and prenatal organ development. Nonetheless, if there are microbial metabolites that encourage hepatic differentiation and maturation *in utero*, that remains to be discovered.

3.2. Postnatal period

The first 1000 days encompassing the period from conception to about 3 years of age, represent a critical window of growth and development in the neonate. Although bacterial colonization has been proposed to begin *in utero*, it is widely accepted that, only during extrauterine life, there is a meaningful colonization of the neonate's gut and progressive alterations towards establishing a more stable and mature microbiome. Stewart et al. [251] described the three different stages of microbiota evolution during the postnatal period (Figure 3), which vary according to the dynamics of the most abundant phyla and the changes in alpha diversity. For instance, in the first phase, or the developmental phase (months 3-14), alpha diversity and phyla proportion change significantly with a predominance of *Bifidobacterium* spp. (*Actinobacteria* phylum). In the second stage, the transitional phase (months 15-30), phyla like *Bacteroidetes* and *Proteobacteria* continue to develop as continuous changes in alpha diversity occur. Finally, in a third phase, or the stable phase (>31

months), phyla and alpha diversity remain unchanged, with a predominance of *Firmicutes*. Many factors have been proposed to play a role in these different stages, which are reviewed in greater depth elsewhere [252,253]. Here we highlight those that might have a more significant influence on neonatal liver development, growth and maturation.

3.2.1. Birth

The mode of delivery is considered the first contributor to establish the early colonization patterns of the neonatal microbiome. According to Dominguez-Bello et al., vaginally delivered babies acquired bacterial communities resembling their mother's vaginal microbiota, dominated by *Lactobacillus*, *Prevotella* or *Sneathia* spp. In contrast, the microbiome of babies born via C-section is not only depleted and delayed in the colonization of the *Bacteriodes* genus, but mainly dominated by *Staphylococcus*, *Corynebacterium* and *Propionibacterium* spp. identical to their mother's skin surfaces [254]. Still, exposing C-section delivered newborns to maternal vaginal fluids at birth proved successful, if only in part, in enriching the gut, oral and skin microbiome with vaginal microbes [255]. Interestingly, Shao et al. noted that, besides disrupted transmission of maternal *Bacteriodes* strains, babies delivered by C-section showed higher levels of ESKAPE pathogenic bacteria typical of hospital environments (including *Enterococcus*, *Enterobacter* and *Klebsiella* spp.) [256]. The abundance of opportunistic ESKAPE strains derived from C-section births positively correlated with the number of respiratory infections over the first year of life [257], suggesting a possible relation of vaginal delivery-mediated gut colonization and neonatal immune priming. Additionally, C-section delivered neonates have a less significant representation of bacteria involved in lipopolysaccharide (LPS) biosynthesis pathway, therewith demonstrating a reduced immunostimulatory potential via secretion of pro-inflammatory cytokines [258]. LPS are some of the various endotoxins filtered by the liver, capable of triggering Kupffer cell inflammatory response [259] but also inducing hepcidin expression via TLR4 signaling in hepatocytes [260] in order to control inflammation-mediated iron homeostasis. Coordinated regulation of these functions is crucial in adult life, but it is not clear how LPS, or other metabolites that arise from the microbes that colonize the newborn

during birth, can onset early hepatic programming. Nevertheless, there is an undoubtable relation between the early microbiome composition and liver function, since newborns are typically diagnosed with signs of jaundice. Hyperbilirubinemia is so common among newborns it is often referred as physiological, showing evidence of being protective against endotoxic shock [261] and early-onset of neonatal sepsis mediated by *Streptococcus agalactiae* [262]. The immaturity of gut microbes is partially responsible for an inefficient bilirubin excretion, especially for C-section born babies with lower abundance of *Bifidobacterium pseudolongum* [263], indicating postpartum functional diversification of the gut microbiome is at least required for hepatic homeostasis.

Birth also imposes remarkable adaptations upon the hepatic circulation and oxygenation. *In utero* oxygenated blood flows through the umbilical recess directly into the main portal vein branches. With the beginning of intestinal function, portal vein trunk markedly dilates to allow a more considerable blood flow volume [69]. It remains elusive as to whether this physiological adaptation modulates microbiome acquisition and hepatic functional maturation after birth through intermediates that originate from the first colonic microbes.

3.2.2. Early feeding practices

Early life feeding practices are one of the greatest contributors for the development of the gut microbiome in the neonate. Evidence suggests that around 25–30% of the neonatal intestinal microbes are originated during the lactation period due to prebiotic effects of the colostrum and breast milk. Breastfed babies showed dominance of Bifidobacterium and Lactobacillus spp. [264], while the microbiota of formula-fed counterparts is enriched with anaerobic organisms such as Bacteroides and Clostridium [265,266]. Breast milk contains various immunomodulatory factors, including maternal antibodies (e.g., IgA), lactoferrin and defensins [267], which are believed to be protective against pediatric diseases such as viral gastroenteritis [268] and allergic asthma [269]. In fact, during the first 4 months of life, the assembly of the gut virome in breastfeeding neonates was delayed compared to formula-fed counterparts [270]. After birth, there is a decrease in gut alpha diversity [271], probably due to the selective pressure of milk substrates, and the neonatal gut microbiome will

remain very similar over the next 6 months, or as long as the only food intake is milk. During this stage, the selective pressure of maternal milk boosts gut mucosal and systemic immunity, as gut microbiota promote regulatory T cell generation [272,273], shape T helper cell immunity [274], encourage Peyer's patch development [275], and maturation of lymphoid follicles via TLR activation [276]. Another recent study showed that maternal betaine supplementation modulated *Akkermansia* abundance in neonates and was associated with decreased adiposity, improved glucose metabolism and long-term metabolic health throughout adulthood [277]. But how can milk intake help shape the development of other organs? Besides its role in microbe-dependent immune priming, could maternal milk also stimulate neonatal liver growth and maturation?

The neonatal microbiota substantially reorganizes after birth, with recognizable enteric functional specification within 6 weeks (e.g., LPS biosynthesis, bile acid deconjugation, metabolism of cofactors and vitamins, among others) [278]. This early microbial inoculum supports critical metabolic processes throughout the body. In fact, within hours after birth the liver parenchymal cells readily uptake vitamin K_2 to synthesize various anticoagulant factors [218,219]. Nevertheless, how the chronological and orchestrated changes to the gut microbial communities and its intermediates affects the developing neonatal organs is poorly understood, even though it is widely accepted they can have early physiological effects. Both vitamin K_2 and the secondary bile acid LCA were able to upregulate the phase-I drug metabolism enzymes CYP3A4 and CYP2C9 in hPSC-hepatocytes in isolated fetal hepatocytes [167]. In germ-free mice, CYP4A enzymes, which participate in fatty acid and prostaglandin hydroxylation, are aberrantly upregulated at neonatal stages [279]. Collectively, this data suggests that both microbial composition and microbial-derived nutrients that arise after birth are linked to postpartum maturation of CYP450, participating both in xenobiotic and energy metabolism programming.

Additionally, indigestible milk glycans, also known as human milk oligosaccharides (HMOs), can be properly metabolized when reaching the gut by *Bifidobacterium* strains [280] and are likely to modulate the severity of certain diseases, such as necrotizing enterocolitis [281] and neonatal rotavirus infections [282]. The main products of HMO catabolism are SCFAs [283], and to a lesser extent BCFAs, which fuel intestinal metabolism but can also reach the liver via portal circulation.

Charbonneau et al. recently described in a cohort of stunted infants, sialylated HMOs are less represented in their mothers' milk [284]. Germ-free mice and piglets colonized with these infants' gut microbes, and only when supplemented with dietary sialylated oligosaccharides, presented higher increment of hepatic acylcarnitines and long-chain fatty acyl CoA species between the fed and fasted states, indicating an increased metabolic flexibility and suggesting a potential role of HMO-derived microbial metabolites in driving postnatal liver energy metabolism.

Prebiotic oligosaccharides are routinely added to infant formula milk in order to promote breastfed-like flora however, Baumann-Dudenhoeffer et al. predicted distinct functional pathways between breastfed and formula fed neonates [285]. In fact, exclusively breastfed infants are more prone to have higher proportions of colonic SCFAs, especially acetate [286]. These differences are likely to influence neonatal hepatic development, as shown by an increase in CYP7A1 expression in formula-fed piglets relatively to their breastfed counterparts, a consequence of reduced bile acid metabolism by the gut microbiome and associated reductions in bile acid recirculation [287]. Formula feeding also appears to increase the biotransformation of caffeine and dextromethorphan by promoting an accelerated maturation of CYP1A2 and CYP3A4 [288], even though it remains elusive if differences in breastmilk composition (free fatty acids, lipase activity, among others) and/or alterations in the availability of certain microbial intermediates could explain these variations. Among probiotics, *Lactobacillus* spp. are popular microbes that are included in formulas, and similarly to prebiotic HMOs, their inclusion is aimed at promoting a microbiome similar to those found in breastfed newborns. *Lactobacillus reuteri* DSM 17938 has been used to attenuate infantile colic and bowel disorders [289]. In neonatal mice, its supplementation exerted changes on the plasma metabolome, upregulating microbial amino acid metabolites used in the urea, tricarboxylic acid (TCA) and methionine cycles, identified as important antioxidants in the liver as well as substrates for anabolism [290]. In contrast, *Lactobacillus ingluviei* promoted an increase in mice hepatic mass, upregulated CYP2E1 and accelerated metabolism [291].

Taken all together, the massive lipid burst associated with milk feeding [292,293] and its nutritional richness, in conjugation with early selective pressure imposed by gut microbes, likely helps setting the first cues for fatty acid oxidation, ketogenesis,

cholesterol/bile acid metabolism and mitochondrial bioenergetic maturation within the hepatic niche, alongside with noteworthy CYP450 specification.

3.2.3. Weaning, solid food intake and antibiotics

The last phase in neonatal gut microbial colonization is the weaning period and the introduction of solid food which results in an adult-like complex microbiome dominated by the phyla *Bacteroidetes* and also *Firmicutes*, that is believed to continue until 3 years of age (Figure 3) [294]. Interestingly, Bäckhed et al. found the cessation of breastfeeding enriched the infant gut microbiota with *Clostridia* spp. similar to those in adults, such as *Roseburia*, *Clostrium*, and *Anaerostipes* [295]. In turn, breastfed 12-month-old infants still present *Bifidobacterium* and *Lactobacillus* spp. as the dominant gut microbiota strains. Bäckhed et al. also noted that microbiota adapts to the availability of substrates, by first promoting bacterial functions vital for early development, such as biosynthesis of vitamins and transport of essential amino acids, and later on by supporting carbohydrate degradation. Indeed, with the start of solid/semisolid food intake the gut microbiota environment becomes less oxidative, encouraging pyruvate utilization and complex sugar and starch metabolism [295], the latter yielding mainly SCFAs that can be further used as an energy substrate in the liver.

Owing to the high-fat low carbohydrate composition of milk, fatty acid oxidation and ketone body production are the main functions of the newborn liver, along with gluconeogenesis due to an inadequate glucose production from absorbed lactate. The dietary transition of weaning brings higher abundance of carbohydrates, with a marked increase in lipogenesis [296]. Naemi et al. showed in mice that the normal expression levels of hepatic enzymes involved in lipid and carbohydrate metabolism was only reached around the weaning period [297]. Moreover, early weaning disturbed the programming of hepatic enzymes, causing elevations in genes associated with fatty acid metabolism, and resulted in longer weaning periods. Early introduction of solid/semisolid foods (i.e., at or before 3 months) has also proved to be associated with alterations of the infant gut microbiome, promoting higher concentrations of the SCFA butyrate [298]. Although it is not clear how gut microbiota encourages metabolic

changes in the liver of weaning neonates, the relationship between their coordinated functional maturation merits investigation.

The weaning period not only changes the neonate's energy metabolism, it is equally instrumental for hepatic immune priming. Gola et al. recently demonstrated the enrichment of myeloid and lymphoid cells in the liver, including Kupffer cells, towards the periportal regions of the lobule, a process that is triggered around weaning in mice [299]. Underlying this asymmetrical organization is a sustained sensing of commensal bacteria products (e.g., LPS) by liver sinusoidal cells in a MYD88-dependent manner that in turn tightly regulates the composition of glycocalyx to establish chemokine gradients. Even though bacterial products that illicit an immune response are often associated with hepatic inflammation and disease, during postnatal development the gut microbiome seems to work alongside the host to establish immune zonation in the liver as a lifelong preventive barrier against pathogens that can inflict damage on the parenchyma.

Environmental insults during this period, especially suboptimal feeding or even malnutrition, may contribute to lifelong and intergenerational deficits in growth and development. Undernutrition in weaning piglets decreased *Lactobacillus* spp. abundance, which increased secondary bile acid synthesis and suppressed CYP7A1 expression [300]. Beyond dysbiosis, infantile malnutrition is associated with a highly immature microbiota depleted of age-discriminatory taxa [301], that when transplanted into germ-free mice or piglets recapitulates abnormal juvenile development patterns [192,302], such as reduced weight and length prior to weaning, besides neuronal, metabolic and immune dysfunctions. Interestingly, Schwarzer et al. showed germ-free mice have a reduced activity of the somatotropic axis caused by an impaired signaling of growth hormone (GH), that instructs the liver to produce insulin-like growth factor-1 (IGF-1) [303]. During undernutrition germ-free mice became severely stunted, and this was partially reversed when colonized with strains of *Lactobacillus plantarum*, demonstrating gut microbes support systemic growth. As it happens, microbial SCFAs are recognized as sufficient to induce IGF-1 secretion [304]. IGF-1 plays a role beyond those associated to mitogenic hormones, being capable of regulating extrahepatic tissue metabolism and insulin sensitivity [305,306]. Thus, it is likely that the interplay

between IGF-1 and the gut microbiota is also required to drive liver energy metabolism programming in early life.

Another relevant insult during weaning is antibiotic exposure, that decreases the overall alpha diversity and was shown to delay microbial maturation during months 6 to 12 [271]. These findings are particularly concerning for hospitalized preterm infants, who often are exposed to antibiotics for extended periods of time due to their increased vulnerability to bacterial infections. Preterm perturbations by antibiotics enriches the gut antibiotic resistome and selects for multidrug-resistant *Enterobacteriaceae* spp. [307], which could predispose preterm neonates for numerous diseases. However, adverse hepatic reactions associated with drug intake at neonatal stages are low, possibly as a result of reduced persistent exposure and xenobiotic metabolism immaturity that in some cases may offer increased resistance (e.g., predominance of sulfation over glucuronidation is protective against acetaminophen toxicity) [308]. Nonetheless, consumption of dysbiotic drugs like antibiotics in neonatal piglets has shown to suppress microbial amino acid catabolism and reduce hepatic ureagenesis [309], but also downregulate *CYP1A2* expression as well as other genes that regulate fatty acid oxidation and amino acid biosynthesis [310]. Moreover, subtherapeutic antibiotic treatment in weaning mice selected gut microbiota fit to overharvest calories from complex carbohydrates, yielding higher proportion of intraluminal intestinal SCFAs that exacerbated hepatic lipogenesis, cholesterol and triglyceride metabolism [311]. Antibiotic treatment even prior to weaning similarly impacts the liver in mice, and despite reestablishment of the gut microbiome following cessation of antibiotics, the metabolic sequalae are lasting [312]. Such phenomena raise sensible questions whether postnatal antibiotic exposure can significantly impact liver development, and if it can possibly correlate with metabolic syndrome later in life.

3.3. Transition to adult microbiome

3.3.1. Infancy

Besides identifying three major phases of gut microbiome acquisition and diversification during the postnatal period, Stewart and colleagues demonstrated that the microbiome becomes relatively stable and adult-like from year 3 onwards [251].

However, other cohorts with longitudinal sampling over extended periods of time revealed children, either during early [313] or late childhood [314], still present a distinct microbiome from those found in adults, supporting the idea gut microbiome development may take longer than expected. Hollister et. al not only concluded school-aged pre-adolescent children (aged 7-12 years) harbor a less diverse microbiome with *Bacteroides* spp. abundances below those of adults, but also revealed there are significant differences in microbial functional pathways between children and adults [314]. While children have higher enrichment of genes involved in vitamin synthesis (e.g., B_{12} and *de novo* synthesis of folate) needed to support ongoing development, the adult microbiome is more oxidative and pro-inflammatory (e.g., TCA cycle, oxidative phosphorylation, LPS biosynthesis). Of note, early-life pre-school events, particularly the duration of breastfeeding, have been associated with differential microbiome composition among children [315]. Even perinatal factors, such as gestational age and mode of delivery, can have a noteworthy impact in progressive maturation of gut microbes in the first 4 years of life [316]. Nonetheless, a child's microbiome gradually evolves, becoming more competent in processing complex nutrients and adapting to environmental insults.

After 2 years of age, it is acknowledged that the infant has a fully mature liver, capable of performing all its function at levels comparable to those of adults [317]. Nonetheless, pediatric pharmacokinetics and pharmacodynamics differ from adults in several ways. For instance, adult-like activity of CYP2D6 is reached by 3-5 years, CYP2C9 and CYP3A4 activities may exceed adult levels during childhood, and most strikingly, UGT1A6 activity reaches adult levels only after 10 years of age [318]. Gut microbial intermediates are thought to participate in postpartum CYP450 maturation, but beyond neonatal stages its influence has not been documented.

A more obvious way gut microbes influence hepatic function in pediatric populations is through diet. A child's diet is nutritionally equivalent to an adult diet, and undoubtedly shapes flora composition. Wu et al. showed gut enterotypes correlate with long-term diet style [319]. While *Bacteroides* genra is associated with animal fat and protein-rich diets, *Prevotella* genra is more commonly related with carbohydrate-rich diets. HFDs are linked to obesity and gut dysbiosis, in turn predisposing to liver diseases such as NAFLD, that may affect even children [320]. In fact, Belei et al. predicted obese

children with small intestine bacterial overgrowth (or intestinal dysbiosis) have increased risk for developing NAFLD [321]. Even if the contribution of gut microbes to fully attain hepatic adult competence during infancy is currently debatable, it seems undeniable that a ‘healthy’ microbiome is vital for proper liver function.

3.3.2. Puberty

During puberty a substantial rise in circulating steroid sex hormones, mainly testosterone in males and the estrogen estradiol in females, stimulates profound physiological changes in the body to achieve reproductive competence. Agans et al. reported adolescents have significantly higher abundances of genra *Bifidobacterium* and *Clostridium*, even though the overall number of species is similar to adults [322], suggesting a potential hormonal impact on the gut microbiome. The microbiome composition is by itself a hallmark of sexual maturity, as transfer of gut microbes from adult male mice to immature female mice changed the recipient’s gut microbiome and resulted in testosterone elevations [323]. Besides gonadal and bodily changes, puberty onsets various sex-specific organ adaptations, including to the cardiovascular system, brain, kidneys and liver. So, could these sexual dimorphic adaptations be associated with the transition of the microbiome towards an adult configuration? Particularly in the liver, do gut microbes have an influence in defining its sex-specific roles?

The liver has, in fact, been acknowledged for a long time as one of the most sexually dimorphic organs, and recent transcriptomic and proteomic data indicates about 72% of its genes are expressed in a sex-specific way [324]. Hepatic sexual dimorphism is thought to be consequence of the gonadal-hypothalamus-pituitary-liver axis action [325]. Perinatal exposure to testosterone imprints a sex-dependent pulsatile pituitary GH secretion, which later on will appear during puberty and result in several organs’ sexual dimorphism that is maintained throughout adulthood. In contrast to the male liver, the female liver has increased capacity for fatty acid uptake, esterification, triglyceride synthesis and VLDL output, and less for fatty acid oxidation, gluconeogenesis and glycogen storage [326–328]. These differences confer an evolutionary advantage under food scarcity but are mainly physiological and related with a required metabolic adaptation during pregnancy, as it allows the mother to spare

glucose and amino acids for the developing neonate and rely on lipid oxidation for herself. Sex biased expression of xenobiotic enzymes (e.g., CYP3A4, CYP2B6, CYP2A6, CYP1A2, CYP2E1, sulfotransferases, glutathione S-transferases, UDP-glucuronosyltransferases) is also evident between males and females [329]. Interestingly, CYP3A enzymes were upregulated during pregnancy in mice possibly due to increases in placental growth hormone and estrogen plasma concentrations [330], suggesting female hormonal inputs may be sufficient to selectively program CYP450 expression for additional detoxification of fetal products.

It has become clear pubertal liver 'masculinization' or 'feminization' is required both for hepatic metabolism and reproductive competency later in life, so perturbations during this period could dampen sexual dimorphism. In fact, the reproductive function of germ-free mice is inferior to their conventionally raised counterparts [331], therefore it is pertinent to wonder if gut microbes are linked to sexual maturation of the liver. In a recent study, Weger et al. showed germ-free mice have perturbed sexual dimorphism and sex-specific rhythmicity, with noticeable alterations in hepatic gene and metabolite signatures belonging to sexually dimorphic pathways such as lipid and xenobiotic metabolism [332]. The resulting male liver feminization and female liver masculinization of germ-free animals is possibly related with altered sexual maturation (perturbed action of testosterone and estradiol) and GH secretion, alongside with dissimilar activation of xenobiotic receptors, in which microbial metabolites can be instrumental to regulate their collective action. Therefore, the gut microbiome appears to be a relevant player in the transition from a 'metabolic mature' towards a 'sexually mature' liver, and future studies may allow to uncover ways to control it in order to manage sex-specific susceptibility in developing metabolic syndromes in adulthood.

3.3.3. Adulthood

The adult gut microbiome has been acknowledged as relatively stable. Faith et al. analyzed fecal samples from 37 healthy adults and observed 60% of strains resided in the subject's gut over the course of 5 years, even though they could potentially remain there for decades [333]. Among the thousands of resident microbes, the ones belonging to the *Firmicutes* and *Bacteriodetes* phyla are by far the most abundant [99], but bacteria from the *Actinobacteria*, *Proteobacteria* and *Verrucomicrobia* phyla are

present nonetheless. A mature gut microbiome is expected to have a high alpha diversity and gene richness [99], which cannot be objectively characterized owed to significant inter-individual variations. This diversity can be attributed to many factors, including host genetics [334], environment [335] and diet [319,336]. Despite this, a fully mature gut microbiome is incredibly plastic and capable of appropriately responding to insults. For example, short-term consumption of either animal-based or plant-based diets can alter the gut microbial communities as to facilitate nutrient harvest in each dietary lifestyle [336]. Antibiotic insults can equally change the composition of the gut microbiome, lowering its overall diversity, which can be reversed back to its initial state after a recovery period [337]. The microbiome persists and adapts throughout life, regardless of the severity of the challenges imposed upon it, and so it is expected its close connection with the liver to be maintained in adulthood, especially as a sort of frontline against extrinsic and intrinsic insults.

Perhaps the most sophisticated way the liver safeguards homeostasis is via xenobiotic metabolism that prevents the body from toxicity. Variations in xenobiotic metabolizing enzyme activity profiles throughout life cannot only be attributed to ontology, but also result from a dissimilar exposure to environmental factors and drugs. Due to a higher consumption of exogenous compounds during adulthood, their efficient detoxification prior to entering systemic circulation is heavy reliant upon first-pass metabolism by the gut and liver, organs that harbor a vast repertoire of CYP450 enzymes. Nonetheless, the bioavailability, efficacy and toxicity of certain drugs is also undeniably influenced by gut microbes. An anecdotal case is prontosil, an agent with no antibacterial activity against *Streptococci in vitro* and effective only *in vivo*, due to the fact gut bacteria cleave its azo bond giving rise to the active component sulfanilamide [338]. Spanogiannopoulos et al. has comprehensively detailed known direct modifications microorganisms can perform on pharmaceuticals, such as activation (e.g., sulfanilamide), inactivation (e.g., digoxin) or toxification (e.g., irinotecan), and even how postbiotics can indirectly affect therapeutic outcome (e.g., simvastatin and secondary bile acid levels are positively correlated, and acetaminophen competes with *p*-cresol for the host sulfotransferase SULT1A1) [339]. More recently, Zimmermann et al. designed a large-scale experiment that assessed the ability of 76 gut-resident bacterial strains to metabolize 271 drugs, and noticed 176 of those drugs underwent considerable chemical transformations, including oxidation, reduction, acetylation,

deacetylation, hydrogenation, hydroxylation and propionylation [340]. Microbial-encoded enzymes appear to be an essential component of first-pass metabolism, even though, for most drugs, they remain unidentified and are often neglected during the drug development pipeline. It comes as no surprise that the absence of gut microbes is capable of changing how the liver processes exogenous drugs. In fact, germ-free or antibiotic treated animals are more efficient at metabolizing the anesthetic pentobarbital [341] and have an attenuated analgesic tolerance to the opioid morphine [342]. These differences are primarily associated with a dissimilar expression of hepatic xenobiotic receptors and phase I/II/III enzymes [341,343,344]. As an example, the antibiotic ciprofloxacin reduces levels of LCA-producing bacteria in the gut, leading to a decreased activation of PXR and reduced expression of the PXR target gene *Cyp3a11* (*CYP3A4* in humans) [345]. Furthermore, the microbiome has rhythmic oscillation patterns of biogeographical localization and metabolite secretion in the gut, that programs and couples with the host's circadian clock to maintain normal diurnal activity in hepatic drug metabolism [346]. The chronopharmacology of acetaminophen is mediated by variations of the microbial metabolite 1-phenyl-1,2-propanedione, whose higher nocturnal concentration detrimentally depletes hepatic glutathione levels and explains diurnal variations of acetaminophen overdose [347]. There is a growing appreciation of how the gut microbiome interacts with the host's hepatic drug metabolism, but further research is required to uncover the mechanisms behind this interaction and whether it could be manipulated for the host's benefit.

As a pivotal organ in detoxification, the liver is prone to damage, that if left unrepaired could result in liver disease and catastrophic multisystemic failure. The incredible regenerative capacity of the liver, following acute injury and partial hepatectomy, is well known, with as much as 51% of the original liver mass that can regenerate back to its full size in adults [33]. This is a complex and dynamic process, with different cell types intervening and specific intra and extracellular regulatory signals driving tissue repair. Interestingly, liver regeneration is substantially depressed in germ-free, athymic and LPS-resistant mice after 2/3 partial hepatectomy [348], suggesting the gut microbiome has a role to play. Liu et al. demonstrated a correlation between hepatic gene expression profiles and the shift in bacterial community composition throughout critical phases of liver regeneration in mice, namely during hepatocyte priming and proliferation [349]. In particular, the concentration of hydrophobic secondary bile acids

(e.g., DCA and LCA) and hepatic genes involved in bile acid metabolism were directly correlated with the transient abundance of certain microbial taxa. As mentioned above, bile acids are critical during hepatic tissue repair. If partial hepatectomy is accompanied by ileal resection, which presumably influences bile acid reabsorption, mice have a reduced liver regeneration due to lower mitosis events in hepatocytes [350]. A shift in bacterial composition seems to also stimulate an immune response, namely through the sensing of LPS produced by Gram-negative bacteria that expand after partial hepatectomy [349]. LPS represent another bacterial product that stimulates liver regrowth, as LPS-resistant mice have lower hepatic DNA synthesis [348]. Many other postbiotics may cooperate with host factors during regeneration, and their precise identification could well mean a way to aid recovery after liver injury and avoid irreversible loss of this unique ability.

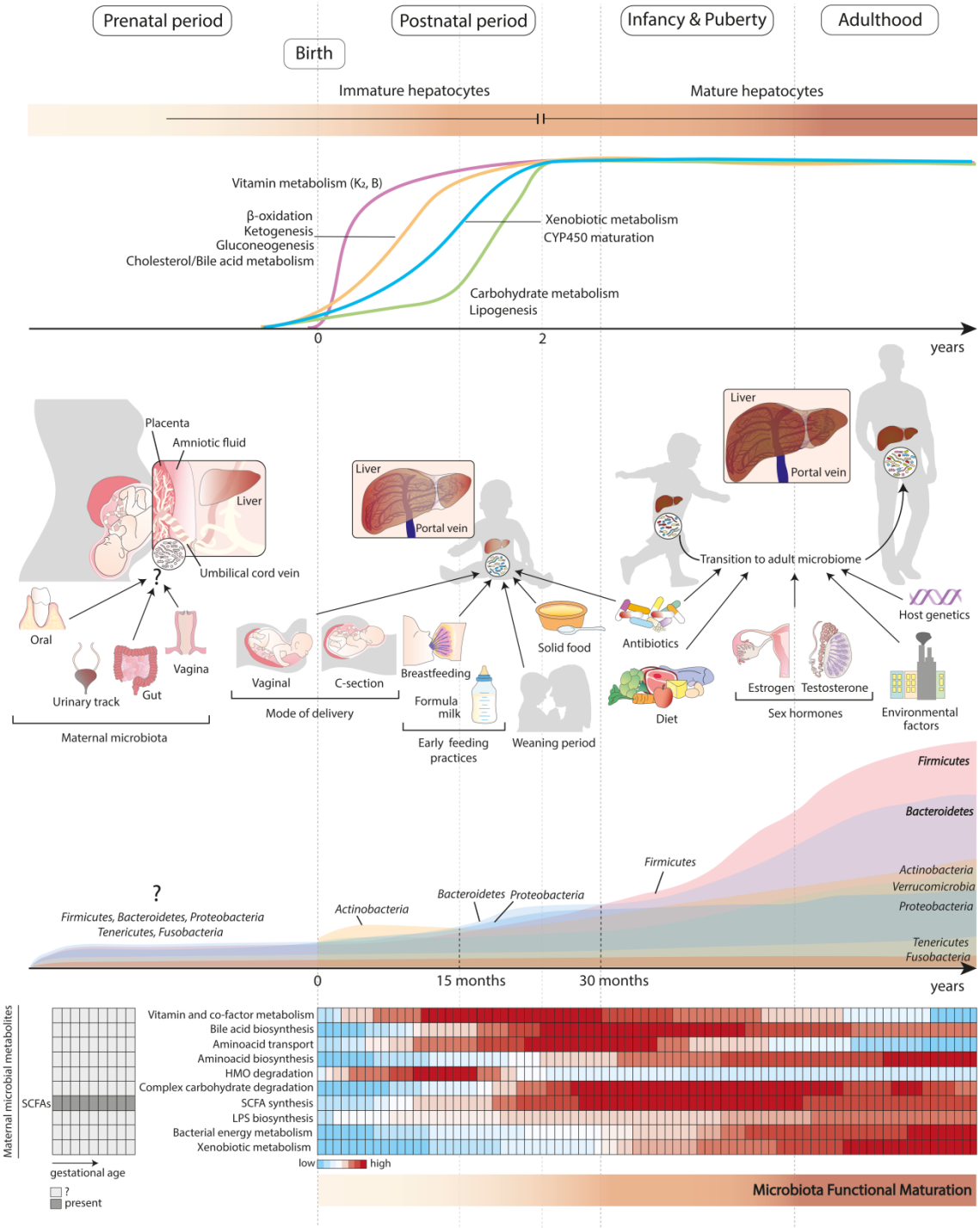

Figure 4. Proposed role of the gut microbiome in shaping liver maturation, function and homeostasis. Postpartum hepatocytes are highly immature, and it takes about 2 years to achieve a mature vitamin, energy and xenobiotic metabolism (and possibly others, not represented due to lack of current evidence correlating with the gut microbiome). The establishment and diversification of the gut microbiome is believed to be shaped by many factors, that ultimately contribute for intestinal phylum specification and functional maturation (as schematically represented by the various phyla abundance and associated metabolic pathways along the time, based on studies referenced in the text). Despite uncertainties regarding placental and amniotic fluid sterility, maternal gut microbial nutrients such as short-chain fatty acids (SCFAs) can still influence embryonic differentiation. Extrauterine gut colonization mediated by mode of delivery and neonatal feeding practices provide the first microbial nutrients used as substrates for vitamin and energy metabolism. The development of such pathways is accompanied by cytochrome P450 (CYP450) maturation, in which both gut microbial composition and nutrients play a role. Carbohydrate metabolism in the neonatal liver intensifies with the introduction to solid food during weaning, which is associated with a shift in microbiome diversity and increased capacity by gut microbes to metabolize complex sugars and starch. Dysbiotic insults such as antibiotics can significantly alter hepatic function at neonatal stages, with unclear developmental and long-term repercussions. As diet diversifies with age, the microbiome gradually changes towards and adult-like state. During puberty, gut microbiota is influenced by sex hormones, and is thought to be implicated in establishing liver sexual dimorphism that persist throughout adulthood. The adult microbiome is more complex and stable, even though dietary inputs, antibiotics, environmental factors and host genetics can disrupt hepatic homeostasis and promote disease onset. Abbreviations: LPS, liposaccharide; HMO, human milk oligosaccharide.

4. Scope of the Thesis

The overall aim of this thesis was to develop novel and robust strategies to generate clinically relevant numbers of mature HLC for regenerative medicine applications. To address that, we combined advanced manufacturing platforms with nature-inspired strategies, by unveiling the role of human microbiome on HLC maturation and function preservation, thus recapitulating more closely the physiological liver development. The specific aims of each chapter of this thesis are summarized in **Figure 5**.

Briefly, **Chapter 1** provides a comprehensive overview of an adult liver, comparing it to its immature and mostly hematopoietic fetal form. Furthermore, it briefly describes hepatic organogenesis, giving extensive insights into the acquisition of function and maturity during the early postnatal period. In particular, this Chapter aims to pinpoint key microbial molecules that have known effects on the liver and to discuss how the microbiome evolves from the perinatal period into adulthood providing evidence that the events that determine microbiome diversification and transformation are potentially linked to the acquisition of hepatic maturation. Therefore, **Chapter 2** was focused on investigating, for the first time, the implications of a microbial secretome, in the function of HLC. Two microbial secretomes (designated as conditioned media) were formulated *in vitro* and, after being characterized for their content in bile acids, vitamins and short-chain fatty acids, they were evaluated for their impact on the maturation and function of HLC generated from hESC and hiPSC, using either 2D or 3D cell culture systems.

Chapter 3 and 4 focused on the establishment of a scalable protocol for generation of HLC as 3D aggregates under controlled culture conditions. In **Chapter 3** an integrated bioprocess that combines 3D hiPSC expansion and hepatic differentiation steps was developed, using stirred-tank bioreactor technology, to improve HLC yields when compared to standard 2D monolayer cultures. Since monitoring cell quality attributes is a critical step for any biologic manufacturing process but remains a challenge in 3D culturing approaches, the potential of dielectric spectroscopy for *in situ* monitoring of 3D hiPSC growth and differentiation status was assessed by incorporating a capacitance sensor in the bioreactor. The modest expansion/differentiation yields observed in 3D culture in bioreactors, motivated to investigate whether alterations in dissolved oxygen concentration at specific stages of

the process would improve further cell proliferation and HLC enrichment. Therefore, in **Chapter 4** the bioprocess was intensified by controlling dissolved oxygen concentration at low levels during hepatic specification. The transcriptome of HLC along differentiation phase was characterized by RNA-Seq analysis, aiming at investigating whether the cell maturation level modulates the “machinery” that mediates cell engraftment and identifying a suitable HLC maturation stage that ensures efficient recellularization of acellular liver scaffolds.

The main achievements obtained in the previous chapters were outlined in **Chapter 5**.

GENERATION AND LARGE-SCALE EXPANSION OF HIGHLY FUNCTIONAL HPSC-DERIVED HEPATOCYTES FOR CELLULAR THERAPIES AND BIOENGINEERED LIVERS: THE UNKNOWN ROLE OF HUMAN MICROBIOME

Chapter 1

HALLMARKS OF THE HUMAN INTESTINAL MICROBIOME ON LIVER MATURATION AND FUNCTION

- A comprehensive review on the influence of the human intestinal microbiome in the acquisition of adult hepatic maturation and homeostasis

Chapter 2

THE EFFECTS OF HUMAN INTESTINAL MICROBIOTA SECRETOME ON HPSC-HEPATOCYTES FUNCTIONALITY

- Formulation and characterization of a human intestinal microbiota secretome
- Investigate the effects of microbial secretome in the functionality of hPSC-HLC *in vitro*

Chapter 3

TOWARDS MASSIVE PRODUCTION OF HIPSC-DERIVED HEPATOCYTES FOR APPLICATION IN REGENERATIVE MEDICINE

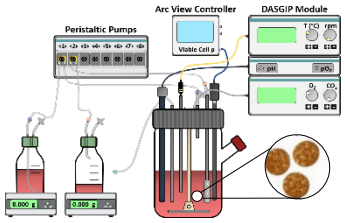

- Development of a scalable protocol for the generation of hiPSC-HLC in STBR

Chapter 4

RECELLULARIZATION OF ACELLULAR LIVER SCAFFOLDS WITH HIGHLY FUNCTIONAL HIPSC-HEPATOCYTES GENERATED USING A SCALABLE AND OPTIMIZED BIOPROCESS

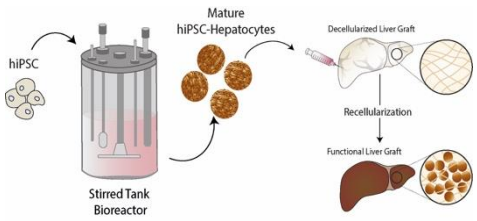

- Investigate the capacity of hiPSC-HLC generated in STBR to engraft in acellular liver scaffolds

Figure 5. Schematic representation of the major aims of the thesis throughout the different chapters.

5. References

[1] Abdel-misih SRZ, Bloomston M. Liver Anatomy. Surg Clin NA 2010;90:643–53. https://doi.org/10.1016/j.suc.2010.04.017.

[2] Thieme S. International Anatomical Terminology (FCA). 1998.

[3] Couinaud C. Le foie; études anatomiques et chirurgicales. 1957.

[4] Henri Bismuth. Surgical Anatomy and Anatomical Surgery of the Liver. World J Surg 1982;6:3–9.

[5] Rogers AB, Dintzis RZ. Hepatobiliary System. Elsevier Inc.; 2018. https://doi.org/10.1016/B978-0-12-802900-8.00013-0.

[6] Teutsch HF. The Modular Microarchitecture of Human Liver. Hepatology 2005:317–25. https://doi.org/10.1002/hep.20764.

[7] Yu Y, Ping J, Chen H, Jiao L, Zheng S, Han Z, et al. A comparative analysis of liver transcriptome suggests divergent liver function among human , mouse and rat. Genomics 2010;96:281–9. https://doi.org/10.1016/j.ygeno.2010.08.003.

[8] The Human Protein Atlas n.d. https://www.proteinatlas.org/humanproteome/tissue/liver (accessed May 25, 2021).

[9] The Johns Hopkins University. Liver: Anatomy and Functions n.d. https://www.hopkinsmedicine.org/health/conditions-and-diseases/liver-anatomy-and-functions (accessed May 25, 2020).

[10] Caripe G, Asa C, Trefts E, Gannon M, Wasserman DH. The liver. Cell Press 2017:1147–51. https://doi.org/10.1016/j.cub.2017.09.019.

[11] Blouin A, Bolender RP, Weibel ER. DISTRIBUTION OF ORGANELLES AND MEMBRANES BETWEEN HEPATOCYTES AND NONHEPATOCYTES IN THE RAT LIVER PARENCHYMA 1977;72:441–55.

[12] Guidotti J, Bre O, Robert A, Debey P, Brechot C, Desdouets C. Liver Cell Polyploidization : A Pivotal Role for Binuclear 2003;278:19095–101. https://doi.org/10.1074/jbc.M300982200.

[13] Gentric G, Desdouets C, Gentric G, Desdouets C, American T. Polyploidization in liver tissue . To cite this version : HAL Id : inserm-01074730 Polyploidization in Liver Tissue. Am J Pathol 2014;184:322–31. https://doi.org/10.1016/j.ajpath.2013.06.035.

[14] Jungermann K, Ph D. Metabolic Zonation of Liver Parenchyma 1988;8.

[15] Gebhardt R. METABOLIC ZONATION OF THE LIVER : REGULATION A N D IMPLICATIONS FOR LIVER FUNCTION 1992;53:275–354.

[16] Benhamouche S, Decaens T, Rickman DS, Moinard C, Vasseur-cognet M, Kuo CJ, et al. Apc Tumor Suppressor Gene Is the ‘“ Zonation-Keeper ”’ of Mouse Liver 2006:759–70. https://doi.org/10.1016/j.devcel.2006.03.015.

[17] Ã RG, Baldysiak-figiel A, Kru V, Ueberham E, Gaunitz F. Hepatocellular expression of glutamine synthetase : An indicator of morphogen actions as master regulators of zonation in adult liver 2007;41:201–66. https://doi.org/10.1016/j.proghi.2006.12.001.

[18] Planas-paz L, Orsini V, Boulter L, Calabrese D, Pikiolek M, Nigsch F, et al. The RSPO – LGR4 / 5 – ZNRF3 / RNF43 module controls liver zonation and size 2016. https://doi.org/10.1038/ncb3337.

[19] Leibing T, Cyrill G, Okun G, Langhans C, Zierow J, Wohlfeil SA, et al. Liver Growth and Metabolic Maturation in Mice 2018;68:707–22. https://doi.org/10.1002/hep.29613.

[20] Kietzmann T. Metabolic zonation of the liver : The oxygen gradient revisited.

Redox Biol 2017;11:622–30. https://doi.org/10.1016/j.redox.2017.01.012.
[21] Monga SPS, Dean A. Hepatic zonation now on hormones! Hepatology 2018. https://doi.org/10.1002/hep.30221.
[22] Chao H, Doi M, Fustin J, Chen H, Murase K, Maeda Y, et al. Circadian clock regulates hepatic polyploidy by modulating Mkp1-Erk1/2 signaling pathway. Nat Commun n.d.:1–14. https://doi.org/10.1038/s41467-017-02207-7.
[23] Soto-gutierrez A, Gough A, Vernetti LA, Taylor DL, Monga SP. Pre-clinical and clinical investigations of metabolic zonation in liver diseases : The potential of microphysiology systems 2017;5:1605–16. https://doi.org/10.1177/1535370217707731.
[24] Day P. The Natural History of Nonalcoholic Fatty Liver : 1995:1714–9.
[25] Ole L, Homeyer A, Schwier M, Dahmen U, Dirsch O, Schenk A, et al. Zonated quanti fi cation of steatosis in an entire mouse liver. Comput Biol Med 2016;73:108–18. https://doi.org/10.1016/j.compbiomed.2016.04.004.
[26] Gebhardt R, Matz-soja M. Liver zonation : Novel aspects of its regulation and its impact on homeostasis 2014;20:8491–504. https://doi.org/10.3748/wjg.v20.i26.8491.
[27] Rui L. Energy Metabolism in the Liver. Compr Physiol 2014;4:177–97. https://doi.org/10.1002/cphy.c130024.Energy.
[28] Almazroo OA, Miah MK. D r u g M e t a b o l i s m in t h e Liver 2017;21:1–20. https://doi.org/10.1016/j.cld.2016.08.001.
[29] Penner N, Woodward C, Prakash C. APPENDIX DRUG METABOLIZING ENZYMES AND 2012.
[30] Montellano O de. Cytochrome P450: Structure, Mechanism, and Biochemistry. 2005.
[31] Achour B, Barber J, Rostami-hodjegan A. Expression of Hepatic Drug-Metabolizing Cytochrome P450 Enzymes and Their Intercorrelations : A Meta-Analysis s 2014:1349–56.
[32] Nelson DR. The Cytochrome P450 Homepage 2009;4:59–65.
[33] Michalopoulos GK, Defrances MC. Liver Regeneration 1997.
[34] Navarro-alvarez N, Soto-gutierrez A, Kobayashi N. Hepatic Stem Cells and Liver Development. 2009. https://doi.org/10.1007/978-1-60327-227-8.
[35] Michalopoulos GK. Liver Regeneration 2007:286–300. https://doi.org/10.1002/JCP.
[36] Gilgenkrantz H, Collin A, Hortet D. Understanding Liver Regeneration. Am J Pathol 2018;188:1316–27. https://doi.org/10.1016/j.ajpath.2018.03.008.
[37] Rmilah AA, Zhou W, Nelson E, Lin L, Amiot B, Nyberg SL. Understanding the marvels behind liver regeneration 2019;8:1–46. https://doi.org/10.1002/wdev.340.Understanding.
[38] Zhou Z, Xu M, Gao B. Hepatocytes : a key cell type for innate immunity 2015;13:301–15. https://doi.org/10.1038/cmi.2015.97.
[39] Lemaigre P, Duncan SA, Si-tayeb K. Organogenesis and Development of the Liver 2010:175–89. https://doi.org/10.1016/j.devcel.2010.01.011.
[40] Roskams T, Van Eyken P, Desmet V. Human liver growth and development. Liver Growth and Repair 1998:541–57. https://doi.org/10.1007/978-94-011-4932-7_21.
[41] Zorn. AM. Liver development. 2008.
[42] Gordillo M, Evans T, Gouon-evans V. Orchestrating liver development 2015:2094–108. https://doi.org/10.1242/dev.114215.
[43] Ober EA, Lemaigre FP. Development of the liver : Insights into organ and tissue

morphogenesis. J Hepatol 2018;68:1049–62. https://doi.org/10.1016/j.jhep.2018.01.005.
[44] Yang L, Wang W, Qiu W, Guo Z, Bi E, Xu C. A single-cell transcriptomic analysis reveals precise pathways and regulatory mechanisms underlying hepatoblast differentiation 2018;66:1387–401. https://doi.org/10.1002/hep.29353.A.
[45] Szpinda MB, Paruszewska-achtel M, Wo A, Mila-kierzenkowska C, Elminowska-wenda G, Dombek MB, et al. Volumetric Growth of the Liver in the Human Fetus : An Anatomical , Hydrostatic , and Statistical Study 2015;2015. https://doi.org/10.1155/2015/858162.
[46] Chou S, Lodish HF. Fetal liver hepatic progenitors are supportive stromal cells for hematopoietic stem cells 2010;107:7799–804. https://doi.org/10.1073/pnas.1003586107.
[47] Linda M. Ernest, Eduardo D. Ruchelli DSH. Color Atlas of Fetal and Neonatal Histology. n.d.
[48] Popescu D, Botting RA, Stephenson E, Green K, Webb S, Jardine L, et al. Decoding human fetal liver haematopoiesis. Nature 2019. https://doi.org/10.1038/s41586-019-1652-y.
[49] Fanni D, Angotzi F, Lai F, Gerosa C, Senes G, Fanos V, et al. Four stages of hepatic hematopoiesis in human embryos and fetuses. J Matern 8 Neonatal Med 2017;0:000. https://doi.org/10.1080/14767058.2017.1297400.
[50] Giancotti A, Monti M, Nevi L, Safarikia S, Ambrosio VD, Brunelli R, et al. Functions and the Emerging Role of the Foetal Liver into Regenerative Medicine n.d.:1–19.
[51] WW. L. Chapter 7.Fetal and Neonatal Hepatic Circulation. Hepatic Circ. Physiol. Pathophysiol., San Rafael (CA): Morgan & Claypool Life Sciences: 2009.
[52] Treluyer JM, Sonnier M, Cresteil T. Cytochrome P-450 Expression in Sudden Infant Death Syndrome 1996;52:497–504.
[53] Developmental Expression of CYP2C and CYP2C-dependent Activities in the Human Liver_ In-Vivo in-Vitro Correlation and Inducibility.pdf n.d.
[54] Alcorn J, Mcnamara PJ. Ontogeny of Hepatic and Renal Part II 2002;41:1077–94.
[55] Ring JA, Ghabrial H, Ching MS, Smallwood RA, Morgan DJ. Fetal hepatic drug elimination 1999;84:429–45.
[56] M W Coughtrie, B Burchell JEL and RH. The inadequacy of perinatal glucuronidation: immunoblot analysis of the developmental expression of individual UDP-glucuronosyltransferase isoenzymes in rat and human liver microsomes. Mol Pharmacol 1988;34:729–35.
[57] Ward M, Deshpande S. Metabolic adaptation at birth 2005. https://doi.org/10.1016/j.siny.2005.04.001.
[58] S.C. K, L.J. D, S.M. S, P.A.J. A. Glucose production in pregnant women at term gestation. Sources of glucose for the human fetus. J Clin Invest 1979:388–94.
[59] Giies M, Hume R. The Ontogeny of Human Hepatic Microsomal Proteins Gestational age (wks) 1990;36:1633–7.
[60] Tomasi TB. Structure and function of alpha-fetoprotein. Annu Rev Med 1977;28:435–65.
[61] IKONEN RS, LINDGREN J, NIEMI E, SORTO AE, SEPPÄLÄ M, RUOSLAHTI E. AlphA FETOPROTEIN LEVELS IN NEONATAL HYPERBILIRUBINAEMIA. Acta Paediatr 1980;69:59–63. https://doi.org/10.1111/j.1651-2227.1980.tb07030.x.
[62] Bakker J, De Mees C, Douhard Q, Balthazart J, Gabant P, Szpirer J, et al. Alpha-

fetoprotein protects the developing female mouse brain from masculinization and defeminization by estrogens. Nat Neurosci 2006;9:220–6. https://doi.org/10.1038/nn1624.
[63] Swartz SK, Soloff MS. The lack of estrogen binding by human a-fetoprotein1. J Clin Endocrinol Metab 1974;39:589–91. https://doi.org/10.1210/jcem-39-3-589.
[64] Hillman NH, Kallapur SG, Jobe AH. Physiology of Transition from Intrauterine to Extrauterine Life. Clin Perinatol 2012;39:769–83. https://doi.org/10.1016/j.clp.2012.09.009.
[65] Chen C, Soto-Gutierrez A, Baptista PM, Spee B. Biotechnology Challenges to In Vitro Maturation of Hepatic Stem Cells. Gastroenterology 2018;154:1258–72.
[66] Edelstone DI, Rudolph AM, Heymann MA. Liver and ductus venosus blood flows in fetal lambs in utero. Circ Shock 1978;42:426–33. https://doi.org/10.1161/01.res.42.3.426.
[67] Poeppelman RS, Tobias JD. Patent Ductus Venosus and Congenital Heart Disease: A Case Report and Review. Cardiol Res 2018;9:330–3. https://doi.org/10.14740/cr777w.
[68] Lind J. Changes in liver circulation at birth. Ann N Y Acad Sci 1963;111:110–20.
[69] Meyer WW, Lind J. Postnatal changes in the portal circulation. Arch Dis Child 1966;41:606–12. https://doi.org/10.1136/adc.41.220.606.
[70] Tilles AW, Baskaran H, Roy P, Yarmush ML. Effects of Oxygenation and Flow on the Viability and Function of Rat Hepatocytes Cocultured in a Microchannel Flat-Plate Bioreactor 2001.
[71] Review C. Oxygen : Modulator of Metabolic Zonation and Disease of the Liver 2000:255–60.
[72] Tanaka Y, Yamato M, Okano T. Evaluation of effects of shear stress on hepatocytes by a microchip-based system 2006:1–5. https://doi.org/10.1088/0957-0233/17/12/S08.
[73] Girard J. Metabolic adaptations to change of nutrition at birth. Neonatology 1990;58:3–15.
[74] SHELLEY HJ. Glycogen Rfserves and Their Changes At Birth and in Anoxia. Br Med Bull 1961;17:137–43. https://doi.org/10.1093/oxfordjournals.bmb.a069888.
[75] Marsac C, Saudubray JM, Moncion A, Leroux JP. Development of gluconeogenic enzymes in the liver of human newborns. Neonatology 1976;28:317–25.
[76] Pégorier JP, Châtelain F, Thumelin S, Girard J. Role of long-chain fatty acids in the postnatal induction of genes coding for liver mitochondrial β-oxidative enzymes. Biochem Soc Trans 1998;26:113–20. https://doi.org/10.1042/bst0260113.
[77] Rando G, Tan CK, Khaled N, Montagner A, Leuenberger N, Bertrand-Michel J, et al. Glucocorticoid receptor-PPARα axis in fetal mouse liver prepares neonates for milk lipid catabolism. Elife 2016;5:1–31. https://doi.org/10.7554/eLife.11853.
[78] Hawdon JM. Hypoglycaemia and the neonatal brain. Eur J Pediatr Suppl 1999;158:9–12. https://doi.org/10.1007/pl00014319.
[79] Bougneres PF, Lemmel C, Ferre P, Bier DM. Ketone body transport in the human neonate and infant. J Clin Invest 1986;77:42–8.
[80] Costa RH, Kalinichenko V V., Holterman AXL, Wang X. Transcription Factors in Liver Development, Differentiation, and Regeneration. Hepatology 2003;38:1331–47. https://doi.org/10.1016/j.hep.2003.09.034.
[81] Sen S, Jumaa H, Webster NJG. Splicing factor SRSF3 is crucial for hepatocyte

differentiation and metabolic function. Nat Commun 2013;4. https://doi.org/10.1038/ncomms2342.
[82] Bhate A, Parker DJ, Bebee TW, Ahn J, Arif W, Rashan EH, et al. ESRP2 controls an adult splicing programme in hepatocytes to support postnatal liver maturation. Nat Commun 2015;6:1–12. https://doi.org/10.1038/ncomms9768.
[83] Gentric G, Celton-Morizur S, Desdouets C. Polyploidy and liver proliferation. Clin Res Hepatol Gastroenterol 2012;36:29–34. https://doi.org/10.1016/j.clinre.2011.05.011.
[84] Anatskaya O V., Vinogradov AE. Genome multiplication as adaptation to tissue survival: Evidence from gene expression in mammalian heart and liver. Genomics 2007;89:70–80. https://doi.org/10.1016/j.ygeno.2006.08.014.
[85] Devi BG, Gupta PD, Habeebullah CM. Changes in membrane fluidity during human liver development. Biochem Int 1992;28:41—49.
[86] Brill S, Zvibel I, Halpern Z, Oren R. The role of fetal and adult hepatocyte extracellular matrix in the regulation of tissue-specific gene expression in fetal and adult hepatocytes. Eur J Cell Biol 2002;81:43–50. https://doi.org/10.1078/0171-9335-00200.
[87] Kjersti Aagaard, Jun Ma, Kathleen M. Antony, Radhika Ganu, Joseph Petrosino and JV. The Placenta Harbors a Unique Microbiome Kjersti. Sci Transl Med 2014;6:1–22. https://doi.org/10.1126/scitranslmed.3008599.
[88] Jimønez E, Fernµndez L, Marín ML, Martín R, Odriozola JM, Nueno-palop C, et al. Isolation of Commensal Bacteria from Umbilical Cord Blood of Healthy Neonates Born by Cesarean Section 2005. https://doi.org/10.1007/s00284-005-0020-3.
[89] de Goffau MC, Lager S, Sovio U, Gaccioli F, Cook E, Peacock SJ, et al. Human placenta has no microbiome but can contain potential pathogens. Nature 2019;572:329–34. https://doi.org/10.1038/s41586-019-1451-5.
[90] Tamburini S, Shen N, Wu HC, Clemente JC. The microbiome in early life: Implications for health outcomes. Nat Med 2016;22:713–22. https://doi.org/10.1038/nm.4142.
[91] M. BJØ, PRYTZ H. Antibodies to intestinal microbes in serum of patients with cirrhosis of the liver. Lancet 1972:58–60. https://doi.org/https://doi.org/10.1016/S0140-6736(72)90060-8.
[92] Volta U, Bonazzi C, Bianchi FB, Baldoni AM, Zoli M, Pisl E, et al. IgA Antibodides to dietary antigens in liver cirrhosis 1987;17:235–42.
[93] Schnabl B, Brenner DA. Interactions between the intestinal microbiome and liver diseases. Gastroenterology 2014;146:1513–24. https://doi.org/10.1053/j.gastro.2014.01.020.
[94] Albillos A, de Gottardi A, Rescigno M. The gut-liver axis in liver disease: Pathophysiological basis for therapy. J Hepatol 2020;72:558–77. https://doi.org/10.1016/j.jhep.2019.10.003.
[95] Inagaki T, Moschetta A, Lee YK, Peng L, Zhao G, Downes M, et al. Regulation of antibacterial defense in the small intestine by the nuclear bile acid receptor. Proc Natl Acad Sci U S A 2006;103:3920–5. https://doi.org/10.1073/pnas.0509592103.
[96] Lee WK, Chang SD, Duddalwar VA, Comin JM, Perera W, Lau WFE, et al. Imaging assessment of congenital and acquired abnormalities of the portal venous system. Radiographics 2011;31:905–26. https://doi.org/10.1148/rg.314105104.
[97] Carneiro C, Brito J, Bilreiro C, Barros M, Bahia C, Santiago I, et al. All about

portal vein: a pictorial display to anatomy, variants and physiopathology. Insights Imaging 2019;10. https://doi.org/10.1186/s13244-019-0716-8.
[98] Da Costa JD, Leão ARDS, Santos JEM, Moulin DS, Sebastianes PM, D'Ippolito G. Measurement of portal blood flow in healthy individuals: A comparison between magnetic resonance imaging and Doppler ultrasound. Radiol Bras 2008;41:219–24. https://doi.org/10.1590/s0100-39842008000400004.
[99] Huttenhower C, Gevers D, Knight R, Abubucker S, Badger JH, Chinwalla AT, et al. Structure, function and diversity of the healthy human microbiome. Nature 2012;486:207–14. https://doi.org/10.1038/nature11234.
[100] Xu J, Gordon JI. Honor thy symbionts. Proc Natl Acad Sci U S A 2003;100:10452–9. https://doi.org/10.1073/pnas.1734063100.
[101] O'Hara AM, Shanahan F. The gut flora as a forgotten organ. EMBO Rep 2006;7:688–93. https://doi.org/10.1038/sj.embor.7400731.
[102] Qin J, Li R, Raes J, Arumugam M, Burgdorf KS, Manichanh C, et al. A human gut microbial gene catalogue established by metagenomic sequencing. Nature 2010;464:59–65. https://doi.org/10.1038/nature08821.
[103] Donaldson GP, Lee SM, Mazmanian SK. Gut biogeography of the bacterial microbiota. Nat Rev Microbiol 2015;14:20–32. https://doi.org/10.1038/nrmicro3552.
[104] Donia MS, Fischbach MA. Small molecules from the human microbiota. Science (80-) 2015;349. https://doi.org/10.1126/science.1254766.
[105] Cummings JH, Pomare EW, Branch HWJ, Naylor CPE, MacFarlane GT. Short chain fatty acids in human large intestine, portal, hepatic and venous blood. Gut 1987;28:1221–7. https://doi.org/10.1136/gut.28.10.1221.
[106] Bergman EN. Energy contributions of volatile fatty acids from the gastrointestinal tract in various species. Physiol Rev 1990;70:567–90. https://doi.org/10.1152/physrev.1990.70.2.567.
[107] Peng L, He Z, Chen W, Holzman IR, Lin J. Effects of butyrate on intestinal barrier function in a caco-2 cell monolayer model of intestinal barrier. Pediatr Res 2007;61:37–41. https://doi.org/10.1203/01.pdr.0000250014.92242.f3.
[108] Barcelo A, Claustre J, Moro F, Chayvialle JA, Cuber JC, Plaisancié P. Mucin secretion is modulated by luminal factors in the isolated vascularly perfused rat colon. Gut 2000;46:218–24. https://doi.org/10.1136/gut.46.2.218.
[109] Smith PM, Howitt MR, Panikov N, Michaud M, Gallini CA, Bohlooly-Y M, et al. The Microbial Metabolites, Short-Chain Fatty Acids, Regulate Colonic T_{reg} Cell Homeostasis. Science (80-) 2013;341:569 LP – 573. https://doi.org/10.1126/science.1241165.
[110] Ahmad MS, Krishnan S, Ramakrishna BS, Mathan M, Pulimood AB, Murthy SN. Butyrate and glucose metabolism by colonocytes in experimental colitis in mice. Gut 2000;46:493–9. https://doi.org/10.1136/gut.46.4.493.
[111] Donohoe DR, Garge N, Zhang X, Sun W, O'Connell TM, Bunger MK, et al. The microbiome and butyrate regulate energy metabolism and autophagy in the mammalian colon. Cell Metab 2011;13:517–26. https://doi.org/10.1016/j.cmet.2011.02.018.
[112] Zhao S, Jang C, Liu J, Uehara K, Gilbert M, Izzo L, et al. Dietary fructose feeds hepatic lipogenesis via microbiota-derived acetate. Nature 2020;579:1–6. https://doi.org/10.1038/s41586-020-2101-7.
[113] Gao X, Lin SH, Ren F, Li JT, Chen JJ, Yao CB, et al. Acetate functions as an epigenetic metabolite to promote lipid synthesis under hypoxia. Nat Commun 2016;7. https://doi.org/10.1038/ncomms11960.

[114] Li X, Chen H, Guan Y, Li X, Lei L, Liu J, et al. Acetic Acid Activates the AMP-Activated Protein Kinase Signaling Pathway to Regulate Lipid Metabolism in Bovine Hepatocytes. PLoS One 2013;8. https://doi.org/10.1371/journal.pone.0067880.
[115] Weitkunat K, Schumann S, Nickel D, Kappo KA, Petzke KJ, Kipp AP, et al. Importance of propionate for the repression of hepatic lipogenesis and improvement of insulin sensitivity in high-fat diet-induced obesity. Mol Nutr Food Res 2016;60:2611–21. https://doi.org/10.1002/mnfr.201600305.
[116] Zhou D, Chen YW, Zhao ZH, Yang RX, Xin FZ, Liu XL, et al. Sodium butyrate reduces high-fat diet-induced non-alcoholic steatohepatitis through upregulation of hepatic GLP-1R expression. Exp Mol Med 2018;50:1–12. https://doi.org/10.1038/s12276-018-0183-1.
[117] Mollica MP, Raso GM, Cavaliere G, Trinchese G, De Filippo C, Aceto S, et al. Butyrate regulates liver mitochondrial function, efficiency, and dynamics in insulin-resistant obese mice. Diabetes 2017;66:1405–18. https://doi.org/10.2337/db16-0924.
[118] Ye J, Lv L, Wu W, Li Y, Shi D, Fang D, et al. Butyrate Protects Mice Against Methionine–Choline-Deficient Diet-Induced Non-alcoholic Steatohepatitis by Improving Gut Barrier Function, Attenuating Inflammation and Reducing Endotoxin Levels. Front Microbiol 2018;9:1–16. https://doi.org/10.3389/fmicb.2018.01967.
[119] Mattace Raso G, Simeoli R, Russo R, Iacono A, Santoro A, Paciello O, et al. Effects of Sodium Butyrate and Its Synthetic Amide Derivative on Liver Inflammation and Glucose Tolerance in an Animal Model of Steatosis Induced by High Fat Diet. PLoS One 2013;8:1–13. https://doi.org/10.1371/journal.pone.0068626.
[120] Yoshida H, Ishii M, Akagawa M. Propionate suppresses hepatic gluconeogenesis via GPR43/AMPK signaling pathway. Arch Biochem Biophys 2019;672:108057. https://doi.org/10.1016/j.abb.2019.07.022.
[121] Ji X, Zhou F, Zhang Y, Deng R, Xu W, Bai M, et al. Butyrate stimulates hepatic gluconeogenesis in mouse primary hepatocytes. Exp Ther Med 2018:1677–87. https://doi.org/10.3892/etm.2018.7136.
[122] Brown AJ, Goldsworthy SM, Barnes AA, Eilert MM, Tcheang L, Daniels D, et al. The orphan G protein-coupled receptors GPR41 and GPR43 are activated by propionate and other short chain carboxylic acids. J Biol Chem 2003;278:11312–9. https://doi.org/10.1074/jbc.M211609200.
[123] Tirosh A, Calay ES, Tuncman G, Claiborn KC, Inouye KE, Eguchi K, et al. The short-chain fatty acid propionate increases glucagon and FABP4 production, impairing insulin action in mice and humans. Sci Transl Med 2019;11:1–14. https://doi.org/10.1126/scitranslmed.aav0120.
[124] den Besten G, Lange K, Havinga R, van Dijk TH, Gerding A, van Eunen K, et al. Gut-derived short-chain fatty acids are vividly assimilated into host carbohydrates and lipids. Am J Physiol - Gastrointest Liver Physiol 2013;305:900–10. https://doi.org/10.1152/ajpgi.00265.2013.
[125] Perry RJ, Borders CB, Cline GW, Zhang XM, Alves TC, Petersen KF, et al. Propionate increases hepatic pyruvate cycling and anaplerosis and alters mitochondrial metabolism. J Biol Chem 2016;291:12161–70. https://doi.org/10.1074/jbc.M116.720631.
[126] Kaiko GE, Ryu SH, Koues OI, Collins PL, Solnica-Krezel L, Pearce EJ, et al. The Colonic Crypt Protects Stem Cells from Microbiota-Derived Metabolites.

Cell 2016;165:1708–20. https://doi.org/10.1016/j.cell.2016.05.018.
[127] Wrzosek L, Miquel S, Noordine M-L, Bouet S, Chevalier-Curt MJ, Robert V, et al. Bacteroides Thetaiotaomicron and Faecalibacterium prausnitzii Shape the Mucus Production and Mucin O-Glycosylation in Colon Epithelium. BMC Biol 2013;11:1–13. https://doi.org/10.1016/s0016-5085(13)60210-3.
[128] Hay DC, Zhao D, Fletcher J, Hewitt ZA, McLean D, Urruticoechea-Uriguen A, et al. Efficient Differentiation of Hepatocytes from Human Embryonic Stem Cells Exhibiting Markers Recapitulating Liver Development In Vivo. Stem Cells 2008;26:894–902. https://doi.org/10.1634/stemcells.2007-0718.
[129] Du C, Feng Y, Qiu D, Xu Y, Pang M, Cai N, et al. Highly efficient and expedited hepatic differentiation from human pluripotent stem cells by pure small-molecule cocktails. Stem Cell Res Ther 2018;9:1–15. https://doi.org/10.1186/s13287-018-0794-4.
[130] Zhu S, Wang H, Ding S. Reprogramming fibroblasts toward cardiomyocytes, neural stem cells and hepatocytes by cell activation and signaling-directed lineage conversion. Nat Protoc 2015;10:959–73. https://doi.org/10.1038/nprot.2015.059.
[131] Oliphant K, Allen-Vercoe E. Macronutrient metabolism by the human gut microbiome: Major fermentation by-products and their impact on host health. Microbiome 2019;7:1–15. https://doi.org/10.1186/s40168-019-0704-8.
[132] Roager HM, Hansen LBS, Bahl MI, Frandsen HL, Carvalho V, Gøbel RJ, et al. Colonic transit time is related to bacterial metabolism and mucosal turnover in the gut. Nat Microbiol 2016;1:1–9. https://doi.org/10.1038/nmicrobiol.2016.93.
[133] Wikoff WR, Anfora AT, Liu J, Schultz PG, Lesley SA, Peters EC, et al. Metabolomics analysis reveals large effects of gut microflora on mammalian blood metabolites. Proc Natl Acad Sci U S A 2009;106:3698–703. https://doi.org/10.1073/pnas.0812874106.
[134] Darkoh C, Chappell C, Gonzales C, Okhuysen P. A rapid and specific method for the detection of indole in complex biological samples. Appl Environ Microbiol 2015;81:8093–7. https://doi.org/10.1128/AEM.02787-15.
[135] Lamas B, Richard ML, Leducq V, Pham HP, Michel ML, Da Costa G, et al. CARD9 impacts colitis by altering gut microbiota metabolism of tryptophan into aryl hydrocarbon receptor ligands. Nat Med 2016;22:598–605. https://doi.org/10.1038/nm.4102.
[136] Chimerel C, Emery E, Summers DK, Keyser U, Gribble FM, Reimann F. Bacterial Metabolite Indole Modulates Incretin Secretion from Intestinal Enteroendocrine L Cells. Cell Rep 2014;9:1202–8. https://doi.org/10.1016/j.celrep.2014.10.032.
[137] Qiu J, Heller JJ, Guo X, Chen ZME, Fish K, Fu YX, et al. The Aryl Hydrocarbon Receptor Regulates Gut Immunity through Modulation of Innate Lymphoid Cells. Immunity 2012;36:92–104. https://doi.org/10.1016/j.immuni.2011.11.011.
[138] Venkatesh M, Mukherjee S, Wang H, Li H, Sun K, Benechet AP, et al. Symbiotic bacterial metabolites regulate gastrointestinal barrier function via the xenobiotic sensor PXR and toll-like receptor 4. Immunity 2014;41:296–310. https://doi.org/10.1016/j.immuni.2014.06.014.
[139] Cason CA, Dolan KT, Sharma G, Tao M, Kulkarni R, Helenowski IB, et al. Plasma microbiome-modulated indole- and phenyl-derived metabolites associate with advanced atherosclerosis and postoperative outcomes. J Vasc Surg 2018;68:1552-1562.e7. https://doi.org/10.1016/j.jvs.2017.09.029.
[140] Rosas HD, Doros G, Bhasin S, Thomas B, Gevorkian S, Malarick K, et al. A

systems-level “misunderstanding”: the plasma metabolome in Huntington’s disease. Ann Clin Transl Neurol 2015;2:756–68. https://doi.org/10.1002/acn3.214.
[141] Krishnan S, Ding Y, Saedi N, Choi M, Sridharan G V., Sherr DH, et al. Gut Microbiota-Derived Tryptophan Metabolites Modulate Inflammatory Response in Hepatocytes and Macrophages. Cell Rep 2018;23:1099–111. https://doi.org/10.1016/j.celrep.2018.03.109.
[142] Ji Y, Gao Y, Chen H, Yin Y, Zhang W. Indole-3-acetic acid alleviates nonalcoholic fatty liver disease in mice via attenuation of hepatic lipogenesis, and oxidative and inflammatory stress. Nutrients 2019;11. https://doi.org/10.3390/nu11092062.
[143] Beaumont M, Neyrinck AM, Olivares M, Rodriguez J, De Rocca Serra A, Roumain M, et al. The gut microbiota metabolite indole alleviates liver inflammation in mice. FASEB J 2018;32:6681–93. https://doi.org/10.1096/fj.201800544.
[144] Zhao ZH, Xin FZ, Xue Y, Hu Z, Han Y, Ma F, et al. Indole-3-propionic acid inhibits gut dysbiosis and endotoxin leakage to attenuate steatohepatitis in rats. Exp Mol Med 2019;51. https://doi.org/10.1038/s12276-019-0304-5.
[145] Chen G, Cue RA, Lundstrom K, Wood JD, Doran O. Regulation of CYP2A6 protein expression by skatole, indole, and testicular steroids in primary cultured pig hepatocytes. Drug Metab Dispos 2008;36:56–60. https://doi.org/10.1124/dmd.107.017285.
[146] Diaz GJ. Metabolism of 3-Methylindole by Porcine Liver Microsomes: Responsible Cytochrome P450 Enzymes. Toxicol Sci 2000;55:284–92. https://doi.org/10.1093/toxsci/55.2.284.
[147] Banoglu E, Jha GG, King RS. Hepatic microsomal metabolism of indole to indoxyl, a precursor of indoxyl sulfate. Eur J Drug Metab Pharmacokinet 2001;26:235–40. https://doi.org/10.1007/BF03226377.
[148] Banoglu E, King RS. Sulfation of indoxyl by human and rat aryl (phenol) sulfotransferases to form indoxyl sulfate. Eur J Drug Metab Pharmacokinet 2002;27:135–40. https://doi.org/10.1007/BF03190428.
[149] Sato T, Yamaguchi H, Kogawa T, Abe T, Mano N. Organic anion transporting polypeptides 1B1 and 1B3 play an important role in uremic toxin handling and drug-uremic toxin interactions in the liver. J Pharm Pharm Sci 2014;17:475–84. https://doi.org/10.18433/j3m89q.
[150] Doran E, Whittington FW, Wood JD, McGivan JD. Cytochrome P450IIE1 (CYP2E1) is induced by skatole and this induction is blocked by androstenone in isolated pig hepatocytes. Chem Biol Interact 2002;140:81–92. https://doi.org/10.1016/S0009-2797(02)00015-7.
[151] Rasmussen MK, Balaguer P, Ekstrand B, Daujat-Chavanieu M, Gerbal-Chaloin S. Skatole (3-methylindole) is a partial aryl hydrocarbon receptor agonist and induces CYP1A1/2 and CYP1B1 expression in primary human hepatocytes. PLoS One 2016;11:1–17. https://doi.org/10.1371/journal.pone.0154629.
[152] Hoyles L, Fernández-Real JM, Federici M, Serino M, Abbott J, Charpentier J, et al. Molecular phenomics and metagenomics of hepatic steatosis in non-diabetic obese women. Nat Med 2018;24:1070–80. https://doi.org/10.1038/s41591-018-0061-3.
[153] Meijers BKI, Evenepoel P. The gut-kidney axis: Indoxyl sulfate, p-cresyl sulfate and CKD progression. Nephrol Dial Transplant 2011;26:759–61. https://doi.org/10.1093/ndt/gfq818.

[154] Barnes KJ, Rowland A, Polasek TM, Miners JO. Inhibition of human drug-metabolising cytochrome P450 and UDP-glucuronosyltransferase enzyme activities in vitro by uremic toxins. Eur J Clin Pharmacol 2014;70:1097–106. https://doi.org/10.1007/s00228-014-1709-7.
[155] Clayton TA, Baker D, Lindon JC, Everett JR, Nicholson JK. Pharmacometabonomic identification of a significant host-microbiome metabolic interaction affecting human drug metabolism. Proc Natl Acad Sci U S A 2009;106:14728–33. https://doi.org/10.1073/pnas.0904489106.
[156] Evenepoel P, Bammens B, Verbeke K, Vanrenterghem Y. Acarbose treatment lowers generation and serum concentrations of the protein-bound solute p-cresol: A pilot study. Kidney Int 2006;70:192–8. https://doi.org/10.1038/sj.ki.5001523.
[157] Ridlon JM, Kang DJ, Hylemon PB. Bile salt biotransformations by human intestinal bacteria. J Lipid Res 2006;47:241–59. https://doi.org/10.1194/jlr.R500013-JLR200.
[158] Setchell KDR, Lawson AM, Tanida N, Sjovall J. General methods for the analysis of metabolic profiles of bile acids and related compounds in feces. J Lipid Res 1983;24:1085–100.
[159] Sayin SI, Wahlström A, Felin J, Jäntti S, Marschall HU, Bamberg K, et al. Gut microbiota regulates bile acid metabolism by reducing the levels of tauro-beta-muricholic acid, a naturally occurring FXR antagonist. Cell Metab 2013;17:225–35. https://doi.org/10.1016/j.cmet.2013.01.003.
[160] Hamilton JP, Xie G, Raufman JP, Hogan S, Griffin TL, Packard CA, et al. Human cecal bile acids: Concentration and spectrum. Am J Physiol - Gastrointest Liver Physiol 2007;293:256–63. https://doi.org/10.1152/ajpgi.00027.2007.
[161] Makishima M, Okamoto AY, Repa JJ, Tu H, Learned RM, Luk A, et al. Identification of a Nuclear Receptor for Bile Acids. Science (80-) 1999;284:1362 LP – 1365. https://doi.org/10.1126/science.284.5418.1362.
[162] Zhang M, Chiang JYL. Transcriptional regulation of the human sterol 12α-hydroxylase gene (CYP8B1): Roles of hepatocyte nuclear factor 4α in mediating bile acid repression. J Biol Chem 2001;276:41690–9. https://doi.org/10.1074/jbc.M105117200.
[163] Chen W, Chiang JYL. Regulation of human sterol 27-hydroxylase gene (CYP27A1) by bile acids and hepatocyte nuclear factor 4α (HNF4α). Gene 2003;313:71–82. https://doi.org/10.1016/S0378-1119(03)00631-0.
[164] Gupta S, Natarajan R, Payne SG, Studer EJ, Spiegel S, Dent P, et al. Deoxycholic acid activates the c-Jun N-terminal kinase pathway via FAS receptor activation in primary hepatocytes: Role of acidic sphingomyelinase-mediated ceramide generation in FAS receptor activation. J Biol Chem 2004;279:5821–8. https://doi.org/10.1074/jbc.M310979200.
[165] Yu J, Lo JL, Huang L, Zhao A, Metzger E, Adams A, et al. Lithocholic acid decreases expression of bile salt export pump through farnesoid X receptor antagonist activity. J Biol Chem 2002;277:31441–7. https://doi.org/10.1074/jbc.M200474200.
[166] Wang H, Chen J, Hollister K, Sowers LC, Forman BM. Wang,m 1999. Mol Cell 1999;3:543–53.
[167] Avior Y, Levy G, Zimerman M, Kitsberg D, Schwartz R, Sadeh R, et al. Microbial-Derived Lithocholic Acid and Vitamin K2 Drive the Metabolic Maturation of Pluripotent Stem Cells-Derived and Fetal Hepatocytes. Hepatology 2015;62:265–78. https://doi.org/10.1002/hep.27803.

[168] Staudinger JL, Goodwin B, Jones SA, Hawkins-Brown D, MacKenzie KI, LaTour A, et al. The nuclear receptor PXR is a lithocholic acid sensor that protects against liver toxicity. Proc Natl Acad Sci U S A 2001;98:3369–74. https://doi.org/10.1073/pnas.051551698.
[169] Xie W, Radominska-Pandya A, Shi Y, Simon CM, Nelson MC, Ong ES, et al. An essential role for nuclear receptors SXR/PXR in detoxification of cholestatic bile acids. Proc Natl Acad Sci U S A 2001;98:3375–80. https://doi.org/10.1073/pnas.051014398.
[170] Makishima M, Lu TT, Xie W, Whitfield GK, Domoto H, Evans RM, et al. Vitamin D receptor as an intestinal bile acid sensor. Science (80-) 2002;296:1313–6. https://doi.org/10.1126/science.1070477.
[171] Kawamata Y, Fujii R, Hosoya M, Harada M, Yoshida H, Miwa M, et al. A G protein-coupled receptor responsive to bile acids. J Biol Chem 2003;278:9435–40. https://doi.org/10.1074/jbc.M209706200.
[172] Watanabe M, Houten SM, Mataki C, Christoffolete MA, Kim BW, Sato H, et al. Bile acids induce energy expenditure by promoting intracellular thyroid hormone activation. Nature 2006;439:484–9. https://doi.org/10.1038/nature04330.
[173] Keitel V, Reinehr R, Gatsios P, Rupprecht C, Görg B, Selbach O, et al. The G-protein coupled bile salt receptor TGR5 is expressed in liver sinusoidal endothelial cells. Hepatology 2007;45:695–704. https://doi.org/10.1002/hep.21458.
[174] Dent P, Fang Y, Gupta S, Studer E, Mitchell G, Spiegel S, et al. Conjugated bile acids promote ERK1/2 and AKT activation via a pertussis toxin-sensitive mechanism in murine and human hepatocytes. Hepatology 2005;42:1291–9. https://doi.org/10.1002/hep.20942.
[175] Studer E, Zhou X, Zhao R, Wang Y, Takabe K, Nagahashi M, et al. Conjugated bile acids activate the sphingosine-1-phosphate receptor 2 in primary rodent hepatocytes. Hepatology 2012;55:267–76. https://doi.org/10.1002/hep.24681.
[176] Ferreira DMS, Afonso MB, Rodrigues PM, Simao AL, Pereira DM, Borralho PM, et al. c-Jun N-Terminal Kinase 1/c-Jun Activation of the p53/MicroRNA 34a/Sirtuin 1 Pathway Contributes to Apoptosis Induced by Deoxycholic Acid in Rat Liver. Mol Cell Biol 2014;34:1100–20. https://doi.org/10.1128/mcb.00420-13.
[177] Rodrigues PM, Afonso MB, Simaõ AL, Borralho PM, Rodrigues CMP, Castro RE. Inhibition of NF-κ B by deoxycholic acid induces miR-21/PDCD4-dependent hepatocelular apoptosis. Sci Rep 2015;5:1–17. https://doi.org/10.1038/srep17528.
[178] Qiao L, Studer E, Leach K, McKinstry R, Gupta S, Decker R, et al. Deoxycholic acid (DCA) causes ligand-independent activation of epidermal growth factor receptor (EGFR) and FAS receptor in primary hepatocytes: Inhibition of EGFR/mitogen-activated protein kinase-signaling module enhances DCA-induced apoptosis. Mol Biol Cell 2001;12:2629–45. https://doi.org/10.1091/mbc.12.9.2629.
[179] Rodrigues CMP, Ma X, Linehan-Stieers C, Fan G, Kren BT, Steer CJ. Ursodeoxycholic acid prevents cytochrome c release in apoptosis by inhibiting mitochondrial membrane depolarization and channel formation. Cell Death Differ 1999;6:842–54. https://doi.org/10.1038/sj.cdd.4400560.
[180] Hino A, Morita M, Une M, Fujimura K, Kuramoto T. Effects of deoxycholic acid and its epimers on lipid peroxidation in isolated rat hepatocytes. J Biochem 2001;129:683–9. https://doi.org/10.1093/oxfordjournals.jbchem.a002907.

[181] Castro RE, Ferreira DMS, Afonso MB, Borralho PM, MacHado M V., Cortez-Pinto H, et al. MiR-34a/SIRT1/p53 is suppressed by ursodeoxycholic acid in the rat liver and activated by disease severity in human non-alcoholic fatty liver disease. J Hepatol 2013;58:119–25. https://doi.org/10.1016/j.jhep.2012.08.008.
[182] Azzaroli F, Mehal W, Soroka CJ, Wang L, Lee J, Crispe N, et al. Ursodeoxycholic acid diminishes Fas-ligand-induced apoptosis in mouse hepatocytes. Hepatology 2002;36:49–54. https://doi.org/10.1053/jhep.2002.34511.
[183] Schoemaker MH, Conde De La Rosa L, Buist-Homan M, Vrenken TE, Havinga R, Poelstra K, et al. Tauroursodeoxycholic acid protects rat hepatocytes from bile acid-induced apoptosis via activation of survival pathways. Hepatology 2004;39:1563–73. https://doi.org/10.1002/hep.20246.
[184] Tanaka M, Tateishi T, Watanabe M. Reduction in Rats With Deoxychok Acid-Induced Liver Injury. Liver 1999;450:263–70.
[185] Rodrigues CMP, Fan G, Wong PY, Kren BT, Steer CJ. Ursodeoxycholic acid may inhibit deoxycholic acid-induced apoptosis by modulating mitochondrial transmembrane potential and reactive oxygen species production. Mol Med 1998;4:165–78. https://doi.org/10.1007/bf03401914.
[186] Mitsuyoshi H, Nakashima T, Sumida Y, Yoh T, Nakajima Y, Ishikawa H, et al. Ursodeoxycholic acid protects hepatocytes against oxidative injury via induction of antioxidants. Biochem Biophys Res Commun 1999;263:537–42. https://doi.org/10.1006/bbrc.1999.1403.
[187] Huang W, Ma K, Zhang J, Qatanani M, Cuvillier J, Liu J, et al. Nuclear receptor-dependent bile acid signaling is required for normal liver regeneration. Science (80-) 2006;312:233–6. https://doi.org/10.1126/science.1121435.
[188] Kren BT, Rodrigues CMP, Setchell KDR, Steer CJ. Modulation of steady-state messenger RNA levels in the regenerating rat liver with bile acid feeding. Liver Transplant 2001;7:321–34. https://doi.org/10.1053/jlts.2001.23062.
[189] Barone M, Francavilla A, Polimeno L, Ierardi E, Romanelli D, Berloco P, et al. Modulation of rat hepatocyte proliferation by bile salts: In vitro and in vivo studies. Hepatology 1996;23:1159–66. https://doi.org/10.1053/jhep.1996.v23.pm0008621149.
[190] Wostmann BS. The germfree animal in nutritional studies. Annu Rev Nutr 1981;1:257–79. https://doi.org/10.1146/annurev.nu.01.070181.001353.
[191] Magnúsdóttir S, Ravcheev D, De Crécy-Lagard V, Thiele I. Systematic genome assessment of B-vitamin biosynthesis suggests cooperation among gut microbes. Front Genet 2015;6. https://doi.org/10.3389/fgene.2015.00148.
[192] Gehrig JL, Venkatesh S, Chang HW, Hibberd MC, Kung VL, Cheng J, et al. Effects of microbiota-directed foods in gnotobiotic animals and undernourished children. Science (80-) 2019;365. https://doi.org/10.1126/science.aau4732.
[193] Kunisawa J, Sugiura Y, Wake T, Nagatake T, Suzuki H, Nagasawa R, et al. Mode of Bioenergetic Metabolism during B Cell Differentiation in the Intestine Determines the Distinct Requirement for Vitamin B1. Cell Rep 2015;13:122–31. https://doi.org/10.1016/j.celrep.2015.08.063.
[194] Scott TA, Quintaneiro LM, Norvaisas P, Lui PP, Wilson MP, Leung KY, et al. Host-Microbe Co-metabolism Dictates Cancer Drug Efficacy in C. elegans. Cell 2017;169:442-456.e18. https://doi.org/10.1016/j.cell.2017.03.040.
[195] Goodman AL, McNulty NP, Zhao Y, Leip D, Mitra RD, Lozupone CA, et al. Identifying Genetic Determinants Needed to Establish a Human Gut Symbiont in Its Habitat. Cell Host Microbe 2009;6:279–89.

https://doi.org/10.1016/j.chom.2009.08.003.
[196] Danner DJ, Davidson ED, Elsas LJ. Thiamine increases the specific activity of human liver branched chain α-ketoacid dehydrogenase. Nature 1975;254:529–30.
[197] Knowles JR. The mechanism of biotin-dependent enzymes. Annu Rev Biochem 1989;58:195–221.
[198] Barile M, Brizio C, Valenti D, De Virgilio C, Passarella S. The riboflavin/FAD cycle in rat liver mitochondria. Eur J Biochem 2000;267:4888–900. https://doi.org/10.1046/j.1432-1327.2000.01552.x.
[199] Rucker RB. Pantothenic Acid. Encycl Food Heal 2015:205–8. https://doi.org/10.1016/B978-0-12-384947-2.00516-X.
[200] Merrill AH, Henderson JM. Vitamin B6 Metabolism by Human Liver. Ann N Y Acad Sci 1990;585:110–7. https://doi.org/10.1111/j.1749-6632.1990.tb28047.x.
[201] Bailey LB, Gregory JF. Recent Advances in Nutritional Science Folate Metabolism and. J Nutr 1999;129:779–82.
[202] Sanches SC, Ramalho LNZ, Mendes-Braz M, Terra VA, Cecchini R, Augusto MJ, et al. Riboflavin (vitamin B-2) reduces hepatocellular injury following liver ischaemia and reperfusion in mice. Food Chem Toxicol 2014;67:65–71. https://doi.org/10.1016/j.fct.2014.02.013.
[203] Bashandy SAE, Ebaid H, Moussa SAA, Alhazza IM, Hassan I, Alaamer A, et al. Potential effects of the combination of nicotinamide , vitamin B2 and vitamin C on oxidative-mediated hepatotoxicity induced by thioacetamide 2018:1–9.
[204] Corrao G, Torchio P, Zambon A, D'Amicis A, Lepore AR, Di Orio F. Alcohol consumption and micronutrient intake as risk factors for liver cirrhosis: A case-control study. Ann Epidemiol 1998;8:154–9. https://doi.org/10.1016/S1047-2797(97)00193-2.
[205] Ganji SH, Kashyap ML, Kamanna VS. Niacin inhibits fat accumulation, oxidative stress, and inflammatory cytokine IL-8 in cultured hepatocytes: Impact on non-alcoholic fatty liver disease. Metabolism 2015:1–9. https://doi.org/10.1016/j.metabol.2015.05.002.
[206] Eidi A, Mortazavi P, Tehrani ME, Rohani AH, Safi S. Hepatoprotective effects of pantothenic acid on carbon tetrachloride-induced toxicity in rats. EXCLI J 2012;11:748–59. https://doi.org/10.17877/DE290R-5373.
[207] Cabrini L, Bergami R, Fiorentini D, Marchetti M, Landi L, Tolomelli B. Vitamin B6 deficiency affects antioxidant defences in rat liver and heart. IUBMB Life 1998;46:689–97.
[208] Yang A, Sun Y, Mao C, Yang S, Huang M, Deng M, et al. Folate Protects Hepatocytes of Hyperhomocysteinemia Mice From Apoptosis via Cystic Fibrosis Transmembrane Conductance Regulator (CFTR)-Activated Endoplasmic Reticulum Stress. J Cell Biochem 2017;118:2921–32. https://doi.org/10.1002/jcb.25946.
[209] Xu Y, Wang H, Wang Y, Zheng Y, Sun G. Effects of folate on arsenic toxicity in Chang human hepatocytes : Involvement of folate antioxidant properties. Toxicol Lett 2010;195:44–50. https://doi.org/10.1016/j.toxlet.2010.02.015.
[210] Halsted CH, Villanueva JA, Devlin AM, Niemelä O, Parkkila S, Garrow TA, et al. Folate deficiency disturbs hepatic methionine metabolism and promotes liver injury in the ethanol-fed micropig. Proc Natl Acad Sci U S A 2002;99:10072–7. https://doi.org/10.1073/pnas.112336399.
[211] Ganji SH, Tavintharan S, Zhu D, Xing Y, Kamanna VS, Kashyap ML. Niacin noncompetitively inhibits DGAT2 but not DGAT1 activity in HepG2 cells 1. J

Lipid Res 2004;45:1835–45. https://doi.org/10.1194/jlr.M300403-JLR200.
[212] Lingyan Ye, Zheng Cao, Xiangru Lai, Ying Shi NZ. Niacin Ameliorates Hepatic Steatosis by Inhibiting De Novo Lipogenesis Via a GPR109A-Mediated PKC–ERK1/2–AMPK Signaling Pathway in C57BL/6 Mice Fed a High-Fat Diet. J Nutr 2019;150:672–684,.
[213] Shibata K, Ph D, Fukuwatari T, Ph D, A SHB, A CSB, et al. Pantothenic acid refeeding diminishes the liver , perinephrical fats , and plasma fats accumulated by pantothenic acid de fi ciency and / or ethanol consumption. Nutrition 2013;29:796–801. https://doi.org/10.1016/j.nut.2013.01.002.
[214] Zhao M, Yuan MM, Yuan L, Huang LL, Liao JH, Yu XL, et al. Chronic folate deficiency induces glucose and lipid metabolism disorders and subsequent cognitive dysfunction in mice. PLoS One 2018;13:1–16. https://doi.org/10.1371/journal.pone.0202910.
[215] Turgut M, Cinar V, Pala R, Tuzcu M, Orhan C, Telceken H, et al. Biotin and chromium histidinate improve glucose metabolism and proteins expression levels of IRS-1, PPAR-γ, and NF-KB in exercise-trained rats. J Int Soc Sports Nutr 2018;15:1–10. https://doi.org/10.1186/s12970-018-0249-4.
[216] Joske RA. The Vitamin B12 Content of Human Liver Tissue Obtained By Aspiration Biopsy. Gut 1963;4:231–5. https://doi.org/10.1136/gut.4.3.231.
[217] Ichihashi T, Takagishi Y, Uchida K, Yamada H. Nutrient Metabolism Colonic Absorption of Menaquinone-4 Menaquinone-9 in Rats and. J Nutr 1992;122:506–12.
[218] Nammacher MA, Willemin M, Gaston LW, Hartmann JR. Vitamin K deficiency in infants beyond the neonatal period. J Pediatr 1970;76:549–54. https://doi.org/doi.org/10.1016/S0022-3476(70)80404-8.
[219] Hope PL, Hall MA, Millward-Sadler GH, Normand ICS. Alpha-1-antitrypsin deficiency presenting as a bleeding diathesis in the newborn. Arch Dis Child 1982;57:68–70.
[220] Qin J, Chang M, Wang S, Liu Z, Zhu W, Wang Y, et al. Connexin 32-mediated cell-cell communication is essential for hepatic differentiation from human embryonic stem cells. Sci Rep 2016;6:1–16. https://doi.org/10.1038/srep37388.
[221] June L. Round* and Sarkis K. Mazmanian. The gut microbiome shapes intestinal immune responses during health and disease. Nat Rev Immunol 2009;9:313–23. https://doi.org/10.1038/nri2515.The.
[222] Belkaid Y, Hand TW. Role of the microbiota in immunity and inflammation. Cell 2014;157:121–41. https://doi.org/10.1016/j.cell.2014.03.011.
[223] BAUER H, HOROWITZ RE, LEVENSON SM, POPPER H. The response of the lymphatic tissue to the microbial flora. Studies on germfree mice. Am J Pathol 1963;42:471–83.
[224] Ruiz L, Hidalgo C, Blanco-Míguez A, Lourenço A, Sánchez B, Margolles A. Tackling probiotic and gut microbiota functionality through proteomics. J Proteomics 2016;147:28–39. https://doi.org/10.1016/j.jprot.2016.03.023.
[225] Blanco-Míguez A, Gutiérrez-Jácome A, Fdez-Riverola F, Lourenço A, Sánchez B. MAHMI database: A comprehensive MetaHitbased resource for the study of the mechanism of action of the human microbiota. Database 2017:1–10. https://doi.org/10.1093/database/baw157.
[226] Hidalgo-Cantabrana C, Moro-García MA, Blanco-Míguez A, Fdez-Riverola F, Lourenço A, Alonso-Arias R, et al. In silico screening of the human gut metaproteome identifies Th17-promoting peptides encrypted in proteins of commensal bacteria. Front Microbiol 2017;8:1–9.

https://doi.org/10.3389/fmicb.2017.01726.
[227] Samuel Fernández-Tomé, Alicia C. Marin LOM, Montserrat Baldan-Martin, Irene Mora-Gutiérrez AL-G, José Andrés Moreno-Monteagudo, Cecilio Santander, Borja Sánchez MC, Javier P. Gisbert DB. Immunomodulatory Effect of Gut Microbiota-Derived Bioactive Peptides on Human Immune System from Bowel Disease. Nutrients 2019;11:E2605.
[228] Sánchez B, Urdaci MC, Margolles A. Extracellular proteins secreted by probiotic bacteria as mediators of effects that promote mucosa-bacteria interactions. Microbiology 2010;156:3232–42. https://doi.org/10.1099/mic.0.044057-0.
[229] Belkaid Y, Naik S. Compartmentalized and systemic control of tissue immunity by commensals. Nat Immunol 2013;14:646–53. https://doi.org/10.1038/ni.2604.
[230] Planer JD, Peng Y, Kau AL, Blanton L V., Ndao IM, Tarr PI, et al. Development of the gut microbiota and mucosal IgA responses in twins and gnotobiotic mice. Nature 2016;534:263–6. https://doi.org/10.1038/nature17940.
[231] Cording S, Fleissner D, Heimesaat MM, Bereswill S, Loddenkemper C, Uematsu S, et al. Commensal microbiota drive proliferation of conventional and Foxp3 + Regulatory CD4 + T cells in mesenteric lymph nodes and Peyer's patches . Eur J Microbiol Immunol 2013;3:1–10. https://doi.org/10.1556/eujmi.3.2013.1.1.
[232] Temraz S, Nassar F, Nasr R, Charafeddine M, Mukherji D, Shamseddine A. Gut microbiome: A promising biomarker for immunotherapy in colorectal cancer. Int J Mol Sci 2019;20:1–11. https://doi.org/10.3390/ijms20174155.
[233] V. Gopalakrishnan et al. Gut microbiome modulates response to anti-PD-1 immunotherapy in melanoma patients. Science (80-) 2017;359:97–103. https://doi.org/10.1126/science.aan4236.
[234] Sommer F, Bäckhed F. The gut microbiota-masters of host development and physiology. Nat Rev Microbiol 2013;11:227–38. https://doi.org/10.1038/nrmicro2974.
[235] Collado MC, Rautava S, Aakko J, Isolauri E. Human gut colonisation may be initiated in utero by distinct microbial communities in the placenta and amniotic fluid. Nat Publ Gr 2016:1–13. https://doi.org/10.1038/srep23129.
[236] Digiulio DB. Seminars in Fetal & Neonatal Medicine Diversity of microbes in amniotic fl uid 2012;17:2–11. https://doi.org/10.1016/j.siny.2011.10.001.
[237] Ardissone AN, Cruz DM De, Davis-richardson AG, Rechcigl KT, Li N, Drew JC, et al. Meconium Microbiome Analysis Identifies Bacteria Correlated with Premature Birth 2014;9:1–8. https://doi.org/10.1371/journal.pone.0090784.
[238] Ma J, Prince AL, Bader D, Hu M, Ganu R, Baquero K, et al. High-fat maternal diet during pregnancy persistently alters the offspring microbiome in a primate model. Nat Commun 2014;5. https://doi.org/10.1038/ncomms4889.
[239] Ge ZJ, Luo SM, Lin F, Liang QX, Huang L, Wei YC, et al. DNA methylation in oocytes and liver of female mice and their offspring: Effects of high-fat-diet-induced obesity. Environ Health Perspect 2014;122:159–64. https://doi.org/10.1289/ehp.1307047.
[240] Dudley KJ, Sloboda DM, Connor KL, Beltrand J, Vickers MH. Offspring of mothers fed a high fat diet display hepatic cell cycle inhibition and associated changes in gene expression and DNA methylation. PLoS One 2011;6. https://doi.org/10.1371/journal.pone.0021662.
[241] Suter M, Bocock P, Showalter L, Hu M, Shope C, McKnight R, et al. Epigenomics: maternal high-fat diet exposure in utero disrupts peripheral circadian gene expression in nonhuman primates . FASEB J 2011;25:714–26. https://doi.org/10.1096/fj.10-172080.

[242] Wankhade UD, Zhong Y, Kang P, Alfaro M, Chintapalli S V., Thakali KM, et al. Enhanced offspring predisposition to steatohepatitis with maternal high-fat diet is associated with epigenetic and microbiome alterations. PLoS One 2017;12:1–21. https://doi.org/10.1371/journal.pone.0175675.
[243] Wankhade UD, Zhong Y, Kang P, Alfaro M, Chintapalli S V., Piccolo BD, et al. Maternal High-Fat Diet Programs Offspring Liver Steatosis in a Sexually Dimorphic Manner in Association with Changes in Gut Microbial Ecology in Mice. Sci Rep 2018;8:1–15. https://doi.org/10.1038/s41598-018-34453-0.
[244] Collado MC, Isolauri E, Laitinen K, Salminen S. Distinct composition of gut microbiota during pregnancy in overweight and normal-weight women. Am J Clin Nutr 2008;88:894–9. https://doi.org/10.1093/ajcn/88.4.894.
[245] Soderborg TK, Clark SE, Mulligan CE, Janssen RC, Babcock L, Ir D, et al. The gut microbiota in infants of obese mothers increases inflammation and susceptibility to NAFLD. Nat Commun 2018;9:1–12. https://doi.org/10.1038/s41467-018-06929-0.
[246] Argenio VD. The Prenatal Microbiome : A New Player for Human Health 2018:1–10. https://doi.org/10.3390/ht7040038.
[247] Pelzer E, Gomez-arango LF, Barrett HL, Dekker M. Review : Maternal health and the placental microbiome. Placenta 2017;54:30–7. https://doi.org/10.1016/j.placenta.2016.12.003.
[248] Thorburn AN, McKenzie CI, Shen S, Stanley D, MacIa L, Mason LJ, et al. Evidence that asthma is a developmental origin disease influenced by maternal diet and bacterial metabolites. Nat Commun 2015;6. https://doi.org/10.1038/ncomms8320.
[249] Zheng W, Zhao W, Wu M, Song X, Caro F, Sun X, et al. Microbiota-targeted maternal antibodies protect neonates from enteric infection. Nature 2020;577:543–8. https://doi.org/10.1038/s41586-019-1898-4.
[250] Kimura I, Miyamoto J, Ohue-Kitano R, Watanabe K, Yamada T, Onuki M, et al. Maternal gut microbiota in pregnancy influences offspring metabolic phenotype in mice. Science (80-) 2020;367. https://doi.org/10.1126/science.aaw8429.
[251] Stewart CJ, Ajami NJ, O'Brien JL, Hutchinson DS, Smith DP, Wong MC, et al. Temporal development of the gut microbiome in early childhood from the TEDDY study. Nature 2018;562:583–8. https://doi.org/10.1038/s41586-018-0617-x.
[252] Kundu P, Blacher E, Elinav E, Pettersson S. Our Gut Microbiome : The Evolving Inner Self. Cell 2017;171:1481–93. https://doi.org/10.1016/j.cell.2017.11.024.
[253] Robertson RC, Manges AR, Finlay BB, Prendergast AJ. The Human Microbiome and Child Growth – First 1000 Days and Beyond. Trends Microbiol 2018;xx:1–17. https://doi.org/10.1016/j.tim.2018.09.008.
[254] Dominguez-bello MG, Costello EK, Contreras M, Magris M, Hidalgo G. Delivery mode shapes the acquisition and structure of the initial microbiota across multiple body habitats in newborns 2010;107:11971–5. https://doi.org/10.1073/pnas.1002601107.
[255] Dominguez-Bello MG, De Jesus-Laboy KM, Shen N, Cox LM, Amir A, Gonzalez A, et al. Partial restoration of the microbiota of cesarean-born infants via vaginal microbial transfer. Nat Med 2016;22:250–3. https://doi.org/10.1038/nm.4039.
[256] Shao Y, Forster SC, Tsaliki E, Vervier K, Strang A, Simpson N, et al. Stunted microbiota and opportunistic pathogen colonization in caesarean-section birth. Nature 2019;574:117–21. https://doi.org/10.1038/s41586-019-1560-1.
[257] Reyman M, van Houten MA, van Baarle D, Bosch AATM, Man WH, Chu MLJN,

et al. Impact of delivery mode-associated gut microbiota dynamics on health in the first year of life. Nat Commun 2019;10:1–12. https://doi.org/10.1038/s41467-019-13014-7.
[258] Wampach L, Heintz-Buschart A, Fritz J V., Ramiro-Garcia J, Habier J, Herold M, et al. Birth mode is associated with earliest strain-conferred gut microbiome functions and immunostimulatory potential. Nat Commun 2018;9. https://doi.org/10.1038/s41467-018-07631-x.
[259] Su GL, Klein RD, Aminlari A, Zhang HY, Steinstraesser L, Alarcon WH, et al. Kupffer cell activation by lipopolysaccharide in rats: Role for lipopolysaccharide binding protein and Toll-like receptor 4. Hepatology 2000;31:932–6. https://doi.org/10.1053/he.2000.5634.
[260] Lee YS, Kim YH, Jung YS, Kim KS, Kim DK, Na SY, et al. Hepatocyte toll-like receptor 4 mediates lipopolysaccharide-induced hepcidin expression. Exp Mol Med 2017;49:e408-9. https://doi.org/10.1038/emm.2017.207.
[261] Lanone S, Bloc S, Foresti R, Almolki A, Taillé C, Callebert J, et al. Bilirubin decreases NOS2 expression via inhibition of NAD(P)H oxidase: implications for protection against endotoxic shock in rats. FASEB J 2005;19:1890–2. https://doi.org/10.1096/fj.04-2368fje.
[262] Hansen R, Gibson S, De Paiva Alves E, Goddard M, MacLaren A, Karcher AM, et al. Adaptive response of neonatal sepsis-derived Group B Streptococcus to bilirubin. Sci Rep 2018;8:1–10. https://doi.org/10.1038/s41598-018-24811-3.
[263] Dong T, Chen T, White RA, Wang X, Hu W, Liang Y, et al. Meconium microbiome associates with the development of neonatal jaundice. Clin Transl Gastroenterol 2018;9. https://doi.org/10.1038/s41424-018-0048-x.
[264] Yoshioka H, Iseki K, Fujita K. Development and Differences of Intestinal Flora in the Neonatal Period in Breast-Fed and Bottle-Fed Infants. Pediatrics 1983;72:317 LP – 321.
[265] Stark PL, Lee A. Clostridia isolated from the feces of infants during the first year of life. J Pediatr 1982;100:362–5. https://doi.org/10.1016/S0022-3476(82)80430-7.
[266] Marcobal A, Barboza M, Sonnenburg ED, Pudlo N, Martens EC, Desai P, et al. Bacteroides in the infant gut consume milk oligosaccharides via mucus-utilization pathways. Cell Host Microbe 2011;10:507–14. https://doi.org/10.1016/j.chom.2011.10.007.
[267] Lönnerdal B. Nutritional and physiologic significance of human milk proteins. Am J Clin Nutr 2003;77. https://doi.org/10.1093/ajcn/77.6.1537s.
[268] Arifeen S, Black RE, Antelman G, Baqui A, Caulfield L, Becker S. Exclusive breastfeeding reduces acute respiratory infection and diarrhea deaths among infants in Dhaka slums. Pediatrics 2001;108:1–8. https://doi.org/10.1542/peds.108.4.e67.
[269] Verhasselt V, Milcent V, Cazareth J, Kanda A, Fleury S, Dombrowicz D, et al. Breast milk-mediated transfer of an antigen induces tolerance and protection from allergic asthma. Nat Med 2008;14:170–5. https://doi.org/10.1038/nm1718.
[270] Liang G, Zhao C, Zhang H, Mattei L, Sherrill-Mix S, Bittinger K, et al. The stepwise assembly of the neonatal virome is modulated by breastfeeding. Nature 2020. https://doi.org/10.1038/s41586-020-2192-1.
[271] Bokulich NA, Chung J, Battaglia T, Henderson N, Jay M, Li H, et al. Antibiotics, birth mode, and diet shape microbiome maturation during early life. Sci Transl Med 2016;8:1–14. https://doi.org/10.1126/scitranslmed.aad7121.
[272] Song X, Sun X, Oh SF, Wu M, Zhang Y, Zheng W, et al. Microbial bile acid

metabolites modulate gut RORγ+ regulatory T cell homeostasis. Nature 2020;577:410–5. https://doi.org/10.1038/s41586-019-1865-0.
[273] Campbell C, McKenney PT, Konstantinovsky D, Isaeva OI, Schizas M, Verter J, et al. Bacterial metabolism of bile acids promotes generation of peripheral regulatory T cells. Nature 2020. https://doi.org/10.1038/s41586-020-2193-0.
[274] Mazmanian SK, Cui HL, Tzianabos AO, Kasper DL. An immunomodulatory molecule of symbiotic bacteria directs maturation of the host immune system. Cell 2005;122:107–18. https://doi.org/10.1016/j.cell.2005.05.007.
[275] Durkin HG, Bazin H, Waksman BH. Origin and fate of IgE-bearing lymphocytes: I. Peyer's patches as differentiation site of cells simultaneously bearing IgA and IgE. J Exp Med 1981;154:640–8. https://doi.org/10.1084/jem.154.3.640.
[276] Bouskra D, Brézillon C, Bérard M, Werts C, Varona R, Boneca IG, et al. Lymphoid tissue genesis induced by commensals through NOD1 regulates intestinal homeostasis. Nature 2008;456:507–10. https://doi.org/10.1038/nature07450.
[277] Ribo S, Sanchez-Infantes D, Martinez-Guino l et al. Increasing breast milk betaine modulates Akkermansia abundance in mammalian neonates and improves long-term metabolic health. Sci Transl Med 2021;13. https://doi.org/10.1126/scitranslmed.abb0322.
[278] Chu DM, Ma J, Prince AL, Antony KM, Seferovic MD, Aagaard KM. Maturation of the infant microbiome community structure and function across multiple body sites and in relation to mode of delivery. Nat Med 2017;23:314–26. https://doi.org/10.1038/nm.4272.
[279] Selwyn FP, Cheng SL, Bammler TK, Prasad B, Vrana M, Klaassen C, et al. Developmental regulation of drug-processing genes in livers of germ-free mice. Toxicol Sci 2015;147:84–103. https://doi.org/10.1093/toxsci/kfv110.
[280] Sela DA, Chapman J, Adeuya A, Kim JH, Chen F, Whitehead TR, et al. The genome sequence of Bifidobacterium longum subsp. infantis reveals adaptations for milk utilization within the infant microbiome. Proc Natl Acad Sci U S A 2008;105:18964–9. https://doi.org/10.1073/pnas.0809584105.
[281] Autran CA, Kellman BP, Kim JH, Asztalos E, Blood AB, Spence ECH, et al. Human milk oligosaccharide composition predicts risk of necrotising enterocolitis in preterm infants. Gut 2018;67:1064–70. https://doi.org/10.1136/gutjnl-2016-312819.
[282] Ramani S, Stewart CJ, Laucirica DR, Ajami NJ, Robertson B, Autran CA, et al. Human milk oligosaccharides, milk microbiome and infant gut microbiome modulate neonatal rotavirus infection. Nat Commun 2018;9:1–12. https://doi.org/10.1038/s41467-018-07476-4.
[283] Pokusaeva K, Fitzgerald GF, Van Sinderen D. Carbohydrate metabolism in Bifidobacteria. Genes Nutr 2011;6:285–306. https://doi.org/10.1007/s12263-010-0206-6.
[284] Charbonneau MR, O'Donnell D, Blanton L V., Totten SM, Davis JCC, Barratt MJ, et al. Sialylated Milk Oligosaccharides Promote Microbiota-Dependent Growth in Models of Infant Undernutrition. Cell 2016;164:859–71. https://doi.org/10.1016/j.cell.2016.01.024.
[285] Baumann-Dudenhoeffer AM, D'Souza AW, Tarr PI, Warner BB, Dantas G. Infant diet and maternal gestational weight gain predict early metabolic maturation of gut microbiomes. Nat Med 2018;24:1822–9. https://doi.org/10.1038/s41591-018-0216-2.
[286] Bridgman SL, Azad MB, Field CJ, Haqq AM, Becker AB, Mandhane PJ, et al.

Fecal Short-Chain Fatty Acid Variations by Breastfeeding Status in Infants at 4 Months: Differences in Relative versus Absolute Concentrations. Front Nutr 2017;4. https://doi.org/10.3389/fnut.2017.00011.
[287] Mercer KE, Bhattacharyya S, Diaz-Rubio ME, Piccolo BD, Pack LM, Sharma N, et al. Infant formula feeding increases hepatic cholesterol 7α Hydroxylase (CYP7A1) Expression and fecal bile acid loss in neonatal piglets. J Nutr 2018;148:702–11. https://doi.org/10.1093/jn/nxy038.
[288] Blake MJ, Abdel-Rahman SM, Pearce RE, Leeder JS, Kearns GL. Effect of diet on the development of drug metabolism by cytochrome P-450 enzymes in healthy infants. Pediatr Res 2006;60:717–23. https://doi.org/10.1203/01.pdr.0000245909.74166.00.
[289] Sung V, Collett S, De Gooyer T, Hiscock H, Tang M, Wake M. Probiotics to prevent or treat excessive infant crying systematic review and meta-analysis. JAMA Pediatr 2013;167:1150–7. https://doi.org/10.1001/jamapediatrics.2013.2572.
[290] Liu Y, Tian X, He B, Hoang TK, Taylor CM, Blanchard E, et al. Lactobacillus reuteri DSM 17938 feeding of healthy newborn mice regulates immune responses while modulating gut microbiota and boosting beneficial metabolites. J Am J Physiol Liver Physiol 2019;317:824–38. https://doi.org/doi.org/10.1152/ajpgi.00107.2019.
[291] Angelakis E, Bastelica D, Ben Amara A, El Filali A, Dutour A, Mege JL, et al. An evaluation of the effects of Lactobacillus ingluviei on body weight, the intestinal microbiome and metabolism in mice. Microb Pathog 2012;52:61–8. https://doi.org/10.1016/j.micpath.2011.10.004.
[292] Hawdon JM, Ward Platt MP, Aynsley-Green A. Patterns of metabolic adaptation for preterm and term infants in the first neonatal week. Arch Dis Child 1992;67:357–65. https://doi.org/10.1136/adc.67.4_Spec_No.357.
[293] Heilig H, Bustos G, Fuentes S, Vos W De, Moles L, Go M, et al. Bacterial Diversity in Meconium of Preterm Neonates and Evolution of Their Fecal Microbiota during the First Month of Life 2013;8. https://doi.org/10.1371/journal.pone.0066986.
[294] Yatsunenko T, Rey FE, Manary MJ, Trehan I, Dominguez-bello MG, Contreras M, et al. Human gut microbiome viewed across age and geography 2012. https://doi.org/10.1038/nature11053.
[295] Bäckhed F, Roswall J, Peng Y, Feng Q, Jia H, Kovatcheva-Datchary P, et al. Dynamics and stabilization of the human gut microbiome during the first year of life. Cell Host Microbe 2015;17:690–703. https://doi.org/10.1016/j.chom.2015.04.004.
[296] Henning SJ. Postnatal development: coordination of feeding, digestion, and metabolism. Am J Physiol Liver Physiol 1981;241:G199–214. https://doi.org/10.1152/ajpgi.1981.241.3.G199.
[297] Nakagaki BN, Mafra K, de Carvalho É, Lopes ME, Carvalho-Gontijo R, de Castro-Oliveira HM, et al. Immune and metabolic shifts during neonatal development reprogram liver identity and function. J Hepatol 2018;69:1294–307. https://doi.org/10.1016/j.jhep.2018.08.018.
[298] Differding MK, Benjamin-Neelon SE, Hoyo C, Østbye T, Mueller NT. Timing of complementary feeding is associated with gut microbiota diversity and composition and short chain fatty acid concentrations over the first year of life. BMC Microbiol 2020;20:56. https://doi.org/10.1186/s12866-020-01723-9.
[299] Gola A, Dorrington MG, Speranza E, Sala C, Shih RM, Radtke AJ, et al.

Commensal-driven immune zonation of the liver promotes host defence. Nature 2021;589:131–6. https://doi.org/10.1038/s41586-020-2977-2.
[300] Lin S, Yang X, Yuan P, Yang J, Wang P, Zhong H, et al. Undernutrition Shapes the Gut Microbiota and Bile Acid Profile in Association with Altered Gut-Liver FXR Signaling in Weaning Pigs. J Agric Food Chem 2019;67:3691–701. https://doi.org/10.1021/acs.jafc.9b01332.
[301] Subramanian S, Huq S, Yatsunenko T, Haque R, Mahfuz M, Alam MA, et al. Persistent gut microbiota immaturity in malnourished Bangladeshi children. Nature 2014;510:417–21. https://doi.org/10.1038/nature13421.
[302] Blanton L V., Charbonneau MR, Salih T, Barratt MJ, Venkatesh S, Ilkaveya O, et al. Gut bacteria that prevent growth impairments transmitted by microbiota from malnourished children. Science (80-) 2016;351. https://doi.org/10.1126/science.aad3311.
[303] Srutkova D, Hermanova P, Martino ME, Balmand S, Hudcovic T, Heddi A, et al. Lactobacillus plantarum strain maintains growth of infant mice during chronic undernutrition. Science (80-) 2016;351:854–7. https://doi.org/10.1126/science.aad8588.
[304] Yan J, Herzog JW, Tsang K, Brennan CA, Bower MA, Garrett WS, et al. Gut microbiota induce IGF-1 and promote bone formation and growth. Proc Natl Acad Sci U S A 2016;113:E7554–63. https://doi.org/10.1073/pnas.1607235113.
[305] LeRoith D, Yakar S. Mechanisms of disease: Metabolic effects of growth hormone and insulin-like growth factor 1. Nat Clin Pract Endocrinol Metab 2007;3:302–10. https://doi.org/10.1038/ncpendmet0427.
[306] Kineman RD, del Rio-Moreno M, Sarmento-Cabral A. 40 years of IGF1: Understanding the tissue-specific roles of IGF1/IGF1R in regulating metabolism using the Cre/loxP system. J Mol Endocrinol 2018;61:T187–98. https://doi.org/10.1530/JME-18-0076.
[307] Gasparrini AJ, Wang B, Sun X, Kennedy EA, Hernandez-Leyva A, Ndao IM, et al. Persistent metagenomic signatures of early-life hospitalization and antibiotic treatment in the infant gut microbiota and resistome. Nat Microbiol 2019;4:2285–97. https://doi.org/10.1038/s41564-019-0550-2.
[308] Piñeiro-Carrero VM, Piñeiro EO. Liver. Pediatrics 2004;113:1097 LP – 1106.
[309] Puiman P, Stoll B, Mølbak L, de Bruijn A, Schierbeek H, Boye M, et al. Modulation of the gut microbiota with antibiotic treatment suppresses whole body urea production in neonatal pigs. Am J Physiol - Gastrointest Liver Physiol 2013;304:300–10. https://doi.org/10.1152/ajpgi.00229.2011.
[310] Wan JJ, Lin CH, Ren E Du, Su Y, Zhu WY. Effects of early intervention with maternal fecal bacteria and antibiotics on liver metabolome and transcription in neonatal pigs. Front Physiol 2019;10:1–12. https://doi.org/10.3389/fphys.2019.00171.
[311] Cho I, Yamanishi S, Cox L, Methé BA, Zavadil J, Li K, et al. Antibiotics in early life alter the murine colonic microbiome and adiposity. Nature 2012;488:621–6. https://doi.org/10.1038/nature11400.
[312] Cox LM, Yamanishi S, Sohn J, Alekseyenko A V., Leung JM, Cho I, et al. Altering the intestinal microbiota during a critical developmental window has lasting metabolic consequences. Cell 2014;158:705–21. https://doi.org/10.1016/j.cell.2014.05.052.
[313] Cheng J, Ringel-Kulka T, Heikamp-De Jong I, Ringel Y, Carroll I, De Vos WM, et al. Discordant temporal development of bacterial phyla and the emergence of core in the fecal microbiota of young children. ISME J 2016;10:1002–14.

https://doi.org/10.1038/ismej.2015.177.
[314] Hollister EB, Riehle K, Luna RA, Weidler EM, Rubio-Gonzales M, Mistretta TA, et al. Structure and function of the healthy pre-adolescent pediatric gut microbiome. Microbiome 2015;3:36. https://doi.org/10.1186/s40168-015-0101-x.
[315] Zhong H, Penders J, Shi Z, Ren H, Cai K, Fang C, et al. Impact of early events and lifestyle on the gut microbiota and metabolic phenotypes in young school-age children. Microbiome 2019;7:1–14. https://doi.org/10.1186/s40168-018-0608-z.
[316] Fouhy F, Watkins C, Hill CJ, O'Shea CA, Nagle B, Dempsey EM, et al. Perinatal factors affect the gut microbiota up to four years after birth. Nat Commun 2019;10:1–10. https://doi.org/10.1038/s41467-019-09252-4.
[317] Beath S V. Hepatic function and physiology in the newborn. Semin Neonatol 2003;8:337–46. https://doi.org/10.1016/S1084-2756(03)00066-6.
[318] Kodidela S, Kumar SS, Rao C, Uppugunduri S. Developmental Pattern of Hepatic Drug-Metabolizing Enzymes in Pediatric Population and its Role in Optimal Drug Treatment. Arch Med Heal Sci 2017;5:115–22.
[319] Wu GD, Chen J, Hoffmann C, Bittinger K, Chen Y-Y, Keilbaugh SA, et al. Linking Long-Term Dietary Patterns with Gut Microbial Enterotypes. Science (80-) 2011;334:105–9. https://doi.org/10.1126/science.1208344.
[320] Leung DH, Yimlamai D. The intestinal microbiome and paediatric liver disease. Lancet Gastroenterol Hepatol 2017;2:446–55. https://doi.org/10.1016/S2468-1253(16)30241-2.
[321] Belei O, Olariu L, Dobrescu A, Marcovici T, Marginean O. The relationship between non-alcoholic fatty liver disease and small intestinal bacterial overgrowth among overweight and obese children and adolescents. J Pediatr Endocrinol Metab 2017;30:1161–8. https://doi.org/10.1515/jpem-2017-0252.
[322] Agans R, Rigsbee L, Kenche H, Michail S, Khamis HJ, Paliy O. Distal gut microbiota of adolescent children is different from that of adults. FEMS Microbiol Ecol 2011;77:404–12. https://doi.org/10.1111/j.1574-6941.2011.01120.x.
[323] Hormone-dependent MD, Markle JGM, Frank DN, Mortin-toth S, Robertson CE, Feazel LM, et al. Sex Differences in the Gut Microbiome Drive Hormone-Dependent Regulation of Autoimmunity. Science (80-) 2013;339:1084–8. https://doi.org/10.1126/science.1233521.
[324] Yang X, Schadt EE, Wang S, Wang H, Arnold AP, Ingram-Drake L, et al. Tissue-specific expression and regulation of sexually dimorphic genes in mice. Genome Res 2006;16:995–1004. https://doi.org/10.1101/gr.5217506.
[325] Mode A, Gustafsson JÅ. Sex and the liver - A journey through five decades. Drug Metab Rev 2006;38:197–207. https://doi.org/10.1080/03602530600570057.
[326] Soler-Argilaga C, Danon A, Goh E, Wilcox HG, Heimberg M. The effect of sex on the uptake of very low density lipoprotein triglyceride fatty acid from the plasma of the rat in vivo. Biochem Biophys Res Commun 1975;66:1237–42.
[327] Kushlan MC, Gollan JL, Ma WL, Ockner RK. Sex differences in hepatic uptake of long chain fatty acids in single-pass perfused rat liver. J Lipid Res 1981;22:431–6.
[328] Ivey PA, Gaesser GA. Postexercise muscle and liver glycogen metabolism in male and female rats. J Appl Physiol 1987;62:1250–4. https://doi.org/10.1152/jappl.1987.62.3.1250.
[329] Waxman DJ, Holloway MG. Sex differences in the expression of hepatic drug

metabolizing enzymes. Mol Pharmacol 2009;76:215–28. https://doi.org/10.1124/mol.109.056705.
[330] Zhang H, Wu X, Wang H, Mikheev AM, Mao Q, Unadkat JD. Effect of pregnancy on cytochrome P450 3a and P-glycoprotein expression and activity in the mouse: Mechanisms, tissue specificity, and time course. Mol Pharmacol 2008;74:714–23. https://doi.org/10.1124/mol.107.043851.
[331] Shimizu K, Muranaka Y, Fujimura R, ISHIDA H, TAZUME S, SHIMAMURA T. Normalization of reproductive function in germfree mice following bacterial contamination. Exp Anim 1998;47:151–8.
[332] Weger BD, Gobet C, Yeung J, Martin E, Jimenez S, Betrisey B, et al. The Mouse Microbiome Is Required for Sex-Specific Diurnal Rhythms of Gene Expression and Metabolism. Cell Metab 2019;29:362-382.e8. https://doi.org/10.1016/j.cmet.2018.09.023.
[333] Faith JJ, Guruge JL, Charbonneau M, Subramanian S, Seedorf H, Goodman AL, et al. The long-term stability of the human gut microbiota. Science (80-) 2013;341. https://doi.org/10.1126/science.1237439.
[334] Turpin W, Espin-Garcia O, Xu W, Silverberg MS, Kevans D, Smith MI, et al. Association of host genome with intestinal microbial composition in a large healthy cohort. Nat Genet 2016;48:1413–7. https://doi.org/10.1038/ng.3693.
[335] Rothschild D, Weissbrod O, Barkan E, Kurilshikov A, Korem T, Zeevi D, et al. Environment dominates over host genetics in shaping human gut microbiota. Nature 2018;555:210–5. https://doi.org/10.1038/nature25973.
[336] David LA, Maurice CF, Carmody RN, Gootenberg DB, Button JE, Wolfe BE, et al. Diet rapidly and reproducibly alters the human gut microbiome. Nature 2014;505:559–63. https://doi.org/10.1038/nature12820.
[337] Dethlefsen L, Relman DA. Incomplete recovery and individualized responses of the human distal gut microbiota to repeated antibiotic perturbation. Proc Natl Acad Sci U S A 2011;108:4554–61. https://doi.org/10.1073/pnas.1000087107.
[338] Colebrook L, Buttle GAH, O'Meara RAQ. The mode of action of p-aminobenzene sulphonamide and prontosil in hemolytic streptococcal infections. Lancet 1936;228:1323–6. https://doi.org/10.1016/S0140-6736(00)48181-X.
[339] Spanogiannopoulos P, Bess EN, Carmody RN, Turnbaugh PJ. The microbial pharmacists within us: A metagenomic view of xenobiotic metabolism. Nat Rev Microbiol 2016;14:273–87. https://doi.org/10.1038/nrmicro.2016.17.
[340] Zimmermann M, Zimmermann-Kogadeeva M, Wegmann R, Goodman AL. Mapping human microbiome drug metabolism by gut bacteria and their genes. Nature 2019;570:462–7. https://doi.org/10.1038/s41586-019-1291-3.
[341] Björkholm B, Bok CM, Lundin A, Rafter J, Hibberd ML, Pettersson S. Intestinal microbiota regulate xenobiotic metabolism in the liver. PLoS One 2009;4. https://doi.org/10.1371/journal.pone.0006958.
[342] Zhang L, Meng J, Ban Y, Jalodia R, Chupikova I, Fernandez I, et al. Morphine tolerance is attenuated in germfree mice and reversed by probiotics, implicating the role of gut microbiome. Proc Natl Acad Sci U S A 2019;116:13523–32. https://doi.org/10.1073/pnas.1901182116.
[343] Claus SP, Ellero SL, Berger B, Krause L, Bruttin A, Molina J, et al. Colonization-Induced Host-Gut Microbial Metabolic Interaction 2011;2:1–8. https://doi.org/10.1128/mBio.00271-10.Editor.
[344] Selwyn FP, Cui JY, Klaassen CD. Special section on drug metabolism and the microbiome RNA-seq quantification of hepatic drug processing genes in germ-

free mice. Drug Metab Dispos 2015;43:1572–80. https://doi.org/10.1124/dmd.115.063545.
[345] Toda T, Ohi K, Kudo T, Yoshida T, Ikarashi N, Ito K, et al. Ciprofloxacin Suppresses Cyp3a in Mouse Liver by. Flora 2009;24:201–8.
[346] Thaiss CA, Levy M, Korem T, Dohnalová L, Shapiro H, Jaitin DA, et al. Microbiota Diurnal Rhythmicity Programs Host Transcriptome Oscillations. Cell 2016;167:1495-1510.e12. https://doi.org/10.1016/j.cell.2016.11.003.
[347] Gong S, Lan T, Zeng L, Luo H, Yang X, Li N, et al. Gut microbiota mediates diurnal variation of acetaminophen induced acute liver injury in mice. J Hepatol 2018;69:51–9. https://doi.org/10.1016/j.jhep.2018.02.024.
[348] Cornell RP, Liljequist BL, Bartizal KF. Depressed liver regeneration after partial hepatectomy of germ-free, athymic and lipopolysaccharide-resistant mice. Hepatology 1990;11:916–22. https://doi.org/10.1002/hep.1840110603.
[349] Liu HX, Rocha CS, Dandekar S, Yvonne Wan YJ. Functional analysis of the relationship between intestinal microbiota and the expression of hepatic genes and pathways during the course of liver regeneration. J Hepatol 2016;64:641–50. https://doi.org/10.1016/j.jhep.2015.09.022.
[350] Medeiros AC, Azevedo ACB, Oséas JM de F, Gomes MDF, de Oliveira FG, Rocha KBF, et al. The ileum positively regulates hepatic regeneration in rats. Acta Cir Bras 2014;29:93–8. https://doi.org/10.1590/S0102-86502014000200004.

Chapter 2

THE EFFECT OF MICROBIOTA SECRETOME ON HPSC-HLC FUNCTIONALITY

Contents

1. Graphical abstract

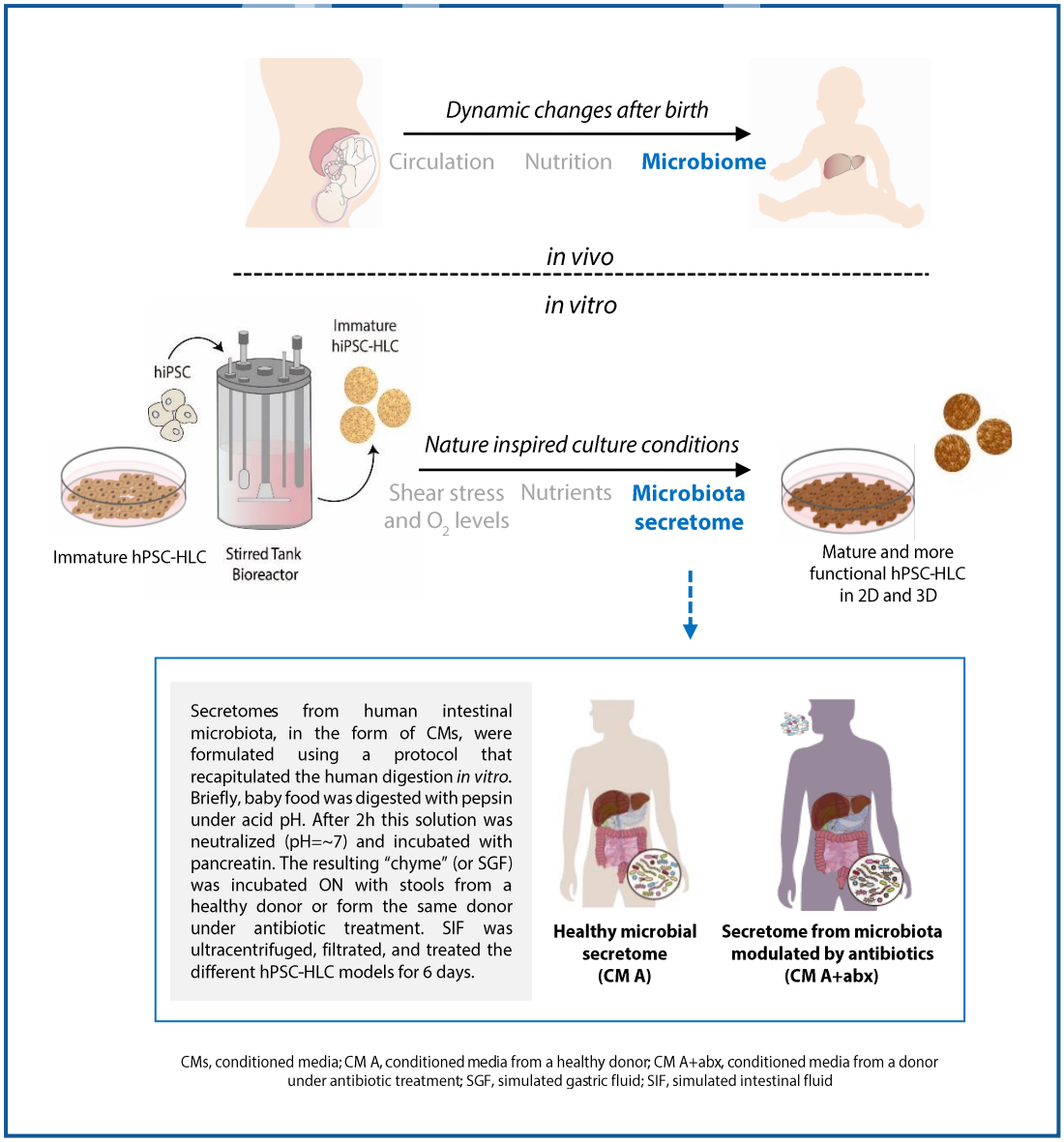

CMs, conditioned media; CM A, conditioned media from a healthy donor; CM A+abx, conditioned media from a donor under antibiotic treatment; SGF, simulated gastric fluid; SIF, simulated intestinal fluid

2. Introduction

Approximately two million people die from liver disease annually. Decompensated cirrhosis and hepatocellular carcinoma are the leading causes of death and together represent 3.5% of global mortality [1]. Epidemiological studies indicate that liver disease is also associated with increased morbidity, low quality of life and high economic costs [2], and its etiology (i.e., viral hepatitis, alcohol-related and non-alcoholic fatty liver diseases, etc.) varies according to the region [1]. Regardless, the natural loss of hepatic function is related to poor clinical prognosis and is usually proceeded by systemic organ decompensation, coma and eventually, death.

Liver transplantation (LT) has been perceived as the ultimate treatment option for these patients but although the liver is the second most common organ transplanted, less than 10% of global transplantation needs are met. According to the Organ Procurement and Transplantation Network, only 8,906 livers were transplanted in 2020, and approximately 20% of patients on the LT waiting list die or become too ill to be transplanted [3]. The sobering prevalence of liver disease, the increasing indications for LT and the consequent shortage of donor organs highlight the need for alternative therapeutic solutions for these patients.

Owing to the exciting preclinical observations [4–8], transplantation of primary human hepatocytes (PHH), derived from unused or deemed unsuitable organs for transplantation, has made the transition from bench to bedside [9–14]. Although significant accomplishments have been made, there are still some clinical limitations regarding PHH transplantation. To our knowledge, there is no evidence of metabolic disease patients (except for acute liver failure patients) that have been completely cured of the long-term symptoms of their disease by PHH transplantation only. Also, PHH are limited in supply, vary in their metabolic activity between donors, showed limited engraftment capacities and loss of long-term functionality *in vitro* [15,16].

Stem-cell therapies using either liver-derived or human pluripotent stem cells (hPSC) have been proposed as alternatives to PHH. The latter consists of human embryonic stem cells (hESC) and human induced pluripotent stem cells (hiPSC) and are characterized by their ability to indefinitely self-renew, the capacity to differentiate into multiple lineages and donor/patient specificity.

The past decade has witnessed significant advances in hPSC technology, and although hPSC-derived hepatocytes (known as hepatocyte-like cells, HLC) can be now successfully differentiated *in vitro* [17,18], their functionality was still more comparable to fetal than adult counterparts [19]. A more recent study claimed the opposite [20]; however, there is still limited consensus regarding what defines the state of “cell maturation” [21].

As HLC showing genomic instability and traits of fetal-adult origin, alternative strategies to improve cell maturation and function have been described [22]. These include, immortalization methods [23]; co-culture with nonparenchymal cells [24–27]; bioprinting techniques [28–30], more sophisticated culture systems [31–34]. Although promising, these approaches showed only modest improvements and are far from resembling nature.

Understanding how cells physiologically mature and get specialized in different tasks is of great importance as it will allow the development of more biological relevant strategies that ultimately will harness the potential of HLC.

Lessons from developmental biology revealed that the liver matures in a 2-year process mediated by events occurring at the environmental and cellular levels during the postnatal period. Among these events, the establishment and diversification of the microbiome in the gut has been extensively associated with acquisition of maturity. This association has been attributed to microbial molecules that are secreted by intestinal bacteria and reach the liver through the portal vein [35]. At the hepatic level, these postbiotics interact with specific membrane and nuclear receptors [36,37], induce transcriptional gene expression via epigenetic modulation [38,39] and have anti-lipogenic, anti-oxidant and anti-inflammatory effects which, ultimately, lead to cell survival and even tissue regeneration [40]. Studies on germ-free animals supported this hypothesis by reporting a dissimilar xenobiotic enzyme profile [41] and an impaired liver regeneration after partial hepatectomy [42] when compared to conventional counterparts.

The potential of microbiome as a biotechnological tool to produce more functional and mature HLC was still not addressed.

3. Aim

In this study, we investigated the effect of human intestinal microbiome on the functionality of HLC differentiated from three hPSC lines.

To address that, we formulated two microbial secretomes (hereafter designated as conditioned medium, CM) using a protocol that mimics the human digestion *in vitro* [43], using stools from an adult donor before and after treatment with antibiotics (hereafter designated as CM A and CM A+abx, respectively). To ensure their correct preparation, both CMs were characterized for their content in bile acids (BA), short-chain fatty acids (SCFA) and vitamins and immediately after formulation.

To evaluate their impact on the hPSC-HLC functionality, both 2D monolayers and 3D aggregates of HLC were treated, for additional 6 days, with CM A or CM A+abx and their phenotype and functionality were compared with untreated counterparts.

4. Materials and methods

4.1. Microbial secretome

4.1.1. Formulation

Microbial secretomes, in the form of conditioned media (CMs), were formulated *in vitro* using a static model of human digestion [43].

In brief, gastric phase was simulated through the digestion of commercial baby food (NESTLE, Naturnes Selección), previously dissolved in sterile Milli-Q water, with pepsin (0.4mg/mL) under acidic pH (incubation parameters: 150 rpm, pH~2.88, 37ºC). Two hours later, simulated gastric fluid (SGF) was neutralized (pH~6.87) and incubated with pancreatin (25.000 U) (incubation parameters: 150 rpm, 2h at 37°C). To recapitulate the intestinal phase, SGF (or chyme) was incubated with different human stools. Thus, conditioned medium adult (CM A) was prepared with feces from a healthy adult while CM adult+antibiotics (CM A+abx) was formulated using feces from the same donor after a treatment with antibiotics*. Bacterial fermentation occurred under anaerobic conditions (incubation parameters: 150 rpm, overnight (ON) at 37ºC).

In the next day, simulated intestinal fluid (SIF) was ultracentrifuged twice (6000 rpm, 4°C, 8min); and the supernatants (CMs) were filtered (Merck, CLS430521) and used to treat different hPSC-HLC models.

*Human stools: stool samples were collected from a 25 years old healthy female and from the same female under a 10 weeks-cycle antibiotic treatment (Clindamycin (600mg/day) and Rifampicin (600mg/day)) for hidradenitis suppurativa [44].

4.1.2. Chemical characterization

Conditioned media were characterized using sophisticated chemical analytic techniques, a service provided by Creative Proteomics (USA). Thereby, bile acids (n=66 kinds), vitamins and vitamin-like compounds (n=35) were quantified by ultra-performance liquid chromatography-multiple reaction monitoring mass spectrometry (UPLC/MRM-MS), while short-chain fatty acids (n=7) were measured by gas chromatography-mass spectrometry (GC-MS) using the methodologies implemented by this company.

4.2. The effect of CMs in hPSC-HLC

4.2.1. The first hepatic model: hESC-HLC

4.2.1.1. Expansion of hESC and differentiation into HLC

In this study, we used the human ESC line ES4. This line was kindly provided by *Banco Nacional de Líneas Celulares del Instituto de Salud Carlos III* and approved by the regional authority, *Comisión de Garantías del Instituto de Salud Carlos III*. Colonies of hESC were routinely expanded in feeder-free Matrigel® coated 6-well plates using mTeSR1™ (StemCell Technologies, 85850) and daily medium changes. Plates were coated with 2.5% v/v Matrigel (Corning, 354234) in KnockOut DMEM (Gibco,10829018) for 1h at room temperature (RT). When reaching 70% confluence, cells were passed 1:6-1:15 using ReLeSR (StemCell Technologies, 05872) between the 20th and 40th passage.

Differentiation of hESC into HLC was based on an adapted protocol from Mallanna et al. that applies sequential addition of growth factors to recapitulate the critical developmental events occurring during *in vivo* hepatogenesis [45] (Fig. 1). To initiate the differentiation process, hESC were cultured to 80% confluence. Cells were detached with Accutase (Sigma, A6964), seeded at a density of 125.000 cells/well in 48-well plates (Biolite, 130187), and cultured in mTeSR1™ supplemented with 2 μM Thiazovivin (Tocris, 3485) in a 4% O2 incubator. In the day after, corresponding to the 1st day of differentiation, hESC were cultured in adv. RPMI medium (Gibco, 12633), containing 1% v/v L-Glutamine (Sigma, G7513) and 1% v/v P/S (Sigma, P0781) and supplemented with 2% v/v B27 without insulin (Gibco, A1895601), 100 ng/mL Activin A (Peprotech, 120-14P), 10 ng/mL BMP4 (Peprotech, 120-05ET), and 20 ng/mL FGF2 (Peprotech, 100-18B). During these two first days of differentiation, medium was changed daily, and cells were cultured at 37°C in 20% O2 and 5% CO2. From days 3 to 5 of differentiation, cells were cultured in adv. RPMI (+1% v/v L-Glutamine and 1% v/v P/S) containing 2% v/v B27 without insulin and 100 ng/mL Activin A. Culture medium was changed daily, and cells were cultured at 37 °C in 20% O2 and 5% CO2. Definitive endoderm (DE) appeared by this day. From the 6-10th of differentiation, cells were cultured in adv. RPMI (+ 1% v/v L-Glutamine and 1% v/v P/S) supplemented with 2% v/v B27 with insulin (Gibco, 17504044), 20 ng/mL BMP4 and 10 ng/mL FGF2. Cells were cultured with daily medium changes for a total

of 5-days at 37°C, 4% O2 and 5% CO2. Hepatic progenitors (or hepatoblasts) emerged after this step. From days 11-15th of differentiation, hepatoblasts were cultured in adv. RPMI (+ 1% v/v L-Glutamine and 1% v/v P/S) supplemented with 2% v/v B27 (with insulin) and 20 ng/mL HGF (Peprotech, 100-39). Medium was changed daily, and cells were kept at 37 °C, 4% O2 and 5% CO2. HLC, in their immature form, appeared by this day. From days 16-20th, immature HLC (imHLC) were cultured in hepatocyte maintenance medium (HMM)** consisting of adv. RPMI (+1% v/v L-Glutamine and 1% v/v P/S) supplemented with 2% v/v B27 (with insulin), 20 ng/mL HGF, 20 ng/mL EGF (Peprotech, AF-100-15), 0.1 µM Dexamethasone (Sigma-Aldrich, D4902), and 20 ng/mL Oncostatin M (Peprotech, 300-10H). Daily medium changes were performed; cells were cultured at 37 °C, ambient O2 / 5% CO2. Mature HLC (mHLC) appeared at the end of differentiation.

**Note: The Clonetics™ Human Hepatocyte Cell Systems (Lonza, CC-3198), used from days 16-20th by Mallanna et al., was replaced by the HMM (section 4.2.1.1), avoiding the use of a commercial and undefined medium.

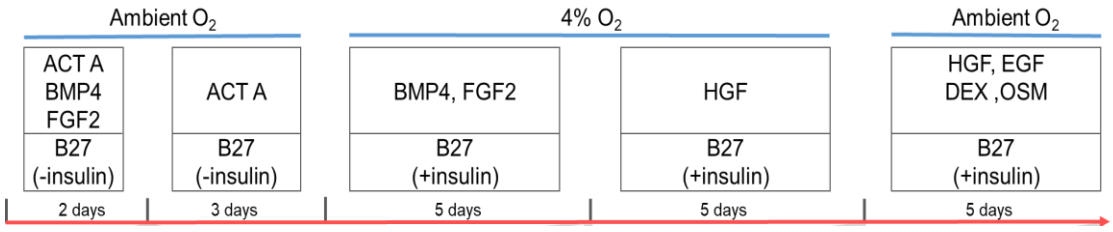

Figure 1. Protocol used to differentiate hESC in HLC.

During hESC differentiation, the commitment of hESC to HLC was monitored by observation of cell morphology and shifts in the transcriptome. HLC obtained at the end of the protocol were characterized and a threshold of >80% Albumin (ALB) positive cells was defined before treatment with microbiome secretome.

4.2.1.2. Treatment of hESC-HLC with CM A or bacterial-derived metabolites

At the end of differentiation, HLC were cultured for 6 additional days with: CM A diluted in HMM (dilution of 1:100); 10 ng/µL lithocholic acid (LA) (Sigma-Aldrich, L6250) and 10 ng/µL vitamin K_2 (Vit.K_2) (Sigma-Aldrich, V9378) or their vehicle dimethyl sulfoxide (DMSO) (Sigma-Aldrich, D8418) in HMM; or HMM only. After these 6-days of

treatment, both phenotype and/or functionality of treated HLC were analysed and compared to untreated counterparts.

4.2.1.3. RNA Isolation, cDNA Synthesis, and RT-PCR

Cells from days 1, 3, 6, 11, 16, 21 of differentiation and HLC treated with CM A; LA+ Vit.K_2; DMSO or untreated HLC were analysed by RT-PCR.
In brief, cells were lysed with TRIzol Reagent (Invitrogen, 15596026) and passed through a 25G needle (Braun, 300600). RNA was separated from DNA, lipids and proteins using chloroform, precipitated using isopropanol and washed using 75% v/v EtOH. Possible DNA contamination was digested by a DNAse treatment (Thermo Scientific, 89836) after which RNA was further purified with an extra phenol/chloroform separation step. The amount of RNA was quantified using the NanoDrop 2000/2000c Spectrophotometer (Thermo Scientific, ND-2000) and 150-250 ng of RNA were reverse transcribed into cDNA using the All-in-One cDNA Synthesis SuperMix (Biotool, B24408). cDNA was subsequently used in a three-step PCR reaction according to the 2 x PCR Super Master Mix (Biotool, B46018) and the primers listed in Table 1. RT-PCR amplicons were run on a 2 % w/v agarose (Invitrogen, 15510-027) gels and visualized using 2 % SYBR Safe (Invitrogen, s33102) in the Bio-Rad Gel Doc™ EZ imager. Expression levels were quantified by the mean pixel intensity of "PCR bands" measured with Image J software and normalized for the housekeeping gene, *GAPDH*.

Table 1. Primer information

Gene Symbol	Gene Name	Primer sequence	Annealing temperature (°C)
POU5F1 (OCT4)	POU Class 5 Homeobox 1	FW-GTGTTCAGCCAAAAGACCATCT RV-GGCCTGCATGAGGGTTTCT	60
FOXA2	Forkhead Box A2	FW-CACCACTACGCCTTCAACC RV-GGTAGTAGGAGGTATCTGCGG	62
GATA4	GATA Binding Protein 4	FW-CCACAAGGCTATGCGTCTC RV-CTTCTTTGCTATCCTCCAAGTC	56
HNF4A	Hepatocyte Nuclear Factor 4 Alpha	FW-GTACTCCTGCAGATTTAGCC RV-CTGTCCTCATAGCTTGACCT	56
AFP	Alpha Fetoprotein	FW-GATGAAACATATGTCCCTCCTG RV-ATGAGAAACTCTTGCTTCATCG	60
ALB	Albumin	FW-AGTGGGCAGCAAATGTTGTAAAC RV-TCAGGACCACGGATAGATAGTCTTC	60
CYP3A4	Cytochrome P450 Family 3 Subfamily A Member 4	FW-TGATGGTCAACAGCCTGTGCTGG RV-CCACTGGACCAAAAGGCCTCCG	60
CYP2C9	Cytochrome P450 Family 2 Subfamily C Member 9	FW-TGAAAGCTTGGAAAACACTGCA RV-GCATATCTCAGGGTTGTGCTTG	60
SULT	Sulfotransferase Family	FW-CCAGTTATTCCCCAAGTCTTTCT RV-AAACATCTCTGGGATTTCTCATGAG	60

GAPDH	Glyceraldehyde-3-Phosphate Dehydrogenase	FW-CTCTCTGCTCCTCCTGTTCG RV-ACGACCAAATCCGTTGACTC	64
TLR1	Toll Like Receptor 1	FW-CAGGCCCTCTTCCTCGTTAGA RV-TTCCTAAAGGTAGAAGCTGTTCTTCA	60
TLR2	Toll Like Receptor 2	FW-CTCTCGGTGTCGGAAT RV-CCCGCTCACTGTAAGAA	60
TLR4	Toll Like Receptor 4	FW-TCTTGGTGGAAGTTGAACG RV-GCCACACCGGGAATAA	60
TLR5	Toll Like Receptor 5	FW-GTACCCTGACTCGTTCT RV-TTCTGCACCCATGTGA	60
TLR6	Toll Like Receptor 6	FW-AGTGGACCCAGACTCG RV-AGTTCGTAATGGCACC	60

4.2.1.4. Immunostaining of Albumin and Alpha-fetoprotein

After treatment, HLC were stained for albumin (ALB) and alpha-fetoprotein (AFP).

Briefly, HLC monolayers were fixed in 4 % v/v formaldehyde for 20 min at RT. After 3 washes with DPBS (Gibco, 14190144) of 5 min each, cells were incubated with 1M NH_4Cl (Sigma-Aldrich, A9434) to reduce possible autofluorescence. Cells were incubated with the "blocking/permeabilization solution" consisting of DAKO protein block (DAKO®, X0909) and 0.1 % v/v saponin (Sigma-Aldrich, 47036-50G-F) (incubation parameters: 1 h at RT). The primary antibodies, goat anti-human ALB (Santa Cruz, sc-46293) and rabbit anti-human AFP (Invitrogen, PA5-16658) in a dilution of 1:250 in DAKO and 0.1% v/v saponin, were added (incubation parameters: 4°C, ON). In the following day, cells were washed and sequentially incubated with the secondary antibodies. The antibody donkey anti-goat 488 (Thermo Fisher, A-11055), at a dilution of 1:200, was added first and incubated for 1 h at 4°C, protected from light. Three washes were followed and the antibody goat anti-rabbit 568 (Thermo Fisher, A-11011) (diluted 1:200) was added and incubated as previously described. Lastly, nuclei were stained with DAPI (Sigma-Aldrich, D9542) (at 1:1000 dilution) for 5 min and mounted in antifade mounting medium (Vector Labs, H-1400). Cells were visualized using the Olympus IX81 inverted fluorescence microscope.

4.2.1.5. Additional characterization of HLC obtained at the end of differentiation

The presence of ALB in HLC was quantified by flow cytometry. In brief, HLC were detached from the plates with Accutase (Sigma, A6964). Approximately 100.000 cells (per condition) were incubated with a LIVE/DEAD® fixable dead cell stain for 30 min and fixed using 4% v/v formaldehyde for 15 min. After 3 washes with DPBS, cells were

incubated with goat anti-human ALB (Santa Cruz, sc-46293) 1:50 diluted in DPBS with 2% v/v FBS and 0.1% v/v saponin (30 min at 4°C). After, cells were washed and incubated with the secondary antibody, donkey anti-goat 488 (Thermo Fisher, A-11055) for 30 min. Cells were acquired on the BD Facs Aria™ III cell sorter and analysed using the Flow Jo version X 10.0.7r2.

Furthermore, HLC were also stained for the epithelial cell adhesion molecule (Epcam) using the protocol described in section 4.2.1.4. As primary antibody, we used the mouse anti-Epcam (Santa Cruz, sc-25308) diluted 1:250, and the goat anti-mouse (Molecular Probes, A11029) as secondary antibody.

Finally, the glycogen content o HLC was visualized by the Periodic acid–schiff (PAS) staining, a procedure carried out by the Histology Unit of IIS-Aragón.

4.2.2. The second hepatic cell model: hiPSC-HLC, as 2D monolayers, in static culture systems

4.2.2.1. Expansion of hiPSC and differentiation in HLC

The hiPSC line Cellartis human iPS Cell Line 18 (ChiPSC18) (Takara Bio Europe, Y00300) was differentiated in HLC. This line was chosen for this work as it demonstrated higher differentiation efficacy when compared to other lines [46].

Cells were routinely propagated in static adherent culture systems (T-flasks) coated with Synthemax® (Corning, 3535), in Cellartis® DEF-CS™ Xeno-Free Culture Medium (Takara Bio Europe AB, Y30040/Y30045), and were placed at 37º C in a humidified atmosphere with 5% CO2. At 80% of cell confluence, cells were detached from the T-flasks by rinsing with DPBS, adding Versene solution (Gibco, 15040066), and incubating the cells for 8 min at 37ºC. Cells were detached with cell scrapers (Sarstedt, 83.3950), resuspended in fresh Cellartis® DEF-CS™ Xeno-Free culture medium and counted using Trypan Blue exclusion method to determine cell number and viability, as described elsewhere [47].

Hepatocyte differentiation as 2D monolayer in static culture systems was carried out using Cellartis iPS Cell to Hepatocyte Differentiation System (Takara BioEurope AB, Y30055), as described by the manufacturer and published in the literature [46].

Differentiation of hiPSC in HLC occurred for 21 days and was monitored by observation of cell morphology by light-microscopy. A threshold of >80% ALB positive cells was defined before the treatment with microbiome secretome.

4.2.2.2. Treatment of hiPSC-HLC with CMs

At the end of differentiation, the culture of HLC was extended for 6 additional days. During these days, HLC were exposed to CM A or CM A+abx (in a dilution of 1:100 in HMM) or cultured in HMM only.

4.2.2.3. Analysis of pluripotency, Sox17, ALB and AFP by flow-cytometry

Before differentiation, pluripotency and the early differentiation maker, Sox17, were assessed by flow cytometry. Likewise, ALB and AFP were analysed after differentiation and before the treatment with CMs.

Briefly, cells were detached from 2D monolayers using with TrypLE Select, (Gibco, 12563011). For detection of cell-surface epitopes (i.e., TRA-1-60, SSEA-4, and TRA-1-81), cells were resuspended in washing buffer (WB) solution (5% v/v FBS in DPBS), centrifuged at 300 x g for 5 min and incubated with the respective antibodies. The antibodies, mouse anti-human TRA-1-60 (Santa Cruz, sc-21705), mouse anti-human SSEA-4 (560126, BD) and TRA-1-81 (Santa Cruz, sc-21706), and respective isotype controls (IgM or IgG3) were diluted in WB (according to supplier instructions) and incubated for 1 h at 4°C. For the intracellular epitopes Sox17, ALB and AFP, cells were washed with WB, fixed, permeabilized using BDCytofix/CytopermTM, (BD Biosciences, 554722) and stained as described in Chapter 4 section XX. Stained cell suspensions were analysed using CyFlowH space (Sysmex PartecGmbH, Görlitz, Germany) instrument. At least ten thousand events were registered per sample. Analysis was performed with FlowJo software (FlowJo LLC, http://www.flowjo.com/).

4.2.2.4. Transcriptomic analysis

The effect of CMs on HLC's transcriptome were analysed by reverse transcription-quantitative real-time PCR (RT-qPCR). RNA was isolated using the High Pure RNA Isolation Kit (Roche, 11828665001) and quantified by optical density with NanoDrop

2000c spectrophotometer. 200ng of RNA were reverse transcribed into cDNA using the Transcriptor First Strand cDNA Synthesis Kit (Roche, 5081963001). mRNA abundance of the selected genes was measured by RT-qPCR using TaqMan probe technology (LightCycler® 480 Probes Master, Roche, 04887301001) and validated primers (Table 2). Relative gene expression was calculated using $2^{-\Delta\Delta CT}$ method and normalized to the housekeeping gene *GAPDH*.

Table 2. Primer information used for RT-qPCR assay

Gene Symbol	Gene Name	Assay ID
FOXA2	Forkhead Box A2	Hs05036278_s1
HNF4A	Hepatocyte Nuclear Factor 4 Alpha	Hs00230853_m1
AFP	Alpha Fetoprotein	Hs00173490_m1
ALB	Albumin	Hs00910225_m1
CYP3A4	Cytochrome P450 Family 3 Subfamily A Member 4	Hs00604506_m1
CYP2C9	Cytochrome P450 Family 2 Subfamily C Member 9	Hs02383631_s1

4.2.3. The third hepatic cell model: hiPSC-HLC generated, as 3D cell aggregates, in bioreactors

4.2.3.1. Expansion and differentiation of hiPSC in HLC in STBR

The hiPSC lines PH1-Fib-hiPSC4F1 and ChiPSC18, henceforth termed hiPSC-1 and hiPSC-2, were used in this work and derived as previously described [46,48]. Before differentiation, hiPSC were routinely propagated in static adherent culture systems (T-flasks) in the Cellartis DEF-CS 500 Xeno-Free Culture Medium w/o antibiotics (Cat. No. Y30045, Takara BioEurope AB, SE) as described in greater depth elsewhere [49,50].

Differentiation of hiPSC in HLC as 3D aggregates was done in stirred-tank bioreactor (STBR) using and integrated strategy combining hiPSC expansion and hepatocyte differentiation steps, as described extensively in the Chapter 4.

4.2.3.2. Treatment of hiPSC-HLC with CMs

At day 21 of differentiation, HLC were harvested from STBR and transferred to different 2D systems according to the analysis. HLC were treated for 6 days, with CM A or CM A+abx (diluted 1:100 in HMM) or cultured in HMM only. Daily media changes were performed during treatment.

4.2.3.3. Cell viability and whole mounting

To assess cell viability and quantify the expression of ALB and AFP by flow-cytometry and immunofluorescence whole mounting, HLC, at a concentration of $1x10^6$ cell/mL, were transferred and cultured in 24-well ultra-low attachment plates (Corning, 3473). Protocols are described in detailed in Chapters 3 and 4.

4.2.3.4. Transcriptomic analysis, secretion of ALB and AFP, release of indocyanine green and activity of CYP3A4

The expression of hepatic specific genes, the quantification of ALB and AFP secreted by HLC, the release of indocyanine green (ICG) and the activity of CYP3A4 are detailed in Chapters 3 and 4. For that, HLC, were seeded in 24w-plate coated with Matrigel (Corning) or in 48w-plate and let to adhere during 24h. After that, HLC were treated with CMs as described.

4.3. Animal models

All animal studies were performed in accordance with portuguese regulations and approved by the Instituto Gulbenkian de Ciência (IGC) ethics committee and Direcção-Geral da Alimentação e Veterinária (the official national entity for regulation of laboratory animal usage). Male C57BL/6 mice with 8 to 12 weeks age, obtained from IGC, were bred and housed under specific pathogen-free (SPF) or germ-free (GF) conditions with 12 h light/dark cycle, humidity 50%–60%, ambient temperature 22 ± 2°C and food and water *ad libitum*. Animals were euthanized with CO2 and livers were harvested and analysed by RT-qPCR.

4.3.1. RNA Isolation, cDNA Synthesis, and RT-qPCR

For RNA isolation, liver lobes (~50 mg) were homogenized in 500 mL TRIzol™ Reagent (Thermo Fisher Scientific, 15596026) using a Tissue Lyser II. Homogenates were then centrifuged at 20000 x g for 3 min at 4°C and 500 mL of supernatant were used for RNA extraction with RNeasy Plus Mini Kit (Quiagen, 74134). Extraction was performed with 100 mL chloroform and the aqueous layer was transferred to a RNeasy

mini spin column. RNA purification was performed according to the manufacturer's instructions including one step of in-column DNase treatment. RNA was quantified in Nanodrop, and 1 mg total RNA was used to synthesize cDNA using SuperScript™ II Reverse Transcriptase (ThermoFisher Scientific, 18064022) and Oligo(dT)12-18 Primer (ThermoFisher Scientific, 18418012). Real-time quantitative PCR was performed using SybrGreen reagent (iTaq™ Universal SYBR® Green Supermix, Bio-Rad) and ABI QuantStudio 7 equipment. Relative gene expression is reported as $2^{-\Delta\Delta CT}$ relative to a control gene (*Gapdh*). A list of the oligonucleotide sequences used can be found in Table 3.

Table 3. List of primers used in section 4.3.1.

Gene	Primers
Alb	FW-CAAGAGTGAGATCGCCCATCG RV-TTACTTCCTGCACTAATTTGGCA
Cyp2c38	FW-CACGGCCCATTGTTGTATTGC RV-TGAGTGTGAAACGTCTTGTCTCT
Cyp2d9	FW-GCTGAAAGATGAGTCTGTCTGG RV-TGGTCTCGTACCACAGCACA
Cyp2e1	FW-CATCACCGTTGCCTTGCTTG RV-GGGGCAGGTTCCAACTTCT
Gapdh	FW- AACTTTGGCATTGTGGAAGG RV- ACACATTGGGGGTAGGAACA

4.4. Statistical analysis

Statistical analysis could not be performed as the results were obtained from experiments performed up to 2 times, in the case of the first and second hepatic models. For the hiPSC-HLC 3D model, statistical analysis could also not be performed as 2 results showed biological duplicates only. The last model using animals was analysed with the Mann-Whitney test. P values are reported for two-tailed tests with a 95% confidence interval, and differences with $P < 0.05$ were considered significant for all statistical tests.

5. Results

5.1. CMs were successfully formulated and were enriched in different organic compounds

To investigate the effect of postbiotics on hepatic function, we formulated two different CMs using stools from a healthy donor which allowed us to simulate a “healthy microbial secretome” and stools from the same donors under a Abx treatment (CM A+abx), allowing us to investigate the effect of a secretome modulated by these drugs (Sup. Fig 2A). Both formulations as well as the basal medium used for HLC culture (HMM) were characterized for their content in BA, vitamins and SCFA.

By UPLC/MRM-MS analysis, a total of 23 BA was identified in CMs, but none could be detected in HMM (Fig. 2A and Sup. Fig. 2B). When comparing both CMs, CM A showed a higher BA diversity than CM A+abx; 8 BA (i.e., dehydrocholic acid; apocholic acid; beta-muricholic acid; taurocholic acid; tauroursodeoxycholic acid; tauro-alpha-muricholic acid; tauro-beta-muricholic acid and tauro-omega-muricholic acid) were only present in CM A while other 2 (chenodeoxycholic acid and glycoursodeoxycholic acid) were exclusive of CM A+abx.

Besides that, CMs showed differences in which regards BA concentration. More specifically, 7 BA (i.e., cholic acid; deoxycholic acid, dehydrolithocholic acid; 7-ketodeoxycholic acid; 7-ketolithocholic acid; nordeoxycholic and ursocholic acid) were enriched in CM A, while 6 others (i.e., lithocholic acid; allocholic acid; dioxolithocholic acid; isolithocholic acid; omega-muricholic acid and norcholic acid) predominated in CM A+abx (Sup. Fig. 2B). Cholic acid was the most enriched BA and its concentration was >80 times higher than CM A+abx. A similar trend was observed for 7-ketodeoxycholic acid and deoxycholic acid, the second and third most enriched BA (Fig. 2A).

Short chain fatty acids were also quantified using GC-MS methodologies. A total of 7 (i.e., acetic acid; propionic acid; isobutyric acid; butyric acid; isovaleric acid; valeric acid and hexanic acid) were identified in both CMs (Fig. 2B) and poorly detected in HMM (Sup. Fig. 2C).

Surprisingly, the CM A+abx was much more enriched in almost all SCFA than CM A, except for acetic acid (Fig. 2B and Sup. Fig. 2C).

Finally, water and fat-soluble vitamins-like were also measured by UPLC/MRM-MS.

Out of the 33 vitamins analysed, 15 were identified in CMs and 20 were found in HMM (Sup. Fig. 2D). In particular, the higher variations between CMs and HMM were in the content of vitamin B3-nicotinic acid, B6-pyridoxine and vitamin B1-Thiamine-phosphate (Fig. 2C).

When comparing both CMs, 8 vitamins (i.e., vitamin B1 thiamine; vitamin B2; vitaminB1-thiamine-pyrophosphate; vitamin B-like-lipoic acid; vitamin A-retinal; vitamin D3-cholecalciferol; vitamin E-alfa-tocopherol; vitamin K2-menaquinone) were enriched, and 7 (i.e., vitamin B3-nicotinamide; vitamin B6-pyridoxamine; vitamin B6-pyridoxine; vitamin B1-Thiamine-phosphate; vitamin B2-riboflavin-5min-phosphate; vitamin B3-nicotinic acid and vitamin B5-pantothenic acid) were decreased in CM A compared to CM A+abx (Sup. Fig. 2D).

Finally, as intestinal bacteria have been shown to secrete proteins and other small peptides, we quantified the total protein content using the commercial BCA Protein Kit.

As showed, both CM formulations were enriched in proteins, which was slightly higher in the CM A (12.2 mg/mL and 10.4 mg/mL for CM A and CM A+abx, respectively) (Fig. 2D and Sup. Fig. 2E). Further experiments are needed to identify the nature of these peptides.

Altogether, these findings suggest that HLC treated with CM A were exposed to a greater BA variety and an overall higher BA concentration compared to cells treated with CM A+abx. Since HMM was free of BA, cells kept in this media only were not exposed to any BA. Moreover, HLC treated with any of the two CMs were exposed to significantly higher SCFA concentrations and to an overall equal amount of vitamins than their untreated counterparts.

Once confirmed that CMs were enriched in various organic compounds, we tested whether these secretomes were biologically active and could therefore modulate hepatic function.

Thus, we treated HLC, derived from 3 different hPSC lines (1 hESC and 2 hiPSC lines) using different differentiation protocols, with CMs and compared their phenotype or functionality to untreated counterparts, as described in the following subsections.

A

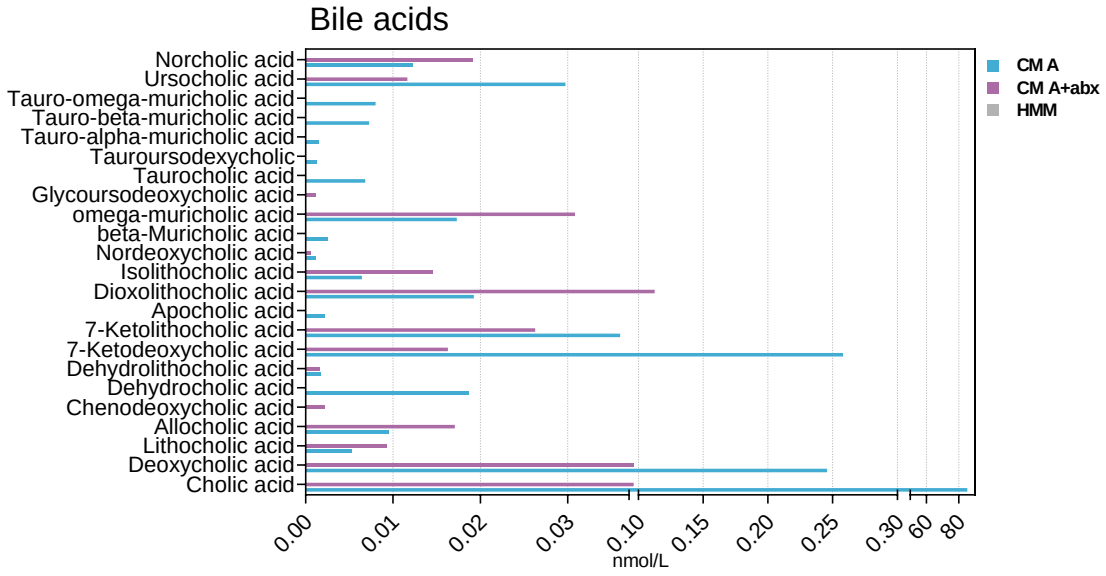

B

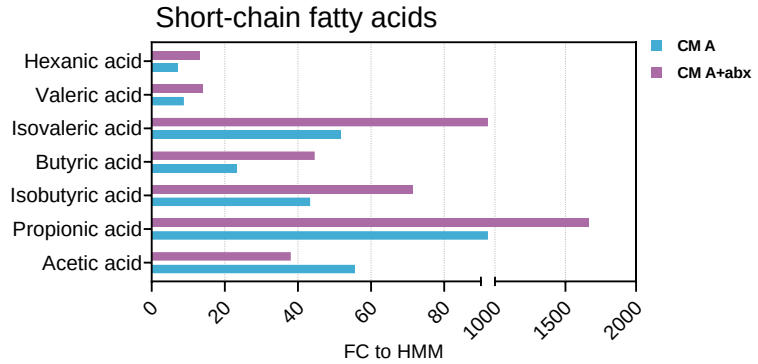

C

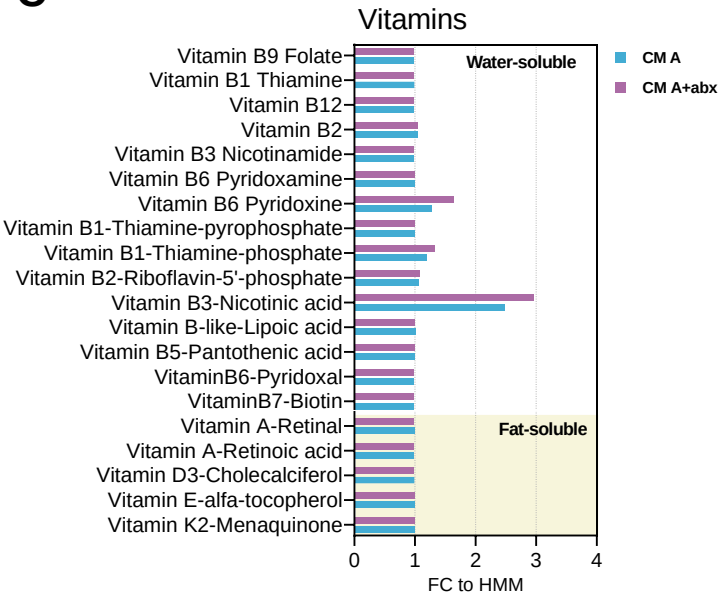

D

Sample	mg/mL
CM A	12.2
CM A+abx	10.4

Figure 2. hPSC-HLC treated with CM A or CM A+abx were exposed to greater diversity and concentration of BA and SCFA and a similar concentration of vitamins compared to untreated counterparts. Different hPSC-HLC were cultured for 6 days in HMM supplemented with CM (CM dilution of 1:100 in 500µl final volume). Before treatment, CMs and HMM were also characterized using different analytical chemistry techniques. (A) Concentration of BA (nmol/L) sensed by HLC considering the dilution and volume mentioned previously. Fold increase in the concentration of (B) SCFA and (C) vitamins sensed by HLC treated with CMs vs untreated cells. (D) Quantification of total protein in CMA and CM A+abx by Pierce BCA Protein Assay Kit. Abbreviations: BA, bile acids; CM, conditioned media; CM A, conditioned media from a healthy adult; CM A+abx, conditioned media from an adult under antibiotic treatment; FC, fold change; hPSC, human pluripotent stem cells; HLC, hepatocyte-like cells; HMM, hepatocyte maintenance media; SCFA, short-chain fatty acids.

.

A

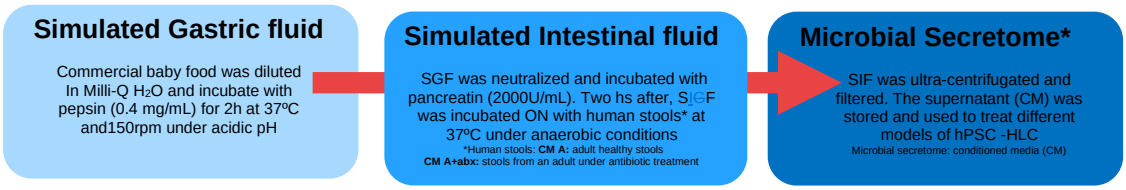

B

Bile Acid (nmol/L)/Sample	CM A	CM A+abx	HMM
Cholic acid	8.535	5.285	0
Deoxycholic acid	24.57	7.553	0
Lithocholic acid	0.525	0.9247	0
Allocholic acid	0.9485	1.707	0
Chenodeoxycholic acid	0	0.2187	0
Dehydrocholic acid	1.871	0	0
12-Ketolithocholic acid	0	0	0
Dehydrolithocholic acid	0.1691	0.1651	0
7-Ketodeoxycholic acid	25.8	1.628	0
7-Ketolithocholic acid	3.6	2.627	0
Alloisolithocholic acid	0	0	0
Apocholic acid	0.2206	0	0
Hyodeoxycholic acid	0	0	0
Murocholic acid	0	0	0
Ursodeoxycholic acid	0	0	0
Dioxolithocholic acid	1.925	11.25	0
Isolithocholic acid	0.6429	1.456	0
Isodeoxycholic acid	0	0	0
12-Ketochenodeoxycholic acid	0	0	0
Nordeoxycholic acid	0.119	0.056	0
3-Oxocholic acid	0	0	0
6,7-Diketolithocholic acid	0	0	0
alpha-Muricholic acid	0	0	0
beta-Muricholic acid	0.2521	0	0
lamda-muricholic acid	0	0	0
omega-muricholic acid	1.731	3.083	0
Glycochenodeoxycholic acid	0	0	0
Glycocholic acid	0	0	0
Glyco-beta-Muricholic acid	0	0	0
Glycodehydrocholic acid	0	0	0
Glycodeoxycholic acid	0	0	0
Glycohyodeoxycholic acid	0	0	0
Glycoursodeoxycholic acid	0	0.1111	0
Glycolithocholic acid	0	0	0
Glycohyocholic acid	0	0	0
Taurodeoxycholic acid	0	0	0
Taurochenodexycholic acid	0	0	0
Taurocholic acid	0.6829	0	0
Taurodehydrocholic acid	0	0	0
Taurolithocholic acid	0	0	0
Tauroursodexycholic acid	0.1292	0	0
Taurohyocholic acid	0	0	0
Tauro-alpha-muricholic acid	0.1484	0	0
Tauro-beta-muricholic acid	0.7281	0	0
Tauro-omega-muricholic acid	0.8008	0	0
Ursocholic acid	2.972	1.164	0
Norursodeoxycholic acid	0	0	0
Norcholic acid	1.227	1.914	0
3beta-OH-5-cholestenoic acid	0	0	0
3beta, 7alpha-diOH-5-cholestenoic acid	0	0	0
7alpha-OH-3-oxo-4-cholestenoic acid	0	0	0
DHCA	0	0	0
THCA	0	0	0
lithocholic acid-3-glucuronide	0	0	0
lithocholic acid-24-glucuronide	0	0	0
deoxycholic acid-3-glucuronide	0	0	0
deoxycholic acid-24-glucuronide	0	0	0
chenodeoxycholic acid-3-glucuronide	0	0	0
chenodeoxycholic acid-24-glucuronide	0	0	0
Hdeoxycholic acid-3-glucuronide	0	0	0
ursodeoxycholic acid-3-glucuronide	0	0	0
ursodeoxycholic acid-24-glucuronide	0	0	0
lithocholic acid-3-sulfate	0	0	0
deoxycholic acid-3-sulfate	0	0	0
chenodeoxycholic acid-3-sulfate	0	0	0
Hyodeoxycholic acid-3-sulfate	0	0	0
ursodeoxycholic acid-3-sulfate	0	0	0
cholic acid-3-sulfate	0	0	0
Allocholic acid-3-sulfate	0	0	0

beta-Muricholic acid-3-sulfate	0	0	0
Glycolithocholic acid-3-sulfate	0	0	0
Glycodeoxycholic acid-3-sulfate	0	0	0
Glycochenodeoxycholic acid-3-sulfate	0	0	0
Glycoursodeoxycholic acid-3-sulfate	0	0	0
Glycohyodeoxycholic acid-3-sulfate	0	0	0
Glycocholic acid-3-sulfate	0	0	0
Taurolithocholic acid-3-sulfate	0	0	0
Taurodeoxycholic acid-3-sulfate	0	0	0
Taurochenodeoxycholic acid-3-sulfate	0	0	0
Tauroursodeoxycholic acid-3-sulfate	0	0	0

C

SCFA (µg/mL)/Sample	CM A	CM A+abx	HMM
Acetic acid	3655.35	2480.42	6.693
Propionic acid	33.701	66.563	0.004
Isobutyric acid	0.847	1.408	0.002
Butyric acid	19.362	37.914	0.087
Isovaleric acid	1.016	2.251	0.002
Valeric acid	1.174	1.951	0.015
Hexanic acid	0.427	0.858	0.007

D

	Vitamins (nmol/L)/Sample	CM A	CM A+abx	HMM
Water-soluble	VitaminB9 Folate	0	0	14563.04
	VitaminB1 Thiamine	40.28	25.61	6661.58
	VitaminB12	0	0	294.37
	VitaminB2	6210.37	4749.1	925.94
	VitaminB3 Nicotinamide	183.17	206.46	7184.37
	VitaminB6 Pyridoxamine	28.91	30.03	289.51
	VitaminB6 Pyridoxine	60.04	131.59	2.01
	VitaminB1-Thiamine-pyrophosphate	1727.6	1182.96	1678.76
	VitaminB1-Thiamine-phosphate	6290.04	10573.6	312.16
	VitaminB2-Riboflavin-5min-phosphate	250.85	319.15	34.65
	VitaminB3-Nicotinic acid	14394.3	18896.1	95.88
	VitaminB-like-Lipoic acid	26.74	18.61	12.41
	VitaminB5-Pantothenic acid	1466.6	1643.17	2417.76
	VitaminB6-Pyridoxal	0	0	13539.9
	VitaminB6-Pyridoxal-phosphate	0	0	0
	VitaminB7-Biotin	0	0	1993.68
	VitaminK3	0	0	0
Fat-soluble	VitaminA-Retinal	1.4711	0	0.8768
	VitaminA-Retinoic acid	0	0	2.525
	VitaminA-Retinol	0	0	0
	VitaminD2-Ergocalciferol	0	0	0
	VitaminD3-Cholecalciferol	0.6414	0.4217	44.733
	VitaminE-alfa-tocopherol	48.4667	30.7638	92.0593
	VitaminE-beta/gamma-tocopherol	0	0	0
	VitaminE-delta-tocopherol	0	0	0
	VitaminE-alfa-tocotrienol	0	0	0
	VitaminE-delta-tocotrienol	0	0	0
	VitaminK1-Phylloquinone	0	0	0
	VitaminK2-Menaquinone	0.1324	0.1247	0.2066
	VitaminE-beta/gamma-tocotrienol	0	0	0
	4-Aminbenzoic acid	0	0	0
	4-Pyridoic acid	0	0	0
	VitaminB12 Cyanocobalamin	0	0	0

E

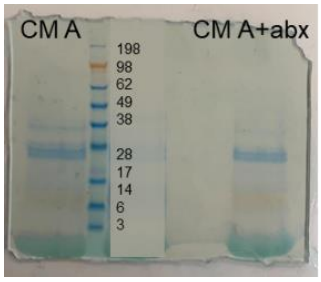

Supporting Figure 2. Secretomes of human intestinal microbiota were successfully formulated *in vitro* and contained different organic compounds. In this study, two CMs were formulated using a protocol that mimics human digestion *in vitro*. CM A and CM A+abx were prepared similarly, varying only the bacterial source. Thus, CM A used stools from a healthy adult while CM A+abx used stools from an adult under antibiotic treatment. Before treat hPSC-HLC with CM, both CMs and HMM were characterized using different analytical chemistry techniques at Creative Proteomics. (A) Protocol used to formulate CMs. (B) Quantitative measurement of BA (nmol/L) by UPLC/MRM-MS; (C) Analysis of SCFA (µg/mL) by GC-MS; (D) Quantification of water and fat-soluble vitamins (nmol/L) by UPLC/MRM-MS; (E) Total protein detection by Coomassie Protein Gel Imaging. Abbreviations: BA, bile acids; CM, conditioned media; CM A, conditioned media from a healthy adult; CM A+abx, conditioned media from an adult under antibiotic treatment; GS-MS, Gas chromatography mass spectrometry; HMM, hepatocyte maintenance media; LC-MS, liquid chromatography–mass spectrometry; ON, overnight; SCFA, short-chain fatty acids; UPLC/MRM-MS, ultraperformance liquid chromatography-multiple reaction monitoring-multi-stage/mass spectrometry.

5.2. hESC-HLC treated with CM A formed ALB+ hepatic cords and showed an increased expression of hepatic specific markers

In the first hepatic model, we used HLC differentiated from hESC.

During differentiation, light microscopy analysis showed alterations in cell morphology from the typical stem binucleated round-shape towards an epithelial-like monolayer (Sup. Fig. 3A). These observations were accompanied by transcriptional shifts that included an initial loss of pluripotency (*OCT-4*) and the consequent activation of hepatic-specific markers (*HNF4A*, *AFP*, *ALB*, *CYP3A4*, *CYP2C9* and *SULT*) (Sup. Fig. 3B).

HLC obtained at the end of differentiation exhibited irregular polygonal shape and expressed ALB (>90% ALB+) and accumulated glycogen (Sup. Fig. 3C a-d), resembling PHH.

Considering these results, the generated hESC-HLC were cultured for 6 additional days with: i) CM A diluted in HMM (HLC+CM A); ii) the microbial products vitamin K2 and lithocholic acid (HLC+Vit.K2+LA) or iii) its vehicle DMSO (HLC+DMSO) diluted in HMM; and iv) HMM only (HLC) (Fig. 3A).

Although HLC+CM A still conserved traits of fetal origin (i.e., AFP) (Fig. 3C), they formed unique “structures”, that by staining for ALB, we believe being hepatic cords (or niches). Interestingly, these “cords” were not observed in HLC kept in HMM only (Fig. 3C).

Moreover, HLC+CM A showed an increased expression of *HNF4A* and *CYP2C9* compared to untreated HLC or even to HLC exposed to the positive inducers Vit.K_2 and LA (Fig. 3D). The increased expression observed for transcripts of *TLR1*, *.-2*, *.-5*, and *.-6* in HLC+CM A suggests a possible signalling transduction pathway mediated by TLR receptors although further experiments will be needed to validate this hypothesis.

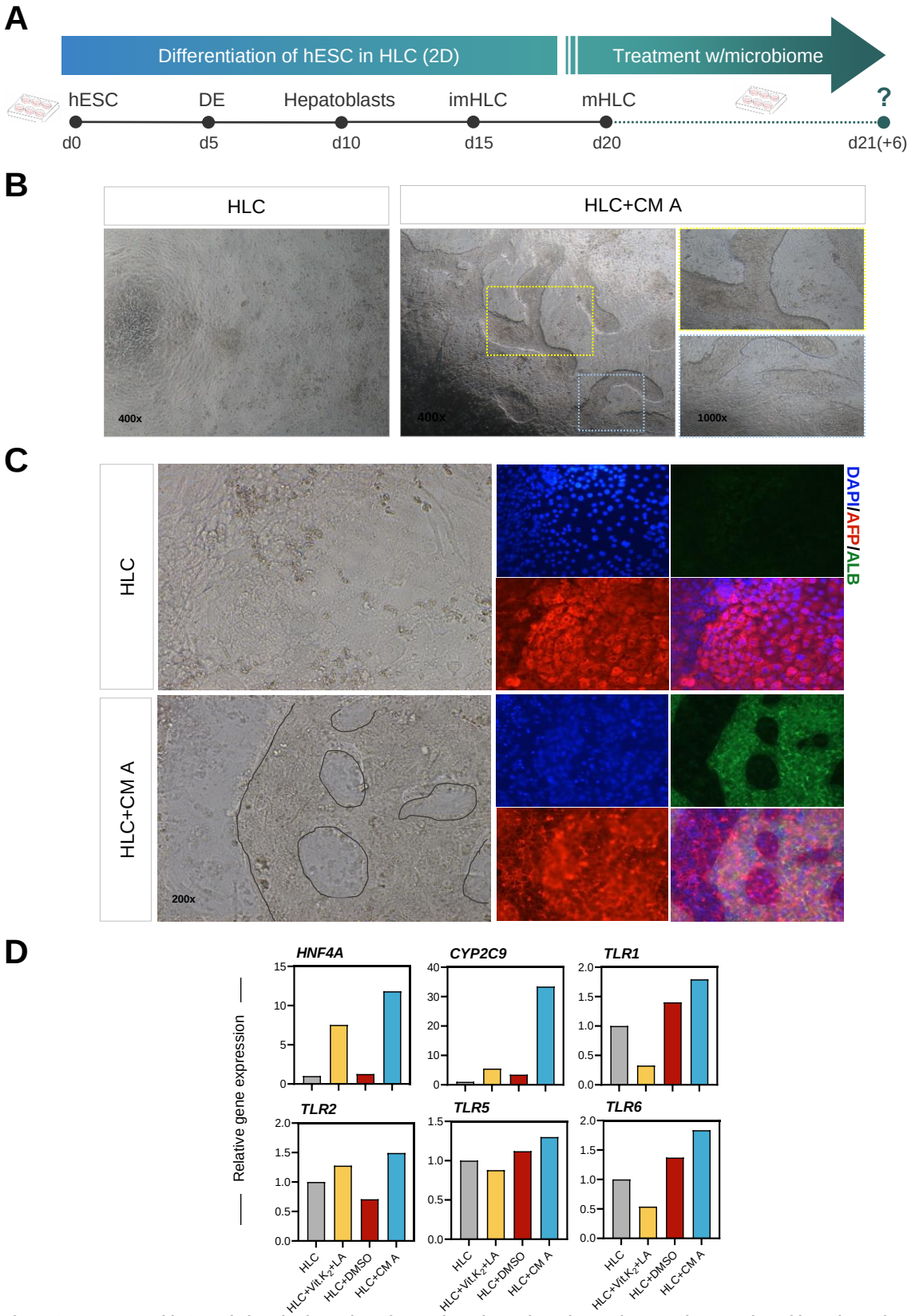

Figure 3. Treatment with CM A led to the formation of ALB+ hepatic cords and to an increased expression of hepatic markers. In this model, HLC were differentiated from hESC and exposed to CM A; Vit.K_2+LA or DMSO (its vehicle) or kept in HMM only for 6 days. (A) Schematic representation of the model. (B) Light microscopy images of untreated HLC and HLC+CM A. Magnifications are indicated on pictures. (C) Staining of ALB and AFP visualized by fluorescence immunocytochemistry after treatment with microbiome. All images were taken with 200x magnification. (D) Expression of *HNF4A*, *CYPC29*, *TLR1*, *-2*, *-5*, *-6* after treatment with microbiome. Gene expression is represented as FC to untreated HLC. No statistical analysis could be performed on quantitative measurements, as the data reported represents single experiments. Abbreviations: CM A, conditioned media from a healthy adult; DE, definitive endoderm; DMSO, dimethyl sulfoxide; FC, fold change; hESC, human embryonic stem cells; HLC, untreated HLC; HLC+CM A, HLC treated with CM A; HLC+Vit.K2+LA, HLC exposed to Vit.K_2 and LA; HLC+DMSO, HLC exposed to DMSO; HMM, hepatocyte maintenance media; imHLC, immature HLC; mHLC, mature HLC.

5.3. Treatment of hiPSC-HLC with CM A increased the expression of hepatic specific genes in contrast to CM A+abx formulation

The influence of CMs on hepatic function was evaluated in a second hPSC model consisting of HLC derived from a hiPSC line. As described above (section 4.2.2), the hiPSC line ChiPSC18 was differentiated in HLC, as 2D monolayers, using the serum- and feeder-free protocol “Cellartis® iPS Cell to Hepatocyte Differentiation Kit” commercialized by Takara Bio Europe-Cellartis AB.

Prior to differentiation, pluripotency was confirmed by the presence of TRA-1-60, SSEA-4 and TRA-1-81 and the absence of the endodermal marker, SOX17 (Sup. Fig. 4A).

Morphological changes during differentiation confirmed that hepatic differentiation occurred as expected (Sup. Fig.4B).

Although HLC displayed the typical PHH morphology with irregular polygonal shape and one or two prominent nucleoli, HLC showed a hybrid fetal-adult phenotype (~79.6%AFP and ~63%ALB) (Sup. Fig. 4C). The accuracy of this analysis was questionable due to technical challenges faced while detaching HLC from the plates, which resulted in poor cell recovery yields and loss of viability (data not shown).

After differentiation, HLC were cultured for six additional days in i) CM A diluted in HMM (HLC+CM A); ii) CM A+abx diluted in HMM (HLC+CM A+abx), or iii) HMM only (HLC) (Fig. 4A).

Our results showed that, only HLC that were treated with CM A displayed an increase in the expression of hepatic-specific markers namely, *HNF4A*, *AFP*, *CYP3A4* and *CYP2C9*. Curiously, none of the formulations improved the transcription of *ALB* (Fig. 4C).

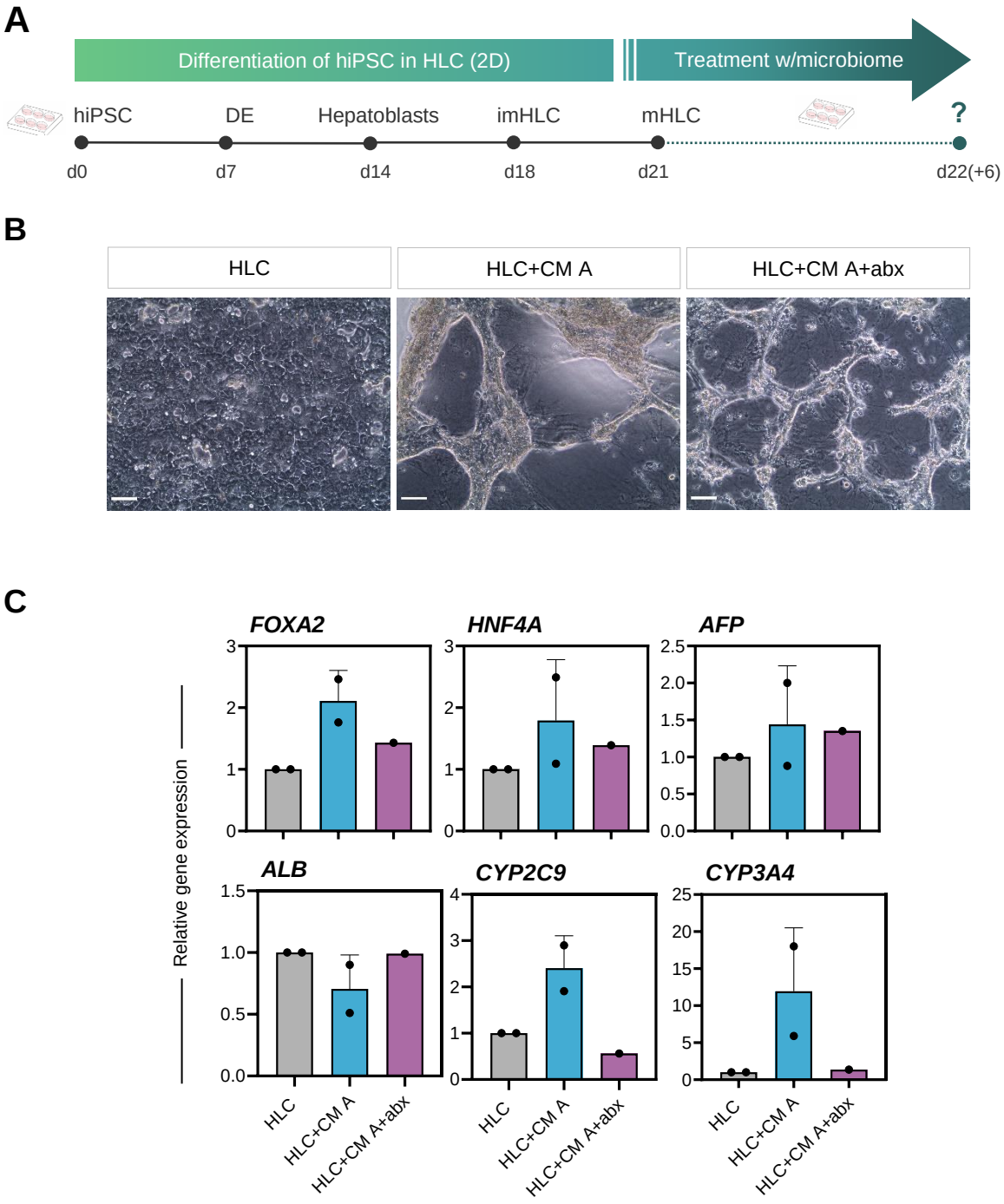

Figure 4. Although both CM formulations were sensed by hiPSC-HLC only CM A led to an increased in the expression of putative hepatocyte markers. In this model, HLC were differentiated from hiPSC and exposed to CM A; CM A+abx or kept in HMM only for 6 days. (A) Schematic representation of the second hepatic cell model. (B) Light microscopy images of untreated HLC, HLC+CM A and HLC+CM A. Scale bar: 200µm. (C) Expression of *FOXA2*, *HNF4A*, *AFP*, *ALB*, *CYP2C9* and *CYP3A4* after treatment with microbiome. Graphs represent the FC expression relative to untreated HLC. Since only two independent experiments were performed, no statistical analysis could be performed. Abbreviations: CM A, conditioned media from a healthy adult; DE, definitive endoderm; DMSO, dimethyl sulfoxide; FC, fold change; hiPSC, human induced pluripotent stem cells; HLC, untreated HLC; HLC+CM A, HLC treated with CM A; HLC+CM A+abx, HLC treated with conditioned media from an adult under antibiotic treatment; HMM, hepatocyte maintenance media; imHLC, immature HLC; mHLC, mature HLC.

5.4. Secretomes of intestinal microbiota preserved the function of 3D aggregates of hiPSC-HLC in 2D culture

In this model, we used hiPSC-HLC generated using a scalable bioprocess described by our group (Chapter 4). Two different hiPSC lines (hiPSC-1 and hiPSC-2) were differentiated in HLC, as 3D cell aggregates, in STBR operating in perfusion.

After 3-4 days of cell expansion and further 21 days of differentiation HLC were harvested and treated for 6 days in static culture systems with i) CM A diluted in HMM (HLC+CM A); ii) CM A+abx diluted in HMM (HLC+CM A+abx) or iii) in HMM only (HLC) (Fig. 5A).

The commitment of hiPSC in HLC and a comprehensive characterization of generated HLC can be found in Chapter 4.

Herein, we firstly demonstrated that transferring cells from 3D dynamic culture conditions to 2D static systems did not compromise cell viability as in all conditions tested HLC remained viable after 6 days of culture (Fig. 5B).

Then, we investigated whether CMs impact HLC by analysing cell phenotype and their ability to perform critical functions of the human liver.

First, we analysed the metabolism of xenobiotics which is carried out mainly by the P450 cytochrome family. We showed that the expression of adult cyp. isoforms (i.e. *CYP1B1*, *-3A4*, *-2C9*, *-2D6* and *-2E1*) was overall increased in HLC+CM A compared to untreated HLC. The same was not that evident for HLC+CM A+abx. Nevertheless, the fetal cyp. isoform, *CYP3A7*, was still transcribed (Fig. 5C-a).

Gene expression analysis was only partially corroborated by function analysis. Although HLC+CM A, derived from both hiPSC lines, showed a higher basal and inducible CYP3A4 metabolism than untreated counterparts, exposure to CM A+abx also improved CYP3A4 metabolism, in contrast to what was demonstrated before by its lower basal expression (Fig. 5C-b).

Next, we analysed the capacity of HLC to express and secrete the liver specific-plasma proteins AFP, ALB and A1AT. HLC treated with both CMs showed higher ALB expression than HLC kept in HMM only (Fig. 5D-b). These mRNA levels were translated in a higher percentage of cells expressing ALB (i.e., 88.8%ALB+ cells in HLC+CM A; 81.4%ALB+ cells in HLC+CM A+abx vs 66.5%ALB+ cells in HLC) and in overall higher ALB secretion (Fig. 5D a-c). Whole mounting immunofluorescence microscopy of HLC+CM A and HLC confirmed these findings (Fig. 5D-d).

Interestingly, the gene expression levels of *AFP* (Fig. 5D-b) and the percentage of AFP+ cells (Fig. 5D-a) in HLC+CM A were superior to HLC, contrary to what was observed in ELISA (Fig. 5D-c) and whole mounting assay (Fig. 5D-d). Although the expression of *AFP* was slightly higher in HLC+CM A+abx than HLC, these were not translated into higher secretion of AFP.

Finally, the expression and secretion of A1AT were superior in HLC+CM A for HLC derived from hiPSC-1 only (Fig. 5D-b-c).

ICG uptake by hepatocytes has been recently used to assess the in vitro function of stem-cell-derived hepatocytes (refs 6, 7). By light-microscopy analysis, we observed that all HLC conditions could uptake ICG. HLC+CM A showed a higher ICG release during the first 5 h post-uptake. This tendency was maintained till 24h, but the highest release was observed for HLC+CM A+abx (Fig.5 E a-b).

Finally, we analysed the expression of other hepatic specific markers. HLC+CM A showed an overall increased expression of the transcriptional factors *HNF4A*, *PPARA* and *FXR* than untreated counterparts. Likewise, the expression of *CPS1*, the master regulator of the urea cycle, and *ABCB1* involved in drug detoxification showed a similar tendency. The same results were not observed in HLC+CM A+abx.

Interestingly, the expression of plasma membrane receptors *TLR1*, *.-2*, *.-6* were also elevated in HLC+CM A, corroborating the results obtained with other models (Fig. 5F).

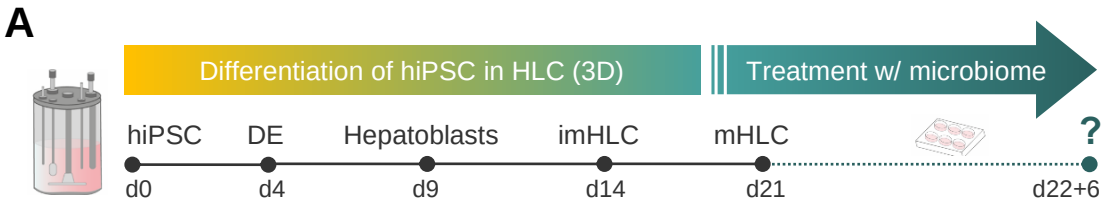
A
Differentiation of hiPSC in HLC (3D)
Treatment w/ microbiome
hiPSC
DE
Hepatoblasts
imHLC
mHLC
?
d0
d4
d9
d14
d21
d22+6

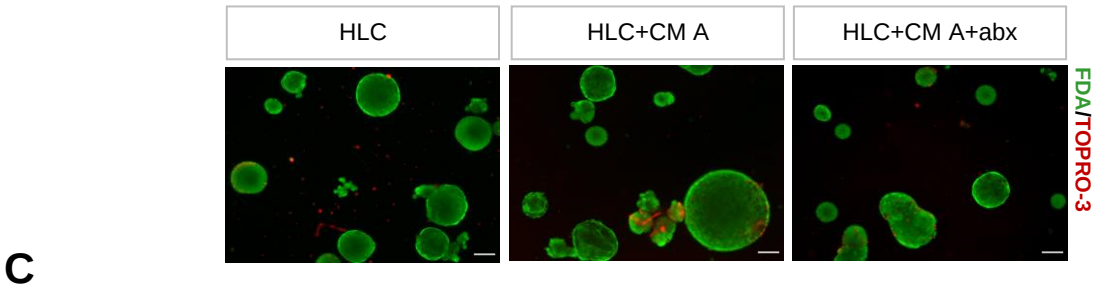
B
HLC
HLC+CM A
HLC+CM A+abx
FDA/TOPRO-3

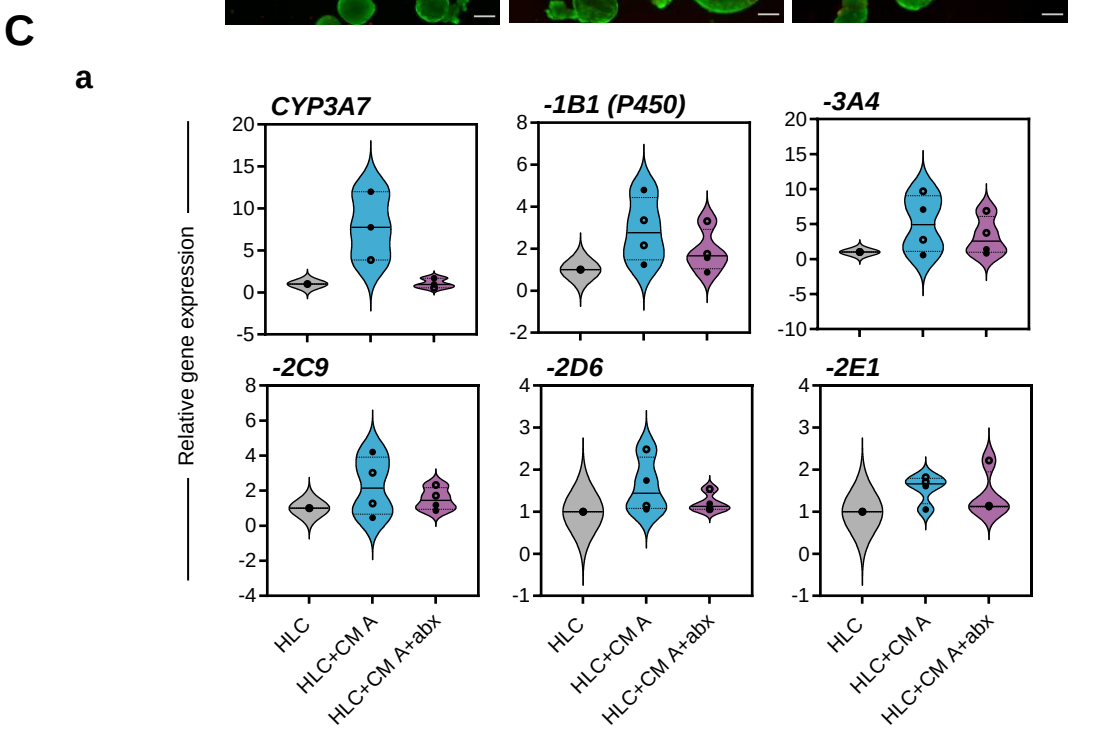
C
a
CYP3A7
-1B1 (P450)
-3A4
-2C9
-2D6
-2E1
Relative gene expression
HLC
HLC+CM A
HLC+CM A+abx

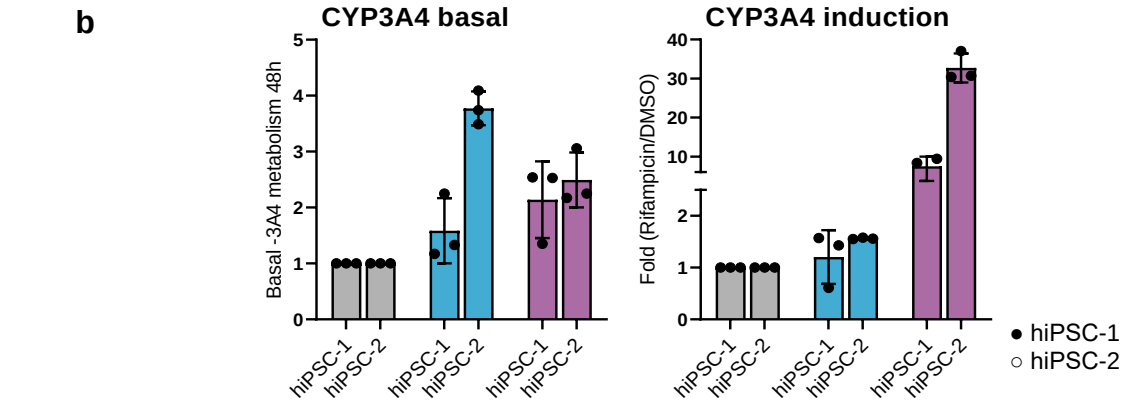
b
CYP3A4 basal
CYP3A4 induction
Basal -3A4 metabolism 48h
Fold (Rifampicin/DMSO)
hiPSC-1
hiPSC-2

D

a

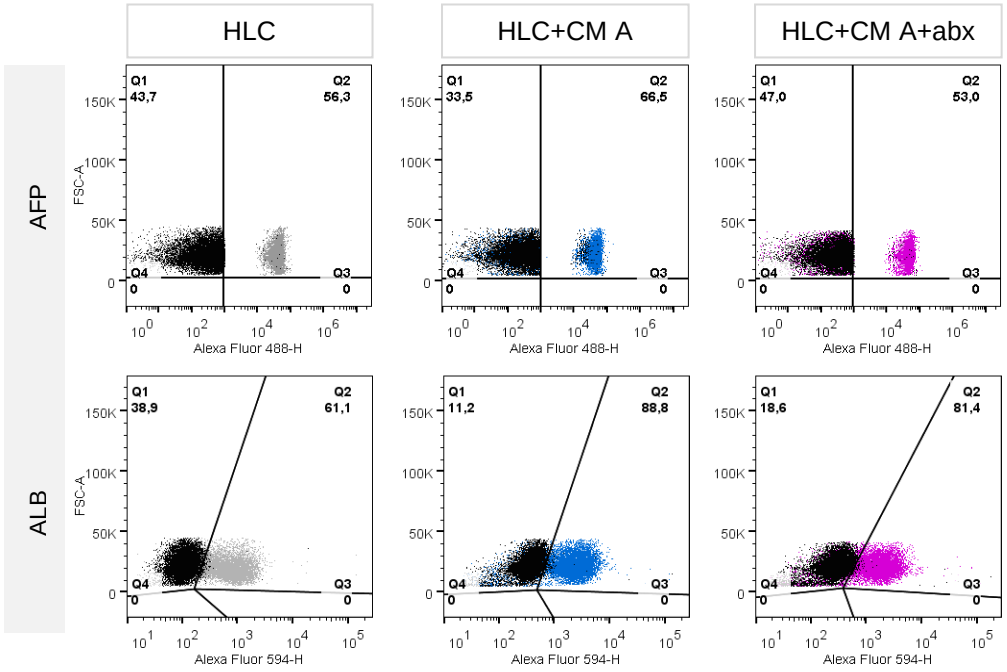
HLC
HLC+CM A
HLC+CM A+abx
AFP
ALB
FSC-A
Alexa Fluor 488-H
Alexa Fluor 594-H
Q1 43,7
Q2 56,3
Q4 0
Q3 0
Q1 33,5
Q2 66,5
Q4 0
Q3 0
Q1 47,0
Q2 53,0
Q4 0
Q3 0
Q1 38,9
Q2 61,1
Q4 0
Q3 0
Q1 11,2
Q2 88,8
Q4 0
Q3 0
Q1 18,6
Q2 81,4
Q4 0
Q3 0

b

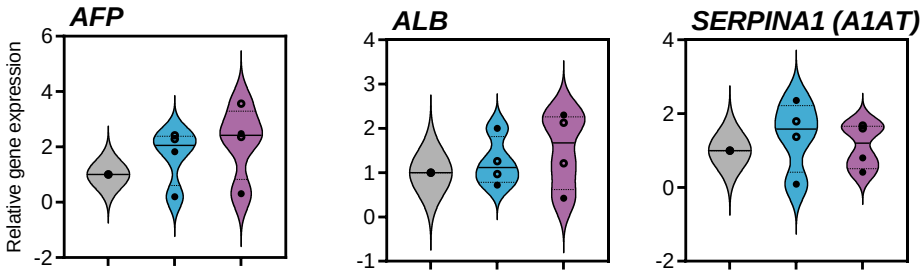
AFP
ALB
SERPINA1 (A1AT)
Relative gene expression

c

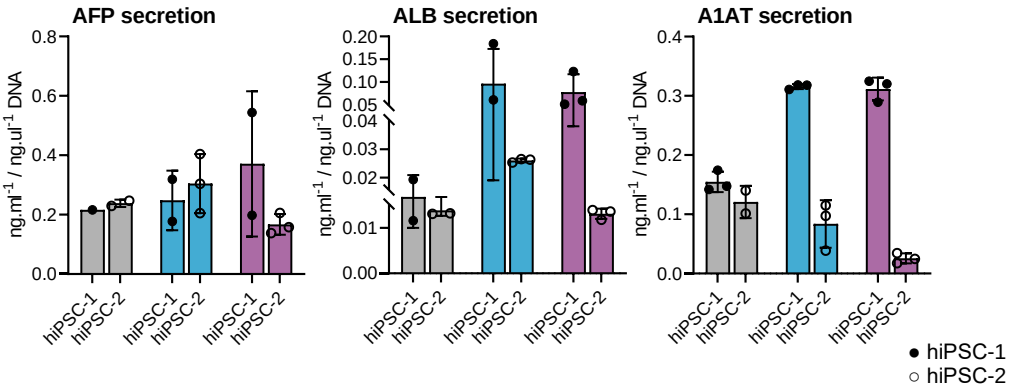
AFP secretion
ALB secretion
A1AT secretion
ng.ml-1 / ng.ul-1 DNA
hiPSC-1
hiPSC-2

d

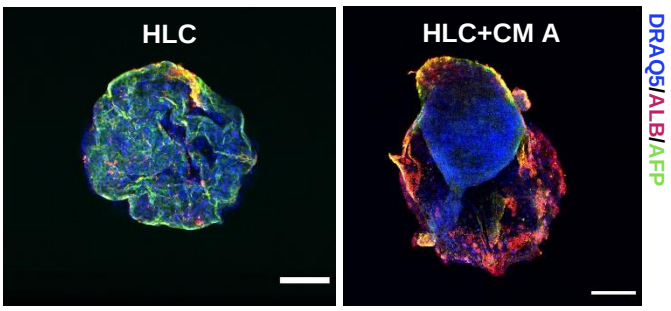
HLC
HLC+CM A
DRAQ5/ALB/AFP

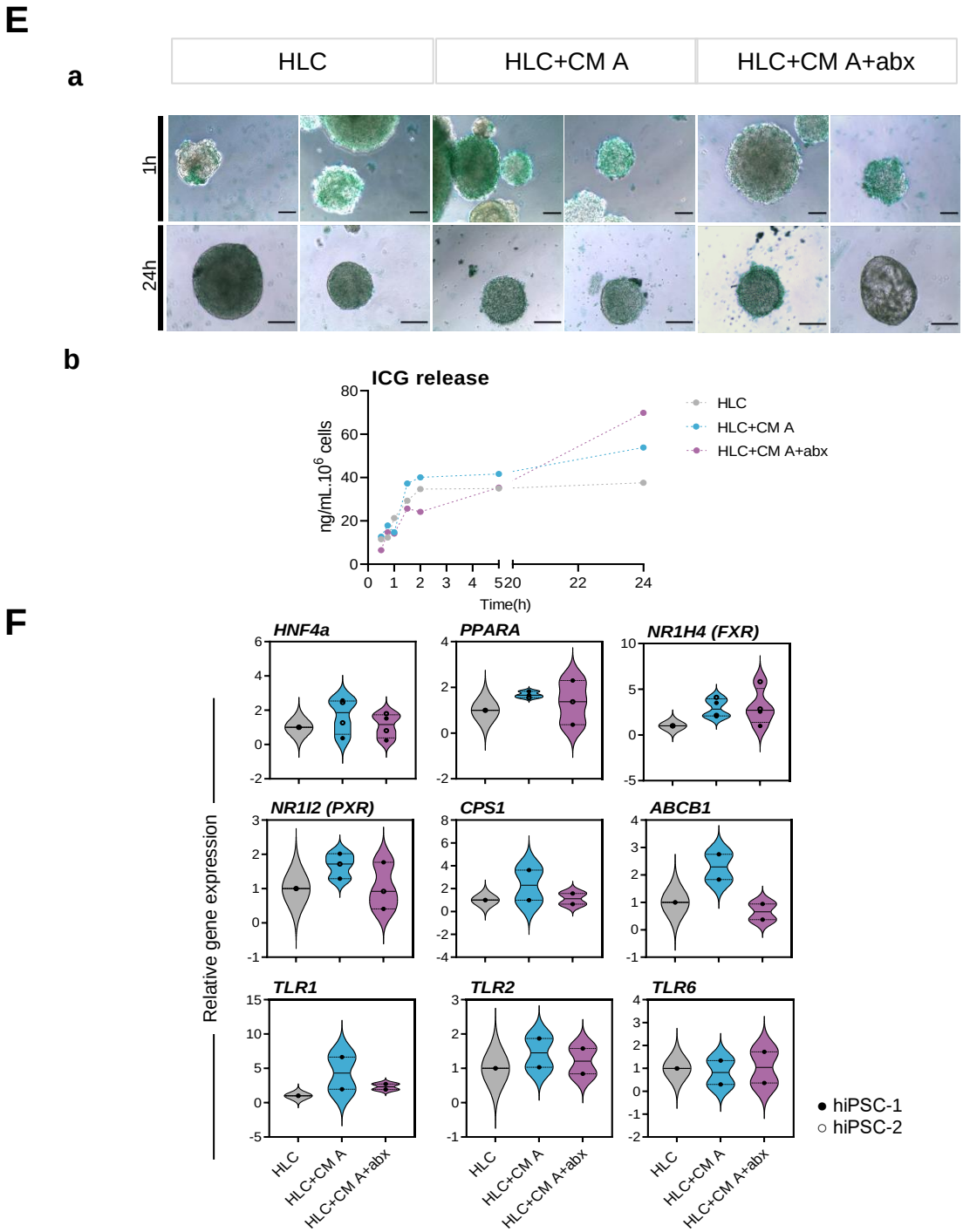

Figure 5. hiPSC-HLC treated with CM A preserved hepatic functionally *in vitro*. In this model, HLC were differentiated from two hiPSC lines in STBR and exposed to CM A; CM A+abx or kept in HMM only for 6 days. After treatment, the phenotype and functionality of both untreated and treated HLC were analysed. (A) Schematic representation of the experimental design. (B) Light microscopy analysis of HLC culture viability after exposure to CM. Live cells internalized FDA and represented as green spheres, whereas death ones stained for TO-PRO™-3 and were identified with red colour. Scale bar: 200 µm. (C) Analysis of xenobiotic metabolism: (a) Relative expression of different *Cyps* by RT-qPCR. mRNA levels were normalized for *GAPDH* and data are represented as FC to untreated HLC. Gene expression values for hiPSC-1 are represented as black dots while white dots represent hiPSC-2; (b) Basal and inducible metabolism CYP3A4 measured 48h after treatment. n=1 experiment for hiPSC-1 and hiPSC-2. (D) Analysis of liver-specific plasma proteins: (a) ALB and AFP analysis by flow-cytometry; (b) Relative expression of AFP, ALB and A1AT by RT-qPCR. (c) Secretion of AFP, ALB and A1AT quantified by ELISA. Concentrations levels were normalized for DNA levels. N=1 experiment per hiPSC-line; (d) Whole-mounting immunofluorescence images of untreated HLC and HLC+CMA A. Scale bar: 50 µm. (E) ICG release: (a) Representative images of HLC after uptake (1 h) and release (24 h) of ICG. Scale bars: 100 µm.; (b) profile of ICG release by HLC after treatment; (F) Expression of *HNF4A, PPARA, FXR, PXR, CPSI, ABCB1, TLR-1., -2* and *-6* by gene expression. mRNA levels were normalized for *GAPDH* and data are represented as FC to untreated HLC. Gene expression values for hiPSC-1 are represented as black dots while white dots represent hiPSC-2. Abbreviations: ALB, albumin; AFP, alpha-fetoprotein; DAPI, 4′,6-diamidino-2-phenylindole; CM A, conditioned media from a healthy adult; CM A+abx, conditioned media from an adult under antibiotic treatment; DE, definitive endoderm; FC, fold change; hiPSC, human induced pluripotent stem cells; HLC, hepatocyte-like cells; HMM, hepatocyte maintance media; ICG, indocyanine green; STBR, stirred-tank bioreactor. Gene nomenclature description can be found in Chapter 4.

6. Discussion

Motivated by the concepts explored in our Seminar [51] and our preliminary results that showed a clear correlation between the presence of intestinal microbiota and the expression of critical hepatic markers (Appendix, Fig.6), in this Chapter, we investigated the potential of microbiome to produce more functional hPSC-HLC that will ultimately harness their potential for cell-therapies.

Altogether our results showed that the secretome from “healthy” bacteria (CM A) could preserve the functionality and phenotype of different hPSC-HLC cultured *in vitro.*

The use of microbial compounds in the culture of PHH or hPSC-HLC is not new. In 2015, Avior *et al*. treated hPSC-HLC and fetal hepatocytes with LA and Vit.K_2 and reported an inducible CYP450 activity, accurate toxicological response, and significant albumin production, comparable to PHH [52]. Five years later, Takeishi *et al*. used ursodeoxycholic acid (UDCA), among other factors, to promote HLC maturation before their recellularization into mini-liver grafts and subsequent transplantation in mice [53].

Although promising, the use of one/two postbiotics could not reflect the complexity of the whole bacterial secretome and the possible synergistic effects between them.

Thus, in this study we investigated, for the first time, the effects of the whole microbiota secretome that grew in our *in vitro* culture conditions, on the functionality of different hPSC-HLC models.

As described, microbiota’s secretomes (CMs) were formulated using an adapted protocol that simulates the human digestion *in vitro* and characterized using sophisticated chemical analytical tools. Worthy of note, to get a more realistic approximation to bacterial secretome itself, we decided not to include a bile acid extract, in contrast to more complex models of human digestion [54].

Beyond the conventional healthy secretome (CM A), we prepared a secretome modulated by antibiotics (CM A+abx).

Although both CM formulations contained BA, SCFA, vitamins and proteins, their concentrations were considerably different. While CM A showed great diversity and

concentration of BA, CM A+abx was enriched in SCFA (except acetic acid). In addition, the content of proteins was also slightly higher in CM A, but vitamins were not different between both CMs (Sup. Fig 2).

When cross-referencing the content of our CMs to what is “expected” to be found in nature [51], we identified 4 compounds that were remarkably decreased in CM A+abx when compared to the healthy formulation.

These compounds included: deoxycholic acid (DCA) (24.57 nmol/L in CM A vs 7.553 nmol/L in CM A+abx); acetic acid (3655.35 µg/mL in CM A vs 2480.42 µg/mL CM A+abx); vitamin-B1 Thiamine (40.28 nmol/L in CM A vs and 25.61 nmol/L in CM A+abx) and vitamin-B2 (6210.37 nmol/L in CM A vs 4749.1 nmol/L in CM A+abx).

DCA, one of most enriched BA in the caecum [55], was 3.3 times reduced in CM A+abx compared to CM A. Likewise, acetic acid (or acetate), a highly prevalent SCFA in human portal blood [56], was also 1.5 times decreased in CM A+abx. Finally, the vitamins B1 and B2, were reduced 1.6 and 1.3 times respectively in CM A+abx when compared to CM A. These findings suggest that the combination of the broad-spectrum antibiotics, clindamycin and rifampicin, to treat hidradenitis suppurativa, affected intestinal microbiota, which was reflected in its altered secretome.

Once it proved that CMs were successfully formulated and enriched in different organic compounds, we tested whether these two CM formulations could impact liver function. For that, we cultured hPSC-HLC obtained with different culture systems, with CMs diluted in HMM for 6 days.

As described, hESC-HLC monolayers treated with CM A formed ALB+ hepatic cords, showed an increased expression of different hepatic specific markers and a possible activation of TLR signaling pathway, compared to untreated HLC (Fig. 3). These observations were partially validated using hiPSC-HLC. We reported that HLC treated with CM A showed upregulated levels of *HNF4A*, *CYP2C9* and *CYP3A4* when compared to HLC treated with CM A+abx and untreated counterparts (Fig. 4). However, more experiments are needed to validate these results and to perform statistical analysis.

We also tested the effects of CMs in hiPSC-HLC obtained using a scalable bioprocess described by our group (Chapter 3 and 4). With superior HLC yields, we could investigate the impact of CMs in some functions that characterize the human liver. Our results showed that the functionality (i.e., the activity of CP3A4, secretion and expression of ALB, ICG release) of HLC was preserved when cells were treated with CM A (Fig. 5). These findings were not that clear for HLC exposed to CM A+abx, but the variability observed between hiPSC lines, makes it difficult to take more assertive conclusions.

Altogether our results show that supplementation with CM A might improve the expression of some putative hepatocyte markers and preserve the functionality of HLC *in vitro*. Whether it can promote cell maturation needs still needs to be carefully analysed [21].

Although promising, this study showed some conceptual and technical limitations.

Before exposing HLC to CM, a more comprehensive studies should have been conducted to discover the optimal CM dilution to be used. Although an initial study was performed testing different conditions of CM (i.e., 1:10; 1:100; 1:1000; 1:10 000; 1:100 000 and 1:1000 000) (data not shown), this study only assessed cell viability by trypan blue assay and microscopic observation. With this preliminary study, only a dilution of 1:10 proved to be toxic and compromised cell viability (data not shown). As so, we chose a CM dilution of 1:100, but more comprehensive studies assessing cellular stress (i.e., ROS and LDH production) or evaluation of apoptotic mediators (e.g., Caspase 3) would be beneficial.

In addition, due to the lack of preliminary results using HLC obtained in 3D, we used the same dilution as 2D, neglecting that these cells were cultured as aggregates and CM might not diffuse adequately.

Regarding the formulation of microbiota secretomes, they should have been prepared with a pool of stools from different donors. Furthermore, stool microorganisms should have been separated from the rest of fecal material using a procedure with a Nycodenz® density gradient as described [57]. After isolation and incubation with the SIF, fecal bacteria could have been identified by 16S rRNA gene sequencing after bacterial DNA isolation with commercially available kits (e.g., Stool DNA Isolation Kit

(NORGEN, Cat. 27600). This would have allowed cross-referencing the species of bacteria and the possible postbiotics found in the CM. This is currently being done at Baptista´s Lab, collecting pools of faeces from 1, 8-9 months-old and adult donors. In addition, new analytical methods, including peptidomics, could have been used, as it would have helped decode CM and reveal novel peptide postbiotics.

Finally, this study brings new opportunities to preserve the functionality hPSC-HLC in vitro and ultimately will harness their potential for cell-therapies.

7. References

[1] Asrani SK, Devarbhavi H, Eaton J, Kamath PS. Burden of liver diseases in the world. J Hepatol 2019;70:151–71. https://doi.org/10.1016/j.jhep.2018.09.014.

[2] Stepanova M, De Avila L, Afendy M, Younossi I, H. P, Cable R, et al. Direct and Indirect Economic Burden of Chronic Liver Disease in the United States. Clin Gastroenterol Hepatol 2017;15:759-766.e5. https://doi.org/10.1016/j.cgh.2016.07.020.

[3] Organ Procurement and Transplantation Network 2022. https://optn.transplant.hrsa.gov/data/.

[4] Matas , A.J., Sutherland, D.E., Steffes, M.W., Mauer, S.M., Sowe, A., Simmons, R.L., Najarian JS. Hepatocellular transplantation for metabolic deficiencies: decrease of plasms bilirubin in Gunn rats. Science 1976;192:892–4. https://doi.org/10.1126/science.818706.

[5] Sutherland, D.E., Numata, M., Matas, A.J., Simmons, R.L., Najarian JS. Hepatocellular transplantation in acute liver failure. Surgery 1977;82:124–32.

[6] Minato M., Houssin D., Demma I., Morin J., Gigou M., Szekely A.M. BH. Transplantation of Hepatocytes for Treatment of Surgically Induced Acute Hepatic Failure in the Rat. Eur Surg Res 1984;16:162–9. https://doi.org/10.1159/000128404.

[7] Yoshida Y, Tokusashi Y, Lee GH, Ogawa K. Intrahepatic transplantation of normal hepatocytes prevents Wilson's disease in Long-Evans Cinnamon rats. Gastroenterology 1996;111:1654–60. https://doi.org/10.1016/s0016-5085(96)70029-x.

[8] De Vree JM, Ottenhoff R, Bosma PJ, Smith AJ, Aten J, Oude Elferink RP. Correction of liver disease by hepatocyte transplantation in a mouse model of progressive familial intrahepatic cholestasis. Gastroenterology 2000;119:1720–30. https://doi.org/10.1053/gast.2000.20222.

[9] Fox I.J., Chowdhury J.R., Kaufman S.S., Goertzen T.C., Chowdhury N.R., Warkentin P.I. et al. Treatment of the Crigler-Najjar syndrome type I with hepatoycte transplantation. N Engl J Med 1998;338:1422–6.

[10] Dhawan A, Mitry RR, Hughes RD, Lehec S, Terry C, Bansal S, et al. Hepatocyte transplantation for inherited factor VII deficiency. Transplantation 2004;78:1812–4. https://doi.org/10.1097/01.TP.0000146386.77076.47.

[11] Meyburg J, Das AM, Hoerster F, M. L, H. K, Engelmann G. et al. One liver for four children: First clinical series of liver cell transplantation for severe neonatal urea cycle defects. Transplantation 2009;87:636–41. https://doi.org/doi: 10.1097/TP.0b013e318199936a.

[12] X. S, Najimi M, Sibille C, Nassogne M-C, Smets F, Sokal EM. Sustained engraftment and tissue enzyme activity after liver cell transplantation for argininosuccinate lyase deficiency. Gastroenterology 2006;130:1317–23. https://doi.org/doi: 10.1053/j.gastro.2006.01.008.

[13] Sokal EM, Smets F, Bourgois A, Van Maldergem L, Buts J-P, Reding R, et al. Hepatocyte transplantation in a 4-year-old girl with peroxisomal biogenesis disease: Technique, safety, and metabolic follow-up. Transplantation 2003;76:735–8. https://doi.org/doi: 10.1097/01.TP.0000077420.81365.53.

[14] Muraca M., Gerunda G., Neri D., Vilei M.T., Granato A., Feltracco P. et al. Hepatocyte transplantation as a treatment for glycogen storage disease type 1a. Lancet 2002;359:317–8. https://doi.org/doi: 10.1016/S0140-6736(02)07529-3.

[15] Dhawan A, Puppi J, Hughes RD, Mitry RR. Human hepatocyte transplantation: current experience and future challenges. Nat Rev Gastroenterol Hepatol 2010;7:288–98. https://doi.org/doi: 10.1038/nrgastro.2010.44.
[16] Gramignoli R, Vosough M, Kannisto K, Srinivasan RC, Strom SC. Clinical hepatocyte transplantation: Practical limits and possible solutions. Eur Surg Res 2015;54:162–77. https://doi.org/10.1159/000369552.
[17] Hay DC, Zhao D, Fletcher J, Hewitt ZA, McLean D, Urruticoechea-Uriguen A, et al. Efficient differentiation of hepatocytes from human embryonic stem cells exhibiting markers recapitulating liver development in vivo. Stem Cells 2008;26:894–902. https://doi.org/10.1634/stemcells.2007-0718.
[18] Si-tayeb K, Noto FK, Nagaoka M, Li J, Battle MA, Duris C, et al. Highly Efficient Generation of Human Hepatocyte–Like Cells from Induced Pluripotent Stem Cells. Hepatology 2010;9:297–305. https://doi.org/10.1002/hep.23354.
[19] Baxter M, Withey S, Harrison S, Segeritz CP, Zhang F, Atkinson-Dell R. Phenotypic and functional analyses show stem cell-derived hepatocyte-like cells better mimic fetal rather than adult hepatocytes. J Hepatol 2015;62:581–9. https://doi.org/10.1016/j.jhep.2014.10.016.
[20] Ghosheh N, Küppers-Munther B, Asplund A, Andersson CX, Björquist P, Andersson TB, et al. Human Pluripotent Stem Cell-Derived Hepatocytes Show Higher Transcriptional Correlation with Adult Liver Tissue than with Fetal Liver Tissue. ACS Omega 2020;5:4816–27. https://doi.org/10.1021/acsomega.9b03514.
[21] Alvarez-Dominguez JR, Melton DA. Cell maturation: Hallmarks, triggers, and manipulation. Cell 2022. https://doi.org/10.1016/j.cell.2021.12.012.
[22] Chen C, Soto-Gutierrez A, Baptista PM, Spee B. Biotechnology Challenges to In Vitro Maturation of Hepatic Stem Cells. Gastroenterology 2018;154:1258–72.
[23] Su S, Di Poto C, Roy R, Liu X, Cui W, Kroemer A, et al. Long-term culture and characterization of patient-derived primary hepatocytes using conditional reprogramming. Exp Biol Med 2019;244:857–64. https://doi.org/10.1177/1535370219855398.
[24] Clement B, Guguen-Guillouzo C, Campion J -P, Glaise D, Bourel M, Guillouzo A. Long-Term Co-Cultures of Adult Human Hepatocytes with Rat Liver Epithelial Cells: Modulation of Albumin Secretion and Accumulation of Extracellular Material. Hepatology 1984;4:373–80. https://doi.org/10.1002/hep.1840040305.
[25] Ahmed HMM, Salerno S, Morelli S, Giorno L, De Bartolo L. 3D liver membrane system by co-culturing human hepatocytes, sinusoidal endothelial and stellate cells. Biofabrication 2017;9. https://doi.org/10.1088/1758-5090/aa70c7.
[26] Danoy M, Tauran Y, Poulain S, Jellali R, Bruce J, Leduc M, et al. Investigation of the hepatic development in the coculture of hiPSCs-derived LSECs and HLCs in a fluidic microenvironment. APL Bioeng 2021;5. https://doi.org/10.1063/5.0041227.
[27] Pettinato G, Lehoux S, Ramanathan R, Salem MM, He LX, Muse O, et al. Generation of fully functional hepatocyte-like organoids from human induced pluripotent stem cells mixed with Endothelial Cells. Sci Rep 2019;9:1–21. https://doi.org/10.1038/s41598-019-45514-3.
[28] Nguyen DG, Funk J, Robbins JB, Crogan-Grundy C, Presnell SC, Singer T, et al. Bioprinted 3D primary liver tissues allow assessment of organ-level response to clinical drug induced toxicity in vitro. PLoS One 2016;11:1–17. https://doi.org/10.1371/journal.pone.0158674.
[29] Ma X, Qu X, Zhu W, Li YS, Yuan S, Zhang H, et al. Deterministically patterned

biomimetic human iPSC-derived hepatic model via rapid 3D bioprinting. Proc Natl Acad Sci U S A 2016;113:2206–11. https://doi.org/10.1073/pnas.1524510113.
[30] Zhong C, Xie HY, Zhou L, Xu X, Zheng S Sen. Human hepatocytes loaded in 3D bioprinting generate mini-liver. Hepatobiliary Pancreat Dis Int 2016;15:512–8. https://doi.org/10.1016/S1499-3872(16)60119-4.
[31] Ortega-Prieto AM, Skelton JK, Wai SN, Large E, Lussignol M, Vizcay-Barrena G, et al. 3D microfluidic liver cultures as a physiological preclinical tool for hepatitis B virus infection. Nat Commun 2018;9. https://doi.org/10.1038/s41467-018-02969-8.
[32] Rajendran, D., Hussain, A., Yip, D., Parekh, A., Shrirao, A., Cho CH. Long-term liver-specific functions of hepatocytes in electrospun chitosan nanofiber scaffolds coated with fibronectin. J Biomed Mater Res A 2017;105:2119–28. https://doi.org/10.1002/jbm.a.36072.
[33] Isidro, I., Vicente, P., Pais, D., Almeida, Joana I., Domingues, M., Abecasis, B., Mertinez-Turrillas, R., Rodriguez-Madoz, Juan R., Aspegren, A., Alves, Paula M., Serra M. On-line monitoring of hiPSC expansion and hepatic differentiation process in a 3D culture system by dielectric spectroscopy. Biotechnol Bioeng n.d.
[34] Yamashita T, Takayama K, Sakurai F, Mizuguchi H. Billion-scale production of hepatocyte-like cells from human induced pluripotent stem cells. Biochem Biophys Res Commun 2018;496:1269–75. https://doi.org/10.1016/j.bbrc.2018.01.186.
[35] Almeida JI, Tenreiro MF, Martinez-Santamaria L, Aspizua SG GJ, Alves PM, Serra M BP. Hallmarks of the human intestinal microbiome on liver maturation and function. J Hepatol 2021. https://doi.org/10.1016/j.jhep.2021.10.015.
[36] Zhao S, Jang C, Liu J, Uehara K, Gilbert M, Izzo L, et al. Dietary fructose feeds hepatic lipogenesis via microbiota-derived acetate. Nature 2020;579:1–6. https://doi.org/10.1038/s41586-020-2101-7.
[37] Makishima M, Okamoto AY, Repa JJ, Tu H, Learned RM, Luk A, et al. Identification of a Nuclear Receptor for Bile Acids. Science (80-) 1999;284:1362 LP – 1365. https://doi.org/10.1126/science.284.5418.1362.
[38] Gao X, Lin SH, Ren F, Li JT, Chen JJ, Yao CB, et al. Acetate functions as an epigenetic metabolite to promote lipid synthesis under hypoxia. Nat Commun 2016;7. https://doi.org/10.1038/ncomms11960.
[39] Zhou D, Chen YW, Zhao ZH, Yang RX, Xin FZ, Liu XL, et al. Sodium butyrate reduces high-fat diet-induced non-alcoholic steatohepatitis through upregulation of hepatic GLP-1R expression. Exp Mol Med 2018;50:1–12. https://doi.org/10.1038/s12276-018-0183-1.
[40] Barone M, Francavilla A, Polimeno L, Ierardi E, Romanelli D, Berloco P, et al. Modulation of rat hepatocyte proliferation by bile salts: In vitro and in vivo studies. Hepatology 1996;23:1159–66. https://doi.org/10.1053/jhep.1996.v23.pm0008621149.
[41] Selwyn FP, Cheng SL, Bammler TK, Prasad B, Vrana M, Klaassen C, et al. Developmental regulation of drug-processing genes in livers of germ-free mice. Toxicol Sci 2015;147:84–103. https://doi.org/10.1093/toxsci/kfv110.
[42] Cornell RP, Liljequist BL, Bartizal KF. Depressed liver regeneration after partial hepatectomy of germ-free, athymic and lipopolysaccharide-resistant mice. Hepatology 1990;11:916–22. https://doi.org/10.1002/hep.1840110603.
[43] Minekus M, Alminger M, Alvito P, Ballance S, Bohn T, Bourlieu C, et al. A

standardised static in vitro digestion method suitable for food-an international consensus. Food Funct 2014;5:1113–24. https://doi.org/10.1039/c3fo60702j.
[44] Gener G, Canoui-Poitrine F, Revuz JE, Faye O, Poli F, Gabison G, et al. Combination therapy with clindamycin and rifampicin for hidradenitis suppurativa: A series of 116 consecutive patients. Dermatology 2009;219:148–54. https://doi.org/10.1159/000228334.
[45] Mallanna SK, Duncan SA. Differentiation of hepatocytes from pluripotent stem cells. Curr Protoc Stem Cell Biol 2013;1:1–15. https://doi.org/10.1002/9780470151808.sc01g04s26.
[46] Asplund A, Pradip A, van Giezen M, Aspegren A, Choukair H, Rehnström M, et al. One Standardized Differentiation Procedure Robustly Generates Homogenous Hepatocyte Cultures Displaying Metabolic Diversity from a Large Panel of Human Pluripotent Stem Cells. Stem Cell Rev Reports 2016;12:90–104. https://doi.org/10.1007/s12015-015-9621-9.
[47] Serra M, Correia C, Malpique R, Brito C, Jensen J, Bjorquist P, et al. Microencapsulation technology: A powerful tool for integrating expansion and cryopreservation of human embryonic stem cells. PLoS One 2011;6:1–13. https://doi.org/10.1371/journal.pone.0023212.
[48] Zapata-Linares N, Rodriguez S, Salido E, Abizanda G, Iglesias E, Prosper F, et al. Generation and characterization of human iPSC lines derived from a Primary Hyperoxaluria Type I patient with p.I244T mutation. Stem Cell Res 2016;16:116–9. https://doi.org/10.1016/j.scr.2015.12.014.
[49] Abecasis B, Aguiar T, Arnault É, Costa R, Gomes-Alves P, Aspegren A, et al. Expansion of 3D human induced pluripotent stem cell aggregates in bioreactors: Bioprocess intensification and scaling-up approaches. J Biotechnol 2017;246:81–93. https://doi.org/10.1016/j.jbiotec.2017.01.004.
[50] Isidro IA, Vicente P, Pais DAM, Almeida JI, Domingues M, Abecasis B, et al. Online monitoring of hiPSC expansion and hepatic differentiation in 3D culture by dielectric spectroscopy. Biotechnol Bioeng 2021:1–8. https://doi.org/10.1002/bit.27751.
[51] Almeida, Joana I., Miguel F. Tenreiro, Lucía Martinez-Santamaria, Aspizua, Sara Guerrero, Javier P. Gisbert, Paula M. Alves, Margarida Serra PMB. Hallmarks of the human intestinal microbiome on liver maturation and function. J Hepatol 2021.
[52] Avior Y, Levy G, Zimerman M, Kitsberg D, Schwartz R, Sadeh R, et al. Microbial-Derived Lithocholic Acid and Vitamin K2 Drive the Metabolic Maturation of Pluripotent Stem Cells-Derived and Fetal Hepatocytes. Hepatology 2015;62:265–78. https://doi.org/10.1002/hep.27803.
[53] Takeishi K, Collin A, Hortet D, Wang Y, Mashimo T, Fox IJ, et al. Assembly and Function of a Bioengineered Human Liver for Transplantation Generated Solely from Induced Pluripotent Stem Cells. CellReports 2020;31:107711. https://doi.org/10.1016/j.celrep.2020.107711.
[54] Hollebeeck, S., Borlon, F., Schneider, Y-J., Larondelle, Y., Rogez H. Development of a standardised human in vitro digestion protocol based on macronutrient digestion using response surface methodology. Food Chem 2013;138:1936–44. https://doi.org/10.1016/j.foodchem.2012.11.041.
[55] Hamilton JP, Xie G, Raufman JP, Hogan S, Griffin TL, Packard CA, et al. Human cecal bile acids: Concentration and spectrum. Am J Physiol - Gastrointest Liver Physiol 2007;293:256–63. https://doi.org/10.1152/ajpgi.00027.2007.
[56] Cummings JH, Pomare EW, Branch HWJ, Naylor CPE, MacFarlane GT. Short

chain fatty acids in human large intestine, portal, hepatic and venous blood. Gut 1987;28:1221–7. https://doi.org/10.1136/gut.28.10.1221.
[57] Hevia A, Delgado S, Margolles A, Sanchez B. Application of density gradient for the isolation of the fecal microbial stool component and the potential use thereof. Sci Rep 2015;5:1–9. https://doi.org/10.1038/srep16807.

8. Supporting Figures

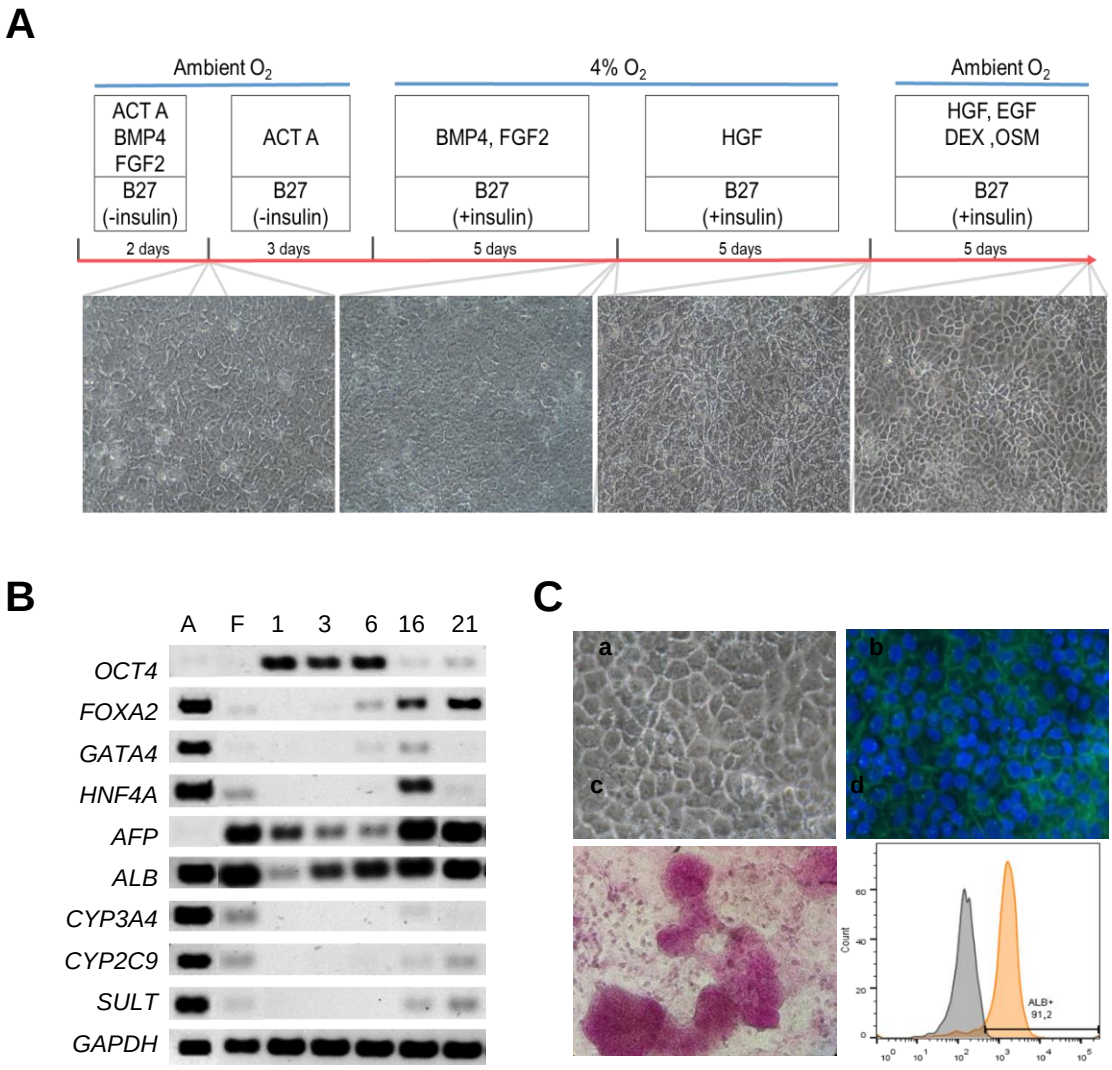

Supporting Figure 3. HLC were successfully generated *in vitro* and exhibited morphology and functional attributes of PHH. The hESC line *ES-4* was differentiated in HLC, as 2D cell monolayers, according to Mallanna's et al. To recapitulate the human hepatogenesis *in vitro*, cells were cultured in adv. RPMI supplemented with a cocktail of different growth factors and exposed to distinct oxygen conditions. Immediately after the critical development phases (at days 1, 3, 6, 16, 21) cells were harvested for further analysis. At the end of differentiation, HLC were characterized in a more comprehensive. (A) Schematic representation of media formulations and culture conditions used throughout hepatic differentiation; and morphological changes observed in cells differentiated from hES to DE (5 days of differentiation), to hepatic progenitors (10 days of differentiation), and finally towards imHLC (15 days of differentiation) and more mature cells (mHLC) (20 days of differentiation). All images were acquired 200x magnification. (B) Transcriptomic analysis during differentiation by RT-PCR. (C) Characterization of HLC obtained at the end of differentiation: (a) Bright-field microscopy image of HLC (400x magnification); (b) EpCAM and DAPI fluorescence immunocytochemistry staining (400x magnification); (c) Glycogen accumulation (PAS staining); (d) Quantification of ALB by flow cytometry. Abbreviations: A, adult liver; ACT A, activin A; ALB, albumin; BMP4, Bone morphogenetic protein 4; CM A, conditioned media from a healthy adult; DE, definitive endoderm; DEX, dexamethasone; EGF, epidermal growth factor; F, fetal liver; FGF2, fibroblast growth factor 2 precursor; hESC, human embryonic stem cells; HGF, hepatocyte growth factor; HLC, hepatocyte-like cells; HLC+CM A, HLC treated with CM A; HMM, hepatocyte maintenance media; imHLC, immature HLC; mHLC, mature HLC; OSM, oncostatin M; O2, oxygen. Pas, periodic acid–Schiff stain. Gene nomenclature can be found in Table 1.

A

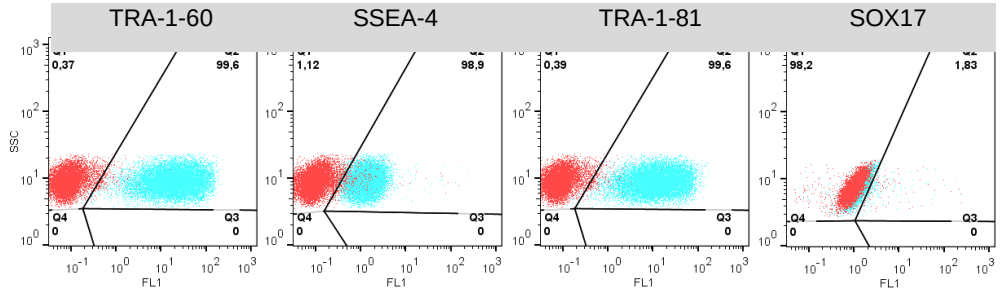

B

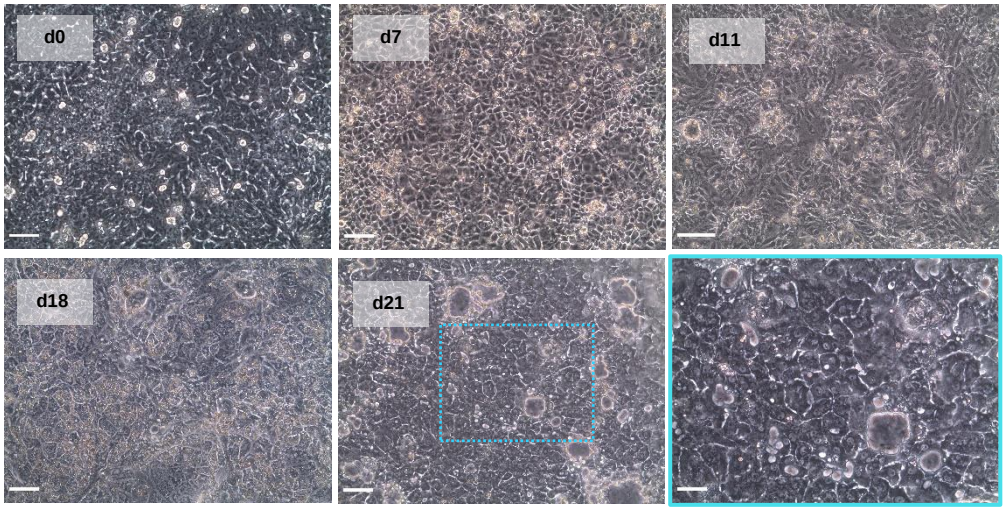

C

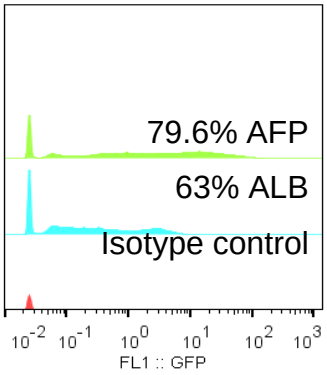

Supporting Figure 4. HLC were successfully differentiated *in vitro* but preserved the fetal marker, AFP. (A) Analysis of pluripotent (TRA-1-60, SSEA-4, TRA-1-80) and the endodermal marker (SOX17) before differentiation by flow cytometry. (B) Light microscopy analysis of cell during differentiation: d0, hiPSC; d7, DE; d18, imHLC; d21, mHLC. Scale bar: 200µm. (C) ALB and AFP quantification in HLC generated after differentiation (day 21 of differentiation) by flow-cytometry.

9. Appendix

5.4. Preliminary Results: Germ-free mice showed reduced expression of hepatic genes when compared to conventional raised animals

With this animal model, we aim to investigate whether the liver function is improved with the administration of CM. To assess that, we firstly analysed if the expression of specific hepatic genes varies in mice colonized by bacteria (SPF) when compared to counterparts that lack intestinal microbes (GF mice) (Fig. 6A).

We showed that GF mice showed reduced expression of *Alb*, *Cyp2c38*, *Cyp2e1* and *Cyp2C9* compared to SPF (Fig. 6B). Hence, we want to test if administration with CM could improve GF hepatic levels to the same levels found in SFP animals. If so, we plan to inject CM in models of acute and chronic liver failure and evaluate if it can restore hepatic functionality.

A

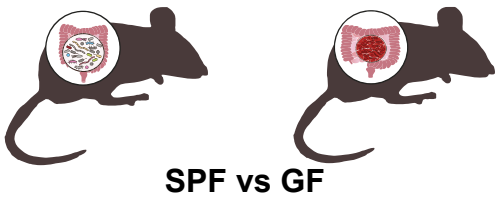

B

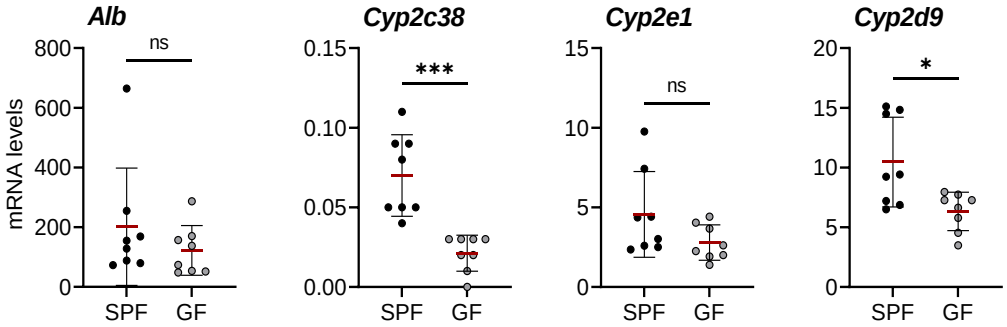

Figure 6. Germ-free animals showed reduced expression of key hepatic markers compared to SPF animals. (A) Livers from SPF or GF mice (n=8) were analysed for the expression of *Alb*, *Cyp2c38*, *Cyp2e1* and *Cyp2d9* by RT-qPCR (B). Data are presented as mean ± SD. Where *p ≤ 0.05; **p ≤ 0.01; ***p ≤ 0.001; and ns – nonsignificant (p > 0.05).

Chapter 3

TOWARDS MASSIVE PRODUCTION OF HIPSC-HLC FOR APPLICATION IN REGENERATIVE MEDICINE

This chapter is adapted from the manuscript:

Isidro, I. A., Vicente, P., Pais, D. A. M., **Almeida, J.I.**, Domingues, M., Abecasis, B., Zapata-Linares, N., Rodriguez-Madoz, J. R., Prosper, F., Aspegren, A., Alves, P. M., Serra, M. Online monitoring of hiPSC expansion and hepatic differentiation in 3D culture by dielectric spectroscopy. 2021. Biotechnology and Bioengineering, 1–8. doi: 10.1002/bit.27751. https://doi.org/10.1002/bit.27751

Author’s contribution

Joana Inês Almeida participated in the bioreactor experiments and performed part of the characterization of hiPSC-HLC. Joana was also involved in the data analysis and interpretation, manuscript writing and revision.

Contents

1. Graphical abstract

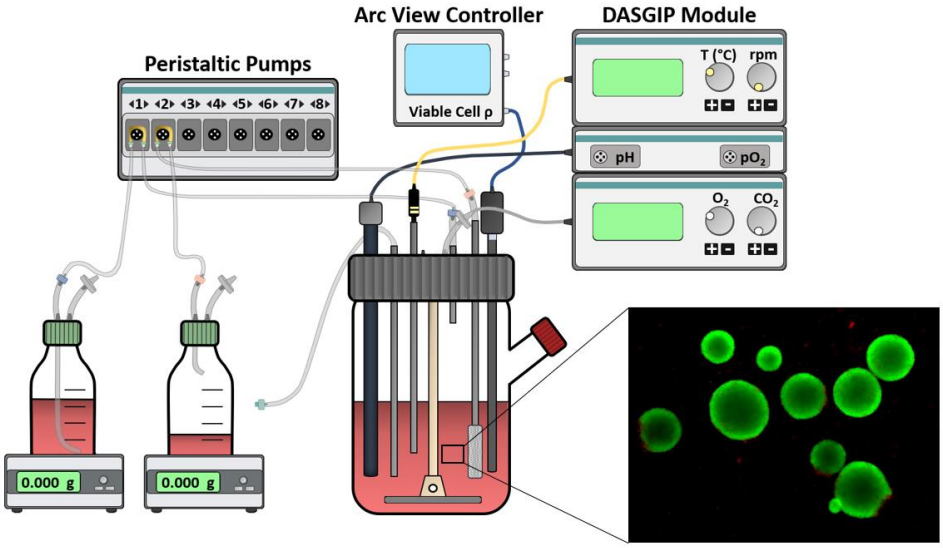

Integrated bioprocess for expansion and hepatic differentiation of hiPSC as 3D aggregates in bioreactors

2. Introduction

Hepatocyte-like cells derived from hiPSC (hiPSC-HLC) hold great promise as an unlimited source of hepatocytes for *in vitro* disease modelling, preclinical drug development and regenerative medicine applications [1]. In the last decade, these cells have been successfully generated as two-dimensional (2D) monolayers exhibiting morphological and functional features of primary human hepatocytes [2,3].

More recently, these protocols have been transferred from standard planar 2D cultures to more physiologic and parameter-controlled 3D cell culturing approaches, allowing the generation of relevant yields of hiPSC-HLC, compatible with both preclinical research and clinical applications [4].

Different bioreactor systems have already been reported for generation of hiPSC-HLC, including a rotary cell culture system [5], stirred-tank [6] and 3D perfused bioreactors [7].

As production technology and process knowledge advances, the opportunity to implement process intensification likewise increases. Indeed, the combination of stem cell expansion and differentiation/maturation steps in an integrated bioprocess enables the biomanufacturing process to be streamlined and automated in a fully enclosed bioreactor system.

Previous work in neuronal and cardiac differentiation of human stem cell in stirred-tank bioreactors (STBR) already demonstrated the advantages of integrated bioprocesses over multi-step approaches including higher robustness and scalability and reduced costs (reviewed in [8]).

Monitoring cell quality attributes is a critical step for any biologic manufacturing process but remains a challenge in 3D culturing approaches. In fact, the conventional assessment of cell viability requires aggressive enzymatic treatments to disrupt cell spheroids which is a laborious and time-consuming step, often resulting in sparse and biased, imprecise, or even incorrect measurements.

Finding process analytical technologies (PAT) that enable *in situ* monitoring of stem cell growth and differentiation status in 3D culture, thus minimizing contamination risks, would have an enormous impact in stem cell bioprocessing.

Dielectric spectroscopy has already been shown to successfully monitor viable cell concentration in single-cell suspension culture systems [9,10] but there are still few published applications in 3D cultures [11,12].

Herein, we established an integrated bioprocess that combines 3D hiPSC expansion and hepatic differentiation steps in STBR operating in perfusion and, for the first time, assessed the potential of dielectric spectroscopy for the *in situ* monitoring of hiPSC growth and differentiation status.

3. Materials and Methods

3.1. hiPSC Culture

The hiPSC PBL-PH1 clone 2.4 was derived from peripheral blood lymphocytes (PBL) obtained from a PH1-diagnosed patient with a p.I244T [13]. The cell line, registered at the Spanish National Cell Bank, was provided by Dr. Juan R. Rodriguez-Madoz (Area of Cell Therapy, Clínica Universidad de Navarra, Spain), within the scope of ERAdicatPH project.

Human iPSCs were routinely propagated in static culture conditions (T-flasks or 6-well plates (Falcon™)), using the Cellartis® DEF-CS 100 Culture System (Cat. No. Y30020, Takara BioEurope AB, Göteborg, Sweden) and were placed at 37°C in a humidified atmosphere with 5 % (v/v) CO_2, according to manufacturer's recommendations. Briefly, hiPSC were seeded at 4-6 x 10^4 cell/cm^2 and sub-cultured every 3-4 days; culture medium was replaced daily. At 80 % cell confluence, hiPSC were detached from the T-flasks by rinsing with Dulbecco phosphate-buffered saline (DPBS, Thermo Fisher Scientific, Waltham, Massachusetts, EUA) and incubating with Versene (Thermo Fisher Scientific, Waltham, Massachusetts, EUA) for 8 min at 37°C. Cells were resuspended in Cellartis® DEF-CS culture medium and counted using Trypan Blue exclusion method to determine cell number and viability, as described elsewhere [14].

3.2. hiPSC expansion and hepatocyte differentiation in STBR

hiPSC were expanded and differentiated into HLC in STBR (DasGip cellferm-pro bioreactor system, Eppendorf AG, Hamburg, Germany) operated in perfusion (200 mL working volume). Flat bottom bioreactor vessels equipped with trapezoid shaped paddle impellers with long arms were used (Fig. 1) based on their mixing performance as reported in previous publications from our group [14–16]. Cells were cultured under defined and controlled conditions of temperature, CO_2, pO_2, aeration, stirring and perfusion rates, as described below.

Data acquisition and process control were performed using DASGIP® Control Software 4.0 (Eppendorf AG). Sensors and pumps were calibrated as described by the manufacturer's instructions.

3.2.1. Expansion of hiPSC as 3D culture

3D hiPSC expansion in bioreactors was performed as described previously by our group [14]. Briefly, hiPSCs single cell suspensions were prepared by harvesting cells from static monolayer cultures with TrypLE^{TM} Select (Gibco Life Technologies), during 5 minutes at 37°C and inoculated at a density of 2.5 x10^5 cell/mL in STBR in 150 mL of Cellartis® DEF-CSTM Xeno-Free 3D Spheroid Culture Medium (Cat. No. Y30047, Takara BioEurope AB, Göteborg, Sweden). During expansion step (duration of 5 days, identified as day -5 to day 0), cells were cultured under defined and controlled conditions (temperature: 37°C; surface aeration rate: 0.1 volumes per volume of medium (vvm); pO_2: 4%). The stirring rate was set to 80 rpm for the first 6 h and then increased to 90 rpm. Perfusion was initiated 24h after inoculation, with dilution rate of 1.3 day^{-1}, according to the protocol developed by our group [14].

3.2.2. Hepatocyte differentiation of hiPSC in 3D culture

Differentiation was performed using hepatocyte suspension differentiation protocol (Cat. No. Y11111, Y11112, Y11132-37 and Y30051, Takara BioEurope AB, Göteborg, Sweden). Endoderm differentiation was initiated 5 days after inoculation (day 0), when cell concentration reached 1x10^6 cell/mL and the average size of aggregates was 150 µm, approximately. During the differentiation step (duration of 28 days, identified as day 0 to day 28, Fig. 1A), cells were cultured under defined and controlled conditions (temperature: 37°C; surface aeration rate: 0.1 vvm; CO_2: 5% (v/v)). Stirring rate was set to 90 rpm until day 4 and increased to 100 rpm from day 4 onwards. At day 0, perfusion was interrupted, and the expansion media was replaced by Definitive Endoderm Day 1 Medium (Basal Medium for Definitive Endoderm Differentiation Cat. No. Y11135, concentrate Day 1 Cat. No. Y11132, Takara BioEurope AB, Göteborg, Sweden). Complete media exchanges were then performed at days 1 (Basal Medium for Definitive Endoderm Differentiation Cat. No. Y11135, concentrate Day 1 Cat. No. Y11133, Takara BioEurope AB, Göteborg, Sweden), 2 (Basal Medium for Definitive Endoderm Differentiation Cat. No. Y11135, concentrate Day 3&4 Cat. No. Y11134,

Takara BioEurope AB, Göteborg, Sweden), 4 (Basal Medium for Progenitor Differentiation Cat. No. Y11136, Hepatocyte Progenitor Medium Concentrate Cat. No. Y11111, Takara BioEurope AB, Göteborg, Sweden), 9 (Basal Medium for Hepatocyte Differentiation Cat. No. Y11137, Hepatocyte Differentiation Medium Concentrate Cat. No. Y11112, Takara BioEurope AB, Göteborg, Sweden) and 14 (Cellartis Hepatocyte Maintenance Medium Cat. No. Y30051, Takara BioEurope, Göteborg, Sweden). Perfusion was operated at defined dilution rates according to the manufacturer's instructions; the values used for dilution rate were indicated in Fig. 1A.

3.3. Hepatocyte differentiation of hiPSC in 2D static culture systems

Hepatocyte differentiation in monolayer static culture conditions was carried out using Cellartis® iPS Cell to Hepatocyte Differentiation System (Cat. No. Y30055, Takara BioEurope AB, Göteborg, Sweden), as described elsewhere [17].

3.3.1. Culture characterization

3.3.1.1. Cell viability, concentration and aggregate diameter

Cell viability: For viability assessment two methods were used: (i) the enzyme substrate fluorescein diacetate (Sigma-Aldrich) and TO-PRO®-3 dye (0.5 µM; Thermo Fisher Scientific) and (ii) the Trypan blue (Thermo Fischer Scientific) exclusion method, as previously described [14,18]. For the first method, direct staining of the aggregates was performed followed by observation at the inverted fluorescence microscope (DMI6000, Leica, Wetzlar, Germany), as described elsewhere [18]. Representative images were taken using a digital camera (Leica DFC 360 FX). For the latter method, aggregates were centrifuged at 100 x g for 5 min, resuspended in DPBS and again centrifuged at 100 x g for 5 min. Supernatants were removed before adding the TrypLE Select for 5 min incubation at 37°C with agitation using a thermomixer (Eppendorf). Viable cells were quantified by Trypan Blue exclusion, as described elsewhere [18].

Aggregate size and concentration: Aggregate samples harvested from the bioreactor were distributed in wells of a 96-well plate (100 µL/well) and counted using an inverted

microscope (CKX31, Olympus). Images of cell aggregates were collected (Leica DFC 360 FX) and analysed in Image J open source software (Rasband, WS, ImageJ, U. S. National Institutes of Health, Bethesda, MD, USA, http://imagej.nih.gov/ij/, 1997–2012) for estimation of aggregate size, as described elsewhere [14].

3.3.1.2. Immunocytochemistry of hiPSC-HLC aggregates

Whole Mount Immunofluorescence Microscopy: Cell aggregates harvested from the bioreactor were fixed in 4% (w/v) paraformaldehyde (PFA) in phosphate-buffered saline (PBS) for 1 hour at RT. Fixed cells were washed with DPBS and permeabilized/blocked in DPBS containing 0.1% (v/v) Triton X-100 and 0.2% (v/v) gelatine from cold water fish skin for 20 min at RT. Subsequently, cells were washed three times with DPBS and incubated, for 2h at RT, with the primary antibodies Albumin (Abcam) and AFP (Sigma) diluted in 0.125% FSG+0.1%Triton X-100 according to supplier instructions. Cells were washed with DPBS and incubated in the dark, with the secondary antibodies Alexa Flour 594 (Invitrogen) and Alexa Fluor 488 (Invitrogen) (diluted 1:1000 in 0.125%FSG+0.1% Triton X-100), for 1h at RT. Finally, aggregates were washed as previously and mounted in ProLong™ Gold Antifade Mount (Invitrogen), containing 40,6-diamidino-2-phenylindole (DAPI), in ibidi® chambers. Cells were visualized under a confocal miscrossope (SP5, Leica).

3.3.1.3. Gene expression analysis

Cells from static culture, dissociated with TrypLE™ Select (Gibco Life Technologies) for 5 min at 37°C, and aggregates collected from the bioreactor were centrifuged at 300 x g for 5 min. These pellets were washed with DPBS, snap-freezed with liquid nitrogen and kept at -80°C. mRNA was extracted using the High Pure RNA Isolation kit (Roche) according to manufacturer's instructions. mRNA was quantified in a NanoDrop 2000c spectophotometer (Thermo Scientific) and cDNA synthesized with 200 ng RNA per sample, using the Transcriptor High Fidality cDNA Synthesis Kit (Roche). RT-qPCR reactions of 10 µL included 2 µL of cDNA (diluted 1:2 in RNase free water), 0.5 µL of forward and reverse primers (5 µM) (Table S1) and 5 µL of LightCycler 480 SYBR Green I Master Kit (Roche) and 2 µL of RNase free water were analyzed in the LightCycler 480 Instrument II-384-well block (Roche). The thermal cycle had an initial pre-incubation step for 10 min at 95°C; 45 cycles of amplification

with denaturation at 95°C for 10 s and annealing at 62°C for 10 s; extension at 72°C for 15 s. Each sample was run in triplicate and data analyzed in LightCycler 480 Software v1.5.0 (Roche). Relative expression levels were calculated using the $2^{-\Delta\Delta Ct}$ method [19] and normalized to housekeeping gene *GAPDH1* expression and represented relative to a control sample (set at 1).

Table 1.Primers used for RT-qPCR analysis.

Gene Symbol	Forward primer (5'-3') sequence	Reverse primer (5'-3') sequence
GAPDH1	AATGAAGGGGTCATTGATGG	AAGGTGAAGGTCGGAGTCAA
A1AT	CACCCACGATATCATCACCA	CCCCATTGCTGAAGACCTTA
SOX17	GAATCCAGACCTGCACAACG	CTCTGCCTCCTCCACGAAG
FOXA2	CACTCGGCTTCCAGTATGCT	GTTCATGTTGCTCACGGAGG
AGXT	GAGATCATGGGTGGCCTTG	GTCACGCGGTCCACATTCT
AFP	TTTGGGCTGCTCGCTATGAC	TTGCTGCCTTTGTTTGGAAGC
CYP3A4	AAGTCGCCTCGAAGATACACA	AAGGAGAGAACACTGCTCGTG
ALB	ACACAAGCCCAAGGCAACAA	TATCGTCAGCCTTGCAGCAC
HNF4α	AGAGCAGGAATGGGAAGGAT	GCAGTGGCTTCAACATGAGA

3.3.1.4. Albumin secretion

Samples collected from the bioreactor and static cultures, at days 21 and 25 respectively, were centrifuged (300 x g, 5 min) and supernatants kept at -20 °C prior to analysis. The concentration of secreted albumin in the supernatant was quantified by enzyme-linked immunosorbent assay (ELISA) kit (Bethyl, Montgomery, TX, USA) according to the manufacturer's instructions. Albumin synthesis rate of hiPSC-HLC aggregates was calculated according to the general mass balance equation for a continuous system: $q = (\Delta C/\Delta t - D \times (C_{in} - C_{out}))/X_V$ average, where q is the specific rate of albumin synthesis, $\Delta C/\Delta t$ is the rate of change of the albumin in the supernatant, D is the dilution rate, Cin and Cout are the inlet and outlet concentrations of albumin, and X_V average is the average of viable cell concentrations during the time period Δt. For static culture system, the specific rate of albumin synthesis was estimated as $q = \Delta C/(\Delta t. X_V)$. Results were expressed as $ng.10^{-6}$ cells.day^{-1}.

3.3.1.5. Indocyanine green uptake and clearance

A stock solution (5mg/mL) of indocyanine green (Cardiogreen, Sigma-Aldrich) was prepared in ddH_20. Then, the working solution (1 mg/mL) was done in hepatocyte maintenance medium at 37°C to dissolve the powder completely. For analysis of indocyanine green (ICG) uptake and clearance, hiPSC-HLC 3D aggregates harvested

at day 25 were seeded at a density of 2 X 10^6 cell/well in 24-well plates (Falcon™), coated with growth factor reduced (GFR) Matrigel®, Phenol Red Free (BD Biosciences). hiPSC-HLC cultured as 2D monolayers in 24-well plates were also used at day 25 of differentiation. Both 3D and 2D hiPSC-HLC were incubated in hepatocyte maintenance medium supplemented with 1 mg/mL ICG for 1 h, at 37ºC in a humidified atmosphere with 5 % (v/v) CO_2. Cells were washed tree times with DPBS and then cultured in hepatocyte maintenance medium for additional 23 h. To determine ICG uptake and release profiles, supernatants from both cultures were collected at specific time points (30 min, and 1, 2 and 24 h) and analyzed by spectrophotometry in Tecan Infinite 200 PRO NanoQuant, microplate reader, at optical density 820 nm (OD820). Cells were visualized using inverted phase contrast microscopy (Leica DMIRB, Leica Microsystems GmbH). Representative pictures were obtained using Leica DFC 295 digital camera.

3.3.1.6. Histological assessment: H&E, MT and PAS staining

hiPSC-HLC aggregates were fixed, overnight, in 10 % (v/v) buffered formalin at RT and added to 1 % (w/v) agarose (Lonza) in DPBS. Spheroids were subsequently processed and included in paraffin-blocks. Transversal sections, with 3 µm of thickness, were stained for hematoxylin and eosin (H&E, Sigma-Aldrich), Periodic acid–Schiff (PAS, Sigma-Aldrich) and Masson's trichrome (MT, Sigma-Aldrich) according to the protocol established at the Histopathology Facility at the Instituto Gulbenkian de Ciência (Oeiras, Portugal). Images were analyzed using NDP.view2 software.

3.4. Dielectric spectroscopy data analysis and calibration

Online dielectric spectroscopy data, acquired every 10 min throughout the bioreactor culture, included measurements of permittivity both at a fixed frequency and as a scan over a range of frequencies.

3.4.1. Calibration of biovolume estimator

Offline measurements were used to calculate the reference culture biovolume along the bioprocess. Biovolume represents the volume occupied by the cell aggregates per

bulk culture volume and was estimated from the average aggregate concentration and diameter, assuming a spherical geometry (Eq. 1).

$$Biovolume = (Aggregate\ concentration) \times \frac{4}{3}\pi(Aggregate\ mean\ radius)^3 \quad \textbf{(Eq. 1)}$$

A capacitance-based biovolume estimator was established by using a linear regression model between the online fixed frequency permittivity and the offline biovolume reference data. Bioprocess stages where electrical properties of the cell culture media were highly different from the remaining, and led to high shifts in the permittivity signal, were not used for calibration.

3.4.2. β-dispersion curve analysis

The frequency scan data was used to plot the characteristic β-dispersion curve for each time point. To enable comparison of β-dispersion plots at different culture phases and with different cell culture media, each time point was normalized between 0 and 1, by subtracting the minimum value and dividing by the range. The characteristic frequency was calculated automatically by the ArcView 265 software (Hamilton, Reno, USA).

4. Results and discussion

We inoculated hiPSC as single cells in STBR (working volume: 200mL) and cultured for 5 days in a defined xeno-free culture medium under controlled conditions of dissolved oxygen (DO, 4% O_2) and perfusion (D = 1.3 day^{-1}), according to the protocol optimized by our group [14] (Fig. 1A).

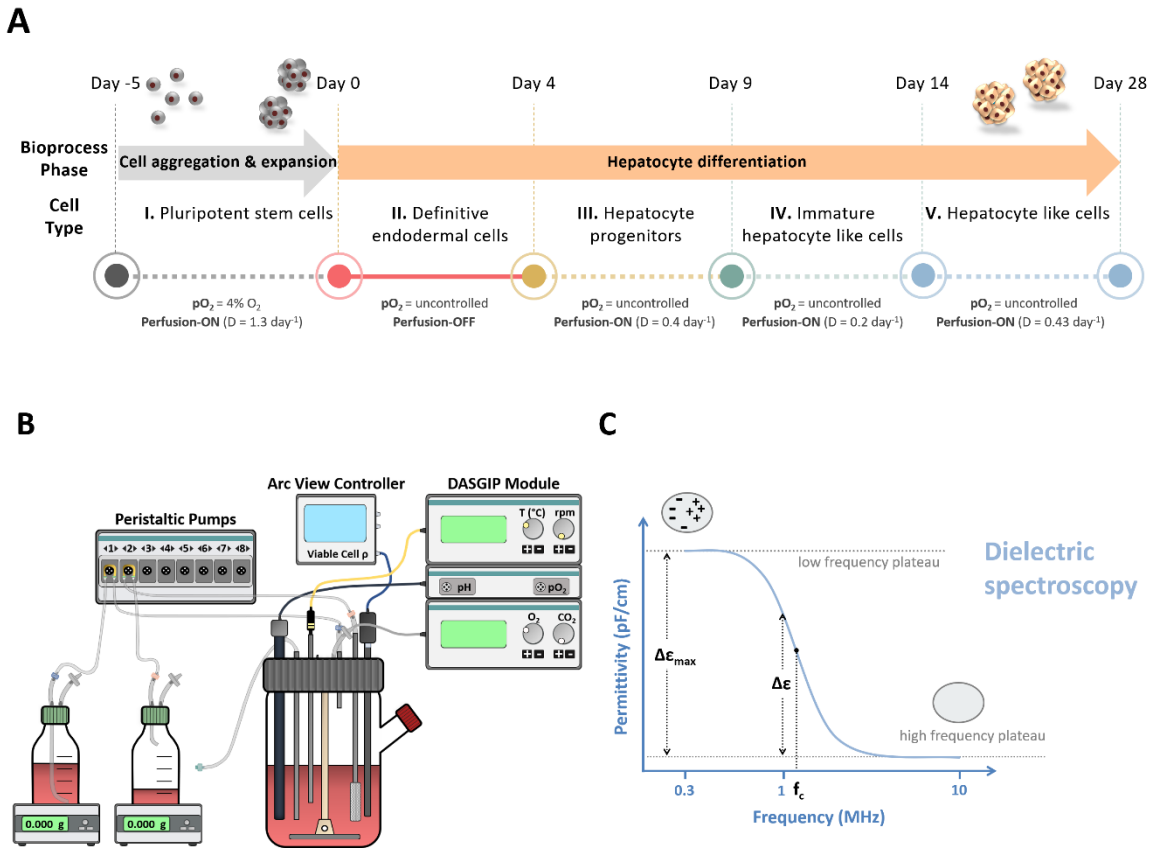

Figure 1. Integrated bioprocess for hiPSC expansion and hepatic differentiation in a STBR system. (a) Schematic representation of the sequential steps used to differentiate hiPSC to HLC as 3D aggregates. The cell type and operation conditions of dissolved oxygen (pO_2) and perfusion are indicated for each step. (b) Illustration of DasGip bioreactor culture setup used for hiPSC expansion and hepatocyte differentiation, operated under perfusion mode. (c) Representation of fixed-frequency permittivity measurement (Δε) and β-dispersion curve (blue line) with respective characteristic frequency (fc). Abbreviations: 3D, three dimensional; hiPSC, human-induced pluripotent stem cells; HLC, hepatocyte-like cells; STBR, stirred-tank bioreactor.

Cells were able to aggregate (Fig. 2A) and proliferate (Fig. 2B) showing a growth kinetics (specific growth rate of 0.8±0.1 day^{-1}), an aggregate size distribution (Fig. 2C) and concentration (Fig. 2D) similar to those reported for other hiPSC lines [14]. The hepatocyte differentiation step was integrated after 5 days (designated by day 0, Fig. 1A), when the cell concentration exceeded 1 x 10^6 cell/mL (Fig. 2B) and aggregate diameter was around 150 µm (Fig. 2C); since it has been demonstrated that this average size resulted in higher HLC productivity and differentiation efficiency [6]. The differentiation was induced by addition of different levels of key soluble factors to

generate populations successively enriched for definitive endoderm, hepatoblasts, hepatocyte progenitors and HLC (Fig. 1A), and perfusion rates were estimated considering preliminary data generated by our group (data not shown) and the protocol described previously [17]. Four days after differentiation induction, a drop in viable cell concentration was observed (Fig. 2B) while the concentration of aggregates and average size maintained constant from this time point onwards (Fig. 2C, D).

Bioreactor culture was monitored with a capacitance sensor to assess the potential of dielectric spectroscopy to estimate viable cell concentration throughout the process. Our results show a delay between changes in cell concentration and in the permittivity, signal measured by the probe. Nevertheless, a good correlation between the biovolume calculated by offline methods and the permittivity signal (R^2 = 0.84) was observed (Fig. 2B), showing the usefulness of this method to monitor cell aggregation in a non-invasive manner. These observations show that cell number expansion requires a few days to result in an increase of the aggregate biovolume and that each cell aggregate behaves as one overall inducible dipole. This relation was previously reported by Heileman and Tabrizian, stating that each cell in an aggregate contributes to increase the permittivity signal and that the aggregate polarization depends on the net contribution of their cells [12].

Differences in the cell culture medium electrical properties, as the conductivity (Fig. 2E), for sequential differentiation steps might also affect the measured cell permittivity leading to shifts and possibly drifts in the signal (Fig. 2B, stage IV). In future work this can be at least partially corrected by measuring baseline electrical properties for each culture medium (without cells) prior to the expansion and differentiation process.

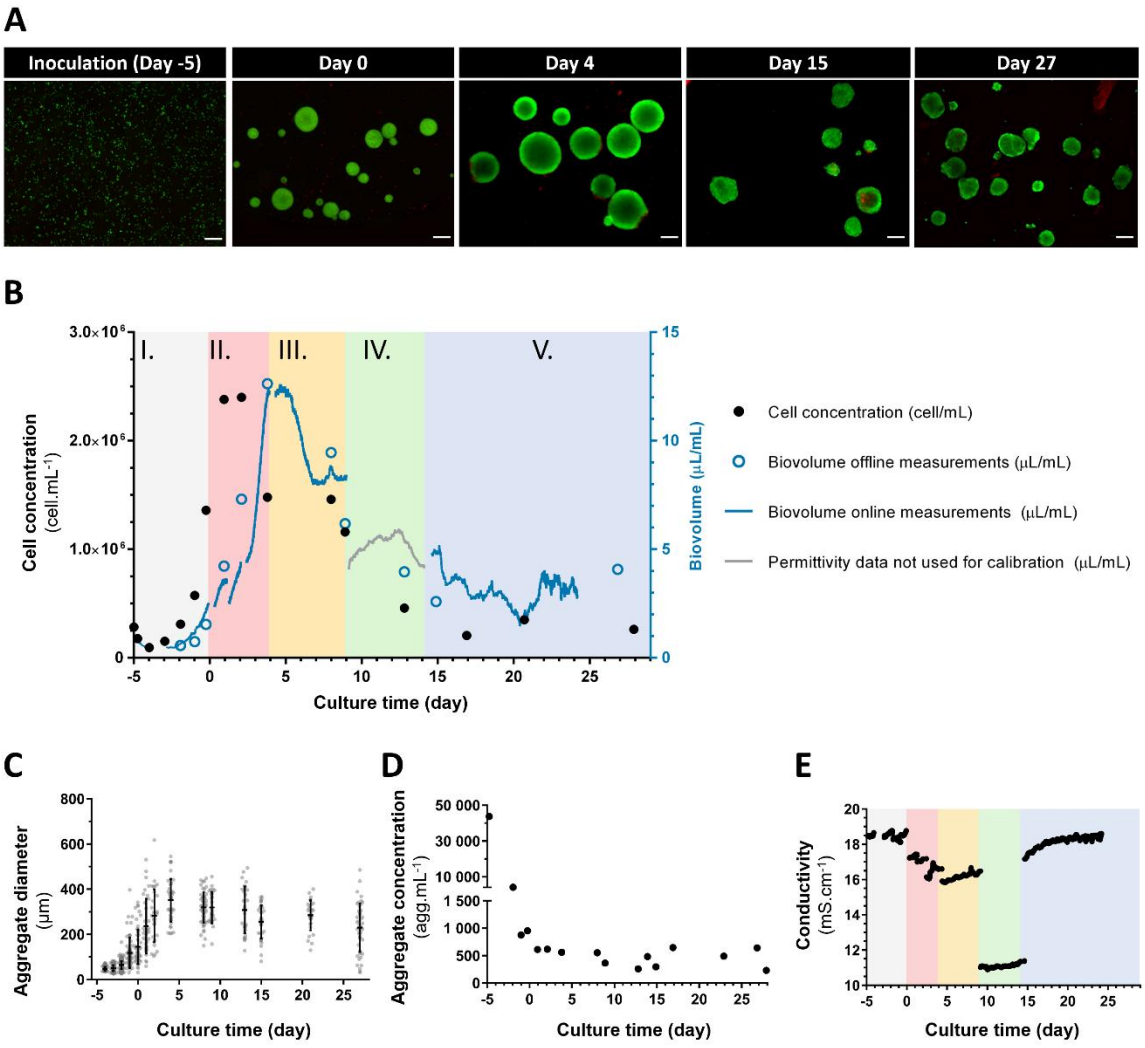

Figure 2. Characterization of hiPSC expansion and hepatic differentiation in stirred-tank bioreactors. (a) Viability analysis of hiPSC stained with fluorescein diacetate (FDA) (live cells, green) and TO-PRO™-3 Iodide (dead cells, red). Scale bar: 200 µm. (b) Cell concentration and biovolume profiles for cell expansion (I—cell aggregation and expansion, gray) and sequential differentiation stages (II—definitive endoderm, red; III—hepatocyte progenitors, yellow; IV—hepatocyte differentiation, green; V—maintenance and maturation, blue). (c) Average aggregate diameter estimated in each time point (n > 30). (d) Average aggregate concentration profile. (e) Electrical conductivity of the cell culture measured online. hiPSC, human-induced pluripotent stem cells.

Gene expression analysis of 3D aggregates along differentiation in STBR showed a coexpression of the fetal alpha fetoprotein (AFP) marker with mature hepatic markers, such as hepatocyte nuclear factor 4α (HNF4a), alanine-glyoxylate and serine-pyruvate aminotransferase (AGXT), albumin (ALB), α-1 antitrypsin (A1AT), and cytochrome P450 subunit 3A4 (CYP3A4) (Fig. 3a). This heterogeneity in the aggregates maturation can be associated with the dispersion in aggregate size observed in culture (Fig. 2C) that was reported to influence the hepatic differentiation efficiency [20]. To overcome this, the use of controlled methods, such as force aggregation or micro-contact patterning and the optimization of stirring rate profile in STBR [21], may be considered in future to modulate cell aggregate size and morphology while minimizing

heterogeneity. Nevertheless, expression of mature hepatic markers AGXT, A1AT and CYP3A4 at day 21 in 3D aggregates closely resembles the hepatoma-derived immortalized cell line HepaRG, used as a positive control (Fig. 3A).

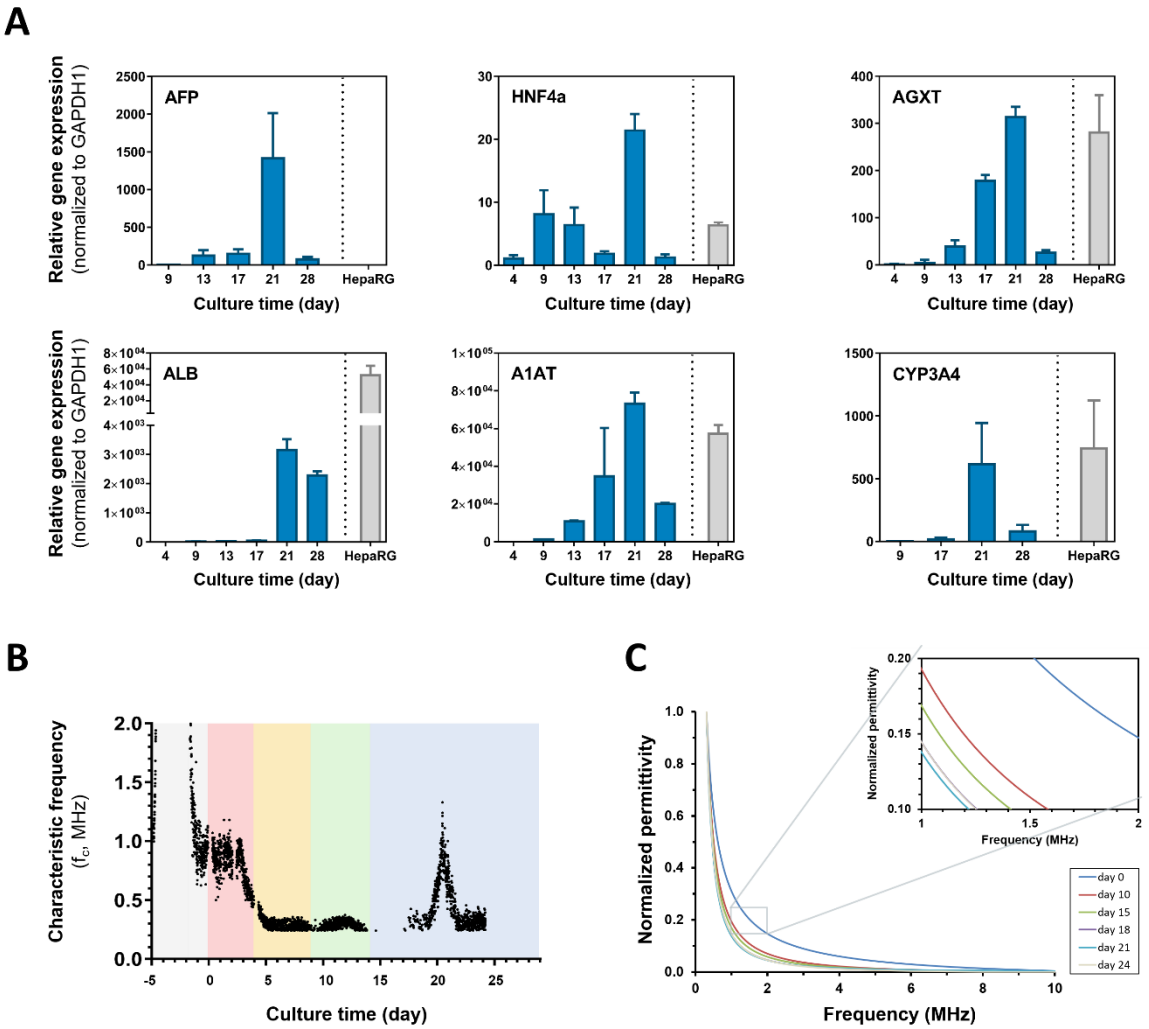

Figure 3. Gene expression and permittivity profile of hiPSC during hepatic differentiation in bioreactors. (a) Relative expression of hepatic specific markers, alpha fetoprotein (AFP), hepatocyte nuclear factor 4α (HNF4a), alanine-glyoxylate and serine-pyruvate aminotransferase (AGXT), albumin (ALB), α-1 antitrypsin (A1AT), and cytochrome P450 subunit 3A4 (CYP3A4) by qRT-PCR quantified using the 2-ΔΔCT method relatively to day 0 of differentiation and normalized for GAPDH housekeeping gene, from hiPSC-HLC (blue bars) and from HepaRG cells (gray bars). (b) Normalized β-dispersion curve for several timepoints throughout the expansion and differentiation processes. The stages of the process are highlighted: Expansion and aggregation (gray), definitive endoderm (red), hepatocyte progenitors (yellow), hepatocyte differentiation (green), and maintenance and maturation (blue). (c) Characteristic frequency (fc) estimated from normalized β-dispersion curve over culture time. GAPDH, glyceraldehyde 3-phosphate dehydrogenase; HepaRG, hepatoma-derived immortalized cell line; hiPSC-HLC, hepatocyte-like cells derived from human-induced pluripotent stem cells; qRT-PCR, quantitative reverse-transcription polymerase chain reaction.

In addition to the monitoring of the culture biovolume, dielectric spectroscopy could also be used to follow differentiation progression. The β-dispersion curve, obtained by reading permittivity over a range of frequencies at each time point, changes over culture time (Fig. 3C) with a characteristic frequency peak at day 21 (Fig. 3B) which is coincident with the higher expression of hepatic markers (Fig. 3A).

Morphological characteristics that change during hiPSC hepatic differentiation, namely cell shape and size, and their heterogeneity within the cell population, are known to influence the shape of the β-dispersion curve [22]. Because aggregates behave as large dipoles, permittivity measurements at lower frequencies would be necessary to ensure full polarization and trace the low frequency plateau of the β-dispersion curve (Fig. 3C). Nevertheless, these results suggest that permittivity signal can also be an indicator for differentiation progression and thus support the potential of dielectric spectroscopy to monitor complex stem cell differentiation processes in stirred cultures.

The 3D hiPSC-HLC aggregates were harvested at day 21, when a peak in the expression of hepatic genes was attained (Fig. 3A), and characterized in terms of morphology, phenotype and functionality.

Noteworthy, hiPSC-HLC showed no expression of SOX17 and FOXA2 endoderm markers and the expression of hepatic specific markers and albumin synthesis significantly improved in the 3D culture strategy compared with the equivalent 2D monolayer protocol [17] that was run in parallel (Fig. 4A, B). The improved functionality features of HLC in 3D culture approaches were already observed by other authors showing the positive effect of cell-cell interaction in 3D conformation for hepatic specification (Subramanian et al., 2014). Additionally, hiPSC-HLC aggregates were able to uptake and release indocyanine green (ICG) compound (Fig. 4C, D), indicating drug metabolization capacity, and the histological assessment shows phenotypic features of hepatocytes within the aggregate. Cells exhibit polygonal shape (Fig. 4E), glycogen storage (Fig. 4E) and positive staining for albumin and AFP markers (Fig. 4F).

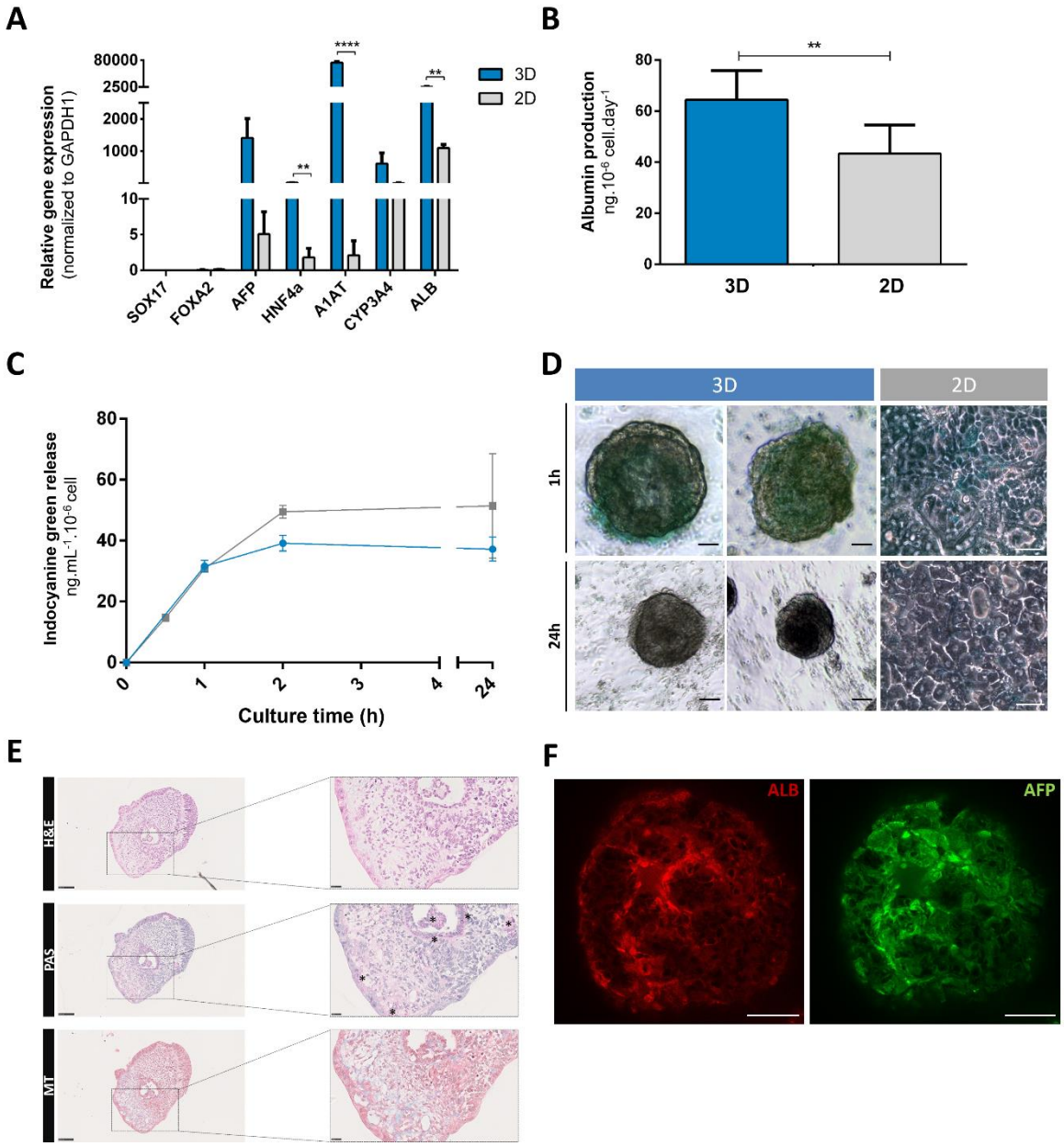

Figure 4. Characterization of hiPSC-HLC phenotype and functionality after expansion and 21 days of differentiation in bioreactors. (a) qRT-PCR-based analysis of the mRNA expression of hepatic differentiation markers of hiPSC-HLC from 3D bioreactor (blue bars) and 2D monolayers (gray bars) culture. (b) Albumin synthesis by hiPSC-HLC generated from 3D bioreactor (blue bar) and 2D monolayers (gray bar) analyzed in the culture medium by enzyme-linked immunosorbent assay (ELISA). (c) Profile of indocyanine green (ICG) release by hiPSC-HLC generated by 3D (blue line) and 2D (gray line) culture. (d) Representative images of hiPSC-HLC generated in 3D (left panel) and 2D (right panel) after uptake (1 h) and release (24 h) of ICG. Scale bars: 100 µm (3D) and 50 µm (2D). (e) Hematoxylin and eosin (H&E) staining of hiPSC-HLC sections, hiPSC-HLC show glycogen storage by periodic acid–Schiff (PAS) staining, and collagen deposition by Masson Trychome (MT) staining. Scale bars: 100 µm (left panel) and 25 µm (right panel). (f) Immunofluorescence microscopy images demonstrating expression of albumin (ALB) and alpha-fetoprotein (AFP) hepatic markers in hiPSC-HLC whole aggregate. Scale bar: 50 µm. Multiple t test (FDR: 0.05) compared between hiPSC-HLC from 3D bioreactor and 2D monolayers, **p < 0.01, ****p < 0.0001. 2D, two dimensional; hiPSC-HLC, hepatocyte-like cells derived from human-induced pluripotent stem cells; mRNA, messenger RNA; qRT-PCR, quantitative reverse-transcription polymerase chain reaction.

In this study, we successfully developed an integrated bioprocess for hiPSC expansion and hepatic differentiation as 3D aggregates using STB operated in perfusion. The 3D differentiation improved hepatic features of differentiated HLC compared with 2D

monolayer culture while the bioreactor and perfusion system potentiate process automation and higher cell productivities [23]. Indeed, a 3.5-fold improvement in the final cell yield was obtained when compared to static 2D cultures, yielding 3.5 x 10^5 cell/mL.

Additionally, this work provides for the first time a demonstration of dielectric spectroscopy tools, measured with an *in situ* capacitance sensor, to monitor an expansion and differentiation bioprocess of hiPSC aggregates in STB.

This PAT tool has the potential to improve bioprocess understanding, reduce the costs and maximize product quality consistency, that are extremely important for the application of hiPSC-HLC in preclinical research and regenerative medicine.

5. References

[1] Li S, Huang S, Zhao Y, Ding Y, Ding Q. Derivation and applications of human hepatocyte-like cells. World J Stem Cells 2019;11:535–48. https://doi.org/10.4252/wjsc.v11.i8.535.

[2] Mallanna SK, Duncan SA. Differentiation of hepatocytes from pluripotent stem cells. Curr Protoc Stem Cell Biol 2013;1:1–15. https://doi.org/10.1002/9780470151808.sc01g04s26.

[3] Wang Y, Alhaque S, Cameron K, Meseguer-ripolles J, Lucendo-Villarin B, Rashidi H, et al. Defined and Scalable Generation of Hepatocyte-like Cells from Human Pluripotent Stem Cells. J Vis Exp 2017;2. https://doi.org/10.3791/55355.

[4] Edmondson R., Broglie J.J, Adcock A.F. YL. Three-dimensional cell culture systems and their applications in drug discovery and cell-based biosensors. Assay Drug Dev Technol 2014;12:207–18. https://doi.org/10.1089/adt.2014.573.

[5] Yamashita T, Takayama K, Sakurai F, Mizuguchi H. Billion-scale production of hepatocyte-like cells from human induced pluripotent stem cells. Biochem Biophys Res Commun 2018;496:1269–75. https://doi.org/10.1016/j.bbrc.2018.01.186.

[6] Heidariyan Z, Ghanian MH, Ashjari M, Farzaneh Z, Najarasl M, Larijani MR, et al. Efficient and cost-effective generation of hepatocyte-like cells through microparticlemediated delivery of growth factors in a 3D culture of human pluripotent stem cells. Biomaterials 2018;159:174–88. https://doi.org/10.1016/j.biomaterials.2018.01.005.

[7] Sivertsson L., Synnergren J., Jensen J., Björquist P., Ingelman-Sundberg M. Hepatic differentiation and maturation of human embryonic stem cells cultured in a perfused three-dimensional bioreactor. Stem Cells Dev 2013;22:581–94. https://doi.org/10.1089/scd.2012.0202.

[8] Lam ATL, Chen AKL, Ting SQP, Reuveny S, Oh SKW. Integrated processes for expansion and differentiation of human pluripotent stem cells in suspended microcarriers cultures. Biochem Biophys Res Commun 2016;473:764–8. https://doi.org/10.1016/j.bbrc.2015.09.079.

[9] Downey, B. J., Graham, L.J., Breit, J.F., Glutting NK. A novel approach for using dielectric spectroscopy to predict viable cell volume (VCV) in early process development. Biotechnol Prog 2013;30:479–87. https://doi.org/10.1002/btpr.1845.

[10] Metze S, Ruhl, S., Greller G, Grimm, C., Scholz J. Monitoring online biomass with a capacitance sensor during scale - up of industrially relevant CHO cell culture fed - batch processes in single - use bioreactors. Bioprocess Biosyst Eng 2020;43:193–205. https://doi.org/10.1007/s00449-019-02216-4.

[11] Lei KF, Wu MH, Hsu CW, Chen YD. Real-time and non-invasive impedimetric monitoring of cell proliferation and chemosensitivity in a perfusion 3D cell culture microfluidic chip. Biosens Bioelectron 2014;51:16–21. https://doi.org/10.1016/j.bios.2013.07.031.

[12] Heileman, K.L., Tabrizian M. Dielectric spectroscopy platform to measure MCF10A epithelial cell aggregation as a model for spheroidal cell cluster analysis. Analyst 2017;142:1601–7. https://doi.org/10.1039/c6an02156e.

[13] Zapata-Linares N, Rodriguez S, Salido E, Abizanda G, Iglesias E, Prosper F, et al. Generation and characterization of human iPSC lines derived from a Primary Hyperoxaluria Type I patient with p.I244T mutation. Stem Cell Res

2016;16:116–9. https://doi.org/10.1016/j.scr.2015.12.014.
[14] Abecasis B, Aguiar T, Arnault É, Costa R, Gomes-Alves P, Aspegren A, et al. Expansion of 3D human induced pluripotent stem cell aggregates in bioreactors: Bioprocess intensification and scaling-up approaches. J Biotechnol 2017;246:81–93. https://doi.org/10.1016/j.jbiotec.2017.01.004.
[15] Correia C, Serra M, Espinha N, Sousa M, Brito C, Burkert K, et al. Combining Hypoxia and Bioreactor Hydrodynamics Boosts Induced Pluripotent Stem Cell Differentiation Towards Cardiomyocytes. Stem Cell Rev Reports 2014;10:786–801. https://doi.org/10.1007/s12015-014-9533-0.
[16] Samaras JJ, Abecasis B, Serra M, Ducci A, Micheletti M. Impact of hydrodynamics on iPSC-derived cardiomyocyte differentiation processes. J Biotechnol 2018;287:18–27. https://doi.org/10.1016/j.jbiotec.2018.07.028.
[17] Asplund A, Pradip A, van Giezen M, Aspegren A, Choukair H, Rehnström M, et al. One Standardized Differentiation Procedure Robustly Generates Homogenous Hepatocyte Cultures Displaying Metabolic Diversity from a Large Panel of Human Pluripotent Stem Cells. Stem Cell Rev Reports 2016;12:90–104. https://doi.org/10.1007/s12015-015-9621-9.
[18] Serra M, Brito C, Sousa MFQ, Jensen J, Tostões R, Clemente J, et al. Improving expansion of pluripotent human embryonic stem cells in perfused bioreactors through oxygen control. J Biotechnol 2010;148:208–15. https://doi.org/10.1016/j.jbiotec.2010.06.015.
[19] Livaka K.J. STD. Analysis of Relative Gene Expression Data Using Real-Time Quantitative PCR and the 2−ΔΔCT Method. Methods 2001;25:402–8. https://doi.org/https://doi.org/10.1006/meth.2001.1262.
[20] Torizal FG, Kimura K, Horiguchi I, Sakai Y. Size-dependent hepatic differentiation of human induced pluripotent stem cells spheroid in suspension culture. Regen Ther 2019;12:66–73. https://doi.org/10.1016/j.reth.2019.04.011.
[21] Sart S, Bejoy J, Li Y. Characterization of 3D pluripotent stem cell aggregates and the impact of their properties on bioprocessing. Process Biochem 2017;59:276–88. https://doi.org/10.1016/j.procbio.2016.05.024.
[22] Dabros M, Dennewald D, Currie DJ, Lee MH, Todd RW, Marison IW, et al. Cole-Cole, linear and multivariate modeling of capacitance data for on-line monitoring of biomass. Bioprocess Biosyst Eng 2009;32:161–73. https://doi.org/10.1007/s00449-008-0234-4.
[23] Cunha B, Aguiar T, Silva MM, Silva RJS, Sousa MFQ, Pineda E, et al. Exploring continuous and integrated strategies for the up- and downstream processing of human mesenchymal stem cells. J Biotechnol 2015;213:97–108. https://doi.org/10.1016/j.jbiotec.2015.02.023.

Chapter 4

RECELLULARIZATION OF ACELLULAR LIVER SCAFFOLDS WITH HIGHLY FUNCTIONAL HIPSC-HLC GENERATED USING A SCALABLE AND OPTIMIZED BIOPROCESS

Contents

1. Graphical abstract

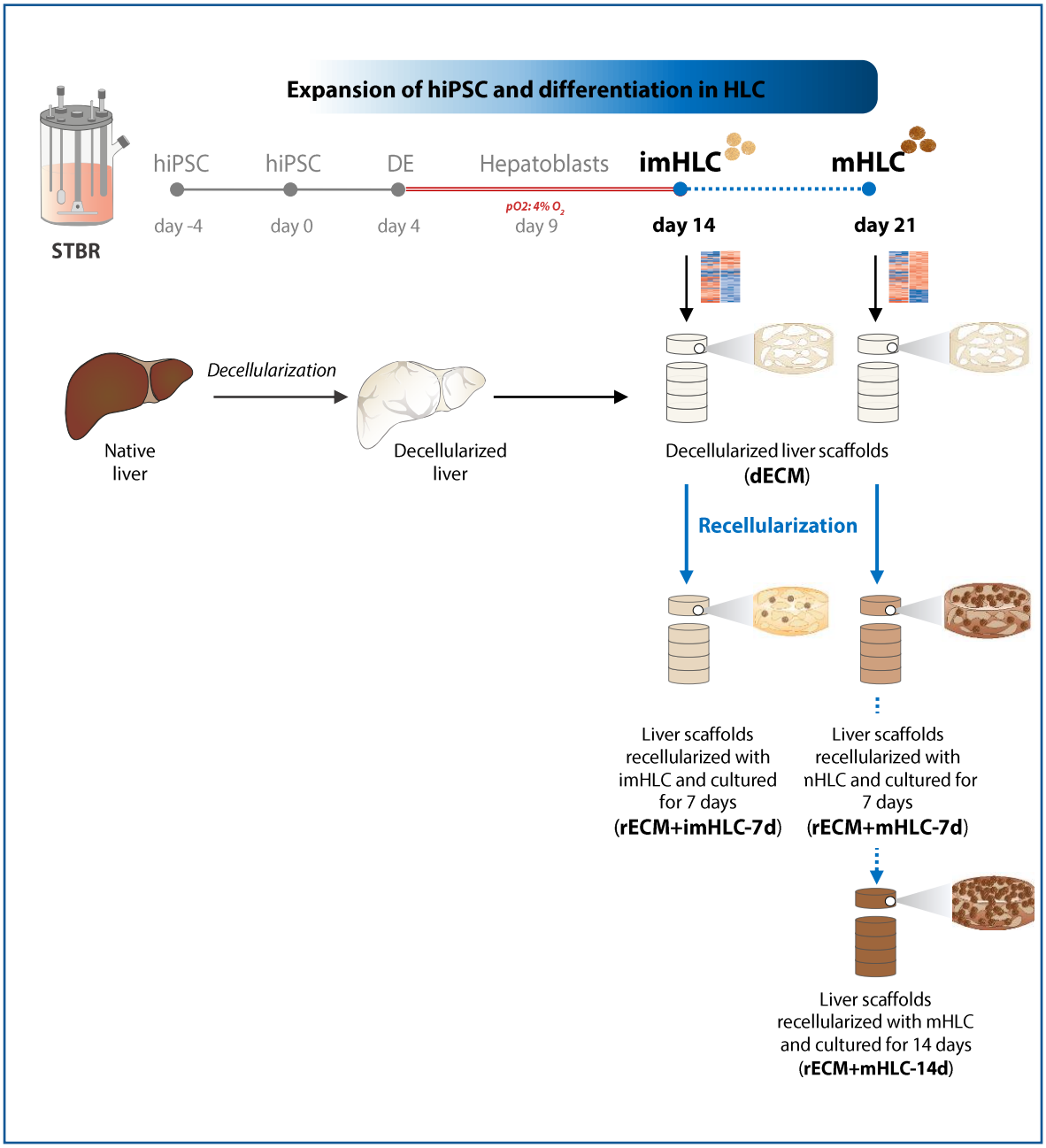

2. Introduction

The global prevalence of people suffering from end-stage liver disease with clinical indications for liver transplantation is sobering [1]. Even though the liver accounts for the second most common solid organ transplanted after kidney, less than 10% of global organ transplantation needs are met, given the current transplantation rates [2].

Allogeneic transplantation of primary human hepatocytes (PHH) isolated from either unused or deemed unsuitable livers for transplantation have shown encouraging preclinical [3,4] and clinical prognosis [5–7]. However, their limited availability and often marginal quality, the low engraftment levels and rapid declining functionality during *in vitro* culture [8,9] have led to the search for a more powerful cell source. Human pluripotent stem cells (hPSC), including embryonic (hESC) and induced pluripotent (hiPSC) stem cells, provide unprecedented opportunities for cell-based therapies due to their unlimited self-renewal ability, capacity to differentiate into different lineages and donor/patient specificity [10,11].

In the past 15 years, the successful generation of functional hepatocytes from hPSC, usually referred to as hepatocyte-like cells (HLC), has raised the hopes for treating poor prognostic liver disorders [12,13,22,14–21].Regrettably, the lack of reliable and reproducible protocols to generate the numbers of functional cells needed for transplantation (i.e. ~$2.41x10^8$ hepatocytes [23,24]) impairs the use of HLC in clinical practice.

In more recent years, different strategies that include hollow-fiber bioreactors (BR) [25–30], spinner-flasks [31–34], rotatory culture system [35] to more sophisticated parameter controlled stirred-tanks BR (STBR) [36] have been described to improve the manufacturing production of HLC (Appendix Table 1). Although some had showed encouraging results, all these studies are exclusively focused on scaling-up HLC production and accomplishing “mature” phenotypes, neglecting the ability of HLC to engraft into tissues. To our knowledge, the few papers that assessed the engraftment ability of HLC only used cells generated with 2D-monolayer protocols [37].

A successful cell engraftment lays the basis of any cell therapy, and if for PHH transplantation this remains a challenge [9,38], for hPSC-HLC there are even more open questions. It is critical to not only confirm if scalable culture systems provide the

key environmental cues for the proper HLC commitment but also to understand the machinery behind cell engraftment in order to identify the optimal differentiation/maturation stage that would lead to efficient cell engraftment into tissues while preserving cell viability and function.

3. Aim

In this study, we generated 3D aggregates of HLC from hiPSC using an optimized bioprocess in STBR, and decoded the transcriptome of HLC, by RNA-Seq analysis, along differentiation phase. We investigated, for the first time, whether the cell maturation level modulate the “machinery” that mediate cell engraftment and identified a suitable HLC maturation stage that ensures efficient repopulation of acellular liver scaffolds with preservation of hepatic functionality for up to 14 days of culture.

4. Materials and Methods

4.1. Human iPSC culture

The hiPSC lines PH1-Fib-hiPSC4F1 and ChiPSC18, henceforth termed hiPSC-1 and hiPSC-2, were used in this work and derived as described below. The hiPSC-1 was derived from peripheral blood lymphocytes (PBL) obtained from a patient diagnosed with primary hyperoxaluria type 1 with a p.I244T (c.731T>C) mutation in the AGXT gene [39], and the hiPSC-2 was derived from human skin fibroblasts from healthy patients [40].

Before differentiation, hiPSC were routinely propagated in static adherent culture systems (T-flasks) in the Cellartis DEF-CS 500 Xeno-Free Culture Medium w/o antibiotics (Takara BioEurope AB, Y30045) as described in greater depth elsewhere [36,41].

4.1.1. Expansion and differentiation of hiPSC in HLC using STBR

hiPSC-1 and hiPSC-2 were expanded and differentiated into HLC, as 3D cellular aggregates, using STBR operated in perfusion, as previously described by our group [36].

In short, STBR (DASGIP ® Bioblock bioreactor system, Eppendorf AG), with 200 mL working volume, were inoculated with $2.5x10^5$ hiPSC/mL in Cellartis® DEF-CS 500 Xeno-Free 3D Spheroid Culture Medium (Takara Bio Europe AB, Y30047). hiPSC were then expanded under defined and controlled conditions (Table 1), and the hepatocyte differentiation was induced after 3-4 days when cell concentration reached $1x10^6$ cell/mL and the average of aggregate size was approximately 200 µm. hiPSC were then differentiated in definitive endoderm (DE), for 4 days, by daily media exchanges. DE specification into hepatic lineage occurred from days 5 to 9 by continuous perfusion of Hepatocyte Progenitor Medium and low O_2 conditions (pO2: 4% O2). Likewise, hepatocyte differentiation (days 10-14) occurred at low O_2 conditions and was preceded by maturation that ended by day 21.

Culture media description and the bioprocess parameters used in this work are extensively detailed in Supplementary Table S1. A continuous perfusion feeding

regimen was used along the integrated bioprocess, except when daily medium exchanges were required.

Table 1. Media and culture parameters used during hiPSC expansion and differentiation in HLC.

Day of culture	Media (Cat. No.)	Culture conditions
-4 - 0	Cellartis DEF-CS 500 Xeno-Free 3D Spheroid Culture Medium w/o Antibiotics (Cat. No. Y30047)	pO_2: 4% O_2 T: 37 ºC CO_2: 5% (v/v) SAR: 0.1 vvm DR:1.3 day^{-1}
1	Definitive Endoderm Differentiation Concentrate Day 1 (Y11132) Definitive Endoderm Differentiation Basal Medium (Y11135)	pO2: uncontrolled (95% air; 5%CO_2) SAR: 0.1 vvm T: 37 ºC
2	Definitive Endoderm Day 2 (Y11133) Differentiation Basal Medium (Y11135)	
3 & 4	Definitive Endoderm Differentiation Concentrate Day 3/4 (Y11134) Definitive Endoderm Differentiation Basal Medium (Y11135)	
5-9	Progenitor Medium Concentrate (Y11111) Hepatocyte Progenitor Medium (Y11111 + Y11135)	**pO_2: 4% O_2** SAR: 0.1 vvm T: 37 ºC DR: 0.6 day^{-1}
10-14	Hepatocyte Differentiation Medium Concentrate (Y11112) Medium for Hepatocyte Differentiation in Suspension (Y11137)	**pO_2: 4% O_2** SAR: 0.1 vvm T: 37 ºC DR: 0.2 day^{-1}
15-21	Hepatocyte Maintenance Medium (Y30051)	pO2: uncontrolled (95% air; 5%CO_2) SAR: 0.1 vvm T: 37 ºC DR: 0.43 day^{-1}

Abbreviations: DR, dilution rate; pO_2, oxygen partial pressure; SAR, Surface aeration rate; T, Temperature.

4.2. Cell culture characterization

4.2.1. Cell viability, concentration and size distribution of 3D cell aggregates

To monitor cell viability, cells were harvested from STBR at days 0, 4, 9, 14 and 21 of differentiation, by aseptic sampling. Cells were directly stained with 5 µg/mL Fluorescein diacetate (FDA) (Sigma-Aldrich, 596-09-8) and 0.5 µM TO-PRO-3 Stain (Thermo Fisher Scientific, T3605) and visualized under an inverted fluorescence microscope (DMI6000, Leica). Representative images were taken using a digital camera (Leica DFC 360 FX).

Using the same images, the diameter of aggregates was calculated using the Ferret diameter measurement algorithm from ImageJ.

Cell concentration was measured by Trypan Blue (Gibco, 15250061) Exclusion Test after enzymatic dissociation of aggregates, as described in [42,43].

4.2.2. Transcriptomic analysis by RT-qPCR

The commitment of hiPSC to HLC was monitored by RT-qPCR following standard procedures. Firstly, RNA from cells along culture in STBR (days 0, 4, 9, 14 and 21) was isolated using the High Pure RNA Isolation Kit (Roche, 11828665001). RNA was quantified by optical density with NanoDrop 2000c spectrophotometer, and 200ng of it were reverse transcribed into cDNA using the Transcriptor First Strand cDNA Synthesis Kit (Roche, 5081963001). mRNA abundance of the selected genes was measured by RT-qPCR using TaqMan probe technology (LightCycler® 480 Probes Master, Roche, 04887301001) and validated primers (Table 2). Relative gene expression was calculated using $2^{-\Delta\Delta CT}$ method and normalized to the housekeeping gene *GAPDH*.

Table 2. Primer list.

Gene Symbol	Gene Name	Assay ID
ABCB1	ATP binding cassette subfamily B member 1	Hs00184500_m1
AFP	Alpha fetoprotein	Hs00173490_m1
ALB	Albμmin	Hs00910225_m1
CDH1	Cadherin 1	Hs01023895_m1
CPS1	Carbamoyl-phosphate synthase 1	Hs00157048_m1
CYP1B1	Cytochrome P450 family 1 subfamily B member 1	Hs00164383_m1
CYP2C9	Cytochrome P450 family 2 subfamily C member 9	Hs02383631_s1
CP2D6	Cytochrome P450 family 2 subfamily D member 6	Hs04931916_gH
CYP2E1	Cytochrome P450 family 2 subfamily E member 1	Hs00559367_m1
CYP3A4	Cytochrome P450 family 3 subfamily A member 4	Hs00604506_m1
CYP3A7	cytochrome P450 family 3 subfamily A member 7	Hs00426361_m1
FOXA2	Forkhead box A2	Hs05036278_s1
GAPDH	Glyceraldehyde-3-phosphate dehydrogenase	Hs99999905_m1
HNF4A	Hepatocyte nuclear factor 4 alpha	Hs00230853_m1
KRT19	Keratin 19	Hs00761767_s1
NANOG	Nanog homeobox	Hs02387400_g1
OCLN	Occludin	Hs05465837_g1
POU5F1	POU class 5 homeobox 1	Hs00999632_g1
PPARA	Peroxisome proliferator activated receptor alpha	Hs00947536_m1
SERPINA1(A1AT)	Serpin family A member 1	Hs00165475_m1
SOX17	SRY-box 17	Hs00751752_s1

4.2.3. RNA Sequencing

RNA from HLC harvested at day 14 and 21 of differentiation was isolated using RNeasy Mini Kit (Quiagen, 74104) according to the manufacturer's instructions. RNA sequencing was carried out by Maren Calleja and Juan R. Rodriguez-Madoz from the Instituto de Investigación Sanitaria de Navarra (Spain).

RNA sequencing reads were demultiplexed using Illumina's bcl2fastqsoftware (version 1.2.4) and the quality was assessed using FastQC. Illumina adapters, polyA tails and short reads (less than 20 bases) were trimmed with Cutadapt [44]. Processed reads were aligned to the human genome (GRCh38) using STAR (2.6.1) [45] and mapped genes were quantified using the feature Counts function within the Subread package [46]. Minimal gene expression was established at 5cpm, and genes with lower levels of expression in more than 20% of samples from at least one sample group were removed for increased consistency.

Differential gene expression analysis was performed using the DESeq function within the R package DESeq2 (1.32.0) [47]. Genes with a fold change difference of ±2 and a Benjamini–Hochberg (BH) adjusted p-value < 0.05 were considered significantly differentially expressed (DE), unless otherwise stated.

For principal component analysis (PCA) and visualization of expression heatmaps, counts were normalized using the variance stabilizing transformation option (vst-normalization) of the package. The R package biomaRt (2.48.3) [48,49] was utilized to annotate DE genes.

To determine if gene ontology (GO) and/or Kyoto Encyclopedia of Genes and Genomes (KEGG) terms were overrepresented in genes found to be differentially expressed, the R package WebGestaltR (0.4.4) [50] was used. Terms were considered differentially enriched with an FDR < 0.05. Heatmaps were plotted with the R package pheatmap (1.0.12) (ref), all other plots were made using the R packages ggplot2 (3.3.5) and ggpubr (0.4.0). Data was processed using Remove Batch Effect function from Limma analysis package for data visualization purposes.

4.2.4. Flow cytometry

Cells as aggregates were harvested from STBR at days 0, 4 and 21 of differentiation and dissociated with TrypLE Select (Gibco, 12563011). Single-cell suspensions were stained as described in *Section 4.2.2.3, Chapter 2* [36,41]. Pluripotency was confirmed by the antibodies: TRA-1-60, mouse anti-human, unlabelled, (Santa Cruz, sc-21705);

SSEA-4 FITC, mouse anti-human, FITC (BD, 560126) and SSEA-1, mouse anti-human FITC (BD, 560127). Endodermal cells were identified with the antibodies: Sox17, mouse anti-human, unlabelled, clone P7-969 (BD, 561590) and Epcam, mouse anti-human, unlabelled, EGP40/826/837/1110/1120 (BD, ab216136). As secondary antibodies, we used: Alexa 488 anti-mouse IgG1 (Invitrogen, A-11001); Alexa 488 anti-mouse IgM (Invitrogen, A-21042); ALB Sheep anti-human, unlabelled (Abcam ab8940) and AFP Mouse anti-human (Abcam, A8452,) (as described in Chapter 2). Stained cell suspensions were analysed using BD FACSCelesta™ Cell Analyzer (BD) and the data acquired with DIVAsoftware (BD). At least ten thousand events were registered per sample. Analysis was performed with FlowJo Software (FlowJo LLC, http://www.flowjo.com/).

4.2.5. Histology analysis

HLC aggregates harvested at day 21 of differentiation were fixed ON in 10 % (v/v) buffered formalin at RT and added to 1 % (w/v) agarose (Lonza) in DPBS. Spheroids were subsequently processed and included in paraffin-blocks. Transversal sequential sections, with 3 µm of thickness, were stained for H&E, PAS, MT and Oil O Red, as described in *Section 3.3.1.6. Chapter 3*.

4.3. Recellularization of hiPSC in acellular liver scaffolds

4.3.1. Preparation of acellular liver scaffolds

Acellular liver scaffolds were obtained from decellularized porcine livers [51] as previously described [52]. Briefly, decellularized liver lobes were cut into small lobes, embedded into optimal cutting temperature (OCT) compound in Tissue-Tek® Cryomold® Molds (Sakura Finetek) and flash-frozen with liquid nitrogen. Sections of 300 µm thickness were cut using a cryotome (Leica CM3050S). Scaffolds in the form of discs were obtained by punching these sections with a 6-mm-diameter biopsy punch. The scaffolds were placed in 96-wells plate and air-dried for 2h at RT. Lastly, scaffolds were washed with DPBS $^{-/-}$ (3 washes of 15min each) and sterilized for 2h under UV light.

4.3.2. Recellularization of acellular liver scaffolds with HLC

Recellularization of acellular liver scaffolds with HLC was adapted from [24,52]. Firstly, cell aggregates, harvested at day 14 or day 21 of differentiation, were mechanically disrupted into small fragments by up-down pipette aspiration movements in a solution containing 0.01 µM of ROCK Inhibitor Y-27632 (StemCell Technologies, 72302) and 0.03 µM of Chir99021 (StemCell Technologies, 72052) and passed through a 250 µm nylon mesh (Labopolis). The cell viability, ultrastructure and size of fragments were evaluated by FDA/TOPRO-3 staining and SEM analysis prior to seeding.

A volume of 10µl containing $1x10^6$ fragments in Hepatocyte Maintenance Medium (HMM) was used for recellularization. Initially, scaffolds were seeded with 5µl of this suspension and incubated for 15 minutes at 37ºC. The remaining 5ul was added to scaffolds and incubated for 1h30 at 37°C. After incubation, 200ul of HMM was gently added to the scaffolds. HLC were cultured in the scaffolds for up to 14 days, and medium changes were performed every two days.

4.3.3. Scanning Electron Microscopy

Decellularized and recellularized liver scaffolds, HLC aggregates and fragments were fixed with 2.5% buffered glutaraldehyde (Sigma-Aldrich) for 2h at RT. Samples were washed with DPBS and dehydrated using graded series of ethanol solutions for 5 minutes each (50%, 70%, 80%, 95% and 100% absolute ethanol) as described [53]. Samples were dried on adhesive carbon tabs (12 mm, Agar Scientific) and sputter-coated with a 30 nm iridium film using a Quorum Q150TES (Quorum Technologies, UK). A Hitachi Regulus 8220 (Hitachi Corporation, JP) operated in SE mode with an accelerating voltage of 1 keV was used to analyse the samples.

4.3.4. Atomic Force Microscopy

Atomic force microscopy (AFM) characterization was performed to assess the microscale mechanical behaviour of decellularized and recellularized liver scaffolds. Force-indentation (F−δ) curves were recorded with an Asylum Research MFP-3D Standalone system (Oxford Instruments, UK) using cantilevers with a polystyrene microsphere of 4.5 µm in diameter attached to their ends (k = 0.03 N/m; Novascan, USA). Prior to microsphere attachment, these cantilevers were calibrated by their manufacturer using the thermal noise method. Liver scaffolds were physically

immobilized on top of microscopy glass slides and F−δ curve acquisition was done while the sample was immersed in PBS buffer at room temperature. For each condition, a minimum of 86 F−δ curves were recorded from at least 3 scaffolds and each scaffold was probed on at least 2 regions. No F−δ curves were generated from points less than 5 μm from a previously indented point. Young's modulus (E) was determined by fitting the F−δ unload curve with the Hertz contact model in Asylum Research's IGOR Pro software package while assuming a Poisson's ratio of 0.5 [54].

4.3.5. Histology analysis

As previously described, longitudinal or transversal 3-μm sections of decellularized and recellularized liver scaffolds were stained with H&E, PAS, and MT. Histological sections were analysed using NDP.view2 software.

4.3.6. Biochemical analysis: DNA, Collagen and Glycosaminoglycans quantification assays

Enzymatic digestion of dECM and rECM was performed using papain (Sigma, P3125) according to the protocol developed in our laboratory [53]. Scaffolds were digested and incubated at 60ºC at 650 rpm for 20h in a ThermoMixer® (Eppendorf). DNA quantification was performed immediately after stopping the digestion, using Quant-iT™ PicoGreen ® dsDNA Reagent and Kit (Invitrogen, P7589). For the composition of the ECM, sulfated glycosaminoglycans (s-GAGs) content was quantified, by the Blyscan™ Glycosaminoglycan Assay (Biocolor, 054B1000), and total collagen content results from the sum of soluble collagen (Sircol™ Soluble Collagen Assay, Biocolor, 054S1000) and insoluble (Sircol™ Insoluble Collagen Assay, Biocolor, 054S2000). TECAN Infinite M200 PRO with the i-control software 1.10 was used for analysis. Results were normalized by mg of wet scaffold.

4.3.7. Quantification of ALB, AFP and A1AT

The functionality of HLC in the scaffolds was quantified by the concentration of ALB (Bethyl laboratories, E88-129), AFP (Abcam, ab108838) and A1AT (Abcam, ab108799) present in the culture media. The proteins secretion rates of rECM (q) were

calculated according to equation (1):

$$q = \frac{\Delta C}{\Delta t \times W_{WT}} \quad (1)$$

where ΔC (ng/ µl) is the variation of protein concentration during the time period Δt (day) and W_{WT} is the weight of wet tissue (mg). Results were normalized for the DNA (isolated with the kit Allprep DNA/RNA Micro Kit (Qiagen, 50980284) and are expressed as $ng.day^{-1}$ / $ng.\mu l^{-1}$ DNA.TECAN Infinite M200 PRO with the i-control software 1.10 was used for analysis.

4.4. Statistical Analysis

GraphPad Prism6 software (GraphPad Software, La Jolla, CA) was used for statistical analysis. According to the nature of the data, one-way ANOVA analysis of variance with Tukey's correction were used. P values are reported for two-tailed tests with a 95% confidence interval, and differences with $P < 0.05$ were considered significant for all statistical tests.

5. Results

5.1. Two populations of hiPSC-HLC, corresponding to distinct maturation stages, were generated in STBR

In this study, hiPSC were successfully differentiated into HLC as 3D cell aggregates according to an optimized version of our integrated bioprocess described in Chapter 3.

Preliminary work from our group showed that controlling the dissolved oxygen concentration at 4%O_2 between the 4th and the 14th day of differentiation, i.e. during hepatic specification (hereafter designated as BR-Hypoxia) (Appendix Fig. 1A-C), improved the production and enrichment of HLC when compared to the standard protocol (hereafter designated as BR-Normoxia). As showed in Appendix Figure 1, in both conditions, hiPSC display high cell viability along culture time (Appendix Fig. 1D) and, at the end of the process (day 21 of differentiation), higher numbers of HLC were attained in BR-Hypoxia (2x10^{6}cell/mL) compared with BR-Normoxia (0.6x10^6 cell/mL) (Appendix Fig. 1E), corresponding to a 3.3-fold improvement in HLC yields. In addition, more than 85% of HLC generated under hypoxic conditions, expressed ALB (vs 43% ALB+ cells from BR-Normoxia; Appendix Fig. 2B) and showed increased expression of the hepatocyte specific markers *HNF4A*, *ALB*, *A1AT* and *CYP3A4* (Appendix Fig. 2A). Considering these findings, BR-Hypoxia was the most efficient strategy for production of HLC. The next step was to validate the protocol for four independent bioreactor cultures using 2 different hiPSC lines (Fig. 1A).

Light microscopy images of cell aggregates stained with FDA and TO-PRO-3 dyes showed high cell viability throughout differentiation process for both hiPSC lines (Fig. 1B). At the start of differentiation, i.e., 3-4 days after hiPSC expansion in STBR, stemness was confirmed by the transcripts of *POU5F1* (OCT4) and *NANOG2* (Fig. 1C), and by the presence of cells expressing TRA-1-60 and SSEA-4 (i.e., 99.9% and 94.4% of TRA-1-60 and 92.4% and 82.0% SSEA-4 positive cells for hiPSC-1 and hiPSC-2, respectively), and the absence of SSEA-1 positive cells (< 1% for both hiPSC-lines; Sup. Fig. 1A). On day 4, the presence of SOX17 confirmed hiPSC differentiation into definitive endoderm (DE) germinative line (Fig. 1C and Sup. Fig. 1B). The resulting DE cells were also EpCAM positive (99.7% and 97% EpCAM

positive cells for hiPSC-1 and hiPSC-2, respectively), suggesting a high ability to proliferate and differentiate (Sup. Fig. 1B). From day 4 onwards, up-regulated mRNA levels of *CDH1* and *OCLN* confirmed DE polarization and epithelialization, possibly mediated by *FOXA2* that appeared on the same day (Fig.1C). The bipotent stem cells, hepatoblasts (or hepatic progenitors), emerged on day 9 and were identified by the simultaneous expression of biliary epithelial cell marker *KRT19* and the liver-enriched transcription factor, *HNF4a* (Fig. 1C). Differentiation of progenitors into hepatocytes was confirmed by the decreasing expression of *KRT19*, and by the increasing expression of *PPARA*. Likewise, the increasing transcription of *CYP1B1*, *-3A4*, *-2C9*, -2D6, *-2E1* and *ABCB1* involved in xenobiotic metabolism; the appearance of the ureogenic enzyme (*CPSI*) and genes encoding for liver plasma proteins (*AFP*, *SERPINA1* (A1AT) and *ALB*) over time (Fig. 1C) allowed us to distinguish between two HLC populations: an immature population that emerged at day 14 (hereafter designated as imHLC) and a more mature population that appeared 7 days later (hereafter designated as mHLC).

Mature HLC were also identified by the expression of ALB (71.1% and 82.2% ALB positive cells for hiPSC-1 and hiPSC-2, respectively; Sup. Fig. 1B) and the synthesis and accumulation of glycogen, collagen, and lipids (Sup. Fig. 1D b-d), hallmarks of PHH. Finally, the proper differentiation efficacies obtained for both hiPSC lines (5.04 and 15.30 HLC /input hiPSC) and the high numbers of mHLC obtained at the end of differentiation ($1.22x10^6$ and $3.19x10^6$ cell/mL for hiPSC-1 and hiPSC-2, respectively) confirmed the potential of our protocol for the manufacturing production of hiPSC-HLC (Sup. Fig. 1E).

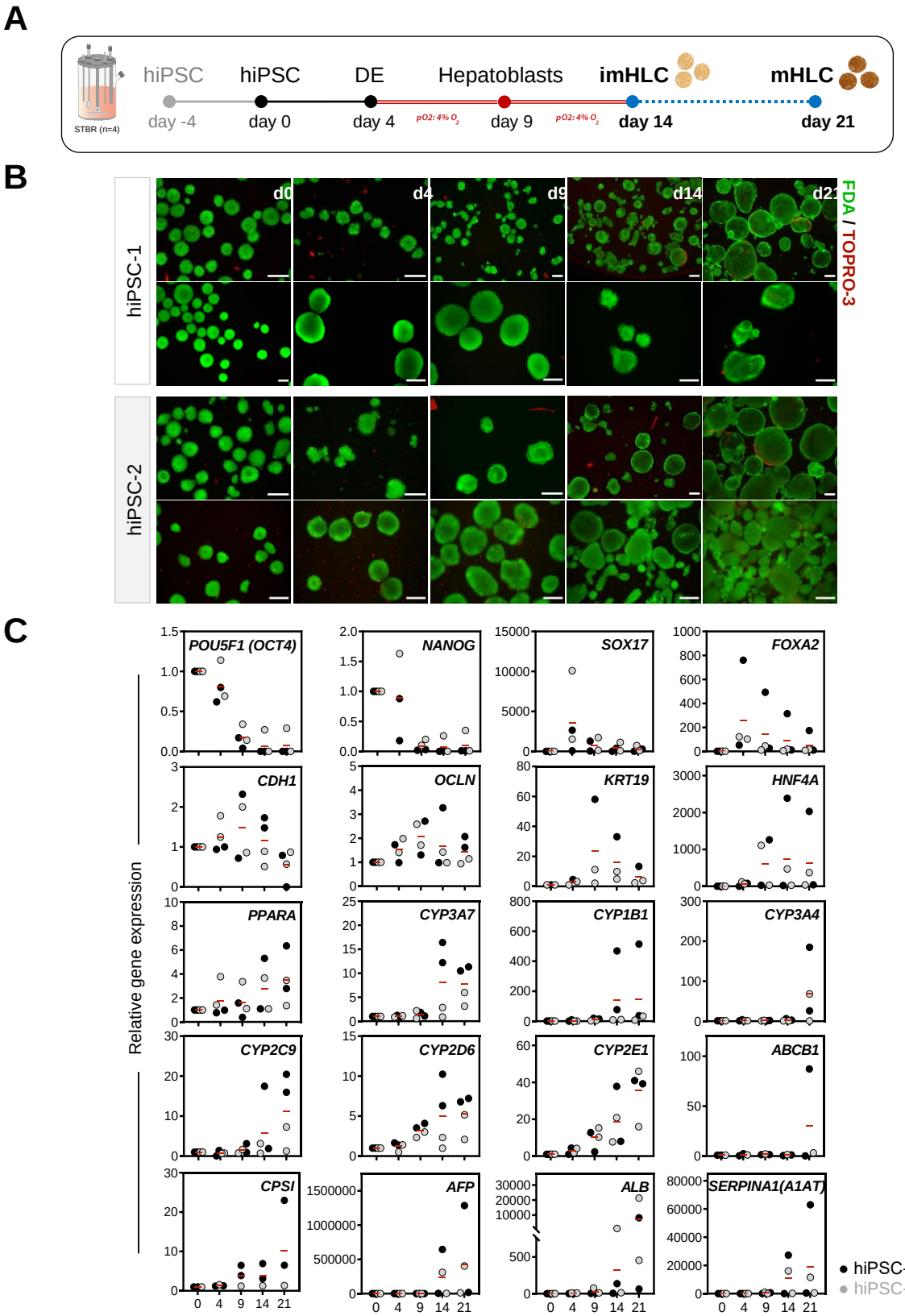

Figure 1. hiPSC were successfully differentiated in HLC with different levels of maturation. In this study, hiPSC-1 and hiPSC-2 were differentiated into HLC as cell aggregates for 21 days using STBR. Cells were harvested at critical differentiation time points (days 0, 4, 9, 14 and 21) to monitor culture viability and differentiation status. (A) Schematic representation of our integrated bioprocess. (B) Light microscopy analysis of culture viability during differentiation. Live cells internalized FDA and are represented as green spheres, whereas death ones stained for TO-PRO-3 and are identified with red colour. Scale bar: 200 µm. (C) Differentiation of hiPSC into HLC. Transcriptomic analysis by RT-qPCR of hiPSC commitment into HLC. Data are normalized for *GAPDH* and are represented as FC increase to d0. Gene expression values for hiPSC-1 are represented as black dots while grey dots represent hiPSC-2. In total, 4 independent STBR were performed, and red bars indicate mean values. Abbreviations: DE, definitive endoderm; FC, fold change; hiPSC, hµman induced pluripotent stem cells; HLC, hepatocyte-like cells; imHLC, immature HLC; mHLC, mature HLC; STBR, stirred-tank bioreactors. Gene nomenclature is described in Table 2.

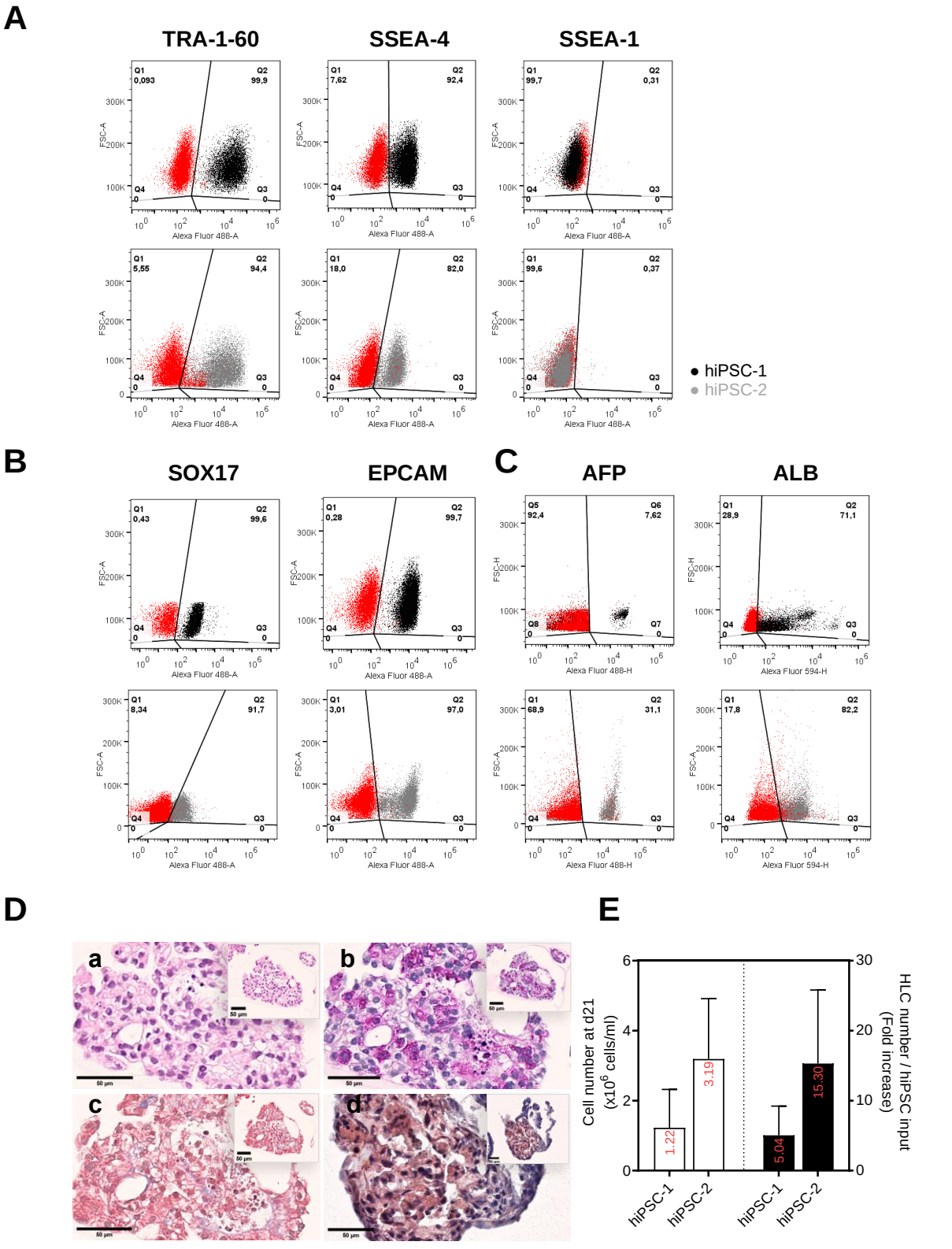

Supporting Figure 1. Production of relevant yields of mHLC in STBR. In this study, hiPSC-1 and hiPSC-2 were differentiated into HLC using STBR. Cells were harvested at critical differentiation time points (days 0, 4 and 21) to monitor differentiation status by flow cytometry: (A) analysis of pluripotency markers (TRA-1-60, SSEA-4) and SSEA-1; (B) analysis of SOX17 and EpCAM; (C) quantification of hepatic markers (AFP and ALB). (D) Histological analysis of mHLC with the stainings of (a) H&E; (b) PAS; (c) MT and (d) Oil O Red. Scale bar: 50 µm. (E) Concentration of HLC obtained at day 21 of differentiation (white bars) and efficacy of differentiation measured by ratio between the nµmber of HLC generated by the input of hiPSC (black bars). Abbreviations: H&E, hematoxylin and eosin; HLC, hepatocyte-like cells; MT, Masson's trichrome; PAS, periodic acid–schiff; STBR, stirred-tank bioreactors.

5.2. The maturation levels of HLC modulated the transcriptome that sustains cell engraftment

We analyzed, by RNA-Seq, the transcriptome of HLC harvested at days 14 (imHLC) and 21 (mHLC) of differentiation to investigate whether dynamic suspension cultures provided HLC with the critical environmental factors to activate and develop the "engraftment machinery". Additionally, we explored whether the maturation level influences these pathways and, therefore, the ability of HLC to repopulate liver extracellular matrix.

Principal component analysis (PCA) of vst-normalized counts revealed that the transcriptome of imHLC and mHLC differed about 35%. Although these states separate clearly on PC2, the primary source of variability was owed to biological differences between the hiPSC lines used that were derived from different donors (Fig. 2A).

Next, we performed differential expression analysis to identify differences in the gene expression between the two HLC populations. From this analysis, we identified a total of 368 statistically significant upregulated genes and 269 statistically significant downregulated when comparing mHLC to imHLC (Fig. 2B). To unveil the underlying mechanisms of such genes and the nature of the pathways upregulated in mHLC, we performed pathway enrichment analysis by evaluating if specific terms (GO and kegg) were significantly over-represented in such genes. Interestingly, 136 enriched terms were found and 24 of those were associated with cell engraftment. As illustrated in Fig. 2C, these pathways included focal adhesion, cell-substrate adhesion (mediated by integrins), glycosaminoglycan binding, sulfur compound binding and extracellular matrix organization. Additional pathways implicated in cell growth, metabolism, survival, and proliferation, possibly mediated by the signaling pathway PI3K-Akt (also increased), were upregulated in mHLC. Pathways associated with stem cell differentiation, pattern specification, morphogenesis of an epithelium/connective tissue development were also increased. Lasty, cell-to-cell communication or even response to oxygen were found enriched in mHLC (Fig. 2C).

Of these pathways, we calculated the z-score for genes that were found differentially expressed and generated 4 heat maps to show their expression pattern (Fig. 2D). As

illustrated, many genes associated with cell engraftment namely *CEACAM6, ICAM1, ITGA2, -4, -7, -8, CX3CL1, CD34, GPC4,* etc.) were upregulated in mHLC and not in imHLC. Similar tendency was observed for *WNT5A* (regulator of cell fate and patterning during embryogenesis); *CDKN1A* (a cyclin-dependent kinase inhibitor involved in cell cycle progression); CCN2 (involved in cell adhesion) and many others (Fig. 2D).

Overall, this set of results suggests that the maturation profile of HLC is associated with different transcriptomic signatures, mainly in pathways involved not only in cell growth and proliferation but also in cell engraftment in tissues.

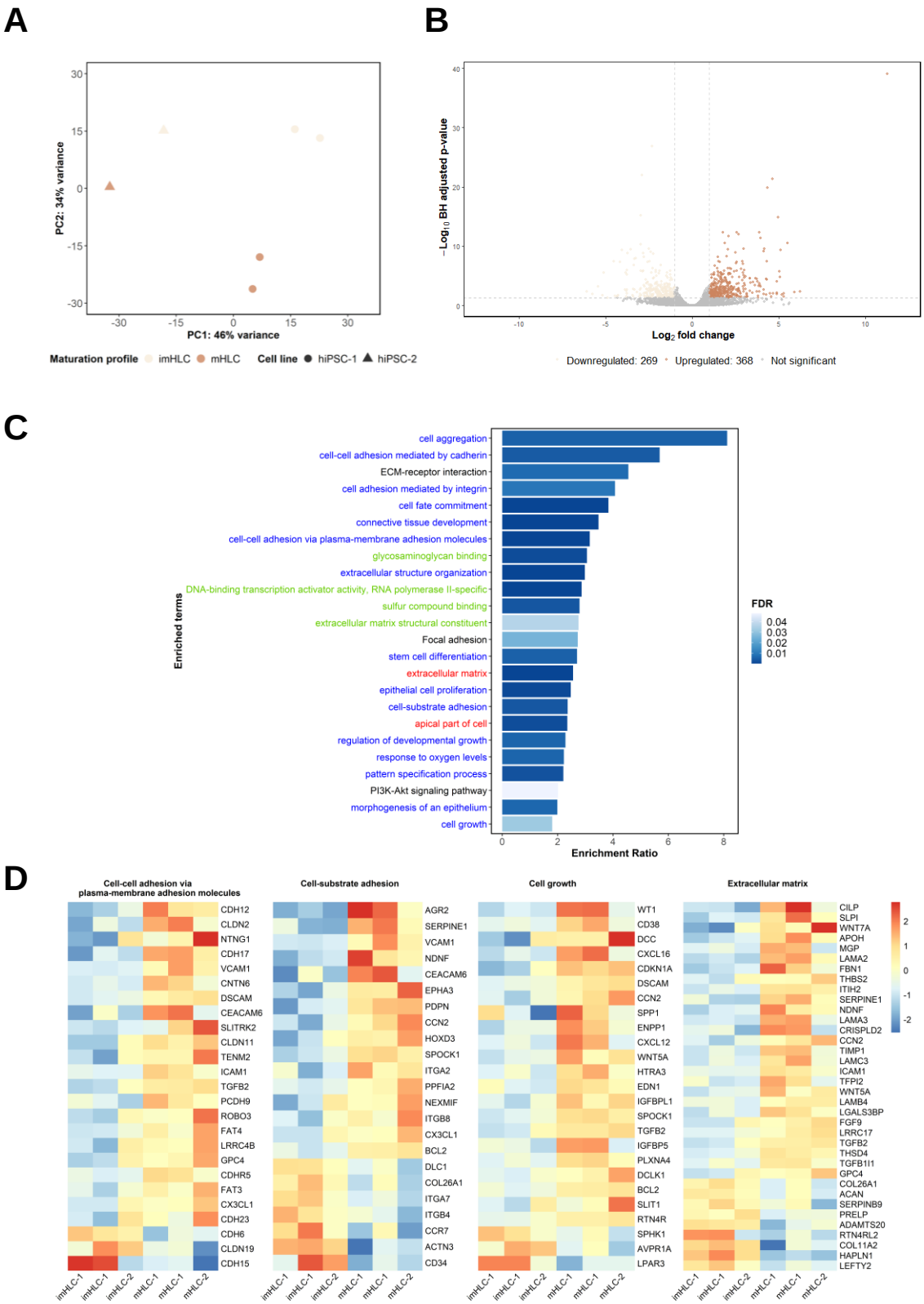

Figure 2. Mature HLC showed enhanced transcription of pathways involved in cell growth, proliferation and engraftment. HLC from hiPSC-1 and hiPSC-2 were harvested from STBR at day 14 (imHLC) and 21 (mHLC) of differentiation and analysed by RNA-Seq. RNA sequencing results of imHLC and mHLC for hiPSC-1 and hiPSC-2. (A) PCA of vst-normalized counts of all expressed genes. (B) Volcano plot of differentially expressed genes between mHLC and imHLC. (C) Overrepresented terms in differentially expressed gene list. Coloured letters indicate to which branch the term belongs. Red = GO: Molecular Function, Blue = GO: Biological Process, Green = GO: Cellular Component and Black = KEGG. (D) Heatmaps representing the z-score of vst-normalized counts for differentially expressed genes within the GO terms cell-cell adhesion via plasma membrane adhesion molecules (GO:0098742), cell-substrate adhesion (GO:0031589), cell growth (GO:0016049) and extracellular matrix (GO:0031012). Abbreviations: imHLC-1, immature HLC from hiPSC-1; imHLC-2, immature HLC from hiPSC-2; mHLC-1, mature HLC from hiPSC-1; mHLC-2, mature HLC from hiPSC-2; PCA, principal component analysis. Gene nomenclature can be found in Gene Cards.

5.3. Mature HLC showed enhanced ability to engraft into scaffolds *versus* immature counterparts

To evaluate whether the transcriptional signatures of imHLC and mHLC can be an indicative of their engraftment ability, we recellularized acellular liver scaffolds with these two HLC populations and analyzed scaffold repopulation after 7 and 14 days of culture.

Acellular liver scaffolds were derived from porcine livers that were decellularized (Fig. 3A a-c) and processed in the form of discs (Fig. 3A d), as previously described [51,52].

The efficiency of the decellularization protocol was confirmed by the absence of cellular material in the scaffolds evidenced by images of SEM (Fig. 3A d-e) and the staining of H&E and Nuclear Fast Red (NFR) (Fig. 3A f-g). Importantly, the presence of ECM fibers and the high collagen content observed (Fig. 3A h-k) confirmed the scaffolds' integrity after decellularization process.

For recellularization of liver scaffolds, aggregates of both imHLC and mHLC were harvested from STBR and mechanically dissociated into smaller fragments using nylon meshes with a pore size of 250 µm. Although fragments showed significantly reduced size when compared to their initial form (Fig. 3B and C), no differences in the size of fragments were observed between imHLC and mHLC (32.51 ± 26.10 µm and 34.36 ± 35.28 µm, respectively; Fig. 3C), and cells presented high viability after mechanical disruption (Fig. 3D).

For both conditions, we seeded approximately $1x10^6$ cells in fragments per scaffold and cultured them in HMM for 7 or 14 days. Histological analysis of scaffolds recellularized with mHLC after 7 days of culture (rECM+mHLC-7d) revealed efficient cell retention (Fig. 4A c-d) contrary to what was observed with scaffolds seeded with imHLC (rECM+imHLC-7d) (Fig. 4A a-b) where very few cells were observed. These observations were corroborated by the content of dsDNA quantified in the scaffolds (Fig. 4B); while the amount of dsDNA present in rECM+imHLC-7d was very low (155.86 ± 110.49 ng/mg of wet tissue) and did not differ significantly from decellularized scaffolds (136.31 ± 51.67 ng/mg of wet tissue), the content of dsDNA in rECM+mHLC-7d (859.86 ± 229.34 ng/mg of wet tissue) was increased by 6 times. Interestingly, when mHLC were left in culture for additional days (rECM+mHLC-14d),

the content of dsDNA present in these scaffolds (945.81 ± 25.92 ng/mg of wet tissue) were 7 times superior to rECM+imHLC-7d and cells presented a more homogenous distribution in these scaffolds (Fig 4A e-f). Finally, when comparing rECM+mHLC-14 to rECM+mHLC-7d, a slight increase in the content of dsDNA was observed that might be an indicative of cell proliferation.

These assumptions were validated by SEM analysis (Fig 5A-C). Images of SEM of scaffolds cultured with mHLC for 7 and 14 days revealed that cells were able to migrate and completely repopulate the scaffolds, showing cell adhesion mechanisms to the substrate and clear evidence of cell-to-cell connections mediated by nanotubular structures (Fig. 5B-C). Interestingly, none of these events were observed in scaffolds recellularized with imHLC (Fig. 5A).

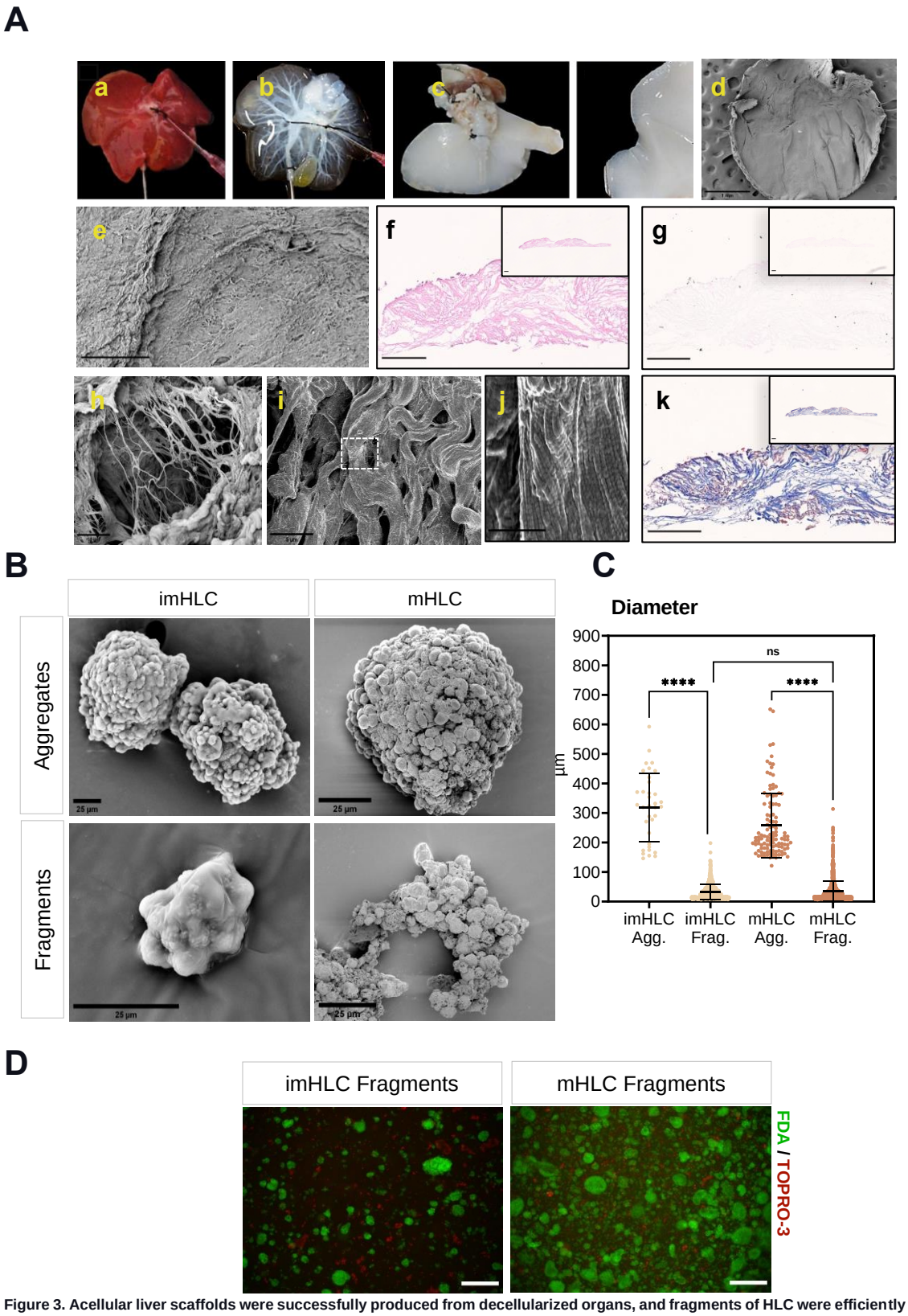

Figure 3. Acellular liver scaffolds were successfully produced from decellularized organs, and fragments of HLC were efficiently obtained from aggregates. (A) Decellularization of liver lobes and production of acellular liver scaffolds: (a) native porcine liver; (b-c) decellularized liver lobe; (d-e) images of acellular liver scaffold by SEM; (f-g) transversal images of scaffolds stained with H&E and NFR. Scale bar: 50 µm (bigger images) and 250 µm (smaller images); (h-j) SEM images of ECM fibers of scaffolds; (k) transversal image of scaffolds stained with MT. Scale bar: 50 µm (bigger image) and 250 µm (smaller image); (B) Images of SEM of HLC aggregates after dissociation and resulting fragments. Scale bar: 25 µm. (C) Size of HLC aggregates and respective fragments. Data is represented as mean ± SD. Statistical analysis by ordinary one-way ANOVA. ****p <0.0001; ns, not significant. (d) Light microscopy analysis of fragments viability after dissociation. Live fragments internalized FDA and appear stained as green, whereas death ones stained for TO-PRO-3 and are identified as red. Scale bar: 200 µm. Abbreviations: HLC, hepatocyte-like cells; H&E, hematoxylin and eosin; imHLC, immature HLC (in the form of 3D aggregates); imHLC fragments, fragments obtained from imHLC; mHLC, immature HLC (in the form of 3D aggregates); mHLC fragments, fragments obtained from mHLC; MT, masson's trichrome; NFR, nuclear fast red; SEM, scanning electron microscopy.

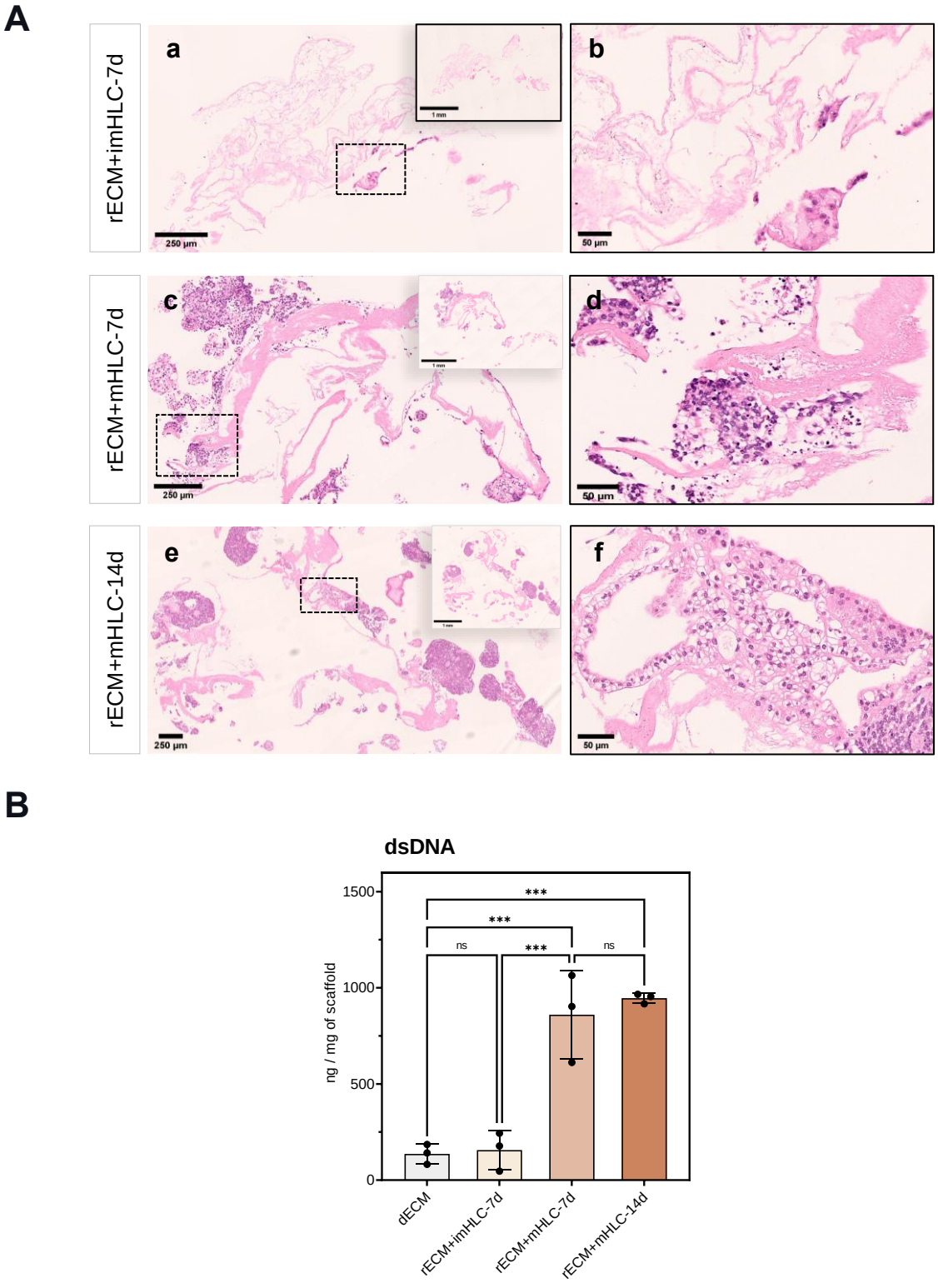

Figure 4. Mature HLC showed enhanced engraftment ability than immature counterparts. Decellularized liver scaffolds, in the form of discs, were seeded with im- or mHLC ($1x10^6$ HLC fragments/scaffold) and cultured for 7 or 14 days. (A) Longitudinal sections of scaffolds stained with H&E: (a-b) rECM+imHLC-7d; (c-d) rECM+mHLC-7d; (e-f) rECM+mHLC-14d. Scale bar: 250µm or 50 µm. (B) Quantification of dsDNA content in the scaffolds after culture (ng/mg of scaffold). Data is represented as mean values ± SD (n=3 technical replicates). Statistical analysis by ordinary one-way ANOVA. ****p <0.0001; ns, not significant. Abbreviations: dECM, decellularized ECM; dsDNA, double-stranded DNA; ECM, extracellular matrix; HLC, hepatocyte-like cells; H&E, hematoxylin and eosin; imHLC, immature HLC; mHLC, mature HLC; rECM+imHLC-7d, acellular liver scaffolds recellularized with imHLC and cultured for 7 days; rECM+mHLC-7d, acellular liver scaffolds recellularized with mHLC and cultured for 7 days; rECM+mHLC-14d, acellular liver scaffolds recellularized with mHLC and cultured for 14 days.

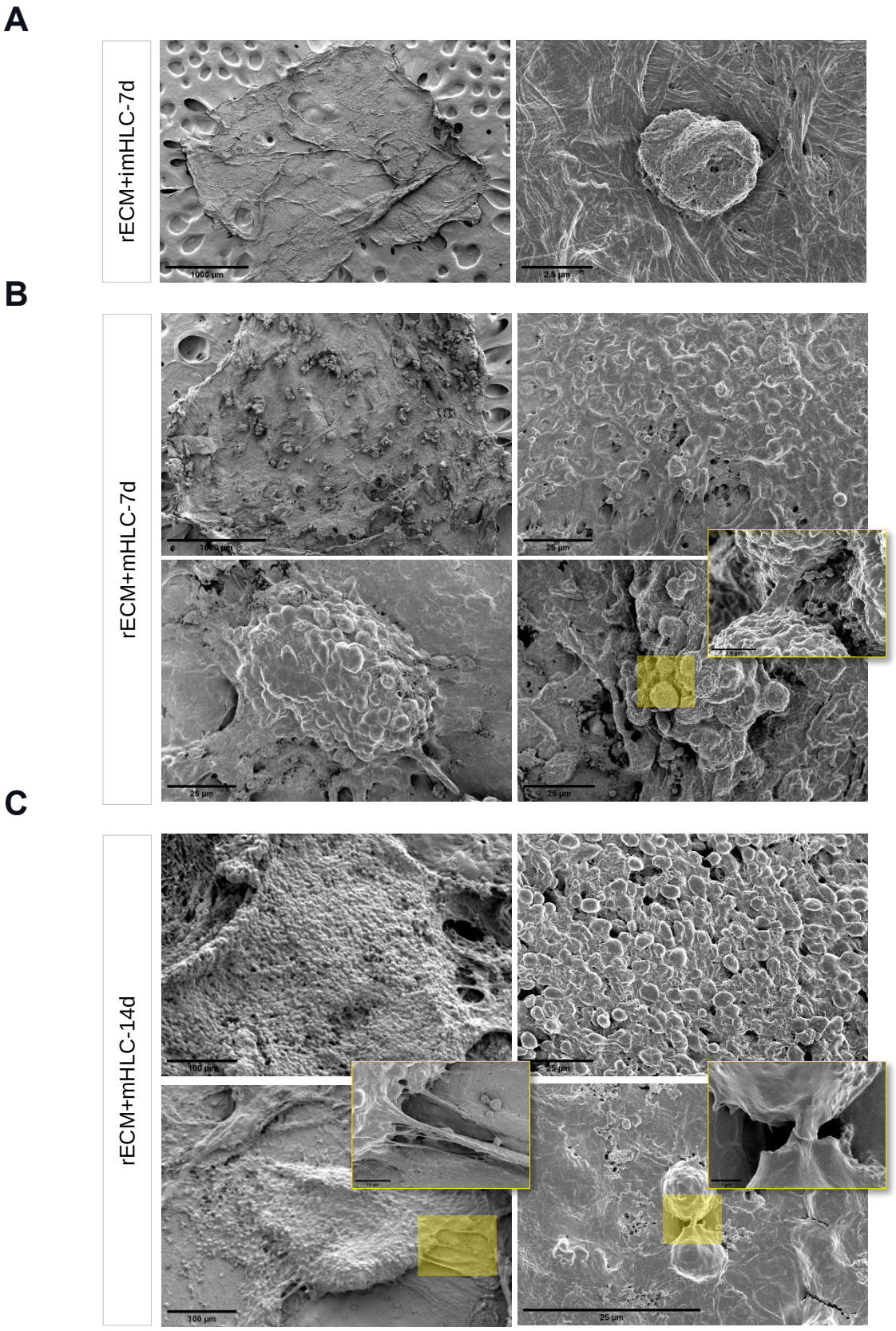

Figure 5. Mature HLC engrafted into liver scaffolds and exhibited mechanisms of adhesion to substrate and cell-to-cell communication. Images of (A) rECM+imHLC-7d; (B) rECM+mHLC-7d and (C) rECM+mHLC-14d by SEM. Scale bars are illustrated in the pictures. Abbreviations: HLC, hepatocyte-like cells; imHLC, immature HLC; mHLC, mature HLC; rECM+imHLC-7d, acellular liver scaffolds recellularized with imHLC and cultured for 7 days; rECM+mHLC-7d, acellular liver scaffolds recellularized with mHLC and cultured for 7 days; rECM+mHLC-14d, recellularized ECM with mHLC for 14 days; SEM, scanning electron microscopy.

5.4. Mature HLC remodelled ECM and remained functional after 14 days of culture in the scaffolds

We then investigated whether these mHLC remain viable and functional *in vitro*.

By atomic force microscopy (AFM), we observed that the stiffness of scaffolds cultured with mHLC were drastically inferior compared to decellularized scaffolds (dECM). Furthermore, we observed a significant increase in the content of s-GAGs (0.193, 1.39 and 1.56 µg/mg of scaffold for dECM, rECM+mHLC-7d and rECM+mHLC-14d, respectively) and collagen (9.50, 30.08 and 24.56 µg/mg of scaffold for dECM, rECM+mHLC-7d and rECM+mHLC-14d, respectively) in scaffolds seeded with mHLC (Fig. 6A). The latter was corroborated by histological analysis of scaffolds stained with MT (Fig. 6B).

Finally, we analyzed the ability of mHLC scaffolds to secrete liver-specific plasma proteins during the culture in scaffolds. We observed that mHLC cultured for 14 days in scaffolds secreted slightly more AFP (0.70±0.03 $ng.day^{-1}/ng.\mu l^{-1}$ of DNA in rECM+mHLC-7d and vs 0.76±0.03 $ng.day^{-1}/ng.\mu l^{-1}$ of DNA in rECM+mHLC-14d), ALB up to 4 times more (0.03±0.01 vs 0.11±0.01 $ng.day^{-1}/ng.\mu l^{-1}$ of DNA in rECM+mHLC-7d and rECM+mHLC-14d, respectively), and A1AT up to 2 times more (0.54±0.11 vs 0.88±0.26 $ng.day^{-1}/ng.\mu l^{-1}$ of DNA in rECM+mHLC-7d and vs rECM+mHLC-14d, respectively) compared to HLC cultured in the scaffolds for 7 days only (Fig. 7A). These cells were also shown to synthetize and accumulate glycogen (Fig. 7B).

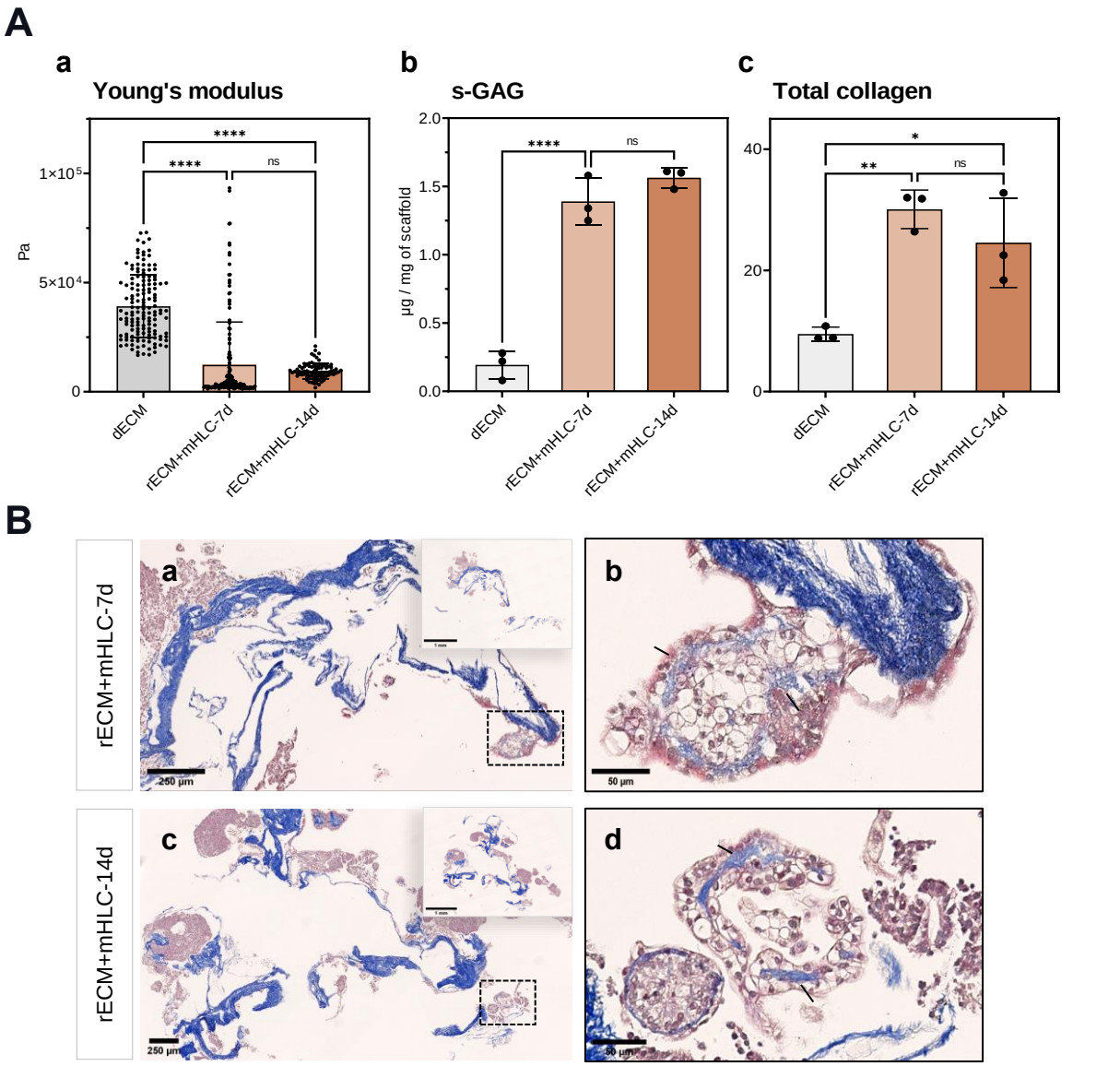

Figure 6. Mature HLC degrade and remodelled ECM. (A) Mechanical and biochemical properties of scaffolds cultured with mHLC: (a) resistance to deformation (Young's Modulus) of dECM, rECM+mHLC-7d and rECM+mHLC-14d (in Pa) measured by AFM; Content of (b) s-GAGs and (c) total collagen in these scaffolds (µg/mg). Data were normalized to tissue wet weight (n=3 technical replicates). Data is represented as mean ± SD. Statistical analysis by ordinary one-way ANOVA. *p ≤ 0.05; **p ≤ 0.01; ***p ≤ 0.001; and ns – nonsignificant (p > 0.05). (B) Images of longitudinal sections of rECM+mHLC-7d and rECM+mHLC-14d stained with MT. Scale bars are illustrated in the pictures. Abbreviations: AFM, atomic force microscopy; ECM, extracellular matrix; HLC, hepatocyte-like cells; imHLC, immature HLC; mHLC, mature HLC; MT, masson's trichrome; Pa, pascal; rECM+mHLC-7d, acellular liver scaffolds recellularized with mHLC and cultured for 7 days; rECM+mHLC-14d, acellular liver scaffolds recellularized with mHLC and cultured for 14 days; SD, standard deviation; s-GAGs, sulphated glycosaminoglycans.

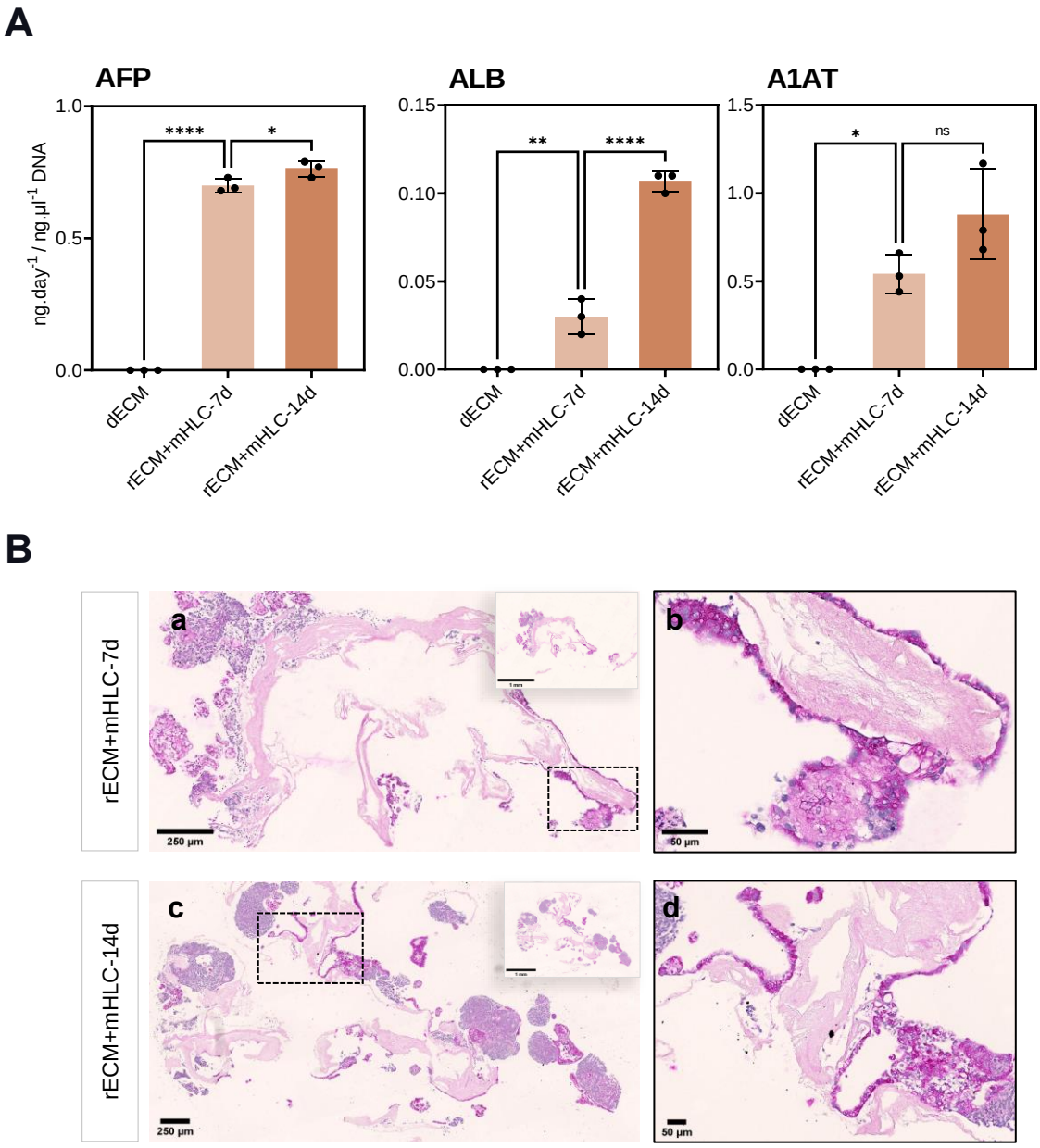

Figure 7. Mature HLC cultured for long-term in the scaffolds showed improved secretion of hepatic plasma proteins. (A) Quantification of AFP, ALB and A1AT secreted by mHLC (ng·day^{-1} / ng·µl^{-1} DNA) after 7 and 14 days of culture in the scaffolds. Protein concentration was normalized to the content of DNA present in the scaffolds (n=3 technical replicates). Data are presented as mean ± SD. Statistical analysis by ordinary one-way ANOVA. *p ≤ 0.05; **p ≤ 0.01; ***p ≤ 0.001; and ns – nonsignificant (p > 0.05). (B) Images of longitudinal sections of rECM+mHLC 7 and rECM+mHLC 14 d stained with PAS. Scale bars are illustrated in the pictures. Abbreviations: AFP, alpha-fetoprotein; ALB, albumin; A1AT; Alpha-1 antitrypsin; ECM, extracellular matrix; HLC, hepatocyte-like cells; imHLC, immature HLC; mHLC, mature HLC; PAS, periodic acid–schiff; rECM+mHLC-7d, acellular liver scaffolds recellularized with mHLC and cultured for 7 days; rECM+mHLC-14d, acellular liver scaffolds recellularized with mHLC and cultured for 14days; SD, standard deviation.

6. Discussion

In this study, we successfully differentiated two hiPSC lines into HLC using STBR, confirming the robustness of our integrated bioprocess already described in Chapter 3.

As shown here, our protocol preserved cell viability during the 21 days of culture, and transcriptomic analysis confirmed hiPSC differentiation into hepatocyte lineage (Fig. 1B-C). Notably, by the end of our bioprocess, we obtained $244x10^6$ and $638x10^6$ of HLC for hiPSC-1 and hiPSC-2, respectively (considering a working volume of 200ml) (Sup. Fig 1E).
Moreover, with a single hiPSC we could obtain approximately five HLC, which confirmed the high differentiation efficacy of our protocol (Sup. Fig. E).
Regarding cellular phenotype, mHLC expressed adult hepatic markers to a greater extent compared to what has been described. Although more than 70-80% of mHLC were positive for ALB and synthesized glycogen, lipids and collagen resembling PHH (Sup. Fig.1 C-D), these cells still preserved traits of fetal origin in accordance with other findings [35,55]. However, the relatively high expression of *AFP* (Fig. 1C) was not translated into protein levels (Sup. Fig. 1C) which led us to believe that our HLC are moving towards more mature phenotypes.

These findings and the fact that STBR culture systems can be scaled up to 2000L make us confident that soon we will achieve the cell numbers and the quality needed to restore at least 10-20% of the hepatocyte liver mass [23].

Additionally, we showed that HLC harvested at the end of differentiation showed increased expression of critical hepatic hallmarks (e.g. *PPARa*, *CYP1B1*, *-.3A4*, *-.2C9*, *-.2E1*, *ABCB1*, *CPSI*, *AFP*, *ALB* and *A1AT*) when compared to counterparts harvested from culture seven days earlier (Fig. 1C). This highlights the interest of our protocol for studies on liver biology and development.

For cell therapy applications, besides the scalability of protocols, cells must engraft into tissues and remain viable and functional after transplantation.

To our knowledge, there is no other study available that investigates the engraftment capacity of HLC derived from hiPSC using bioreactors.

In this study, we proved that although cells grown in suspension cultures free from microcarriers, HLC were able to transcribe pathways associated with cell engraftment. These pathways included cell-adhesion to substrate (by cadherins and integrins), cell-cell communications, epithelial proliferation, etc. (Fig. 2C).

Secondly, we showed that the maturation profile of HLC is critical for cell engraftment. We showed that with a difference of 35% only, imHLC did not express some of these pathways and this might justify their poor engraftment capacity. We demonstrated that mature HLC successfully repopulated and migrated in liver scaffolds whereas immature counterparts did not (Fig. 4 and Fig. 5).
Furthermore, we showed that mHLC could remodel ECM stiffness, possibly mediated by MMPs and synthesized ECM components like GAGs and collagen (Fig. 6). Most importantly, mHLC showed enhanced ALB, AFP and A1AT secretion and accumulation of glycogen after 14 days in culture. More studies should be performed for long-term follow-up to assess the safety and functionality of engrafted cells.

In conclusion, the findings presented here, provide a robust platform for efficient development of functional HLC from hiPSC by a simple and reproducible method in a carrier-free suspension STBR. Moreover, we proved, for the first time, that HLC obtained in suspension cultures, express the machinery that sustained cell engraftment and unveiled some genetic markers that could serve as indicators for a successful engraftment.

This work proved that hiPSC-HLC generated in scalable conditions showed hepatic function and repopulated liver scaffolds.

We are aware of all the challenges regarding hiPSC reprogramming methods and genome instability, however, we believe that HLC derived exclusively from hiPSC represent a more powerful strategy than hepatic organoids since the use of Matrigel and the variability between batch-to-batch is excluded [24].

We are conscious that studies using more realistic scaffolds like whole organs or even mice models will be needed. However, this study represents a considerable first step towards the engraftment of HLC that hopefully will make HLC therapies a tangible reality and a solution for patients with end-stage liver disease.

7. References

[1] Asrani SK, Devarbhavi H, Eaton J, Kamath PS. Burden of liver diseases in the world. J Hepatol 2019;70:151–71. https://doi.org/10.1016/j.jhep.2018.09.014.

[2] Global Observatory on Donation and transplantation 2016. http://www.transplant-observatory.org/who-ont/.

[3] Matas AJ, Sutherland DER, Steffes MW, Mauer SM, Lowe A, Simmons RL, et al. Hepatocellular Transplantation for Metabolic Deficiencies : Decrease of Plasma Bilirubin in Gunn Rats. Science (80-) 1976;192:892–4.

[4] D E Sutherland, M Numata, A J Matas, R L Simmons JSN. Hepatocellular transplantation in acute liver failure. Surgery 1977;82:124–32.

[5] Robin D. Hughes, Ragai R. Mitry, Anil Dhawan, Sharon C. Lehec, Raffaele Girlanda, Mohamed Rela, Nigel D. Heaton and PM. Isolation of Hepatocytes from Livers from NonHeart-Beating Donors for Cell Transplantation. Liver Transplant 2006;12:713–7.

[6] Puppi J, Tan N, Mitry RR, Hughes RD, Lehec S, Mieli-Vergani G, et al. Hepatocyte transplantation followed by auxiliary liver transplantation - A novel treatment for ornithine transcarbamylase deficiency. Am J Transplant 2008;8:452–7. https://doi.org/10.1111/j.1600-6143.2007.02058.x.

[7] Meyburg J, Das AM, Hoerster F, M. L, H. K, Engelmann G. et al. One liver for four children: First clinical series of liver cell transplantation for severe neonatal urea cycle defects. Transplantation 2009;87:636–41. https://doi.org/doi: 10.1097/TP.0b013e318199936a.

[8] Fraczek J, Bolleyn J, Vanhaecke T, Rogiers V, Vinken M. Primary hepatocyte cultures for pharmaco-toxicological studies: At the busy crossroad of various anti-dedifferentiation strategies. vol. 87. 2013. https://doi.org/10.1007/s00204-012-0983-3.

[9] Dhawan A, Puppi J, Hughes RD, Mitry RR. Human hepatocyte transplantation: current experience and future challenges. Nat Rev Gastroenterol Hepatol 2010;7:288–98. https://doi.org/doi: 10.1038/nrgastro.2010.44.

[10] Cahan P, Daley GQ. Origins and implications of pluripotent stem cell variability and heterogeneity. Nat Rev Mol Cell Biol 2013;14:357–68. https://doi.org/10.1038/nrm3584.

[11] Yamanaka S. Pluripotent Stem Cell-Based Cell Therapy—Promise and Challenges. Cell Stem Cell 2020;27:523–31. https://doi.org/10.1016/j.stem.2020.09.014.

[12] Duan Y, Catana A, Meng Y, Yamamoto N, He S, Gupta S, et al. Differentiation and Enrichment of Hepatocyte-Like Cells from Human Embryonic Stem Cells In Vitro and In Vivo. Stem Cells 2007;25:3058–68. https://doi.org/10.1634/stemcells.2007-0291.

[13] Cai J, Zhao Y, Liu Y, Ye F, Song Z, Qin H, et al. Directed differentiation of human embryonic stem cells into functional hepatic cells. Hepatology 2007;45:1229–39. https://doi.org/10.1002/hep.21582.

[14] Hay DC, Zhao D, Fletcher J, Hewitt ZA, McLean D, Urruticoechea-Uriguen A, et al. Efficient differentiation of hepatocytes from human embryonic stem cells exhibiting markers recapitulating liver development in vivo. Stem Cells 2008;26:894–902. https://doi.org/10.1634/stemcells.2007-0718.

[15] Mallanna SK, Duncan SA. Differentiation of hepatocytes from pluripotent stem cells. Curr Protoc Stem Cell Biol 2013;1:1–15. https://doi.org/10.1002/9780470151808.sc01g04s26.

[16] Si-tayeb K, Noto FK, Nagaoka M, Li J, Battle MA, Duris C, et al. Highly Efficient Generation of Human Hepatocyte–Like Cells from Induced Pluripotent Stem Cells. Hepatology 2010;9:297–305. https://doi.org/10.1002/hep.23354.
[17] Asgari S, Moslem M, Bagheri-Lankarani K, Pournasr B, Miryounesi M, Baharvand H. Differentiation and Transplantation of Human Induced Pluripotent Stem Cell-derived Hepatocyte-like Cells. Stem Cell Rev Reports 2013;9:493–504. https://doi.org/10.1007/s12015-011-9330-y.
[18] Sullivan GJ, Hay DC, Park IH, Fletcher J, Hannoun Z, Payne CM, et al. Generation of functional human hepatic endoderm from human induced pluripotent stem cells. Hepatology 2010;51:329–35. https://doi.org/10.1002/hep.23335.
[19] Touboul T, Hannan NRF, Corbineau S, Martinez A, Martinet C, Branchereau S, et al. Generation of functional hepatocytes from human embryonic stem cells under chemically defined conditions that recapitulate liver development. Hepatology 2010;51:1754–65. https://doi.org/10.1002/hep.23506.
[20] Chen YF, Tseng CY, Wang HW, Kuo HC, Yang VW, Lee OK. Rapid generation of mature hepatocyte-like cells from human induced pluripotent stem cells by an efficient three-step protocol. Hepatology 2012;55:1193–203. https://doi.org/10.1002/hep.24790.
[21] Baxter M, Withey S, Harrison S, Segeritz CP, Zhang F, Atkinson-Dell R. Phenotypic and functional analyses show stem cell-derived hepatocyte-like cells better mimic fetal rather than adult hepatocytes. J Hepatol 2015;62:581–9. https://doi.org/10.1016/j.jhep.2014.10.016.
[22] Li Z, Wu J, Wang L, Han W, Yu J, Liu X, et al. Generation of qualified clinical-grade functional hepatocytes from human embryonic stem cells in chemically defined conditions. Cell Death Dis 2019;10. https://doi.org/10.1038/s41419-019-1967-5.
[23] Bilir BM, Guinette D, Karrer F, Kumpe DA, Krysl J, Stephens J, et al. Hepatocyte Transplantation in Acute Liver Failure 2000;6:32–40.
[24] Baptista PM, Spee B. Large-Scale Production of LGR5-Positive Bipotential Human Liver Stem Cells 2020;72:257–70. https://doi.org/10.1002/hep.31037.
[25] Toshio Miki, Alexander Ring JG. Hepatic differentiation of human embryonic stem cells is promoted by three-dimensional dynamic perfusion culture conditions. Tissue Eng Part C Methods 2011;17:557–68. https://doi.org/10.1089/ten.TEC.2010.0437.
[26] Sivertsson L., Synnergren J., Jensen J., Björquist P., Ingelman-Sundberg M. Hepatic differentiation and maturation of human embryonic stem cells cultured in a perfused three-dimensional bioreactor. Stem Cells Dev 2013;22:581–94. https://doi.org/10.1089/scd.2012.0202.
[27] Cipriano M, Freyer N, Knöspel F, Oliveira NG, Barcia R, Cruz PE, et al. Self-assembled 3D spheroids and hollow-fibre bioreactors improve MSC-derived hepatocyte-like cell maturation in vitro. Arch Toxicol 2017;91:1815–32. https://doi.org/10.1007/s00204-016-1838-0.
[28] Freyer N, Knöspel F, Strahl N, Amini L, Schrade P, Bachmann S, et al. Hepatic Differentiation of Human Induced Pluripotent Stem Cells in a Perfused Three-Dimensional Multicompartment Bioreactor. Biores Open Access 2016;5:235–48. https://doi.org/10.1089/biores.2016.0027.
[29] Meier F, Freyer N, Brzeszczynska J, Knöspel F, Armstrong L, Lako M, et al. Hepatic differentiation of human iPSCs in different 3D models: A comparative study. Int J Mol Med 2017;40:1759–71. https://doi.org/10.3892/ijmm.2017.3190.

[30] Fonsato V, Herrera MB, Buttiglieri S, Gatti S, Camussi G, Tetta C. Use of a rotary bioartificial liver in the differentiation of human liver stem cells. Tissue Eng - Part C Methods 2010;16:123–32. https://doi.org/10.1089/ten.tec.2008.0634.
[31] Massoud Vosough, Eskandar Omidinia, Mahdi Kadivar, Mohammad-Ali Shokrgozar, Behshad Pournasr, Nasser Aghdami HB. Generation of Functional Hepatocyte-like Cells from Human Pluripotent Stem Cells in a Scalable Suspension Culture. Stem Cells Dev 2013:2693–705.
[32] Yonsil Park, Yemiao Chen, Laura Ordovas CMV. Hepatic differentiation of human embryonic stem cells on microcarriers. J Biotechnol 2014;174:39–48. https://doi.org/10.1016/j.jbiotec.2014.01.025.
[33] Gu C, Chai M, Liu J, Wang H, Du W, Zhou Y, et al. Expansion of Transdifferentiated Human Hepatocytes in a Serum-Free Microcarrier Culture System. Dig Dis Sci 2020;65:2009–23. https://doi.org/10.1007/s10620-019-05925-8.
[34] Feng S, Wu J, Qiu WL, Yang L, Deng X, Zhou Y, et al. Large-scale Generation of Functional and Transplantable Hepatocytes and Cholangiocytes from Human Endoderm Stem Cells. Cell Rep 2020;33:108455. https://doi.org/10.1016/j.celrep.2020.108455.
[35] Yamashita T, Takayama K, Sakurai F, Mizuguchi H. Billion-scale production of hepatocyte-like cells from human induced pluripotent stem cells. Biochem Biophys Res Commun 2018;496:1269–75. https://doi.org/10.1016/j.bbrc.2018.01.186.
[36] Isidro IA, Vicente P, Pais DAM, Almeida JI, Domingues M, Abecasis B, et al. Online monitoring of hiPSC expansion and hepatic differentiation in 3D culture by dielectric spectroscopy. Biotechnol Bioeng 2021:1–8. https://doi.org/10.1002/bit.27751.
[37] Ebrahim N, Badr OAM, Yousef MM, Hassouna A, Sabry D, Farid AS, et al. Functional recellularization of acellular rat liver scaffold by induced pluripotent stem cells: Molecular evidence for wnt/b-catenin upregulation. Cells 2021;10:1–26. https://doi.org/10.3390/cells10112819.
[38] Dagher I, Nguyen TH, Groyer-Picard MT, Lainas P, Mainot S, Guettier C, et al. Efficient hepatocyte engraftment and long-term transgene expression after reversible portal embolization in nonhuman primates. Hepatology 2009;49:950–9. https://doi.org/10.1002/hep.22739.
[39] Zapata-Linares N, Rodriguez S, Salido E, Abizanda G, Iglesias E, Prosper F, et al. Generation and characterization of human iPSC lines derived from a Primary Hyperoxaluria Type I patient with p.I244T mutation. Stem Cell Res 2016;16:116–9. https://doi.org/10.1016/j.scr.2015.12.014.
[40] Asplund A, Pradip A, van Giezen M, Aspegren A, Choukair H, Rehnström M, et al. One Standardized Differentiation Procedure Robustly Generates Homogenous Hepatocyte Cultures Displaying Metabolic Diversity from a Large Panel of Human Pluripotent Stem Cells. Stem Cell Rev Reports 2016;12:90–104. https://doi.org/10.1007/s12015-015-9621-9.
[41] Abecasis B, Aguiar T, Arnault É, Costa R, Gomes-Alves P, Aspegren A, et al. Expansion of 3D human induced pluripotent stem cell aggregates in bioreactors: Bioprocess intensification and scaling-up approaches. J Biotechnol 2017;246:81–93. https://doi.org/10.1016/j.jbiotec.2017.01.004.
[42] Abecasis B, Aguiar T, Arnault É, Costa R, Gomes-Alves P, Aspegren A, et al. Expansion of 3D human induced pluripotent stem cell aggregates in bioreactors: Bioprocess intensification and scaling-up approaches. J Biotechnol

2017;246:81–93. https://doi.org/10.1016/j.jbiotec.2017.01.004.
[43] Serra M, Brito C, Sousa MFQ, Jensen J, Tostões R, Clemente J, et al. Improving expansion of pluripotent human embryonic stem cells in perfused bioreactors through oxygen control. J Biotechnol 2010;148:208–15. https://doi.org/10.1016/j.jbiotec.2010.06.015.
[44] Martin M. Cutadapt removes adapter sequences from high-throughput sequencing reads n.d.
[45] Dobin A, Davis CA, Schlesinger F, Drenkow J, Zaleski C, Jha S, et al. STAR: ultrafast universal RNA-seq aligner. BIOINFORMATICS 2013;29:15–21. https://doi.org/10.1093/bioinformatics/bts635.
[46] Liao Y, Smyth GK, Shi W. featureCounts : an efficient general purpose program for assigning sequence reads to genomic features. BIOINFORMATICS 2014;30:923–30. https://doi.org/10.1093/bioinformatics/btt656.
[47] Love MI, Huber W, Anders S. Moderated estimation of fold change and dispersion for RNA-seq data with DESeq2. Genome Biol 2014. https://doi.org/10.1186/s13059-014-0550-8.
[48] Durinck S, Moreau Y, Kasprzyk A, Davis S, Moor B De, Brazma A, et al. BioMart and Bioconductor : a powerful link between biological databases and microarray data analysis. BIOINFORMATICS 2005;21:3439–40. https://doi.org/10.1093/bioinformatics/bti525.
[49] Durinck S, Spellman PT, Birney E, Huber W. Mapping identifiers for the integration of genomic datasets with the R / Bioconductor package biomaRt. Nat Protoc 2009;4:1184–91. https://doi.org/10.1038/nprot.2009.97.
[50] Liao Y, Wang J, Jaehnig EJ, Shi Z, Zhang B. WebGestalt 2019 : gene set analysis toolkit with revamped UIs and APIs. Nucleic Acids Res 2019;47:199–205. https://doi.org/10.1093/nar/gkz401.
[51] Baptista PM, Vyas D, Moran E, Wang Z, Soker S. Human Liver Bioengineering Using a Whole Liver. Methods Mol Biol 2013;1001:289–98. https://doi.org/10.1007/978-1-62703-363-3.
[52] Vyas D, Baptista PM, Brovold M, Moran E, Gaston B, Booth C, et al. Self-assembled liver organoids recapitulate hepatobiliary organogenesis in vitro. Hepatology 2018;67:750–61. https://doi.org/10.1002/hep.29483.
[53] Almeida H V., Tenreiro MF, Louro AF, Abecasis B, Santinha D, Calmeiro T, et al. Human Extracellular-Matrix Functionalization of 3D hiPSC-Based Cardiac Tissues Improves Cardiomyocyte Maturation. ACS Appl Bio Mater 2021;4:1888–99. https://doi.org/10.1021/acsabm.0c01490.
[54] Jorba I, Uriarte JJ, Campillo N, Farré R, Navajas D. Probing Micromechanical Properties of the Extracellular Matrix of Soft Tissues by Atomic Force Microscopy. J Cell Physiol 2017;232:19–26. https://doi.org/10.1002/jcp.25420.
[55] Takeishi K, Collin A, Hortet D, Wang Y, Mashimo T, Fox IJ, et al. Assembly and Function of a Bioengineered Human Liver for Transplantation Generated Solely from Induced Pluripotent Stem Cells. CellReports 2020;31:107711. https://doi.org/10.1016/j.celrep.2020.107711.

8. Appendix

Table 3. Scalable culture systems for expansion and differentiation of hPSC in HLC. Not disclosed.

Culture System	Cell type	Cell yields/ Culture period	Main achievements	Reference
Hollow-fiber bioreactor	hESC aggregates	N/D 20 days	↑ expression of *HNF4A*, *A1AT*, *ALB*, *CYP450* ↑ ALB secretion and urea production ~29% positive cells for *ASPGR1*	[25]
	hESC aggregates	N/D 26 days	↑ expression of *ALB, CYP450, A1AT, BCRP* ↑ pathways involved in energy metabolism (glycolipid metabolism, lipid transport, cholesterol transport and homeostasis	[26]
	hnMSC spheroids	N/D 27 days	↑ expression of *ALB, AFP, HNF4α, CK18, CYP450, CEBP* ↑ *ALB* secretion and urea production Inducible CYP450 activity (EROD and luminescence assays) and UGT activity (4-MU quantification) ↑ drug metabolization (bupropion and diclofenac conversion)	[27]
	hiPSC aggregates	N/D 16 days	↑ ALB, AFP, Urea secretion Majority of HLC positive for *ALB, CK18* and *HNF4α* Inducible CYP450 activity (phenacetin, bupropion, diclofenac, and midazolam) Formation of bile ducts by CK19 staining	[28]
	hMSC-BM and hLSC aggregates	N/D 24-48h	↑ CYP450 genes expression (*CYP1A1, CYP2B6, CYP2C19, CYP2C8, CYP2D6, CYP1E1, CYP2J2, CYP3A5*) Expression of hepatic-specific genes (*CK18, CK8, ALB*) ↓ expression of *AFP* and MSC markers (*CD73, CD146, CD29, CD105, CD44*) hLSC produced the highest concentration of ALB and Urea Production of high amounts of HGF by LSC Application in BAL systems	[30]
	hiPSC aggregates	$5x10^6$ cell/ml 18 days	↑ expression of *ALB, CYP3A4, HNF4α* and ↓ *AFP* ↑ secretion of liver-specific proteins (ALB, A1AT) Inducible CYP450 activity (midazolam, bupropion, phenacetin)	[29]
Spinner Flask Bioreactor	hiPSC and hESC spheroids	$1.7x10^6$ cell/ml 21 days	↑ expression of hepatic-specific markers (*ALB, AFP, HNF4α*) ↑ secretion of ALB and production of urea **↑ Production of ECM components (e.g., collagen)** Inducible CYP450 activity (incubation with rifampicin and PROD test) HLC transplanted into mice's spleen resulted in 60% survival after 14 days	[31]
	hESC microcarriers	$2.52x10^6$ cell/ml 18 days	Expression of hepatic-specific markers (*ALB, AFP and ASPGR1*) Secretion of liver-specific proteins (ALB) and production of Urea Inducible CYP450 activity (Luciferin-IPA tests) Use of dextran microcarriers to support differentiation	[32]
	Fibroblasts aggregates with microcarriers	$2.53x10^6$ cell/ml 14 days	Fibronectin promotes hepatocytes attachment and proliferation on microcarriers mediated by integrin pathway Expression of hepatic-specific markers (*ALB, CYP2A6, HNF1α, HNF4α, TAT, TTR, A1AT, CK18)*	[33]
	hEnSC aggregates	$6.67x10^6$ cell/ml 30 days	Generation two hepatic cell lineages (hepatocytes and cholangiocytes) Production of hepatocytes with 85 % purity HLC and cholangiocytes were identified and characterized by sc-RNA-seq 50% of mature hepatocytes Inducible CYP450 activity (rifampicin) Encapsulated hepatocytes are able to rescue rats with acute liver failure Secretion of liver-specific proteins (ALB) and production of Bile Acids, Urea and NH_3 Drug metabolization capacity (amiodarone, diclofenac, acetaminophen, or chlorpromazine)	[34]
Rotatory Cell Culture	hiPSC spheroids	$1.5x10^6$ cell/ml 25 days	High expression of hepatic-specific markers (*CYP1A2, CYP2D6*, *A1AT*, *HNF4α*) ~90% HLC positive for *ALB* **Production of ECM components (collagen type I)**	[35]
Stirred-Tank Bioreactor	hiPSC aggregates	$3.5x10^5$ cell/ml 28 days	Expression of hepatic-specific markers (*ALB, AFP, AGXT, HNF4α, A1AT, CYP3A4*) Improved secretion of hepatic-specific proteins (ALB) **Production of ECM components (collagen)** Drug metabolization capacity (uptake and release of IGC)	[36]

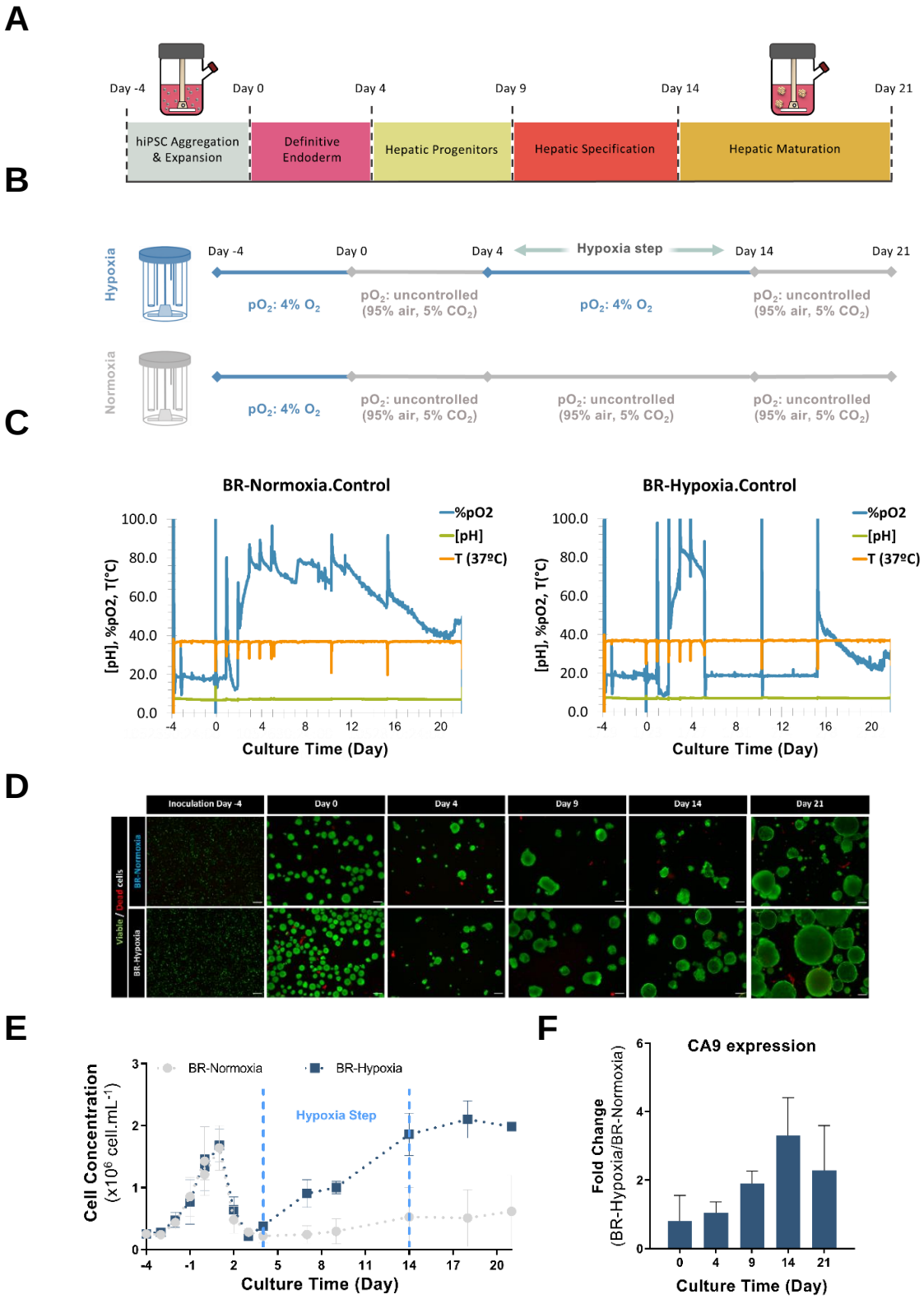

Appendix Figure 1. Low oxygen levels during hepatic specification resulted in higher HLC yields. (A) Schematic representation of the integrated bioprocess for the expansion and differentiation of hiPSC in HLC using STBR. (B) STBR under uncontrolled (BR-Normoxia) or under controlled dissolved oxygen (pO_2: 4%, BR-Hypoxia) between day 4 and day 14 of differentiation. (C) Online monitoring trend lines of $\%pO_2$, pH and temperature for BR-Normoxia and BR-Hypoxia. (D) Viability analysis of cell culture during hiPSC expansion and differentiation. Live cells internalized FDA and are represented as green spheres, whereas death ones stained for TO-PRO-3 and are identified with red colour. Scale bar: 200 µm. (E) Cell density along hiPSC expansion and hepatic differentiation process from BR-Normoxia (grey) and BR-Hypoxia (Blue). (F) Hypoxia inducible gene (CA9) expression in BR-Hypoxia relatively to the expression in BR-Normoxia by qRT-PCR quantified using the $2^{-\Delta\Delta CT}$ method. Data showed represent three pools of independent biological experiments (two independent experiments for hiPSC-1 and one independent experiment for hiPSC-2). Abbreviations: BR, bioreactor; CA9, carbonic anhydrase 9; hiPSC, hµman-induced pluripotent stem cells.

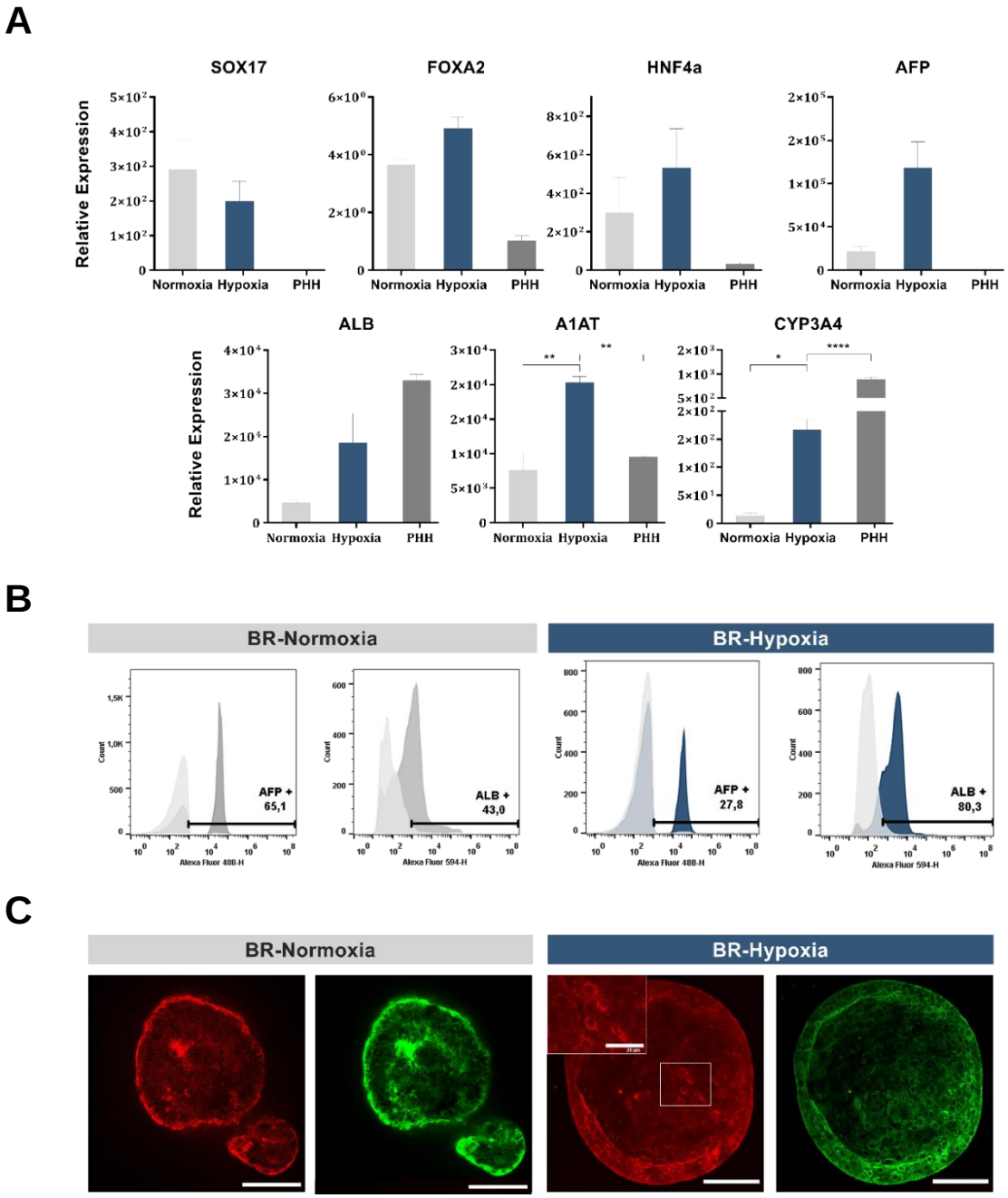

Appendix Figure 2. HLC generated in BR-Hypoxia showed improved expression of hepatic specific markers hepatic. (A) Relative gene expression of *SOX17*, *FOXA2*, *HNF4a*, *AFP*, *ALB*, *A1AT*, *CYP3A4* in HLC (day 21) generated under normoxia (grey) and hypoxia (blue). Data is shown as relative gene expression levels and compared to PHH. (B) Quantification of ALB and AFP in HLC (day 21) by flow-cytometry. BR-Hypoxia (Blue) and BR-Normoxia (Grey). (C) Whole mounting immunofluorescence images of HLC stained for ALB and AFP. Scale bar: 50 µm. hiPSC-HLC, hepatocyte-like cells derived from hµman-induced pluripotent stem cells; ALB, albµmin; AFP, alpha-fetoprotein; PHH, primary hµman hepatocytes.

Chapter 5

CONCLUDING REMARKS

This chapter is adapted from the Seminar:

Almeida J.I., Tenreiro M.F., Martinez-Santamaria, L., Guerrero-Aspizua, S., Gisbert, J.P., Alves P.M, Serra, M., Baptista, P.M. Hallmarks of the human intestinal microbiome on liver maturation and function. Journal of Hepatology 2022. 76(3):694-725. doi: 10.1016/j.jhep.2021.10.015.

1. Concluding Remarks and future directions

After NIH launched the Human Microbiome Project, allowing a deep characterization of microbiome, the interest in this microbial community has been growing steadily [1]

Over the past years, microbiome research has transitioned from cataloguing the diversity of the microorganisms that inhabit us to acknowledging them as a dynamic functional unit, which synergistically develops across spatial and temporal gradients in parallel with the host's physiologic development.

Even though the gut-liver axis is recurrently discussed in the context of acute and chronic liver diseases, recent evidences revealed its contribution to a proper liver development and acquisition of adult hepatic maturity. More specifically, its impact on liver physiology is attributed to different postbiotics that, after being absorbed across the intestinal lumen and reach the hepatic sinusoids via portal vein circulation, influence the liver throughout life [2].

This thesis investigated the effects of the bacterial secretome on liver function, using a biotechnological approach. We successfully formulated two bacterial secretomes *in vitro*, and showed that these secretomes, enriched in BA, SCFA, and vitamins, were critical to preserve the functionality and phenotype of HLC derived from different hPSC lines using 2D or 3D differentiation protocols (Chapter 2).

The work developed in this thesis also aimed at overcoming critical challenges in hPSC bioprocessing namely, the establishment of efficient and scalable protocols for generation of HLC. We developed and optimized an integrated bioprocess for the expansion and differentiation of hPSC into HLC as 3D aggregates using STBR technology. In particular, we showed that HLC generated under hypoxic atmospheric conditions (dissolved oxygen controlled at 4% O2) during hepatic specification step, exhibited phenotypical and functional hallmarks of PHH, and were able to engraft and survive in decellularized liver scaffolds (Chapter 3 and 4).

In conclusion, this thesis described a scalable protocol to produce relevant numbers of functional hPSC-HLC with high purity and provide important insights on the use of microbial secretome as a biotechnological tool to mature and/or preserve the functionality of hPSC-HLC *in vitro*.

In future, additional studies should be performed to identify the role of the key component(s) (and synergistic effects) in the microbial secretome that are driving HLC maturation to potentiate the design of chemically defined medium formulations for efficient generation of fully functional HLC in a cGMP-compliance manner (**Figure 1 d**). Emerging ‘omics methodologies such as metabolomics and single-cell/nuclei RNA-seq, could clear the path to decode the full composition of microbial secretome and understand what the missing cues in HLC differentiation are and how such maturation strategies accurately mimic development.

2. Current and future trends: microbiome-based strategies for precision medicine in hepatology

As the view of the negative impact of microbiome in liver physiology is gradually changing, further work will be required to place the microbiome in the center of basic and clinical hepatology research. Bellow, it is briefly highlighted some of the promising areas of research attempting to advance the hepatology field by taking advantage of the gut microbiome.

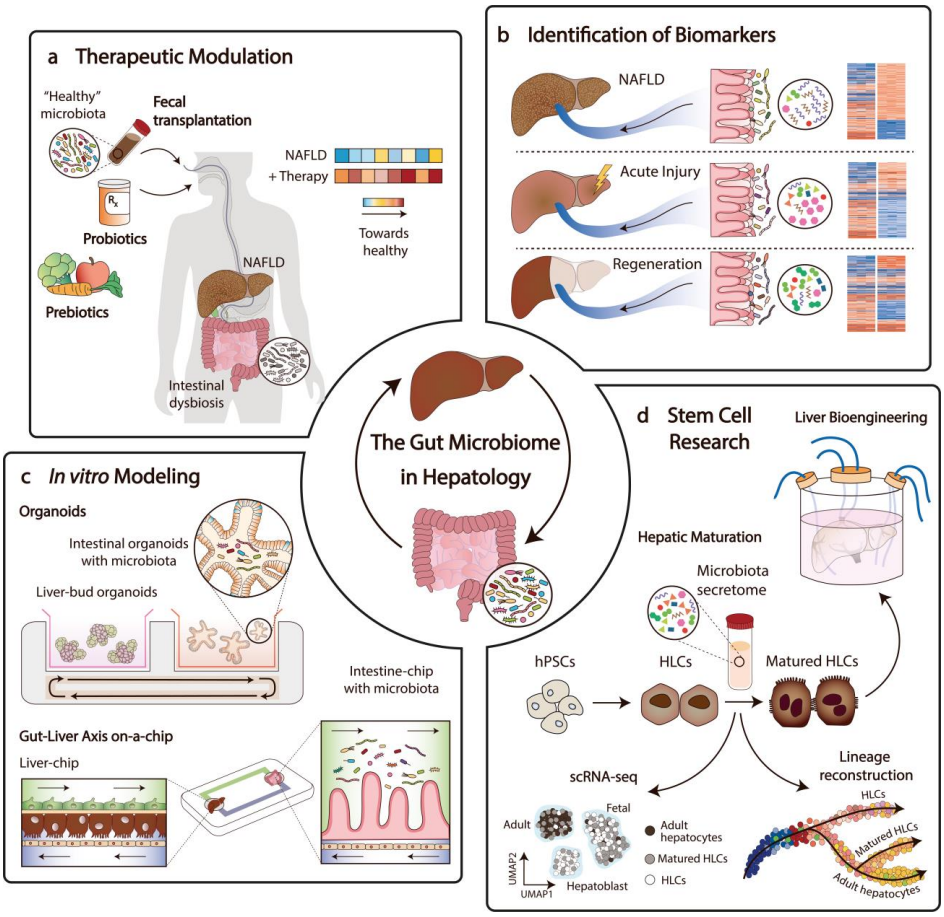

Figure 1. Current and future trends: Microbiome-based strategies for precision medicine in hepatology. a. Several therapeutic strategies can be envisaged to promote the reestablishment of a normal gut microbiome in the case of hepatic disease, namely through prebiotics, probiotics and fecal transplantation. b. Increased knowledge regarding the homeostatic composition of the gut microbiome can provide valuable insight to identify biomarkers responsible for hepatic disease onset and exacerbation, and potentially also in case of acute injury, therapy management and surgery. c. *In vitro* models, such as organoids and organ-on-a-chip platforms, can be useful to study host-microbiome interactions in the gut-liver axis in a personalized manner, surpassing limitations associated with animal models that lack human specificity. d. The microbiota secretome can be a powerful tool to promote the maturation of hepatocytes derived from human pluripotent stem cells (hPSC). These maturation strategies can be designed to mimic as closely as possible the *in vivo* development, expediting the translational use of these cells, namely in precision medicine and organ bioengineering. Abbreviations: NAFLD, non-alcoholic liver disease; HLC, hepatocyte-like cell; scRNA-seq, single-cell RNA sequencing.

2.1. Therapeutic modulation

Attenuating dysbiosis and restoring the balance between pathobionts and beneficial bacteria in the gut, two hallmark events of liver diseases, are usually managed by targeted antibiotic therapies (e.g., ciprofloxacin, rifaximin, etc.); prebiotics/probiotics supplementation (e.g., oligofructose enriched inulin, *Lactobacillus rhamnosus* and *Bifidobacterium animalis*, etc.); drugs that mimic gut-derived hormones (e.g. GLP1-analog) or specifically inhibit molecules involved in liver etiology (e.g. SGLT2-inhibitor). Recently, the use of the gut microbiome itself as therapeutic agent has been changing the paradigm of conventional therapies. Fecal microbiota transplantation (FMT), which consists on transferring the fecal microbial ecosystem of a healthy donor to a diseased recipient to induce therapeutic effects, is being increasingly recognized [3]. In hepatology, the clinical significance of FMT is being assessed (according to https://clinicaltrials.gov) to attenuate liver cirrhosis (NCT02862249), NAFLD/metabolic syndrome (NCT02496390, NCT02469272) and primary sclerosing cholangitis (NCT02424175) (**Figure 1a**). Despite the promising therapeutic benefits of FMT, the exact mechanisms by which fecal recipients benefit from the fecal intervention are not well understood and with the rising number of FMT clinical trials, there is an urgent need for standardized regulations to ensure patient safety.

2.2. Identification of biomarkers

The realization that bacterial composition in the gut is altered in patients with liver disease raised the possibility of using microbiome-derived signatures as non-invasive diagnostic tools. In fact, different studies combining stool metagenomic and untargeted metabolomic profiling were able to predict NAFLD and advanced fibrosis in children [4] and non-obese NAFLD patients [5]. Oh et al. combine these technologies with AST serum levels and machine learning algorithms to predict cirrhosis and advanced fibrosis in racially and geographically independent cohorts [6]. Similar findings were also reported for ALD [7], autoimmune hepatitis [8] and hepatocellular carcinoma [9], confirming the potential of using intestinal microbiome parameters as indicators of a ‘pre-disease state’. The potential of using the microbiome as non-invasive biomarker for hepatic diseases is gaining significantly more interest by public and private

investors. For instance, the MICROB-PREDICT Project, combines the joint efforts of 22 European institutions to develop novel diagnostic tools, based on the microbiome, to early-diagnose and stratify patients with liver disease and envisage personalized therapies (https://microb-predict.eu/). If the microbiome can be used as a diagnosis tool to predict liver disease, perhaps it could be equally valuable to foresee response to therapy or prognosis after liver surgery (e.g., partial hepatectomy due to liver tumors) (**Figure 1b**).

2.3. *In vitro* modeling

Despite the advances in model systems for human biology and medicine, the still high number of therapeutic compounds that fail to be translated in clinical trials highlights the need for advanced models that more closely resemble human physiology. Human organoids cultured in 3D systems are in vitro miniaturized cell-based models of organs that have gained enormous interest for modelling tissue development and disease, and for personalized medicine, drug screening and cell therapy. In recent years, liver organoids have been successfully generated [10], large-scale expanded [11] and were shown to maintain their hepatic and proliferative capacities during long-term cultures [12], exciting the scientific community. However, these models are still minimalistic by its incapacity to reproduce interorgan communication and by neglecting host-microbiome interactions, a critical hallmark of liver pathophysiology. Interestingly, recent advances in the field have allowed the production of physiologically relevant intestinal organoids that are susceptible to microbial [13] and viral infection [14] or that can be injected with microbiota [15]. Therefore, current and future experiments with organoid models that mimic the biology of the gut-liver axis could be established by culturing these two independent organoids separately on the same plate (**Figure 1c**).

More advanced microphysiological systems, including organ-on-a-chip devices, allow continuous co-culture of gastrointestinal tract epithelium and three-dimensional primary liver tissue. Such a system was used by Yang et al. as an in vitro human model of the gut–liver axis (without microbiome) for the initiation and progression of NAFLD [16]. In turn, Fritz et al. were able to successfully co-culture microbial cells and human intestinal cells in a microfluidic device [17]. A model including all the participants involved in the gut-liver axis is still lacking and, if possible, to be engineered, this

system could allow studying on an individual and personalized basis how the gut microbiome promotes health and onsets disease.

3. Conclusiones Finales

En este estudio, investigamos los efectos del secretoma bacteriano sobre la función hepática, siguiendo un enfoque biotecnológico. Formulamos con éxito dos secretomas bacterianos, utilizando un protocolo que recapitula la digestión humana; y mostramos que estos secretomas, enriquecidos en BA, SCFA y vitaminas, eran fundamentales para preservar la funcionalidad y el fenotipo de diferentes hPSC-HLC cultivadas *in vitro* (Capítulo 2).

Ambicionando el desarrollo de terapias celulares, describimos un protocolo para la expansión y diferenciación de hPSC en HLC usando STBR. Mostramos que las HLC generadas utilizando nuestro bioproceso integrado y condiciones de hipoxia, exhibieron características fenotípicas y funcionales de PHH, y fueron capaces de adherirse y sobrevivir en andamios hepáticos descelularizados (Capítulos 3 y 4).

En conclusión, esta tesis describe un protocolo para producir hPSC-HLC de alta calidad a gran escala y revela, por primera vez, el uso del secretoma microbiano como herramienta biotecnológica para madurar y/o preservar la funcionalidad de hPSC-HLC *in vitro*.

4. References

[1] Peterson J, Garges S, Giovanni M, McInnes P, Wang L, Schloss JA, et al. The NIH Human Microbiome Project. Genome Res 2009;19:2317–23. https://doi.org/10.1101/gr.096651.109.

[2] Almeida, Joana I., Miguel F. Tenreiro, Lucía Martinez-Santamaria, Aspizua, Sara Guerrero, Javier P. Gisbert, Paula M. Alves, Margarida Serra PMB. Hallmarks of the human intestinal microbiome on liver maturation and function. J Hepatol 2021.

[3] Giles EM, Adamo GLD, Forster SC. The future of faecal transplants. Nat Rev Microbiol 2019;17:41579. https://doi.org/10.1038/s41579-019-0271-9.

[4] Schwimmer JB, Johnson JS, Angeles JE, Behling C, Belt PH, Borecki I, et al. Microbiome Signatures Associated With Steatohepatitis and Moderate to Severe Fibrosis in Children With Nonalcoholic Fatty Liver Disease. Gastroenterology 2019;157:1109–22. https://doi.org/10.1053/j.gastro.2019.06.028.

[5] Lee G, You HJ, Bajaj JS, Joo SK, Yu J, Park S, et al. Distinct signatures of gut microbiome and metabolites associated with significant fibrosis in non-obese NAFLD. Nat Commun 2020;11:1–13. https://doi.org/10.1038/s41467-020-18754-5.

[6] Oh TG, Kim SM, Caussy C, Fu T, Guo J, Bassirian S, et al. A Universal Gut-Microbiome-Derived Signature Predicts Cirrhosis. Cell Metab 2020;32:878-888.e6. https://doi.org/10.1016/j.cmet.2020.06.005.

[7] Liu Y, Meric G, Havulinna AS, Teo SM, Ruuskanen M, Sanders J, et al. Early prediction of liver disease using conventional risk factors and gut microbiome-augmented gradient boosting. MedRxiv 2020:1–21. https://doi.org/10.1101/2020.06.24.20138933.

[8] Wei Y, Li Y, Yan L, Sun C, Miao Q, Wang Q, et al. Alterations of gut microbiome in autoimmune hepatitis. Gut 2020;69:569–77. https://doi.org/10.1136/gutjnl-2018-317836.

[9] Ren Z, Li A, Jiang J, Zhou L, Yu Z, Lu H, et al. Gut microbiome analysis as a tool towards targeted non-invasive biomarkers for early hepatocellular carcinoma 2019:1014–23. https://doi.org/10.1136/gutjnl-2017-315084.

[10] Broutier L, Andersson-rolf A, Hindley CJ, Boj SF, Clevers H, Koo B, et al. Culture and establishment of self-renewing human and mouse adult liver and pancreas 3D organoids and their genetic manipulation 2016. https://doi.org/10.1038/nprot.2016.097.

[11] Baptista PM, Spee B. Large-Scale Production of LGR5-Positive Bipotential Human Liver Stem Cells 2020;72:257–70. https://doi.org/10.1002/hep.31037.

[12] Hepatocytes H, Hu H, Gehart H, Artegiani B, Peters PJ, Jong YP De, et al. Long-Term Expansion of Functional Mouse and Article Long-Term Expansion of Functional Mouse and Human Hepatocytes as 3D Organoids 2018:1591–606. https://doi.org/10.1016/j.cell.2018.11.013.

[13] Zhang Y, Wu S, Xia Y, Sun J. Salmonella -infected crypt-derived intestinal organoid culture system for host – bacterial interactions. Physiol Rep 2014;2:1–11. https://doi.org/10.14814/phy2.12147.

[14] Zhou J, Li C, Liu X, Chiu MC, Zhao X, Wang D, et al. Infection of bat and human intestinal organoids by SARS-CoV-2. Nat Med 2020;26. https://doi.org/10.1038/s41591-020-0912-6.

[15] Karve SS, Pradhan S, Ward D V, Weiss AA. Intestinal organoids model human

responses to infection by commensal and Shiga toxin producing Escherichia coli 2017:1–20.
[16] Yang J, Hirai Y, Iida K, Ito S, Trumm M, Terada S, et al. Integrated gut – liver-on-a-chip platform as an in vitro human model of non-alcoholic fatty liver disease. BioRxiv 2020.
[17] Fritz V, Glaab E, Desai MS, Greenhalgh K, Frachet A, Shah P, et al. A microfluidics-based in vitro model of the gastrointestinal human–microbe interface. Nat Commun 2016. https://doi.org/10.1038/ncomms11535.